Declaration

Metric 3.3.1

I declare that all the data, reports and other information enclosed in the metric are authentic to the best of my knowledge.

Criteria In-charge

Dr. Goutam Varma

Index

Graphical Representation of
Research Papers Published in Journals (2018-2022)

RESEARCH PAPERS PUBLISHED IN JOURNALS

■ **Research Paper Published**

Bar chart showing Research Papers Published in Journals:
- 2022-23: 9
- 2021-22: 12
- 2020-21: 4
- 2019-20: 9
- 2018-19: 0
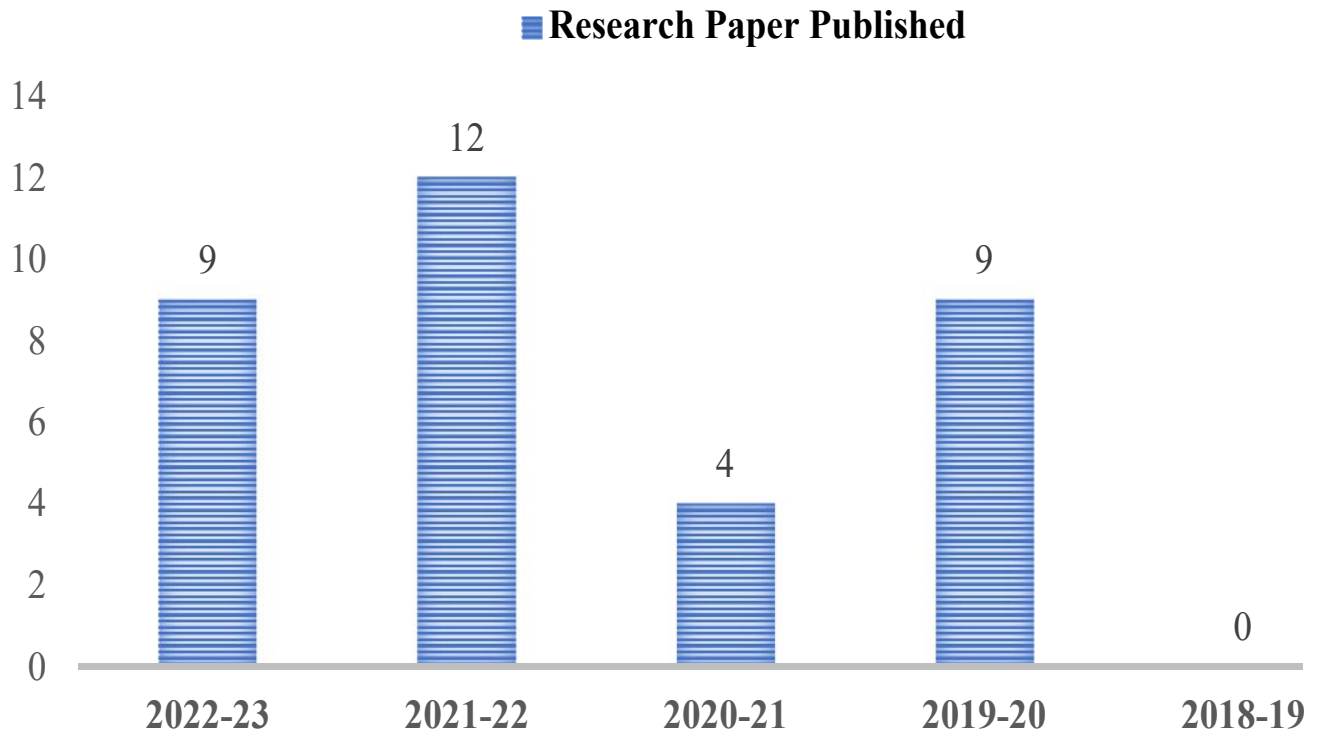
Vibration analysis of Vertical axis wind turbine (VAWT) using Ansys

Kshitij Bachhania

PG Scholar, Swami Vivekanand College of Engineering, Indore452020, India

Mr. Sandeep Badlani

Assistant Professor, Swami Vivekanand College of Engineering, Indore 452020, India

Dr. Rahul Joshi

Associate Professor, Swami Vivekanand College of Engineering, Indore 452020, India

Mr. Manoj Sharma

Assistant Professor, Swami Vivekanand College of Engineering, Indore 452020, India

Mr. MayankLadha

Assistant Professor, Swami Vivekanand College of Engineering, Indore 452020, India

Abstract **- Wind turbines are the most common type of equipment used to transform wind energy into mechanical energy. Understanding the vibration characteristics of wind turbines is essential for reducing blade failure caused by resonance-induced amplitude build-up. The current study investigates a vertical axis wind turbine subjected to free and forced vibration conditions using ANSYS FEA software. In the VAWT test, conventional aluminium alloy and aluminium MMC were used. Natural frequencies and mode shapes for both materials are determined using free vibration (modal) analysis, which is essential for the design of VAWT and the reduction of resonance.The Campbell diagram developed by free vibration analysis found no critical velocities for the operating ranges of 178.02 rpm, 263.89 rpm, 350.81 rpm, 413.64 rpm, 462.86 rpm, and 481.71 rpm. The spin direction and harmonic responses are also investigated using modal analysis. The harmonic response of the system revealed that using Aluminum MMC (composite material) rather than Aluminum alloy material resulted in less stress on the blades. The mode shapes and mass participation factor for both materials offered critical information on vibration properties under free vibration conditions**

Index Terms - Modal Analysis, Harmonic Analysis, vertical axis wind turbine

INTRODUCTION

There is a clear need for the development of renewable energy sources, especially in light of recent studies suggesting that fossil fuel stocks such as oil and natural gas may be depleted in the not-too-distant future. Renewable energy sources include solar, wind, and geothermal energy, to name a few. With wind energy being one of the most well-known sources of renewable energy, it stands out among the other renewable energy alternatives. To transform wind energy into mechanical energy, wind turbines are the most extensively utilised piece of equipment on the planet. Wind turbines transform wind energy into electricity via the use of rotating blades in the generator. The development of substantial technological advances has made it possible to Manuscript Click here to view linked References construct wind turbines [6] [2] that are more practical, dependable, and trustworthy sources of energy, notably for power generation. Wind turbines provide a significant amount of electricity in several countries. Wind energy production increased dramatically in the globe from 1996 to 2015. Wind turbines are devices that generate electricity by using the kinetic energy of the wind as a power source. Prior to the invention of the computer, they were more often used as a mechanical device that spun machinery. It is now possible to use turbines to generate considerable amounts of electrical energy in both onshore and offshore wind farms, and the Vertical Axis Wind Turbine is one of the options available to you (VAWT). Even though a large number of VAWTs are already being used to produce electricity, the HAWT continues to be more practical and popular than the VAWT and is considered to be the focal point of most wind turbine discussions. Wind turbines are a fantastic method to create electricity for our homes and businesses while also using a clean and sustainable resource. 1.1 Theory of Free Vibration [2]: When a mechanical system is started with an initial input and then allowed to vibrate at its own speed, it is referred to as free vibration. When a mechanical system is subjected to a different force or motion on a regular basis, it suffers forced vibration. Washing machines that shake owing to an imbalance, transportation vibration (produced by the vehicle's engine, springs, the road, and so on), and building vibration during an earthquake are all examples of this kind of vibration. The frequency of forced vibration is equal to the frequency of the applied force or motion, with the order of magnitude varying depending on the mechanical system. Once the system is begun in motion, it will inevitably oscillate at its natural frequency, which is a characteristic of the system. Figure 1: Spring-Mass System and Free-Body Diagram The basic foundation for evaluating the motion of the system is Newton's second law.
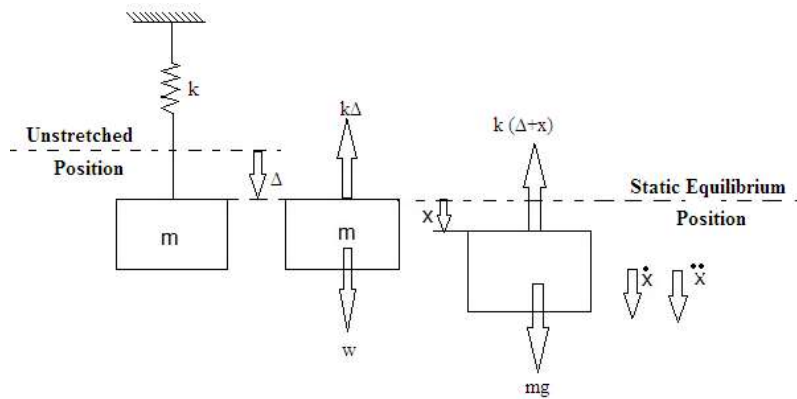
Page 1

Figure 1: Spring-Mass System and Free-Body Diagram

The spring deformation in the static equilibrium position is Δ , as illustrated in Fig. 1 and the spring force $k\Delta$ is equal to the gravitational force w acting

$$k\Delta = w = mg \qquad (1.1)$$

The forces on m are $k(\Delta + x)$ and w when the displacement x from the static equilibrium position is measured. All numbers, including force, velocity, and acceleration, are positive in the downhill direction when x is selected to be positive.

The mass m is now subjected to Newton's second law of motion: \

$$m\ddot{x} = \sum F = w - k(\Delta - x) \qquad (1.2)$$

And because $k\Delta = w$, we obtain:

$$m\ddot{x} = -kx \qquad (1.3)$$

It is evident that by utilising the static equilibrium position as a reference for x, w, the gravitational force, and the static spring force $k\Delta$ have been eliminated from the equation of motion, leaving only the spring force due to the displacement x to operate on m.
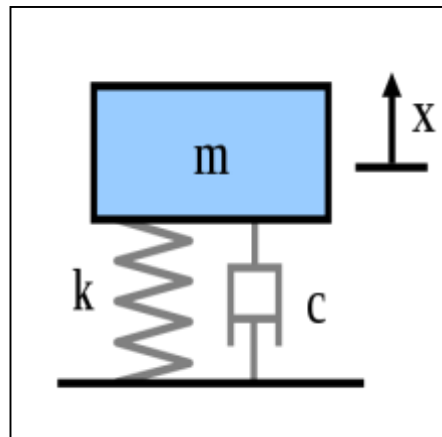

Figure 2: Spring-Mass and damper System

After adding a "viscous" damper to the model, which produces a force proportionate to the mass's velocity. Because it simulates the actions of an item inside a fluid, the damping is termed viscous. The damping coefficient, c, is a proportionality constant with velocity (lbf s/in or N s/m).

METHODOLOGY OF ANALYSIS IN ANSYS

ANSYS is a multipurpose, large-scale finite element programme that may be used to address a number of engineering problems. ANSYS can do static and dynamic structural analyses, steady-state and transient difficulties, mode frequency and buckling eigenalue problems, static or time variable magnetic analyses, and other types of field and coupled field applications. Plasticity, large strain, hyperelasticity, creep, swelling, large deflections, contact, stress, stiffening, temperature dependency, material anisotropy, and radiation are just a few of the non-linearities or secondary effects that may be integrated into the solution using this application. As the programme grew, further sophisticated capabilities such as sub structuring, sub modelling, random vibration, kinetostatics, kinetodynamics, free convection fluid analysis, acoustics, magnetic, piezoelectric, coupled field analysis, and design optimization were included. These capabilities contribute to ANSYS's versatility as an analytical tool for a wide range

Page 2

of engineering specialisations. ANSYS software has been extensively used in the aerospace, automotive, construction, electronics, energy services, manufacturing, nuclear plastics, oil, and steel industries since its launch in 1970. ANSYS is also utilised for analysis, research, and teaching by a huge number of consulting firms and hundreds of institutions.

Figure 3 Flow Chart Shows the Process of Methodology

Design of Vertical Axis Wind Turbine [6]

The design of vertical axis wind turbine is taken from literature and dimensions are given in table 1 below

Table 1: Dimensions of Vertical Axis Wind Turbine

Parameter	Value (cm)
Chord length	12
Height of the blade	40
Length of the shaft	48
Diameter of the shaft	3.2
Diameter of the frame	36
Diameter of support –I	30.5
Diameter of support- II	23.6

The vertical axis wind turbine CAD model was created using PTC's Creo 2.0 software, which is a sketch-based, feature-based, parametric 3d modelling programme with parent-child relationships and bidirectional associativity. Extrude, rotate, sweep, and pattern tools are used to create the CAD model. Initially, the aerofoil is developed in accordance with the NACA 0012 standard. The sketch and extrude tool is used to create the aerofoil. To build wind turbine blades, the aerofoil profile is extruded up to 400mm. As demonstrated in Figure 3, a single blade is patterned to produce many copies in the final assembly file.

To build wind turbine blades, the aerofoil profile is extruded up to 400mm. As demonstrated in Figure 4 a single blade is patterned to produce many copies in the final assembly file.
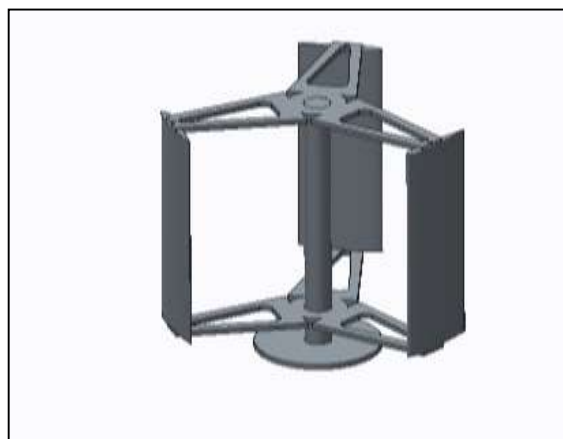

Figure 4: CAD model of vertical axis wind turbine assembly

Table 2 display the material properties of the vertical axis wind turbine used in the study, including structural, physical, and thermal properties.

Table 2: Vertical axis wind turbine material properties

Properties	Aluminium Alloy	Al MMC
Youngs Modulus (MPa)	$7.1 * 10^4$	113000
Density (Kg/m³)	2770	2820
Poisson's ratio	.34	.33

The model is applied with moment load on top geometry after importing and meshing the CAD model. The moment load is 178.02 rpm, 263.89 rpm, 350.81 rpm, 413.64 rpm, 462.86 rpm, and 481.71 rpm, as indicated by literature [9], total deformation, and maximum primary stress are created for each loading condition.
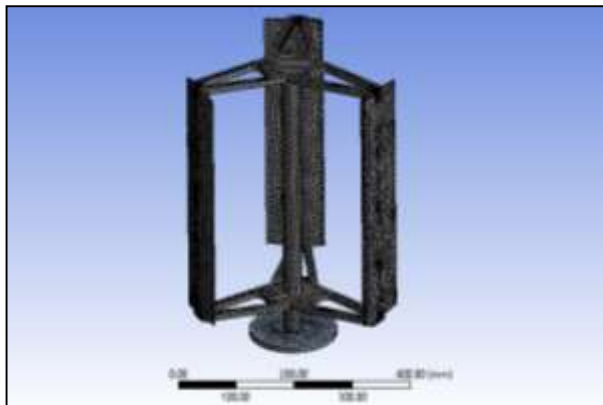

Figure 5: Meshed model of vertical axis wind turbine

During meshing conditions total 80653 nodes created and 45586 elements designed.

Boundary conditions

For the examination of wind turbine blades, two kinds of loading circumstances were considered, one with normal speed and the other with critical speed.
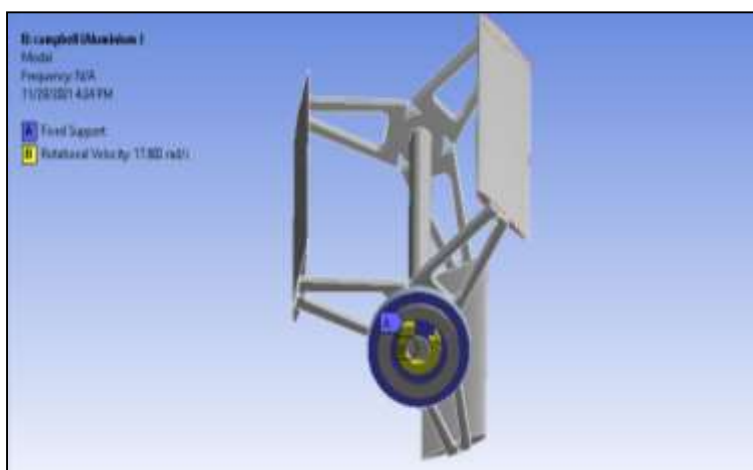

Figure 6: Moment applied on upper geometry

The simulation has now progressed to the solution step, which entails matrix formulations, multiplication, and inversions after the application of loads and boundary conditions. The results are calculated at nodes and the length of each element's edge is interpolated.

RESULT AND DISCUSSION OF ANALYSIS IN ANSYS

ANSYS software is used to calculate mode shapes, mass participation factor, campbell diagram, and 6 fundamental frequencies for a vertical axis wind turbine. This section discusses the results.

Case 1 Normal angular velocity:
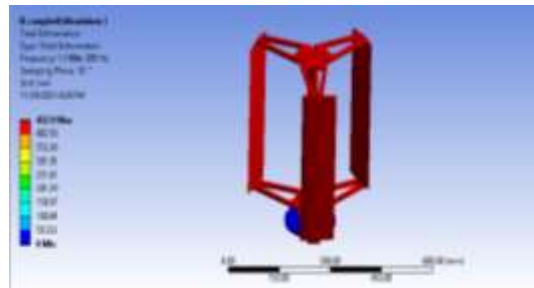
Figure 7:1ˢᵗ mode shape of VAWT
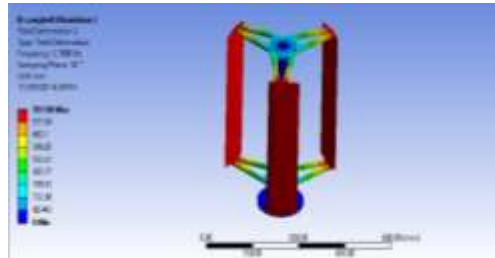
Figure 8: 2ⁿᵈ mode shape of VAWT
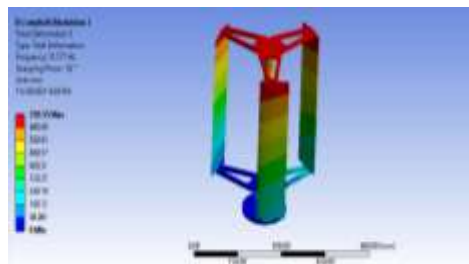
Figure 9: 3ʳᵈ mode of Shape of VAWT
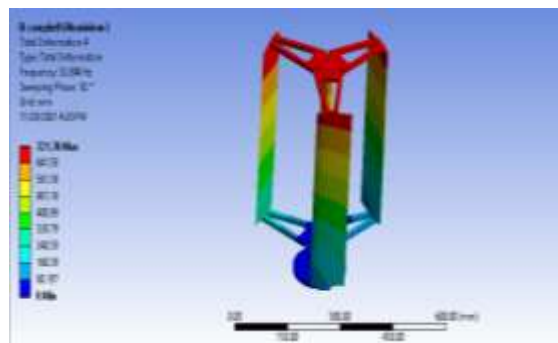
Figure 10: 4ᵗʰ mode shape of VAWT
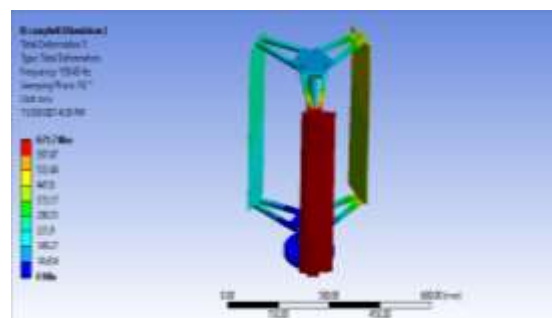
Figure 11: 5ᵗʰ mode Shape of VAWT
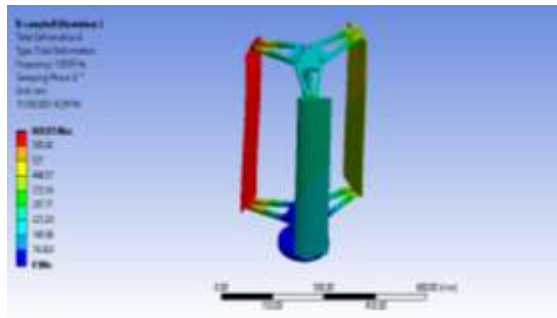
Figure 12: 6th mode shape of VAWT
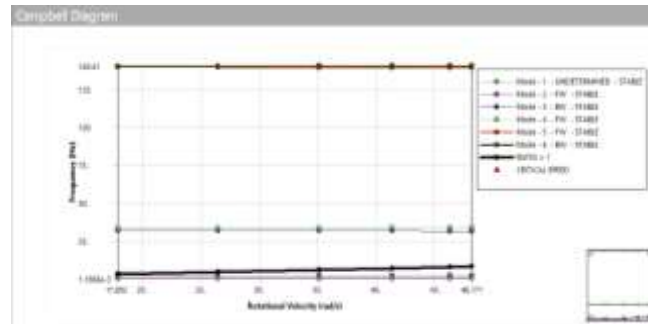
Figure 13: Cambell Diagram of Normal angular Speed

➢ All modes are stable
➢ No critical speeds are observed
➢ 2nd,4th and 5th mode shows forward frequency (clockwise)
➢ 3rd and 6th mode shows backward frequency (anti-clockwise)

Case 2: High Angular Velocity

Points	✔ Rotational Velocity [rad/s]
1	178.02
2	263.89
3	350.81
4	413.64
5	462.86
6	481.71
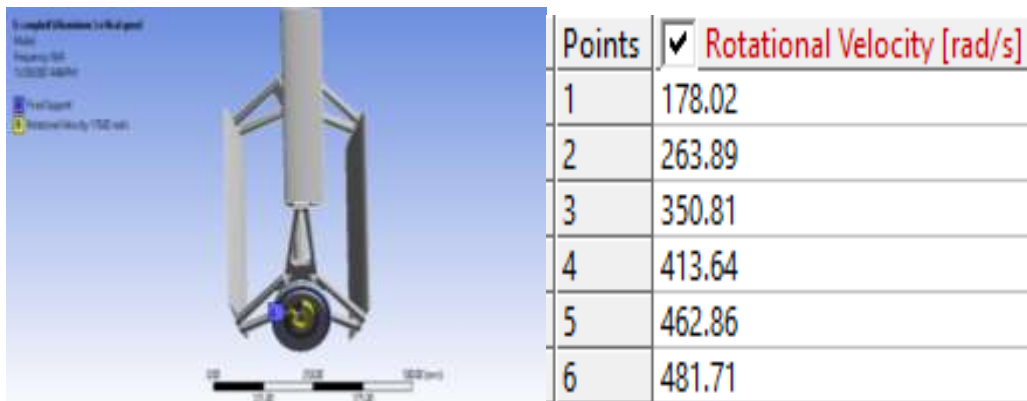
Figure 14: Load and Boundary Condition
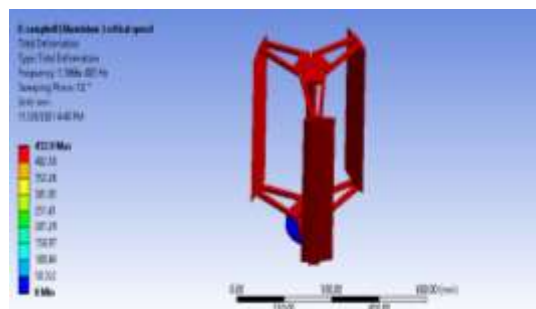
Figure 15: 1st mode Shape
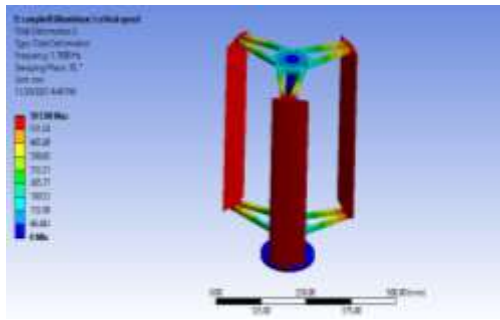
Figure 16: 2nd mode Shape
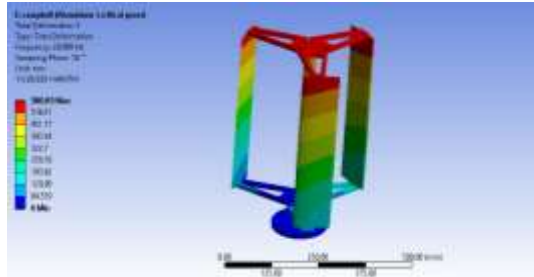
Figure 17: 3rd mode Shape
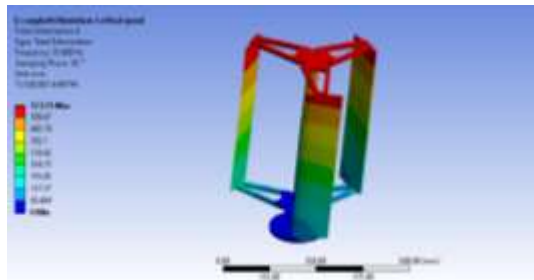
Figure 18: 4th mode Shape
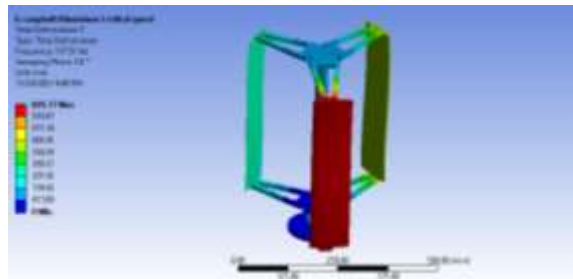
Figure 19: 5th mode Shape
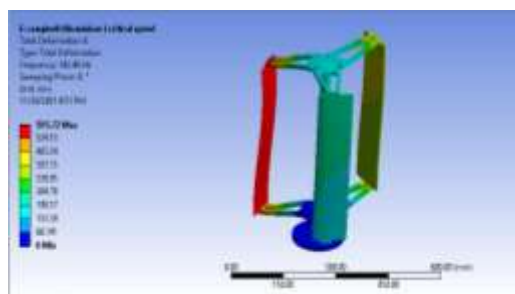
Figure 20: 6th mode shape

In dynamic analysis, two related phenomena, resonance and modal participation, must be investigated. Resonance happens when the excitation frequency of the input load matches one of the structure's intrinsic frequencies. In this circumstance, the load amplifies the mode, resulting in significant displacements. The participation factor reveals how much a certain mode influences the answer. As a result, although the stimulation may match a natural frequency (i.e., a resonance condition), the mode's participation factor is near to zero, implying that little energy will enter the mode and no dynamic response will occur. The mass participation factor for different fundamental frequencies is shown in the tables. The important observations are:

• Because the motion in 1st mode is entirely in the global Z direction, we may anticipate zero EMPF in the X and Y directions and a very big EMPF in the Z direction. In this example, 2.1744 EMPF of the system's mass is involved in the Z direction of this mode form.

• The motion is completely in the global Y direction for the 2nd fundamental frequency, with low EMPF in the X and Z directions and a comparatively big amount for EMPF in the Y direction compared to Z and Z.

• The motion is completely in the global X direction for the third fundamental frequency, with low EMPF in the Y and Z directions and a comparatively big amount for EMPF in the X direction compared to Y and Z.

• The motion for the fourth fundamental frequency is entirely in the global Y direction, with low EMPF in the X and Z directions and a comparatively significant EMPF in the Y direction compared to the X and Z directions.

• The motion is completely in the global X direction for the 5th fundamental frequency, with low EMPF in the Y and Z directions and a comparatively big value for EMPF in the X direction when compared to X and Z.

• The motion is completely in the global Y direction for the 6th fundamental frequency, with low EMPF in the X and Z directions and a comparatively big value for EMPF in the Y direction compared to X and Z.

A Campbell diagram represents the vibration frequencies of a system at various operating RPMs. The campbell diagram for aluminium alloy VAWT [4] is shown in figure 6.11 below. The plot shows description of stability of VAWT at different frequencies and rotational velocities and also enables to determine critical speed.
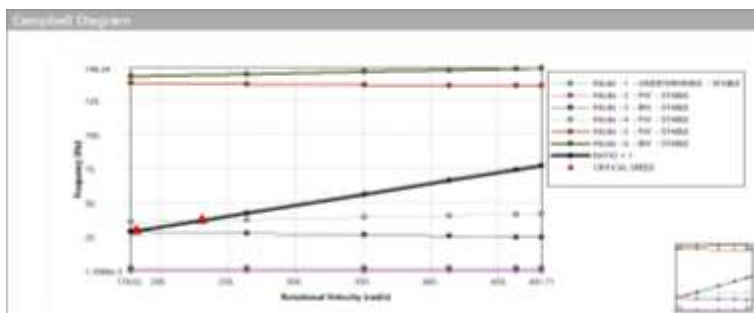

Figure 21: Cambell Diagram for High angular speed

➢ All modes are stable
➢ 2 critical speeds are observed. 1st critical speed is nearly 181.81 rad/s and 2nd critical speed is nearly 230.71 rad/s.
➢ 2nd,4th and 5th mode shows forward frequency (clockwise)
➢ 3rd and 6th mode shows backward frequency (anti-clockwise)

The variation in natural frequency of VAWT is very slightly as shown in in above figure and table below. The whirl direction is shown in 1st column of table 3 below.

Table 3: Vibration frequencies at High Angular Velocity for Aluminium Alloy Material

Mode	Whirl Direction	Mode Stability	Critical Speed	178.02 rad/s
1	Undetermined	Stable	None	1.1866e-003 Hz
2	FW	Stable	None	1.7808
3	BW	Stable	181.81 rad/s	28.999
4	FW	Stable	230.71 rad/s	35.689
5	FW	Stable	NONE	137.51
6	BW	Stable	NONE	142.46

Table 4: Vibration frequencies at Normal Angular Velocity for Aluminium Alloy Material

Mode	Whirl Direction	Mode Stability	Critical Speed	17.802 rad/s
1	Undetermined	Stable	None	1.1866e-003 Hz
2	FW	Stable	None	1.7808 Hz
3	BW	Stable	None	31.577 Hz
4	FW	Stable	None	32.894 Hz
5	FW	Stable	None	139.45 Hz
6	BW	Stable	None	139.97 Hz

Table 5: Vibration frequencies at High Angular Velocity for MMC Material

Mode	Whirl Direction	Mode Stability	Critical Speed	17.802 rad/s
1	Undetermined	Stable	None	1.0276e-003 Hz
2	FW	Stable	None	2.1687 Hz
3	BW	Stable	None	38.182 Hz
4	FW	Stable	None	39.848 Hz
5	FW	Stable	None	174.37 Hz
6	BW	Stable	None	174.9 Hz

CONCLUSION AND FUTURE SCOPE

ANSYS software is used to calculate mode shapes, mass participation factor, campbell diagram, and 6 fundamental frequencies for a vertical axis wind turbine. Under both free and forced vibration conditions, the VAWT is subjected to FEA vibration analysis. The free vibration analysis yields the mode shapes, natural frequencies, and Campbell diagram, which provide crucial information on VAWT vibration qualities. When compared to Aluminium alloy material with higher natural frequencies, the FEA findings showed that there were no critical velocities throughout the operating range for critical speeds of 178.02 rpm, 263.89 rpm, 350.81 rpm, 413.64 rpm, 462.86 rpm, and 481.71 rpm and normal speed 17.80 rpm, 26.38 rpm, 35.08 rpm, 41.36 rpm, 46.28.

REFERENCES

[1] AmericanWind Energy Association (AWEA). Wind Powers America Annual Report; AmericanWind Energy Association (AWEA):Washington, DC, USA, 2019.

[2] Wilburn, D.R. Wind Energy in the United States and Materials Required for the Land-Based Wind Turbine Industry from 2010 through 2030; US Department of the Interior: US Geological Survey: Washington, DC, USA, 2011.

[3] Bianchini, A.; Balduzzi, F.; Di Rosa, D.; Ferrara, G. On the use of Gurney Flaps for the aerodynamic performance augmentation of Darrieus wind turbines. Energy Convers. Manag. 2019, 184, 402–415.

[4] Han, H.; Liu, L.; Cao, D. Dynamic modeling for rotating composite Timoshenko beam and analysis on its bending-torsion coupled vibration. Appl. Math. Modell. 2020, 78, 773–791.

[5] Minhui Tong, Weidong Zhu, Xiang Zhao, MeilinYu ,Kan Liu and Gang Li, Free and Forced Vibration Analysis of H-type and Hybrid Vertical-Axis Wind Turbines Energies 2020, 13, 6747; doi:10.3390/en13246747

[6] S. Brusca • R. Lanzafame • M. Messina Design of a vertical-axis wind turbine: how the aspect ratio affects the turbine's performance Int J Energy Environ Eng (2014) 5:333–340 DOI 10.1007/s40095-014-0129-x

[7] Theory pf Vibration Mechanical Engineering series. Springer, Cham. https://doi.org/10.1007/978-3-319-94271-1_3.

[8] Rumin R, Bergander M, CieslikJ, KulpaM. Extended active vibration control for wind turbines. 2017 XIIIthintconfperspecttechnolmethodsMEMSdes2017.p. 38 40. https://doi.org/10.1109/MEMSTECH.2017.7937528.

[9] C. Chang, Damage detection of cracked thick rotating blades by a spatial wavelet based approach, Applied Acoustics, vol. 65, Nov. 2004, pp. 1095-11.11.` https://doi.org/10.1002/tal.421.

[10] Kalakanda Alfred Sunnya, "Vertical axis wind turbine: Aerodynamic modelling and its testing in wind tunnel" Procedia Computer Science 93 (2016) 1017 – 1023

TuEngr Group

Secure IoT Architecture in Mobile Ad-hoc Network Against Malicious Attacks Using Blockchain-based BATMAN

Neha Khandelwal[1*], Shashikant Gupta[1]

[1]*Department of Computer Science Engineering, ITM University, Gwalior, INDIA.*
Corresponding Author (Email: neha19khandelwal8@gmail.com).

Abstract

It is possible to build a decentralised wireless network using Internet of Things (IoT) sensors and other IoT-based devices. Wireless connections allow all network nodes to be moved around at will. They can connect and construct a network without current network infrastructure. Using blockchain technology in a wireless ad-hoc context, an IoT-based MANET is a fresh research topic. The key challenge for ad-hoc blockchain applications is to cope with the high computational cost of block validation while keeping blockchain features and incorporating nodes. This article presents a blockchain-based mobile network as a potential application of the ensemble approach, which has been covered in other articles. The suggested technique for MANETS routing uses the Byzantine Fault Tolerance (BFT) protocol. It is possible to integrate Blockchain into an IoT-based MANET (BATMAN) using advanced mobile ad-hoc networking (MANET) (BATMAN). Extended-BATMAN (E-BATMAN) is a method of integrating blockchain technology into the BATMAN protocol using IoT-based MANETs. Blockchain is a safe, distributed, and trustworthy platform, with each node performing its security procedures. Four characteristics are used to evaluate the proposed ensemble method: pdr, average e2e latency, network throughput, and algorithm vitality use. All of these components outperform the existing traditional techniques using the recommended ensemble approach.

Disciplinary: Information Technology.

Cite This Article:

Khandelwal, N., Gupta, S. (2022). Secure IoT Architecture in Mobile Ad-hoc Network Against Malicious Attacks Using Blockchain-based BATMAN.*International Transaction Journal of Engineering, Management, & Applied Sciences & Technologies, 13*(6), 13A6R, 1-15. http://TUENGR.COM/V13/13A6R.pdf DOI: 10.14456/ITJEMAST.2022.123

IQAC COORDINATOR
SWAMI VIVEKANAND
COLLEGE OF ENGINEERING
KHANDWA ROAD, INDORE

PRINCIPAL
SWAMI VIVEKANAND
COLLEGE OF ENGINEERING
KHANDWA ROAD, INDORE

1 Introduction

Blockchain technology, first announced by Satoshi Nakamoto in 2008, is still used today (Nakamoto, 2019). Network segmentation happens when two separate chains split apart. Because two chains cannot coexist, one of the links is routinely removed. Data loss may be the root of the problem. Thoughts on the long-term value of a new kind of Blockchain with high network distribution capabilities (Cordova et al., 2020). On-demand distance vector routing (AODV) (Perkins et al., 2003) and BATMAN (Clausen et al., 2003) are three innovative MANET protocols designed to overcome this issue (Sanchez-Iborra et al., 2014). Varaprasad The nodes determine the optimum forward route and push packets appropriately.

According to Laube et al. (2019), a DAG-based architecture may handle the partitioning problem in a MANET with mobile nodes. When the network topology changes, the partition problem arises. The BATMAN routing protocol, presently being developed by the German "Freifunk" community, enabled this. It will be replaced by the more efficient OLSR (Kulla et al., 2012a). The lack of trustworthiness of blockchains has only recently been realized as a mechanism to produce the demand for collaborative components in diverse frameworks, on the current situation of agreements with blockchain-enabled in-process sending motivations for multi-hop (Machado and Westphall, 2021).
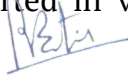
Many researchers have been working on developing a secure network communication system. (Omar et al., 2012) devised an authentication technique that verifies connections are safe before any network communication can occur. Because MANETs are continually changing, a hostile actor may get the private key even if no unauthorized outsiders are present (Eschenauer et al., 2002). Yang et al. A protocol based on the system's ability to withstand Byzantine Generals faults (BFT) was designed to conduct blockchain operations (Kotla and Dahlin, 2004). A few nodes fail or behave maliciously, but the BFT system continues to operate (Aublin et al., 2013). We use DCFM (L, 2020a; S., 2015) to identify hostile intruders from trustworthy nodes. Lwin and coworkers (Lwin et al., 2020a) call it one of the most efficient systems recently suggested (2020a). The suggested system assessment mechanism, based on blockchain technology, can satisfy MANET goals.

When it comes to our work, we divide it into four separate phases that we call our framework: When the Trust value is determined, the second stage, delegated BFT, is used to pick the speaker, and the third stage uses delegated BFT based on the Extended-BATMAN protocol for transaction claims/node validation and block construction, and the fourth stage does maintenance.

2 Literature Review

This part describes several ways the suggested algorithm may be supported in various circumstances.

IQAC COORDINATOR
SWAMI VIVEKANAND
COLLEGE OF ENGINEERING
KHANDWA ROAD, INDORE

PRINCIPAL
SWAMI VIVEKANAND
COLLEGE OF ENGINEERING
KHANDWA ROAD, INDORE

2.1 BATMAN: A Brief Overview

Please remember that the Batman protocol decentralizes route information, which means that routing tables are not available to the whole network through the Batman protocol (Sliwa and colleagues, 2019). It is decided which single-hop neighbours will be assigned to each node in the mesh to offer the best feasible gateway for communication with the destination node. The result is developing an efficient and very fast routing system that allows for establishing a collective intelligence network while using little CPU and, therefore, requiring less energy consumption on the side of each node (Johnson et al., 2008).

This strategy has piqued the scientific community's curiosity. As a result, a lot of effort is done to evaluate routing efficiency under various scenarios. For example, Kulla et al. (2012)b analyze their system's performance in multiple settings and node situations (Kulla et al., 2011, 2010).

2.2 BATMAN's Attack Mitigation Scheme

As an example of a normal project, we have taken the concepts from this project and incorporated them into the recommended project. It is necessary first to discuss NIAs (Node Isolation Attacks), which are attacks that are specially addressed by denial contradictions with fake node mechanism, before moving on to the topic of denial contradictions with fake node mechanism itself. It was Kannhavong et al. who first reported about NIAs, which are a kind of denial-of-service attack on the OLSR (2006).

2.3 Trust Management in MANET via the Use of Blockchain

A blockchain is a chain of records linked together. In addition to the date, each Block contains a hash reference to the previous Block. Each successive Block binds itself to the previous Block's hash by connecting to it, and the Blockchain is established as a result of this linking. When it comes to data manipulation, blockchain architecture has shown to be quite durable.

The development of blockchain-based applications has accelerated significantly in recent years. These applications are being used in various fields, including concurrent IoTOS (IoT), economic facilities, standing schemes, and others. Mining produces a block, which requires a substantial amount of computer power and is also a probabilistic endeavour. While block mining is challenging, determining whether or not a block is valid is not tricky (Dennis and Owen, 2015). A distributed reputation model based on Blockchain technology was created by Peiris and colleagues (2020) to ensure trust, and it is now being tested. B4SDC is a blockchain-based approach for gathering security-related data in MANETs developed by several academics, including Liu et al. (2020) and other researchers.
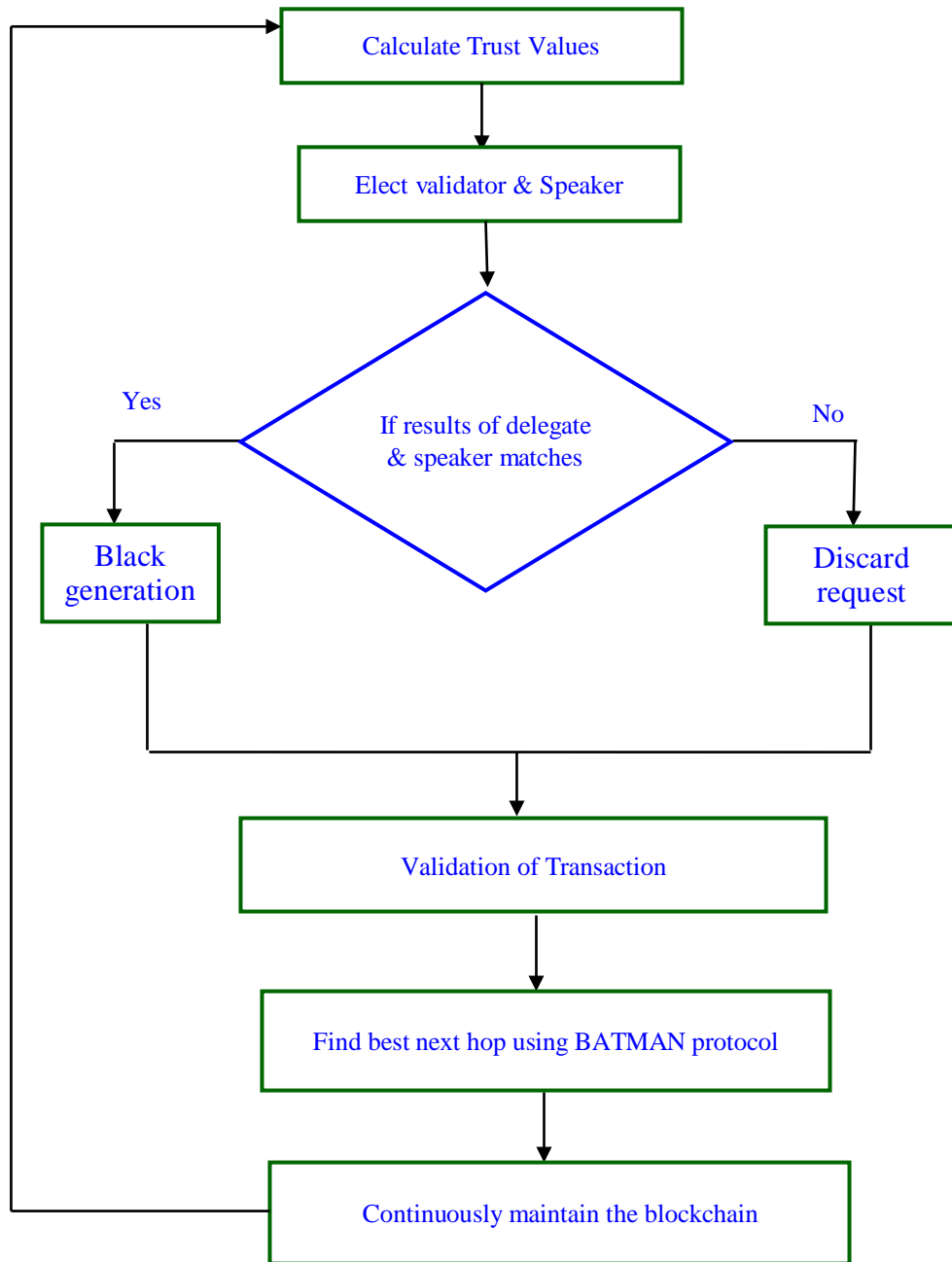
Figure 1: The suggested architecture's workflow diagram.

3 Method

We propose a distributed trust installation system based on blockchains throughout this article. We chose a blockchain-based architecture to handle trust in the IoT-based MANET ecosystem to accomplish so. Its high resource usage and extended validity time make it unsuitable for use in dynamic and latency-sensitive situations. The suggested system has multiple components, as shown in Figure 1.

IQAC COORDINATOR
SWAMI VIVEKANAND
COLLEGE OF ENGINEERING
KHANDWA ROAD, INDORE

PRINCIPAL
SWAMI VIVEKANAND
COLLEGE OF ENGINEERING
KHANDWA ROAD, INDORE
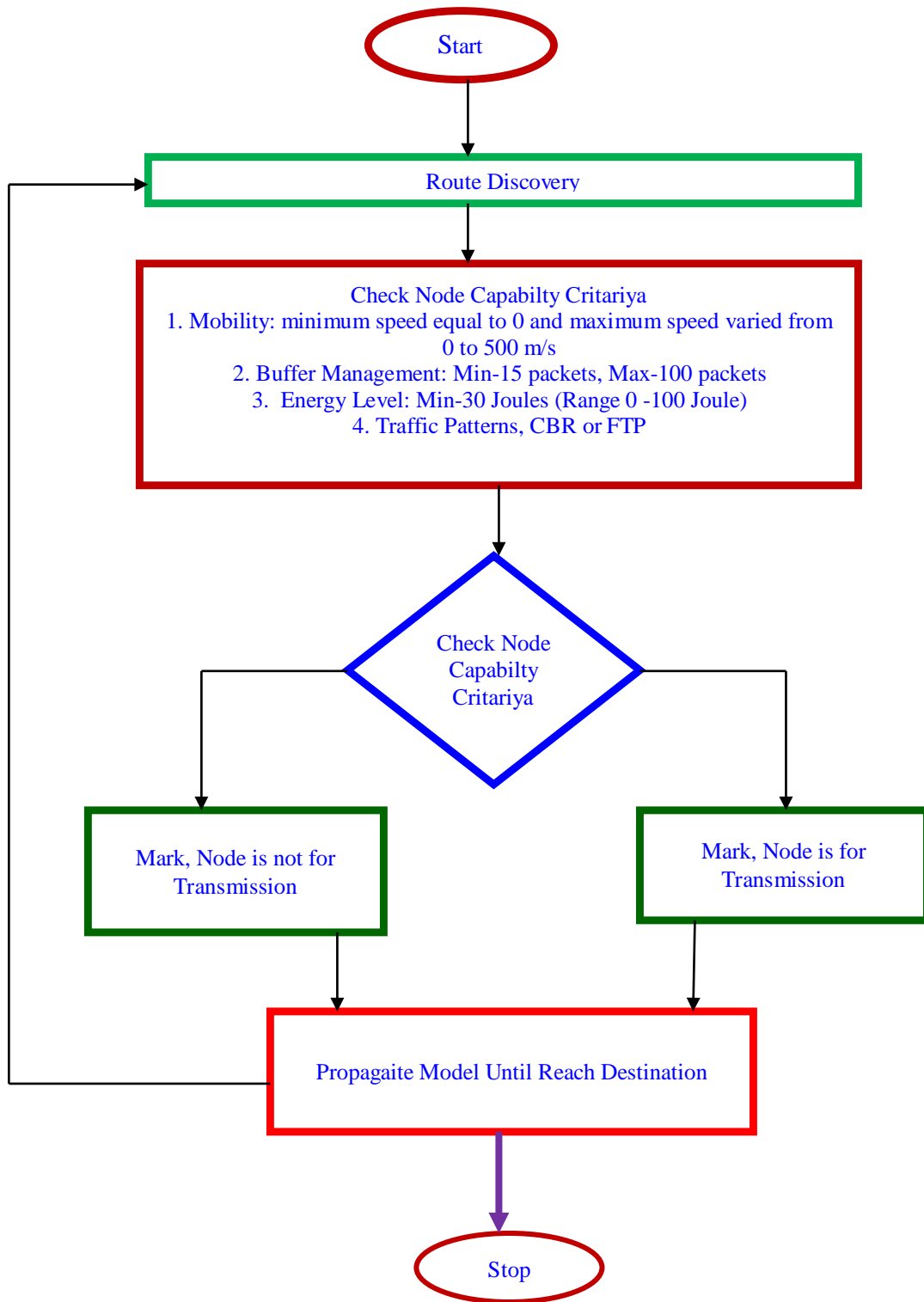
Figure 2: The Flow for computing the Trust Value.

3.1 Step 1: Calculation of the Threshold Value

This investigation was conducted to determine whether a distributed trust mechanism might be developed to improve the stability and scalability of networks. Rather than concentrating on the computation of trust value, we focus on creating the trusted network instead. The presence of an adversary near a node results in information about the attacking node being propagated across the network, reducing the possibility of that same attacker striking again. Our proposed system uses several different discovery and belief models; however, we chose denial contradictions with a fake

node mechanism (Schweitzer and colleagues, 2015) as an example of a typical scheme suited for the solution presented in this research.

An enemy node is identified in the network, and information about it is broadcast across the web for it to be removed from the network. This is made possible by the use of blockchain technology. Figure 2 illustrates the process of determining how to determine Trust Value.

As the AIMD system (Marti et al., 2000) regulates each node's Trust Value (TV), it provides clear and fair incentives and punishments for residential nodes and MANET enemies. Because of the moniker "addition and multiplication," the TVs of the node are added and multiplied together, with addition and multiplication factors () and () being used in the equations for addition and multiplication, respectively, to accomplish this. The denial contradicts the fake node mechanism detection technique using a heuristic approach to detection. To compute a network penalty, multiply the TV of the attacker node by the -1 number, which is the harshest network penalty that may be applied. As a result, negative TV node information is propagated throughout the network.

Since each resident owns the information, they may exclude particular nodes from the connection check. A trust rating of -1 signifies that the node cannot join the network. In equation 2, selfish nodes are represented by a different value. On the other hand, a functional node will contribute to the growth of the TV by increasing its value. To guarantee that the trust level decision is fair, a high TV of MPR nodes should be maintained.

As a consequence, it should be maintained at all times. Consequently, following equation 3, the value is altered. The MPR node's default value is 0.7. In the near term, it will be based on honest nodes that are not MPRs, and in the long run, it will be based on MPRs. Every node starts with a zero value but may gain the maximum trust value of "1" throughout the game. Each node has a TV value of zero when the network is created. In Equation 3, the numerator, i.e., $\sum_{k=1}^{n-1} m_{i}j^{k} m_{i}j^{k} + 1$ I pick j as its MPR node to relay packets for k iterations from when j connects to I to when I calculate j^s TV.

$$TV = \begin{cases} TV * \beta & if\ nodes\ misbehabes \\ TV + \alpha, & otherwise \end{cases} \tag{1}$$

$$\beta = \begin{cases} -1 & if\ nodes\ is\ attack \\ 0.7, & otherwise \end{cases} \tag{2}$$

$$\alpha = \begin{cases} \max\left[\dfrac{\sum_{k=1}^{n-1} M_{ij}^k}{\sum_{k=1}^{n-1} M_{ij+1}^k},\ 0.5\right] & if\ node\ is\ MPR \\ 0.5, & otherwise \end{cases} \tag{3}$$

$MPR \rightarrow$ multipoint relay selector set.

Algorithm 1. Trust Value Computation

1. Begin()
2. {
3. Routs discovery initialize, current position initialize

4. Motion = 0 <motion< 500m/s
5. Buffer_Queuemanaging = 15 < Buffer_Queue< 100
6. Vitalitynear = 0 <vitality< 100
7. Traffic flowoutline = CBR or FTP
8.   }
9. If(Node ability == yes)
10. {
11. Mark node for transmission
12. }
13. Else
14. {
15. Leave the node
16. }
17. While(current position == destination0
18. {
19. Repeat (3 to 16)
20. }

A collaborative approach to our security solutions is also being implemented to boost total system efficiency via collaboration. Even though MANETs (Hernandez Orallo et al., 2014) were previously classified as cooperative networks, early nodes undertake distinct detection processes for most security modes. This is illustrated in Figure 1 and is contrary to previous assumptions about cooperative networks. In denial of contradictions with the fake node mechanism, the search is performed after each Hello interval. However, since our strategy reduces the investigation duration in proportion to the number of neighbours around the node, the synergistic impacts of near surrounding nodes may aid in lengthening the inquiry interval in some circumstances, as shown in Figure 1. Rather than evaluating nodes individually, nodes that meet the following criteria may be examined collectively, as shown in the accompanying picture (Lwin et al., 2020a).

The first method, referred to as Algorithm 1, specifies the procedures that must be followed to calculate the trust value (TV). Line 1 has been finished with completing the route finding process and identifying the present location. On-Line 2, there is a check for node capability performed. Then, as noted in Line 5, you may either select the node for transmission or leave the node undesignated for the message. This is followed by a comparison of the current location and target position. If the current location matches the target position, the procedure is repeated from step 1 through step 5 until the target position is reached.

3.2 Step 2: Algorithm of dBFT

It is necessary to determine the trust values before proceeding with the construction of the proposed model. In the case of the nodes, this is true. The model is generated when the trust values of the nodes have been computed. The selection algorithm chooses a validator node from among the candidates. After that the Delegated Byzantine Fault Tolerance (dBFT) system selects a speaker from among the available candidates. The node that survives acts as a delegate for the remainder of

the network's operations. Following that speaker's presentation, delegates are handed a proposal once the claims have been validated and hashes have been created. Algorithm 2 shows the dBFT steps.

Procedure 2: Delegated_Byzantive_fault_tolerance

TV- Array of belief number of hig_hours

Begin()

{

V = max(TV)

Bully election(V);

Return coordination validator

}

V→ Arrays of nodes eligible to become a validator

A popular vote selects the Validator. These are the nodes qualified to serve as validators in the network, and they are those with the highest TVs. The bully election approach (Hernandez-Orallo et al., 2014) determines which node is the block creator node among a set of similar nodes.

The permission of a nearby node is required for a trustworthy election, unlike a bully election. Neighbours with TVs over the threshold will send claim messages to each other. I j, TV-Claim, one-hop-count) prKeyi j's beliefworth and single-hop neighbour total are placed into single-hop-counter, correspondingly. The claim message is signed using I prKeyi's private and i's public keys. Also, any node with TVs over the threshold may broadcast a claim message to the whole network by piggybacking on a transmission control message (TCM). The Validator is the letter j if all of the following conditions are satisfied. This node has the highest TV and no false allegations against it. No fraudulent claims were made against nodes I and j. Unable to pick between dual or additional nodes with a similar belief value, a claim message has an extra one-hop count. In this case, the Validator is the node with the most one-hop counts. By broadcasting a claim message for node j, node I save energy. The most frequent voter should be rewarded since MANET is resource-intensive.

It's a process. A decision method is used to choose specific nodes from the list of accessible nodes to function as validation nodes. Assigning a speaker node and all other functions to representations simplifies the procedure. Inquiry representatives get hashed values for each outstanding accusation from the speaker. Next, a novel chunk of privileges or communications is supplementary if the comparison between the speaker and the representative is more than 68.9%—algorithm three delegated authority.

Algorithm 3: Delegation Process

1. Begin()

2. {
3. CN = Validators   // CN contains array of validators
4. Choicepresenter S from CN, and cogitate all remains as representatives D.
5. S is answerable for buildingnovelchunk from to comeprerogatives.
6. S confirm and analyze hash
7. D validate(outcomes of S)
8. D portion&relate (results of S)
9. IF (sk_P ≥ 68.9%)

   {

   Chunksupplementary

   }

   Else

   {

   Rejectinvitation

   }

10. }
11. End()

3.3 Step 3: Block Authentication and Block Creation

It's a process. A decision method is used to choose certain nodes from the list of accessible nodes to function as validation nodes. Assigning a speaker node and all other functions to representations simplifies the procedure. Inquiry representatives get hashed values for each outstanding accusation from the speaker. Next, a novelchunk of prerogatives or communications is additional if the comparison between the speaker and the representative is more than 68.9 percent—algorithm 3 delegated authority.

3.4 BATMAN Extended Version (EBATMAN)

It is possible to summarise the BATMAN protocol in the following way in a simplified form: The initial message, also known as the OGM, is sent to the whole network by each node to alert its neighbours that it has been discovered and is functioning properly. The IP and UDP overhead associated with the transmission is typically 52 bytes. To begin with, the OGM has the following data: the sender's address, the node that delivered the packet, the time between packets (TTL), and the sequence number.

The network selectively floods the overlay mesh network (OGM), notifying receiving nodes of other nodes' existence and letting them connect with them. The fact that an X node obtains its OGM from another node implies a Y node. It occurs when one of node Y's one-hop neighbours requests OGM from the other node. Node X receives messages quicker and more reliably with several single-hop neighbours. This improves throughput and reliability. The neighbour must transfer data via the network to connect with the distant node. Determining this neighbour as the optimal next hop for the message sender at that moment, the protocol configures its routing table

to use this neighbour. As seen in Process 4, the various stages of The Improved Method to IoT based MANET protocol are described.

Algorithm 4: The Better Approach to Mobile Ad-hoc Networking Routing Protocol Algo:

Begin()

{

1. Respectively node Brodcost O_G_Ms to her neighbours
2. Neighbours re-Broadcast O_G_M'S to prove their existence

   O_G_M's areoringator msg's of size 52 byte.

   Counting IP SUDP over_head

3. If(node_neighbour > 1)
4. {
5. Best nop node= current node;
6. }
7. Else {
8. Repeated (1,3)
9. }
10. }
11. End()

Blocks are organized in a certain way. The block structure must also contain information about how the representative node configures the Block. A block of transactions recorded in a blockchain system binds the network together. Because the hash value is produced directly from the transaction data, it must provide a hash value using the SHA-256 technique in the Block. As a consequence of this, instability is brought into the blockchain ecosystem.

3.5 Maintenance on the Block

Full and lite nodes are the two kinds of nodes in a blockchain ecosystem. Both maintain the whole Blockchain, but the latter relies significantly on the information provided by the entire node community to work successfully. This is due to the nature of MANETs. A new node is allowed admittance to the network's blockchain information.

First, a lightweight nodule is deployed to the system, able only to download data from the blocker's header. This is the first step. Although a new node enters the network as a light node, it may quickly create transactions for attacker detection/TV calculation. Until a full node becomes available, the mass node actions as a temporary complete node for the communicate chunk headers.

4 Result and Discussion

The investigational findings acquired via the suggested technique are described in this segment. Experiment 1: Results Network performance is measured by characteristics including pdr,

average e2e latency, setup throughput, and vitality use. This outcome subdivision contains 105 moveable nodes connected to the network for 105 mobile nodes.

4.1 NS2 Simulation Constraints

This evaluation of the planned method and the current algorithm is shown next. The simulation parameters are presented in Table 1.

Table 1:- Simulation Constraints

Parameters	Specification	Parameters	Specification
Network Simulator	NS-2, Version 2.35	PHY/MAC Protocol	IEEE 802.11
Network Size	1km x 1km	Propagation Model	Two-ray ground
Connection Protocol	UDP/TCP	Mobility Model	Random Way Point
Traffic type	Constant Bit Rate (CBR)/FTP	Channel Type	Wireless Channel
Source/Destination	Random	Antenna Model	Test-parabolic
Data packet size	256 bytes	Simulation time	200 Second
Data packet size	256 bytes, 512 bytes, and 1024 bytes	Language	Tcl,oTcl,C++, AWK Scripting
Simulation Protocol	BATMAN, E-BATMAN	No. of Malicious Node	5% out of the scenario
Simulation Scenario (No. of Mobile Nodes)	25,50,75,100,125	Channel Type	Wifiphy Standard

4.2 Performance Calculation

Throughput: The throughput (TP) of a network equals the total of the data sent to the based station divided by the time it takes to simulate the network.

Average end-to-end delay: The average end-to-end delay (AED) is the total time it takes for all data chunks to transit from the source nodes to the base station.

The term "end-to-end delay" refers to the time it takes a packet to transit from its point of origin to its point of destination.

Packet delivery ratio: The PDR is the fraction of informations packets transferred to packets received at a certain time (Taha et al., 2017).

4.3 Outcomes

The Extended-BATMAN algorithm is compared to the present BATMAN protocol. This study's average throughput and E-BATMAN approach are shown in Figure 3. Figure 3 explain throughput, units of throughput are kbps. We have to compare three scenarios on different numbers of nodes. Scenarios like BATMAN _MANET Normal Scenario, BATMAN_MANET Under Attackers, BATMAN_MANET [Lwin MT [2020b]] with Attackers, Proposed _BBATMAN_MANET with Attackers. Nodes like 25, 50,75,100,125 are compared to all these scenarios. In normal scenarios maximum of 1024 kbps and a minimum of 942 kbps of throughput. In Under Attackers scenarios maximum of 226 kbps and a minimum of 215 kbps of throughput. In [Lwin MT [2020b]] with Attackers scenarios maximum of 1032 kbps and a minimum of 978 kbps of throughput. In Proposed

_BBATMAN_MANET with Attackers scenarios maximum of 1245 kbps and a minimum of 1235 kbps of throughput.
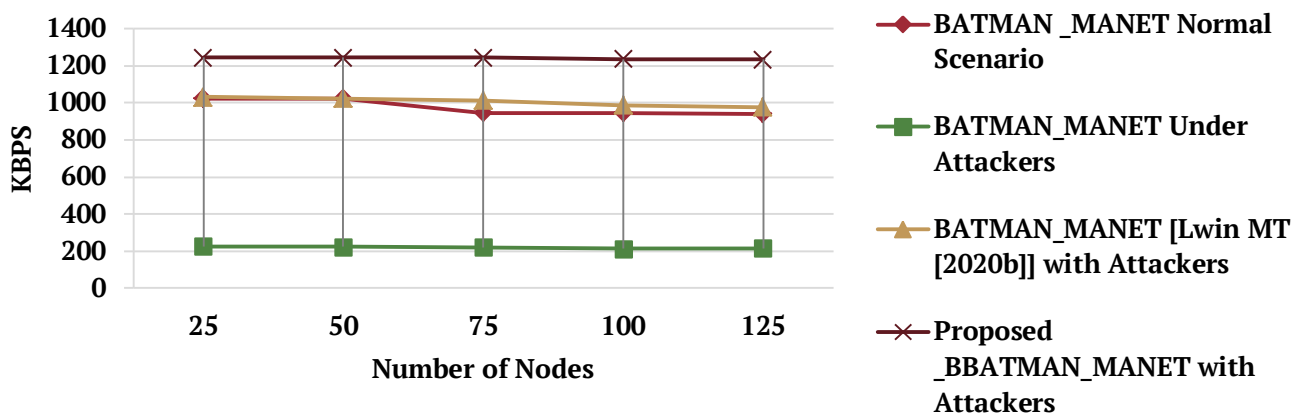
Figure 3: Average throughput (kbps) under attack
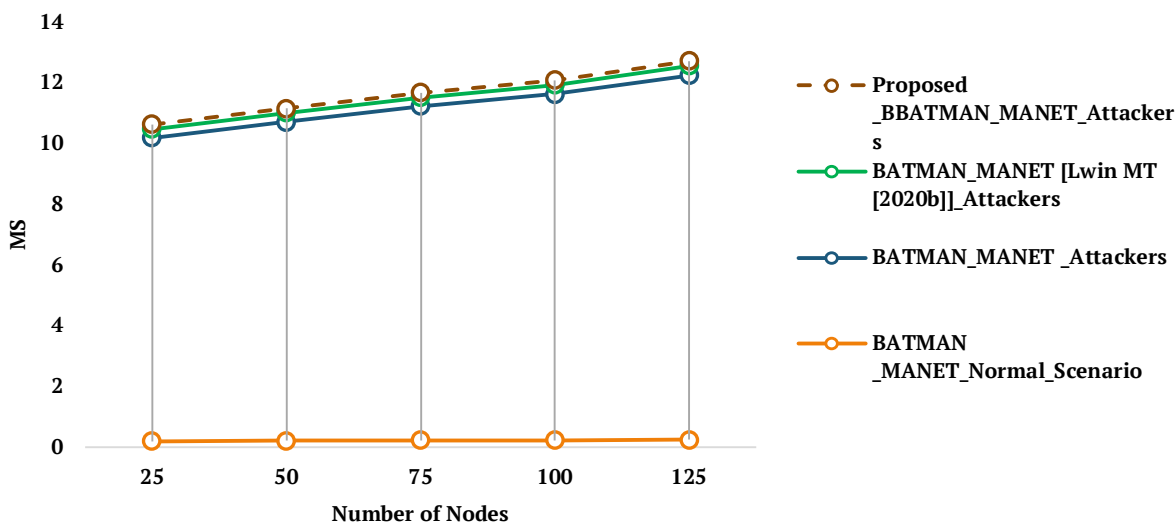
Figure 4: Average e2e-delay test results.

Figure 4 explains e2e-delay, units of end-to-end delay are milliseconds. We have to compare three scenarios on different numbers of nodes. Scenarios like BATMAN _MANET Normal Scenario, BATMAN_MANET Under Attackers, BATMAN_MANET [Lwin MT [2020b]] with Attackers, Proposed _BBATMAN_MANET with Attackers. Nodes like 25, 50, and 75,100,125 are compared to all these scenarios. In normal scenarios maximum of 0.26 ms and a minimum of 0.21ms of e2e delay. In Under Attackers scenarios maximum of 12ms and a minimum of 10ms of e2e delay. In [Lwin MT [2020b]] with Attackers scenarios maximum 0.31ms and minimum 0.28ms of e2e delay. In Proposed _BBATMAN_MANET with Attackers scenarios maximum of 0.17 ms and a minimum of 0.15 ms of e2e delay.
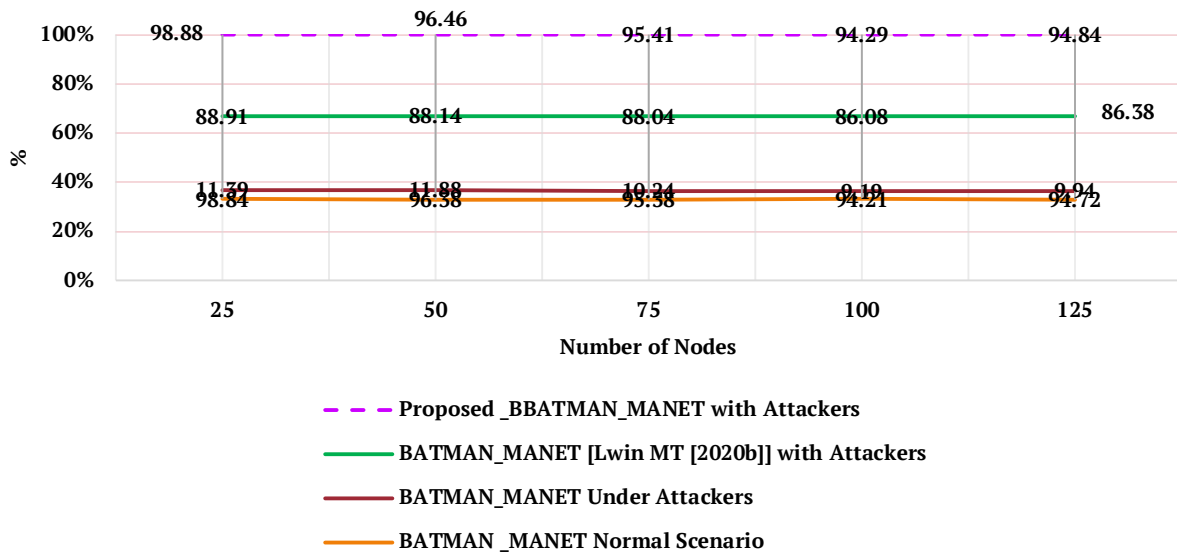
Figure 5: Average Packet Delivery Ratio under Attack.

Figure 5 explain about Packet Delivery Ratio (PDR), units of PDR are percent (%). We have to compare three scenarios on different numbers of nodes. Scenarios like BATMAN _MANET Normal Scenario, BATMAN_MANET under Attackers, BATMAN_MANET [Lwin MT [2020b]] with Attackers, Proposed _BBATMAN_MANET with Attackers. Nodes like 25, 50, 75, 100, and 125 are compared to all these scenarios. In normal scenarios maximum of 98.84 % and a minimum of 94.72 % of the Packet Delivery Ratio. In Under Attackers scenarios maximum of 11.39 % and a minimum of 9.94 % of Packet Delivery Ratio. In [Lwin MT [2020b]] with Attackers scenarios maximum of 88.91 % and a minimum of 86.38 % of Packet Delivery Ratio. In Proposed _BBATMAN_MANET with Attackers scenarios maximum of 98.88 % and a minimum of 94.84 % of Packet Delivery Ratio.
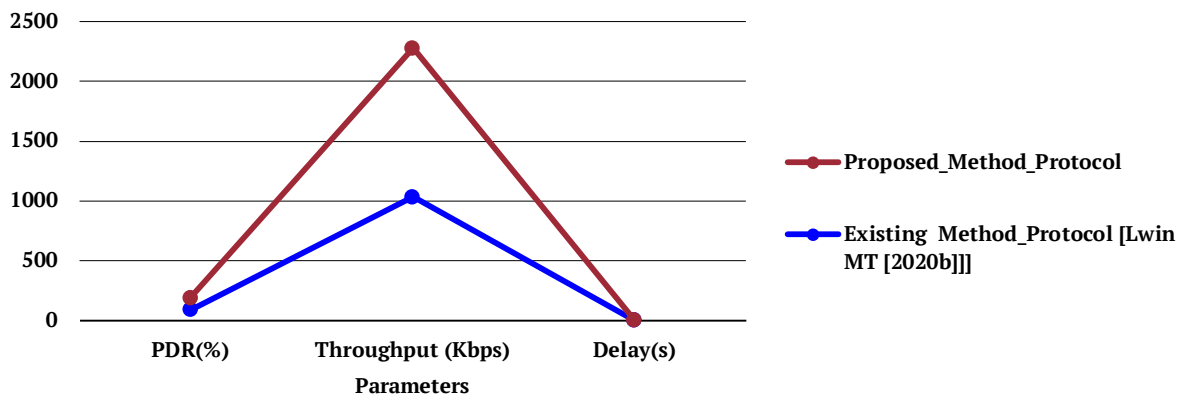
Figure 6: An evaluation of the proposed E-BATMAN protocol compared to the current BATMAN protocol using evaluation parameters (Lwin et al., 2020b).

Figure 6 shows the results of comparing parameters such pdr (%), latency (s) and throughput (kbps). The suggested method outperforms earlier work (Lwin et al., 2020b) on all criteria.

5 Conclusion

This research suggested a unique technique for generating distributed trust value in MANETs, which is described in detail below. The blockchain idea was applied in the Better Approach to Mobile Ad-hoc Networking protocol, dubbed Extended the Improved Method to

Mobile Ad-hoc Networking (Enhance-BATMAN). The model outcomes indicated that a distributed trust value gives high network safety. Using the proposed E-BATMAN protocol ensures no data is lost even if the attacker moves and attacks other network nodes, lowering overall complexity. The network is safe. Aside from that, respectively node's role is summary. Our MANET-based blockchain-based proposed system is also consistent and accessible. We want to examine our suggested solution in MANETs with various routing protocols in the future.

6 Availability of Data and Material

All information is included in this study.

7 References

Aublin PL, Mokhtar SB, Que'ma V.Rbft: Redundant byzantine fault tolerance. In 2013 IEEE 33rd International Conference on Distributed Computing Systems. 2013: 297-306.

Clausen T, Jacquet P, Adjih C, Laouiti A, Minet P, Muhlethaler P, Qayyum A, Viennot L. Optimized link state routing protocol (OLSR). 2003. http://hal.inria.fr/inria-00471712

Cordova D, Laube A, Pujolle G, et al. Blockgraph: A blockchain for mobile ad hoc networks. In 2020 4th Cyber Security in Networking Conference (CSNet), IEEE. 2020:1-8.

Dennis R, Owen G. Rep on the Block: A next generation reputation system based on the Blockchain. In 2015 10th International Conference for Internet Technology and Secured Transactions (ICITST), IEEE.2015:131-8.

Eschenauer L, Gligor VD, Baras J (2002) On trust establish- ment in mobile ad-hoc networks. In: International workshop on security protocols, Springer.2002:47-66.

Hernandez-Orallo E, Olmos MDS, Cano JC, Calafate CT, Manzoni P.Cocowa: A collaborative contact-based watchdog for detecting selfish nodes. IEEE transactions on mobile computing. 2014;14(6):1162-75.

Johnson D, Ntlatlapa NS, Aichele C (2008) Simple prag- matic approach to mesh routing using batman.2nd IFIP International Symposium on Wireless Communications and Information Technology in Developing Countries, CSIR, Pretoria, South Africa.

Kannhavong B, Nakayama H, Kato N, Nemoto Y, Ja- malipour A.Analysis of the node isolation attack against olsr-based mobile ad hoc networks.In 2006 International Symposium on Computer Networks, IEEE, 2006:30-5.

Kotla R, Dahlin M. High throughput byzantine fault tolerance. In 2004International Conference on Dependable Systems and Networks, IEEE. 2004:575-84.

Kulla E, Ikeda M, Barolli L, Miho R. Impact of source and destination movement on manet performance considering batman and aodv protocols. In 2010 International Conference on Broadband, Wireless Computing, Communication and Applications, IEEE. 2010:94-101.

Kulla E, Ikeda M, Hiyama M, Barolli L, Miho R. Performance evaluation of olsr and batman protocols for vertical topology using indoor stairs testbed. In2011 International Conference on Broadband and Wireless Computing, Communication and Applications, IEEE. 2011:159-66.

Kulla E, Hiyama M, Ikeda M, Barolli L. Performance comparison of OLSR and BATMAN routing protocols by a MANET testbed in stairs environment. Computers & Mathematics with Applications. 2012;63(2):339-49.

Kulla E, Ikeda M, Oda T, Barolli L, Xhafa F, Takizawa M. Multimedia transmissions over a manet testbed: problems and issues. In the6th International Conference on Complex, Intelligent, and Software Intensive Systems, IEEE.2012b:141-147.

Laube A, Martin S, Al Agha K. A solution to the split & merge problem for blockchain-based applications in ad hoc networks. In the 8th International Conference on Performance Evaluation and Modeling in Wired and Wireless Networks (PEMWN), IEEE. 2019:1-6.

Liu G, Dong H, Yan Z, Zhou X, Shimizu S. B4SDC: A blockchain system for security data collection in MANETs. IEEE Transactions on Big Data. 2020.DOI: 10.1109/TBDATA.2020.2981438

Lwin MT, Yim J, Ko YB.Blockchain-based lightweight trust management in mobile ad-hoc networks.Sensors. 2020;20(3):698.

Machado C, Westphall CM. Blockchain incentivized data forwarding in manets: Strategies and challenges. Ad Hoc Networks. 2021;110:102321.

Marti S, Giuli TJ, Lai K, Baker M. Mitigating routing misbehaviour in mobile ad hoc networks. In: Proceedings of the 6th annual international conference on Mobile computing and networking, 2000;255-265.

NaOmar M, Challal Y, Bouabdallah A. Certification- based trust models in mobile ad hoc networks: A survey and taxonomy. Journal of Network and Computer Applications. 2012;35(1):268-286

Peiris P, Rajapakse C, Jayawardena B. Blockchain-based distributed reputation model for ensuring trust in mobile adhoc networks. In 2020 International Research Conference on Smart Computing and Systems Engineering (SCSE), IEEE.2020:51-56.

Perkins C, Royer EM, Das S. Ad-hoc on demand distance Vector routing (AODV). 2003. http://media.gradebuddy.com/documents/3107203/4e440567-1f3b-4e47-8585-8d2c24b05758.pdf

Sanchez-Iborra R, Cano MD, Garcia-Haro J. Performance evaluation of batman routing protocol for voip services: a qoe perspective. IEEE Transactions on Wireless Communications. 2014;13(9):4947-4958.

Neha Khandelwal is a Research Scholar at the Department of Computer Science Engineering, ITM University, Gwalior, India. She got a Masters's degree in Artificial Intelligence from VaishnavCollege of Engineering, Indore, India. Her research is related to Computer Applications and Modern Computer Technology.

Dr.Shashikant Gupta is an Associate Professor at the Department of Computer Science Engineering, ITM University, Gwalior, India He got his Master's and Ph.D. degrees in Information Technology in Engineering. His research encompasses Computer Applications and Modern Computer Technology.

Note: This article is an extended work of the previous article entitled "Blockchain-based BATMAN protocol using Mobile ad-hoc Network (MANET) with an Ensemble Algorithm" https://doi.org/10.21203/rs.3.rs-673489/v1

IQAC COORDINATOR
SWAMI VIVEKANAND
COLLEGE OF ENGINEERING
KHANDWA ROAD, INDORE

PRINCIPAL
SWAMI VIVEKANAND
COLLEGE OF ENGINEERING
KHANDWA ROAD, INDORE

A Security Assessment Framework for Routing and Authentication Protocols of Mobile Ad-hoc Networks

Brijendra Kumar Joshi
Military College of Telecommunication Engineering, Mhow, India
Email: brijendrajoshi@yahoo.com
Megha Soni
Swami Vivekanand College of Engineering, Indore, India
Email: meghasoni@svceindore.ac.in

--- ABSTRACT---
Security assessment of routing and authentication protocols is based on the comparison of basic and secured versions of protocols such as AODV, SAODV, DSDV, SEAD, ZRP, SRP, LHAP, HEAP etc. In this paper, a framework for security assessment is presented. It is a complete system that attempts to provide the promised services to each user or application. To assess the security of different protocols, a security index is assigned. The value of security index shows how much a protocol is secured. To assign the security index, security parameters have been found out and the performance of different protocols have been analyzed under normal condition, Black Hole attack, Wormhole attack, and DoS attack.

Keywords- **Routing; Authentication; Framework; Security Index; Performance Index**

----

1. INTRODUCTION

Early designers of protocols focused only on issues related to providing efficient communication paths within highly dynamic networks and disregarding importance of network security. As a result, Mobile Ad-hoc Networks (MANETs) are susceptible to attacks which threaten proper routing of messages within a network.

MANET security is very challenging and it is best attempted by taking into account the types of attacks which are possible and developing a comprehensive security analysis and solutions for secure transmission of information.

Network security demands features like Access Control, Integrity, Confidentiality and Authentication Support. Among these features, authentication is primary, as access or availabilities of all other services follow it. During authentication, validation and verification between the entities, prior to exchanging secret information, provides privacy protection.

2. SECURITY ANALYSIS OF BASIC ROUTING PROTOCOLS

The comparison is based on the basic protocol parameters suchas routing approach, loop freedom, routing metric, route recovery etc.

Table1. Basic routing protocols

Table 1 shows the comparative analysis of basic reactive, proactive and hybrid routing protocols [1].

Parameter	AODV	DSDV	ZRP
Routing Approach	On-demand	Table Driven	Hybrid
Loop Freedom	Yes	Yes	Yes
Routing Metric	Shortest path	Shortest path	Shortest path
Route Recovery	New route	Periodic	Start repair at failure point
Communication Overhead	High	High	Medium

2.1 Causes and Effects of Attacks on basic routing Protocols

Now let us consider the causes and effects of Black Hole, Gray Hole, Wormhole and (Denial of Service(DoS) attacks on the performance parameters of AODV protocol. The main causes of attacks on AODV are the following [2]-

- It is completely on-demand protocol.
- It uses message broadcasting process.
- It has flat routing.
- No mobility management.
- Uses shortest path algorithms.
- Does not have any process of authentication of non-mutable field.
- Only keeps track record of next hop.
- Real time attack is possible.
- No mechanism to observe the neighbor node activities.

Both Black Hole and Gray Hole attacks degrade the performance of AODV but the impact of Black Hole attack is more serious. AODV acts as a counter measure for Gray Hole attack and minimizes its effect and improves the reliability and effectiveness of the Ad-hoc network [2].

The communication overhead limitation in DSDV protocol makes attacker's efforts more communication efficient.

3. SECURITY ANALYSIS OF SECURE ROUTING PROTOCOLS

Secure routing protocols like Secure Ad-hoc On Demand Distance Vector Routing (SAODV), Secure Efficient Ad-hoc Distance Vector Routing (SEAD),Secure Routing Protocol (SRP) are compared in Table 2.

Table 2. Secure routing protocols

Parameters	SAODV	SEAD	SRP
Routing approach	On-demand	Table driven	On-demand
Loop freedom	√	√	√
Routing metric	Distance	Distance	Distance
Shortest path identification	×	×	×
Black Hole attack	×	×	×
Wormhole attack	×	×	×
DoS attack	×	√	√

Table 2 to highlight set of operational requirements and attack analysis.

In SAODV, use of digital signatures [3] prevents impersonation of source and destination nodes. It also uses the one way hash for hop authentication to prevent reduction of the hop count. But two malicious nodes can advertise that they have link between them and they can hold certain traffic in SAODV. It is also possible that intermediate node can corrupt the route discovery.On the other hand, use of public key cryptography imposes a high processing overhead.

SEAD is a robust routing protocol against multiple attackers. It uses efficient and inexpensive cryptographic primitives which play an important role in computation in bandwidth-constrained nodes.

As SEAD relies on doing neighbor authentication, it is unable to provide a way to prevent an attacker from tampering with "next hop" or "destination".

In case of SRP, route signaling cannot be spoofed. Alteration and fabrication of routing messages are not possible. And finally, malicious nodes cannot redirect routes from the real shortest paths.

On the basis of the various studied protocols a comparison of security against attacks is given in Table 2. It shows that a lot of work has been done for DoS attack but for Wormhole attack and Black Hole attack secure protocols are required.

4. SECURITY ANALYSIS OF AUTHENTICATION PROTOCOLS

Timed Efficient Stream Loss-Tolerant Authentication(TESLA), Light-Weight Hop-by-Hop Authentication Protocol (LHAP)and Lu and Pooch's algorithms are vulnerable to DoS attack [4]. LHAP is vulnerable to Wormhole and Man-in-the-Middle attack as periodic delayed key disclosure is not used in this algorithms (ReferTable 3).

Table 3. Attacks on authenticationProtocols
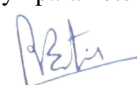
Protocol	Man in-the Middle Attack	Wormhole Attack	DoS Attack
Lu and Pooch's	×	×	√
TESLA	×	√	√
LHAP	√	√	√
HEAP	×	×	×

Hop-By-Hop Efficient Authentication Protocol(HEAP) offers some level of protection against insiders who forge packets and impersonate other insiders' nodes. HEAP successfully guards against many attacks by the outsider, such as DoS attack, Wormhole attack, Man-in-the-Middle attack, and flooding etc.

5. FRAMEWORK FOR SECURITY ASSESSMENT

A framework for security assessment is a complete system that attempts to provide the promised services to each user or application.

The key components of the framework are protocols, attacks, performance parameters, security parameters, *SI* and *PI etc*.
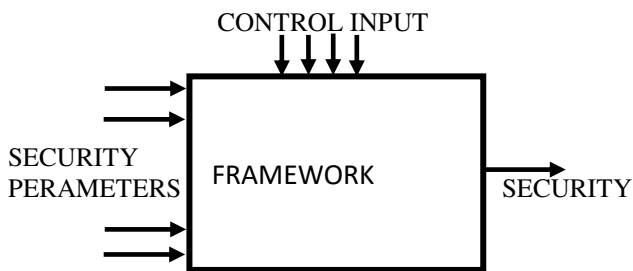
Fig. 1 Security assessment Framework

The objectives of designing the framework are the following:

- Security assessment of routing and authentication protocols.
- Performance analysis of routing and authentication protocols.
- To suggest the suitable routing and authentication protocol as per the user requirements.

In brief, the framework looks like a black box as shown in Fig. 1. The framework accepts the input values for different parameters and outputs a single value between 0 and 1. Here, the value 1 means the strongest system on which no attack can be launched. Obviously, we did not find any set of parameters for which this value could be achieved.The framework may be suitable for developing proposals for potentially new protocols for routing and authentication.

5.1 Control Input (CI) of Framework

The design parameters that serve the desired service to the user areProtocol Version(CI_1), Throughput (CI_2), PDR(CI_3), Delay(CI_4), Memory Overhead (CI_5), Routing Overhead(CI_6),Scalable(CI_7), CPU Time (CI_8).

5.2 Security parameters

Primary Security Parameter(PSP) andSecondary Security Parameter (SSP)are the security parameters of routing protocols. As a result of the study, it is found that the following are the PSPs:

5.2.1 Basic / Secure Version

A protocol may be basic protocol like AODV or secure version of the basic protocol like SAODV.

5.2.2 Routing approach

There are different routing approaches such as on-demand, table driven or both, used to implement protocols. These approaches play an important role in the security assessment of routing protocols (refer Table 1 and 2).

5.2.3 Effect of Attacks

PSPs can assess the security of any protocol by considering the effect of different attacks like Black Hole attack, Gray Hole attack,Wormhole attack, DoS attack and Man in-the Middle attack etc.

5.2.4 Security Schemes

Different security schemes such as Secret key,Message Authentication Code(MAC), Hash chain and Digital signature etc. are called SSPs. They are used to secure the basic protocols. These are the key parameters of security assessment.

5.3 Security parameters of Authentication protocol

When the authentication protocols were explored, it was found that the security of such protocols can be assessed with the help of following PSPs [5]-

- Effect of Attacks
- Source / Hop-by-Hop authentication.
- Application of MAC
- Trust bootstrapping
- Trust maintenance
- Use of Digital signature
- Delay time or varied delay in key disclosure

5.4 Protocol Index Value(PIV) of protocols

To assess the security in designed framework, the PIV shave been assigned forCI, PSPs and SSPs of each protocol. The assignment of values is based on the study of performance and behavior of different protocols [1], [4], [6-16].

5.4.1. PIV for CI of routing protocol

The range of $PIV$is different for different parameters. The range of PIV in the framework is $0 \leq PIV \leq 10$. The selection of "None" as an input, shows that no CI is applicablein assessment process.PIV can be assigned by the following relations:

$$PIV = \begin{cases} 0, \text{CI}_1 = \text{SP} \vee \text{AP} \\ 1, \quad\quad \text{CI}_1 = \text{BP} \end{cases}$$

$$PIV = \begin{cases} 0\,, 0 < C1_2 \leq 20\% \\ 1, 20\% < C1_2 \leq 40\% \\ \quad\quad . \\ \quad\quad . \\ 5, 80\% < C1_2 \leq 100\% \end{cases}$$

$$PIV = \begin{cases} 0, 0 < C1_3 \leq 20\,\% \\ 1, 20\,\% < C1_3 \leq 40\,\% \\ \quad\quad . \\ \quad\quad . \\ 5, 80\,\% < C1_3 \leq 100\,\% \end{cases}$$

$$PIV = \begin{cases} 10, C1_4 \leq .001ms \\ 8, .001ms < C1_4 \leq .01ms \\ \quad\quad . \\ \quad\quad . \\ 2, 10ms < C1_4 \leq 100ms \end{cases}$$

$$PIV = \begin{cases} 1, C1_5 < .1 \\ 2, .5 < C1_5 \leq .75 \\ 1, C1_5 < .1 \end{cases}$$

$$PIV = \begin{cases} 3, 0 < C_6 \\ 2.25, 25\% < C1_6 \le 50\% \\ 1.5, 75\% < C1_6 \le 75\% \\ .75, 75\% < C1_6 \le 100\% \end{cases}$$

$$PIV = \begin{cases} 1, C1_7 \le 100 \\ 2, 100 < C1_7 \le 100 \\ 3, 1000 < C1_7 \end{cases}$$

5.4.2. *PIV for* PSP *of routing protocol*

- If protocol version is secure, the assigned *PIV* is between 2 and 3 and for basic protocol it is 1.
- *PIV* is 1, if routing approach is on- demand; for table driven and hybrid protocols, the assigned *PIV* is 2 and 3 respectively.
- *PIV* is assigned for each attack analysis. It is low if the severity of attack is high. If Black Hole attack, Gray Hole attack and Wormhole attack unable to degrade the performance of the protocol, the $PIV = 3$ else $PIV < 3$.

5.4.3. *PIV for SSP of routing protocol*

If any one of SSP- Secret key, MAC, Digital signature, Hash chain and Cryptography mechanism is used in the protocol, $PIV = 3$ else $PIV = 0$.

5.4.4. *PIV for PSP of authentication protocol*

- The assigned value of *PIV* is 1 for authentication protocol, as they are secure version.
- *PIV* is 1, if Man in-the Middle attack, Wormhole attack and DoS attack are unable to affect the performance of protocols.
- *PIV* is assigned for following PSP or security schemes separately. If Source / Hop by Hop authentication, MAC, Trust bootstrapping, Trust maintenance, Digital signature in trust management, Delay time / varied delay in key disclosure are applicable in protocol, $PIV = 1$ else $PIV = 0$.

5.5 Security Index (SI) and Performance Index (PI)

SI of any protocol can be defined as the normalized value of the summation of the assigned PIV of security parameters.

The value of SI shows that how much a protocol is secure. A protocol is highly secure if SI is high (Refer Table 4). SI of routing and authentication protocols can be calculated by using the following formula.

$$I_{PSP} = \sum PIV \ of \ PSP \qquad (1)$$

$$I_{SSP} = \sum PIV \ of \ SSP \ (2)$$

$$SI = \frac{I_{PSP} + PIV \ of \ CI_1 \ (I_{SSP})}{N} \ (3)$$

Table4. Framework for SI of routing protocol

Where N is the sum of maximum PIV of SSP and PSP. It is 30 for routing protocol and 10 for authentication protocol.

Security Parameter	PIV of protocol					
	AODV	SAODV	DSDV	SEAD	ZRP	SRP
Secure	1	3	1	2	1	2
Routing approach	1	1	3	3	2	-
Black Hole attack	1	3	1	3	2	3
Wormhole attack	1	3	1	2	1	3
DoS attack	1	3	2	2	1.5	2
Secret key	0	3	0	3	0	3
MAC	0	0	0	0	0	3
Digital signature	0	3	0	0	0	0
Hash chain	0	3	0	3	0	0
SI	.16	.73	.26	.6	.25	.6

PI of any protocol can be defined as the normalized value of summation of assigned value of all CI.

$$PI = \frac{\sum PIV \ of \ CI}{n} \ (4)$$

Where n is the sum of maximum PIV of all applicable CIs. The maximum value of n is 30.

PI is required either to find the suitable solution as per the user requirements or to analyze and compare the performance of protocols (Refer Table 5).

Table5. Framework for *PI* of routing Protocol

CI	PIV of protocol					
	AODV	SAODV	DSDV	SEAD	ZRP	SRP
CI_1	0	1	0	1	0	1
CI_2	2.5	2	4	3.5	3.5	3
CI_3	5	4.5	4	4.5	5	4.5
CI_4	3.5	1	10	8	10	9
CI_5	3	2.5	1	1.5	2	2.5
CI_6	2	1	1.5	1	3	2
CI_7	2	1.5	1	.5	3	2.5
CI_8	-	-	-	-	-	-
None	-	-	-	-	-	-
PI	.6	.45	.7	.67	.83	.81

SI and *PI* are independent of each other. A protocol which has high *PI* can perform better than others and also suitable for required service. *PI* can be calculated for minimum one *CI*. For no control input it is 0.

Table6. Framework for *SI* of authentication protocol

Security Parameter	SI value of protocol			
	LHAP	HEAP	TESLA	Lu and Pooch's
Secure	1	1	1	1
Man in-the Middle attack	0	1	1	1
Wormhole attack	0	1	0	1
Dos attack	0	1	1	0
Source / Hop by Hop authentication	1	1	0	1
MAC	0	1	1	1
Trust bootstrapping	1	1	1	1
Trust maintenance	1	1	0	1
Digital signature	1	1	0	0
Delay time / varied delay in key disclosure	0	0	1	1
SI	.5	.9	.6	.8

Table7. Framework for *PI* of authentica-tion protocol

Performance Parameter	PI value of protocol			
	LHAP	HEAP	TESLA	Lu and Pooch's
CI_1	1	1	1	1
CI_2	4	4	4	2
CI_3	2.5	2.5	2.5	1
CI_4	6	10	1	1
CI_5	1	3	.5	.5
CI_6	-	-	-	-
CI_7	2.5	.5	2.5	-
CI_8	2	3	1	1
None	-	-	-	-
Overall *PI*	.63	.8	.41	.2

6. RESULTS AND DISCUSSION

Table 4 and Table 5 show the *SI* and *PI* of different routing protocols for which the framework is designed. By comparing the *SI* of protocols it can be found that which protocol is more secured.

For example, if we assess the security of basic protocols such as AODV, DSDV and ZRP, it is found that DSDV is more secure than AODV. It is due to table driven routing approach of DSDV protocol.

ZRP offers almost same level of security as it uses both on demand and table driven routing approaches. On the other hand if we analyze the performance of these protocols, it is found that the overall *PI* value of ZRP is more than AODV and DSDV. But if we consider only one *CI* such as delay than the performance of DSDV protocol is much better than other basic protocols.

To assess the security of different secured routing protocols, the SI values were compared and are given in Table 4. It is found that SAODV is highly secured among all. It is due to the use of digital signatures in routing process. But it is not completely secured protocol.

The *PI* value of SAODV is very low as compared to SEAD and SRP. It is due to on demand routing approach. The overall performance of SRP is better than that of other given protocols as it is secured version of a hybrid protocol. But it is less secured than SAODV and SEAD protocol.

It is also found that the basic protocols have very low security index as compared to their secured versions. It is due to the application of different security schemes in secured routing.

The performance of HEAP, TESLA, LHAP and Lu and Pooch's algorithms were compared in Table 3 and it is found that TESLA is vulnerable to DoS attacks and thus it is important to secure time synchronization of all the nodes. Further, TESLA introduces very large latencies of several seconds making it unsuitable for real time applications.

LHAP is vulnerable to Wormhole and Man-in-the Middle attacks. Also, it needs very large memory at every node.

Lu's scheme suffers from overall poor performance as throughput and PDR are significantly low; though it has extremely low memory requirements.

HEAP is resistant to many outsider attacks such as DoS and Wormhole. It is suitable for use in MANETs for unicast, multicast or broadcast applications.

Table 6 and Table 7 show the *SI* and *PI* of different authentication protocols and it is found that HEAP

is highly secured and performs better as compared to other protocols which have been taken into consideration in the framework. It is due to the use of Hop by Hop authentication, digital signature, keys in trust bootstrapping and trust maintenance.

7. CONCLUSION

No protocol is able to cover all the threats and accomplish all security goals. This work also underscores the need for a more secured protocol that would deal with demanding requirements of MANETs.

First, most secured routing protocols have been designed by focusing on certain known attacks. Thus when an unknown attack may come up, one or more of these protocols may collapse.

Second, requirement of higher security demands more computational resources on each mobile node, something which is not easy to come by in a MANET environment. Therefore in MANETs, there always exists a tradeoff between higher security and higher performance.

Third, any security option is selected on the basis of what security aspects must prevail in a given operating environment; and in more ways than one these security options are not exclusive to one another.

Fourth, none of these provides complete security in MANETs operation. From the work emerges a table that demonstrates the fact that every secure protocol works within different limitations and to that extent provide security against limited threats.

A framework has been presented that assesses the security of routing and authentication protocols. The framework assigns a numerical value and suggests how much it is secured. In case of an unknown protocol, it suggests that which of the existing protocols the nearest one to satisfy the requirements.

REFERENCES

[1] A. Y. Zomaya, Algorithms and protocols for Wireless and Mobile Ad-hoc Networks: *A Taxonomy of Routing Protocols for Mobile Ad Hoc Networks,*(John Wiley Canada2009).

[2] M. Soni, and B. K. Joshi, Security Assessment of Routing Protocols in Mobile Ad-hoc Networks,*Proceeding of the International Conference on ICT in Business, Industry and Government,* Indore, India, 2016, 24

[3] M. Soni, and B. K. Joshi, Security Assessment of SAODV Protocols in Mobile Ad-hoc Networks.*Proceeding of the International Symposium Data Science and Big Data Analytics,* Indore, India, 2018, 347-355.

[4] R. Akbani,T. Korkmaz, and G.V.S. Raju, HEAP: Hop-by-hop Efficient Authentication Protocol for Mobile Ad-hoc Networks,*Proceedings of the Spring Simulation Multi conference,* Virginia, USA, 2007, 157-165.

[5] M. Soni, and B. K. Joshi, Security Assessment of Authentication Protocols inMobile Adhoc Networks, *International Journal of Computer Scence and. Information Security,*19(5), 2021, 36-40.

[6] S.Kaur, andA. Gupta, A Review On Different Secure Routing Protocols And Security Attacks In Mobile Ad Hoc Networks,*International Journal of Advance Engineering Technology5*(4), 2014,01-05.

[7] Argyroudis P. G. and O'Mahony D., Secure Routing For Mobile Ad Hoc Networks,*IEEE Journal on Communications Surveys & Tutorials,7*(3), 2005, 2-21.

[8] Shawkat, K. and Saaid G. O. S., Evaluating the performance of secure routing protocols in Mobile Ad-hoc Networks,*International Journal of Advanced Research in Computer and Communication Engineering, 1*(9), 2012, 710-716.

[9] A.Mohamed, Abdelshafy and P. J.B. King, AODV and SAODV under Attack Performance Comparison, *Proceeding of 13th International Conference on Ad-Hoc Networks and Wireless ADHOC-NOW,* Benidorm, Spain, 2014, 318-331

[10] P. Singh, N. Mann and T.G. Kaur, Study the impact of different attacks on Zone routing protocol in MANET. *International Journal of Modern Computer Science and Applications, 4*(3), 2016, 14-17.

[11] M. C.Trivedi, S. Yadav, and V. K. Singh, Securing ZRP Routing Protocol Against D DoS Attack in Mobile Ad Hoc Network,*Proceeding of International Conference on Data and Information Systems,* Singapore, 2019, 387-394.

[12] A. Saini and Anu, Analysis of Security Attacks and Solution on Routing Protocols in MANETs, *International Journalof Computer Science and Mobile Compting, 5*(6), 2016, 182-189.

[13] M. F. Juwad and H. S. Al- Raweshidy, Experimental Performance Comparisons between SAODV & AODV,*Proceeding of the 2nd Asia International Conference on Modeling & Simulation,*Kuala Lumpur, Malaysia, 2008, 247-252.

[14] S. M.Basha, S. R. Kumar, and R.V.Matam, Inclusive performance scrutiny of DSDV AODV and ZRP MANETs Routing Protocols, *International Journal of Advanced Computer Technology, 2*(5), 2014, 31-42.

[15]   Ashwin Perti, Evaluate Dynamic Source Routing ProtocolPerformance in Wireless MANET,*Int. J. Advanced Networking and Applications, 5*(5) , 2016, 2056-2059.

[16]   Nitish Balachandran,Surveying Solutions to Securing On-Demand Routing Protocols in MANETs, *Int. J. Advanced Networking and Applications, 4*(1), 2012, 1486-1491

AUTHORS PROFILE

Dr. Brijendra Kumar Joshi is a Professor of Electronics & Telecommunication and Computer Engineering at Military College of Telecommunication Engineering, MHOW (MP), India. He has obtained BE in Electronics and Telecommunication Engineering from Govt. Engg. College, Jabalpur; ME in Computer Science and Engineering from IISc, Banglore, PhD in Electronics and Telecommunication Engineering from Rani Durgavati University, Jabalpur, and M.Tech. in Digital Communication from MANIT, Bhopal. He has more than 38 years of teaching experience. His research interests are programming languages, compiler design, digital communications, mobile ad-hoc and wireless sensor networks, image processing, software engineering and formal methods. He has number of research publications to his credit. He has supervised 12 Ph D thesis and currently supervising two research scholars. He has authored two books on Data Structures and Algorithms in C/C++ published by Tata McGraw-Hill, New Delhi.

Megha Soni Ph.D.in Electronics and Telecommunication Engineering from MCTE, Mhow, DAVV University Indore, India. She has obtained BE in Electronics and Telecommunication Engineering from Govt. Engg College, Sagar; M.E in Digital Communication from Davi Ahilya University Indore. She joined as an Assistant Professor in Electronics & Communication in Dec. 2005. Her research interest is in security assessment of routing and authentication protocols of Mobile Ad- hoc Networks.

Trust-based Secure IoT Architecture in Mobile Ad-hoc Network Against Malicious attacks

Neha Khandelwal
Ph.D. Scholar, ITM University, Gwalior, India
Neha19khandelwal88@gmail.com

Dr. Shashikant Gupta
Associate Professor, ITM University, Gwalior, India
shashikantgupta@itmuniversity.ac.in

Abstract:

 Recently, the Internet of Things (IoT) has seen a meteoric rise in popularity, enabling a diverse range of Internet-enabled devices to communicate with one another in a number of contexts and environments. Networks of the Internet of Things are particularly susceptible to a range of hazards, including insider attacks, as a result of their distributed nature. When rogue nodes are detected, it takes a substantial amount of time for them to be identified and eliminated. A coordinated and simultaneous collection of attacks against Internet of Things networks has the potential to do major harm to the networks, which is logically plausible. As a result of our research, we have developed an approach to addressing this problem that is both theoretical and empirically sound. When it comes to analysing the difficulties affecting the security of Internet of Things (IoT) networks based Mobile Ad-Hoc Network (MANET), game theory is an effective tool. Having portable nodes coordinate with one another in a MANET-IOT environment is becoming increasingly important, as it protects them from numerous security threats and their inability to function securely, while also storing its resources and managing safe routing between nodes in an IoT network, which is becoming increasingly important. As a result, it is critical to build an efficient routing protocol in order to safeguard all nodes from the occurrence of unexpected events. The game-theory technique is being employed for analytical objectives in the present research endeavour, and it is also being used to tackle the security challenges that IoT networks are now experiencing. It is standard practise to use a game-theoretic method in order to discover possibly harmful actions in Internet of Things networks. In particular, the proposed study presents a Bayesian-Signaling game model, which investigates the behaviour of both regular/normal and malevolent nodes in a network. A further advantage of the game model that has been offered is that it allows for finer actions of autonomous strategies for each node in the Internet of Things network to be taken. Games that use Bayesian Equilibrium (BE) may be able to resolve incomplete information by linking tactics and players' rewards, resulting in the achievement of an equilibrium in the game. A network of normal and malicious nodes in an Internet of Things network may be distinguished from one another using the BE technique, which is implemented in the system. It is expected that as a consequence of the Efficient Computational Modelling based on Game Theory (ECM-GT) technique, the utility of malicious nodes in the Internet of Things network would be reduced, while the usefulness of legitimate nodes will be increased. Additionally, by using the reputation system, it encourages the greatest possible cooperation among the nodes in the Internet of Things network. We found that the proposed method outperformed existing systems in terms of malicious node identification, throughput, PDR, E2E latency, energy

6222

consumption, and routing over head parameters when our findings were compared to those of existing systems.

I. INTRODUCTION

Internet of Things (IoT) is becoming more popular as a platform for a variety of contemporary applications and services, including smart homes and health care; public security; industrial monitoring; and environmental protection. IoT networks with many hops can be built by the majority of smart gadgets on the market today. For example, these devices may either collect data from their surroundings, or they could be used to design plans based on that data. In addition to ZigBee, WiFi, and Bluetooth, various Internet of Things protocols [1,2] may be used to connect to these devices.

Insider attacks, in which an attack is launched from inside the network, are a problem for multihop IoT systems. There are several ways in which an attacker may get access to critical information, alter data, or conduct a denial-of-service (DoS) attack from a small number of compromised devices in a multihop IoT network. Because of this, an Internet of Things (IoT) security solution that can detect rogue nodes is essential.

There is no need for a physical infrastructure in MANETs because of the Internet of Things, which is driving the development of these networks. Changeable topology, quick setup, and multihop wireless communication are just some of the features that set IoT networks apart. MANET-IOT is a suitable match for a broad variety of time-critical applications because of these qualities [3, 4]. An ad hoc network may be utilised to provide a functioning communication facility in the absence of a physical infrastructure. In addition, IoT networksenable mobile nodes to communicate information without the need for a physical foundation or the execution of administrative tasks. The result is a dynamic, self-organizing and self-configuring network

that allows nodes to roam freely throughout the network while still being connected. As part of the Fourth Industrial Revolution, IoT networks also play a crucial role. These networks may be expanded and combined with new technologies such as cloud computing, the Internet of Things, and machine learning methodologies in order to build intelligent applications that automate industrial operations. In the IoT networks, developing a secure routing protocol while maintaining quality of service (QoS) is a difficult challenge [7–9]. [7–9] It is possible for any adaptive node to join the network and participate in data transmission, as MANET is an open communication architecture [10]. IoT networkssecurity breaches are made possible in part by the network's open communication design [11].

In such a network, it is difficult to keep data secure and to route it in an efficient manner. Routing protocols for MANETs are often divided into three groups: proactive routing protocols (i), reactive routing protocols (ii), and hybrid routing protocols. Proactive routing protocols are the most widely used (iii). Routing protocols that are proactive in nature construct and maintain all routes in a routing table before any communication takes place. On a regular basis, routing protocols in this category transmit control packets to enable them to undertake route setup and maintenance. Control packets for route creation and maintenance, which are required for the formation and maintenance of routes, add to the routing overhead of a MANET-IOT by increasing the number of packets sent and received. These proactive routing algorithms are particularly well suited to tiny networks.

Nodes request routes from reactive routing systems only when they need them, unlike proactive routing protocols. This route design strategy reduces network congestion by

6223

minimising the network overhead associated with proactive routing techniques' frequent exchange of control packets. Reactive approaches, rather than proactive routing systems, may select the ideal route with minimal packet delay and network overhead. It is also possible to employ larger networks with higher efficiency using reactive routing technologies. The hybrid nature of routing protocols is another kind of routing protocol. In a single protocol, proactive and reactive routing algorithms are merged with the advantages of both approaches.

Ad-hoc on-demand distance vector routing (AODV) is a popular method for routing traffic in metropolitan area networks (MANs). Numerous academics examined AODV's performance in-depth, taking into account a wide variety of criteria. Other possible causes for security breaches were also found. There are a number of issues with this procedure, including the following:

I To date, there is no system in place to alleviate traffic congestion. (iii) Multipath routing is not supported by the existing protocol. [12] As previously indicated, (iii) it has a broad spectrum of security vulnerabilities. When packets go missing, there isn't a standard way to deal with the problem. (v) It lacks any methods for ensuring high levels of customer satisfaction. There is nothing without the concept of energy optimization.

Motivation. A skilled attacker might employ an intelligent approach to damaging behaviour, such as changing certain packets with a probability, despite the fact that most current research focuses on a single and unique attack in an IoT setting [13–15]. In the IoT environment, a skilled attacker may instead choose for a single and singular attack. This work discusses a more powerful and sophisticated attacker who may be able to gain unlawful control of certain nodes in IoT networks and launch a multiple-mix attack with a high likelihood of performing three harmful acts, such as altering data, dropping packets, and transmitting duplicated packets. This is a significant point. As a result, it is more difficult

to identify and capture a culprit when many criminal actions are being carried out concurrently.

AODV is very susceptible to a wide range of attacks, including black hole attacks, wormhole attacks, and denial of service attacks, amongst other things. It is necessary to update the AODV protocol in order to fix these security issues. A large number of academics have created versions of the AODV protocol in order to overcome the issues raised above. The AODV protocol does not, however, solve all of the issues described above in a single version that is easy to understand and use. Consequently, the fundamental goal of the proposed protocol is to provide safe and efficient routing by minimising packet losses and so increasing the overall quality of service provided by the MANET. For the purpose of maximising the efficiency of the network, we provide a Proposed TAODV protocol for routing that takes the following factors into consideration: I Have the Capacity (TP). (ii) The average amount of time it takes from start to end (AED). (iii) The proportion of packets that are delivered. (iv) Routing-related overhead costs are incurred. (V) The use of energy

The rest of this article will be organised in the following manner. Section II addresses existing attacks and countermeasures against selective forwarding in IoT networks, as well as possible future attacks. The Bayesian signalling game model is discussed in detail in the third part. The proposed attack strategy is discussed in Section IV of this document. In Section V, you will learn about execution and result, and in Section VI, you will learn about conclusion.

II. LITRACTURE REVIEW
Secure data transmission and recording/storage may be achieved using the suggested model, which is based on the TOPSIS (Technique for Order Preference by Similarity to the Ideal Solution). Internet of Things (IoT) device trust may be gauged by these characteristics. There are less unneeded and poorly organised elements in the model because of the adoption of Simple Additive Weighting (SAW).

6224

Comparatively, it's compared to a standard IIoT strategy that employs multiple spectrum sensors and security capabilities, amongst others For malicious nodes and Denial-of-Service (DoS) attacks, the proposed method is around 85% more effective than the baseline technique [16] compared to the baseline technique.

There is a way to allocate resources in a heterogeneous Internet of Things network so that there are more communication channels between two nodes or to keep links safe from attacks, like when there are more communication channels. Predicting strategic cyber attacks is an important part of designing safe IoT networks. This is done by setting a lower limit on the number of secure connections needed to meet a certain budget of protected links, and then coming up with a way to build networks that meet heterogeneous network design rules. Each layer of the heterogeneous IoT network is supposed to be able to withstand a certain amount of damage while using the least amount of resources possible. At the end of the study, we give examples of how the Internet of Battlefield Things (IoBT) can be used to support and show our findings.

The reason our certificate-based device access control strategy for the Internet of Things (IoT) works well is because it protects against attacks like the ones above, but it also keeps your identity hidden. In order to show that the proposed system is safe from a wide range of known attacks, it has been subjected to a thorough security analysis that used the widely used "Automated Validation of Internet Security Protocols and Applications" (AVISPA) tool to check for security flaws. This includes the widely used "Real-Or-Random" formal security analysis, an informal security analysis, and formal security verification. In addition, it's been shown that the proposed system has better security and functionality features, communication and computation costs, as well as system performance than other systems of its kind[18].

TBSMR, a trust-based multipath routing system, was created by the researchers to improve the overall performance of the MANET. In order to improve the MANET network's quality of service (QoS), the proposed protocol takes into account a vast number of parameters, including congestion management, packet loss reduction, malicious node identification, and secure data transfer. The suggested protocol's performance is evaluated using the NS2 simulator. It has been shown via simulation results that the suggested routing protocol is superior to current routing strategies.

Attackers create and carry out a series of complex selective forwarding attacks, which may dynamically pick the kind and proportion of forwarding packets while being energy efficient, and even harm other innocent nodes in the network. According to the research, the advised attacks may have a bigger influence on the attack's repercussions (for example, the amount of lost packets) while remaining undetected.. In addition, there is a simple trust-based security mechanism that can be easily implemented to detect and remove rogue selective forwarding nodes from a network. Using just 3.4 percent of the total energy available, the suggested defence system is able to achieve high detection accuracy [20].

Here, we present an approach called Perceptron Detection (PD), which combines both perceptron and K-means algorithms to determine the trustworthiness of Internet of Things (IoT) nodes and to identify malicious nodes in an acceptable way. In addition to tweaking network routing, a novel perceptron learning technique called Perceptron Detection with Enhancement has been created to further increase detection accuracy (PDE). More than a factor of 20–30 percent [21] better than comparable strategies, PD and PDE were shown to be able to detect malicious nodes in the testing.

Edge Computing allows end devices to outsource calculations to servers on the network's perimeter. Traditional cloud communication's latency and bandwidth utilisation are lowered as a consequence of this.

6225

Secure SEAL use fuzzy logic to identify and isolate rogue nodes in an IoT network. Reaction-based trust evaluation reputation value is used to reexamine the suspicious nodes to see whether they are still suspicious. At the conclusion of the procedure, the proposed trustworthy environment was assessed for its performance. [22] More than 90% of the time, the recommended effort is quite effective in minimising the effects of coordinated attacks.

It is the job of internal security to make sure that both users and resources interact with each other and with resources. When looking for services and choosing people to be found, outside security may help to make things more safe. People who aren't supposed to be on the network can have less of an effect on it by not allowing them to use it. It is up to the access control system to decide whether the devices can be neighbours or resources in service communications. Communication between IoT devices improves a lot with the suggested RRAC. It shortens detection time, reduces service overhead and loss, and reduces false positives and misdetections [23].

Sybil attacks and wormhole attacks, two serious dangers to RPL, are well explained in this page. In addition, we provide two methods for identifying these threats in RPL-based IoT networks. Specifically, we utilise the Greatest Rank Common Ancestor (HRCA) concept to find the common ancestor of two nodes in the target network tree whose rank is the greatest among all of their ancestors. Our two detection methods not only identify an active attack, but they also pinpoint the location of the attacker inside the network, which is quite helpful. Because of this, the mitigation strategy becomes easier and more effective to implement. You can download Cooja, a Contiki network emulator, to use either of these methods. Considerable options exist for true positive rate, detection time, packet loss ratio (PLR), memory use and network overhead as a result of our research. Future eventualities may be dealt with by our methods since they seem to be adaptable [24].

It's proposed that a two-tier detection method be used, with the first level consisting of neighbouring nodes determining their own trust. A consortium's blockchain-based approach collects trust ratings for automobile nodes in the second phase of development by using RSUs as validators. According on the trust ratings supplied by other nodes in the near neighbourhood, the blacklist databases are regularly updated. For an actual-size network, experimental results show that the suggested solution is both efficient and scalable. As a final result, we demonstrate that the proposed method enhances VANET performance by reducing the number of nodes initiating insider attacks and blocking such nodes [25].

For two reasons: first, visitors may use any network node to get access to the network; second, once a visitor's identity has been validated, they can use any network node without having to re-authenticate. Our five protocols for synchronising dispersed TPMs include the Synchronization Protocol (SYNP), the Node Access Protocol (NAP), the Crossing-Node Access Protocol (CNAP), and the Updating Protocol (UPDP) (NRP). Using Raspberry Pis and Infineon TPM2.0 chips, we've built a prototype system that can develop and distribute these protocols. As a consequence of our time-saving tests, we can conclude that these techniques are not only feasible but also accessible. It is also possible to use these procedures in an efficient way by examining the experimental data [26].

This paper proposes a global sensor network attack-detection and prevention protocol that uses the Two-Fish (TF) symmetric key technique to identify and prevent attackers from infiltrating the network. Approaches described in this paper are grounded on the Authentication and Encryption Model (AEM) (ATE). The Eligibility Weight Function (EWF) is used to pick the sensor guard nodes, and then a complex symmetric key technique is used to conceal them. With the combination of OLSR and the Ad hoc On-Demand Multipath Distance Vector (AOMDV) routing approach, a safe hybrid routing system is now being developed

for application in wireless sensor networks. According to the results of this research, the suggested routing system has a higher proportion of monitoring nodes than current routing systems. This routing technique also protects against a variety of mobile attacks and guarantees multiple paths of delivery[27].]

This document authenticates and verifies the current DMSN routing protocols. In addition, a novel GAN-based intrusion detection system is presented in this research, which may be installed in the DMSN nodes to enhance the communication network's security. The GBCRP aims to build volatile block chains using decentralised authentication principles and robust intrusion detection techniques since block chain-based routing protocols are inherently unsafe. Fully Decentralized Generative Adversarial Network (FDGAN)-based intrusion detection system is used to keep track of safe routing transactions (FDGAN). A new study finds that the proposed GBCRP provides better secure routing than current systems, in terms of security, energy usage, and routing metrics [28].

Clusters may detect a trustworthy CH using a trust-based clustering approach. Trust-based CH selection, for example, takes into account a node's reputation, expertise, and experience in addition to other variables. In addition, the trustworthiness of each node in a cluster is evaluated in order to build a back-up head for it. When trust is built into a cluster, malicious or compromised nodes may be identified and removed from the network. By identifying these nodes, it is possible to reduce the risk of collecting inaccurate data. It is also capable of providing security and stability by increasing the lifetime of CHs and decreasing the calculation cost connected with CH selection while also reducing the computation cost associated with CH re-selection. StabTrust, on the other hand, is excellent at identifying and guarding against a broad variety of possible dangers [29].

III. BAYESIAN SIGNALLING GAME MODEL

In general, the games can be either cooperative or non-cooperative. In the non-cooperative

scheme, two or multi-players compete, while in the cooperative plan, number of players team up to reach the highest possible benefits. Cooperative games are those in which there is cooperation among the players which scrutinize optimal strategies for the group of players whereas non-cooperative games analyse the environment in which players exist, and the autonomous decision of nodes determines the node payoff. One of the non-cooperative game models is a Bayesian game model where the player performs an action even without complete information of the competent [29] [30].

A game contains a group of players, payoffs, and some moves/strategies. Each player has a strategy for the action of the probable state in the game. Players' payoffs give an incentive scheme where the player loses or wins in a specific state in the game. Since all the nodes are portable, they can travel arbitrarily. Payoff scheme supports the players to forward the packets to one another. Security guarantee is inefficient in resource consumption. Therefore, to overcome this problem, the MANETs are divided into a set of distinct clusters. In every cluster, the nodes select a head-node which serves as IDS for the whole cluster. In this system, a single node is motivated by providing a reputation model. In other game models, 'Bayesian interaction' games offer a solution for distributing the endogenous interaction model, which defines some asymptotic statistics for co-operating with other players [31]. Therefore, this approach can solve various critical issues in which there is a delay among private information and player reaction. The present study provides a 'Bayesian Signaling' model to solve the security issues in MANETs.

IV. PROPOSED WORK

The framework presented in this paper considers a dynamic multi-stage Bayesian Signaling game. Every mobile node in a Bayesian game is set with some classified information which has a considerable effect on the game evolution whereas the remaining mobile nodes are assumed to hold information about the classified data of the belief system. Those belief

values are denoted by a probability distribution and updated by the application of Bayes rules if novice information is available. The mobile nodes choose the most optimum action in the course of the game based on the classified data as well as the existing belief information. The proposed framework adopts Perfect Bayesian Equilibrium ensuring belief formation for a particular node type about its competing mobile node type, updating the belief information at the termination of each stage and approving the actions performed with the help of the belief system in the present stage.

In the framework, a cluster is formed in which mobile nodes associate or depart autonomously owing to their mobility in the collective simulation environment. The identity of mobile nodes is regulated by the physical features of the nodes that are permanently static. When there is a new incoming node that desires to add to the cluster, other nodes existing in the cluster allot their initial beliefs to that node. In case a malicious node enters a cluster that has not been visited previously, other nodes of that

cluster consider the malicious node as the newcomer and allot their initial beliefs to it. Every node in that cluster receives the reporting information broadcast from the regular mobile node. If the information reported is positive, the malicious node shall be reprimanded. Nevertheless, if the information reported about malicious node identification is false, the regular node liability shall be affected severely. The proposed approach evaluates results by considering the expected failure of false alarm (F) and expected gain of genuine reporting action (G_{rep}).

Mobile nodes monitor the outgoing data of the neighbour by utilizing the uninhibited environment ofMANET, but the origin of communication disruption cannot be comprehended by them. Such a process is called Neighbour Monitoring in MANETs. Thus, parameters like φ, ψ and δ are used for distinguishing the actions of neighbour nodes in a better way, and such a phenomenon is referred to as Neighbour Surveillance.
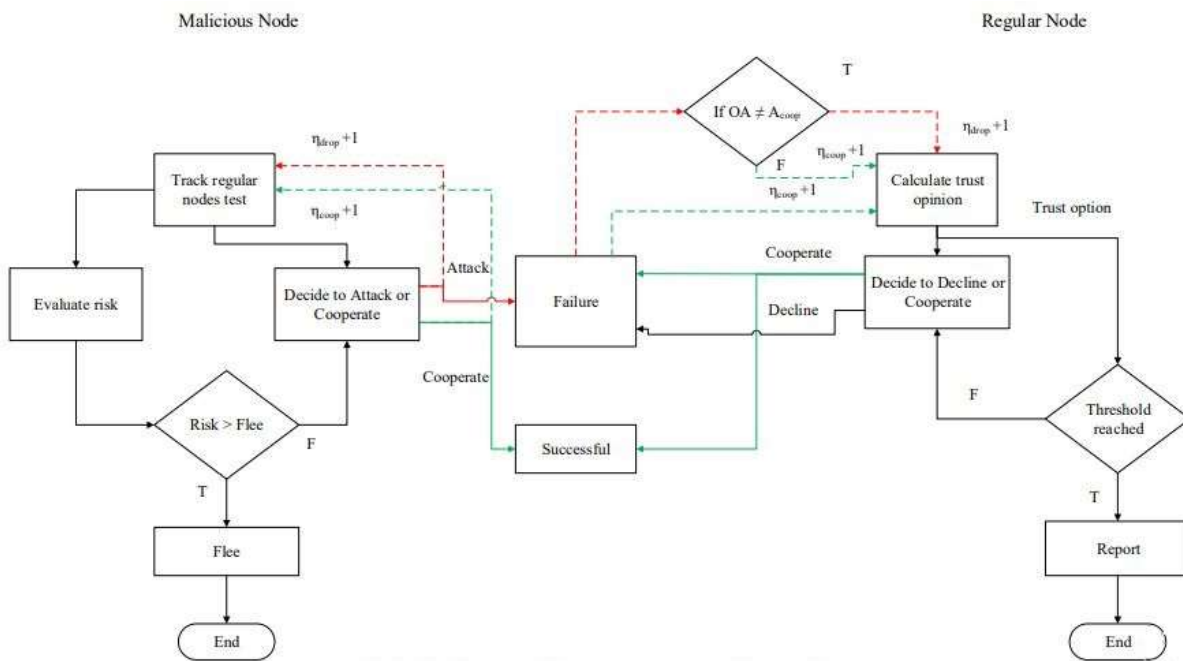
6228

Fig.1. Regular vs malicious node decision-making model

The proposed framework employs a decision-making model that is a cognitive process resulting in the determination of actions to be performed among the variety of available options. The decision-making model of regular vs malicious nodes in the proposed system has

been shown in Fig. 1. The regular node examines the belief option (Op_{belief}) and evidence adequacy (Op_{uncer}) continuously for the competing nodes from feedback received from neighbour monitoring. After each successful communication, the regular nodes raise the ηcoop by one and the opponents' strategy is checked on communication failure. In case the opponent chose A_{dec} / A_{att}, then $η_{drop}$ would be raised by one else $η_{coop}$ is increased by one. The regular nodes follow a threshold policy for taking the reported decision against the competent node. If the regular nodes fail to reach the threshold, the current belief held by the regular nodes for opponents and the

selfishness characteristic for itself determines the cooperate or decline action. Malicious nodes can also be modelled as rational and as such shall assess its trust factor with regular nodes continuously. A decision rule for fleeing is also followed by the malicious node to avoid being reported. Malicious nodes shall develop attacking frequency so that it becomes tough for regular nodes to determine their type.

In comparison to the existing works, the proposed work involves factors to depict selfishness and collaboration while formulating the node strategies in the game. Table I holds the essential parameters considered in the proposed system.

Table I. Parameters involved in the proposed system

Actions to be taken by Regular/Malicious nodes	
A_{att}	Attack
A_{cop}	Cooperate
A_{dec}	Decline
A_{flee}	Flee
A_{rep}	Report
Gain and Cost of Actions Adopted	
G_{att}	Gain associated with A_{att}
G_{coop}	Gain associated with A_{coop}
G_{rep}	Gain associated with A_{rep}
C_{att}	Cost associated with A_{att}
C_{coop}	Cost associated with A_{coop}
C_{flee}	Cost associated with A_{flee}
C_{rep}	Cost associated with A_{rep}
List of Opinion Formulation	
Op_{uncer}	Opinion of Uncertainty
$Op_{disbelief}$	Opinion of Disbelief
Op_{belief}	Opinion of Belief
Other Parameters	
F	Failure caused by false alarm
δ	Probability of the node being malicious
φ	Probability of attack by malicious node
$η_{coop}$	Quantity of identified A_{cop}
$η_{drop}$	Quantity of identified A_{att} or A_{dec}
Ψ	Probability of cooperating by regular node

6229

In mobile ad-hoc networks, a node is malicious if it reveals anomalous action which reduces the network performance. In this study, "Bayesian-signaling" (BS) game model is adopted to exhibit

the finest actions of selfish strategy and to control the malicious nodes' behavior. This game model can provide secure and reliable communication between the nodes. The

scenario is contemplated in this way to deal with the limitations in security in large-scale MANETstaking into account the multi-stage game theory.

This scheme considers the two-player strategy, i.e., sender and receiver, both are involved in the BS game model. Node behavior provides the sender type. The receiver will not observe the nature of the sender. The sender elects to forward the data from a set of possible messages {I → [i_1, i_2,....i_n]} depending on its behavior type and the receiver notices the message from the sender without realizing the sender type. Then, the receiver selects the possible actions in the set of actions A = {C, D} where C indicates 'cooperate' and D indicates 'decline'. Two players collect the payoff values which depend on sender type; here sender selects the data (message) whereas the receiver chooses the action.

Bayesian-Equilibrium (BE) is a game plan under the BS model which illustrates the following deliberations; like as the sender type (S_t) forward a message [$i*(S_t)$] in the set of probability distribution on I. The nodes probability, S_t considersany message 'i' from the set of I while the receiver performs an action from the action sets (i.e., C or D).

In addition, the node strategy is determined by how the payoffs are evaluated and how the belief system is updated. In the node strategy, there are three ways to do things: you can BE, mix, or do them all. Pure strategy doesn't change how nodes behave in any situation. In mixed strategy, node types can be changed at any time. This is how the Bayesian equilibrium works. It gives a strategy profile and changes the belief based on how many nodes there are. Pure strategy chooses an action based on its payoff value, while mixed strategy changes the beliefs of the other nodes. In this approach, relay and sender nodes are thought of as bad. The algorithm that follows shows the best way for game players to act.

6230

Algorithm

Input: Sender node (S_n) and Receiver node (R_n)
Output: Find the malicious action

Start.
      Init Sender node and Receiver node
      Define a profile strategy for S_n and R_n.
      Decide the Node type {Regular or Malicious}.
      Revisethe S_n and R_n beliefs by applying
      Bayes rule.
      Find optimal payoff value for S_n and
      R_n revised beliefs
      Realize the reasonable action {C,D}.
      if action not reasonable then
      Report to the corresponding nodes as
      malicious node
      else
            Determine action C and D
      end if End

A. Multi-Attacker Node Collusion Model

The proposed framework is designed considering the system has incomplete information about the node types, meaning that the user has no control over the behaviour of the attack, the user distributes merely the malicious nodes created within the simulation area. Nevertheless, understanding the working

of collusion attacks appears discerning, but the main point is if collusion can be targeted for colossal collateral network damage. Thus, for supporting the huge network damage, innovation has been introduced in the proposed attacker module in the form of auto-coordination among the attacker nodes within the simulation area.

The example given in Fig. 2 shows a malicious node at cluster position CP1 having limited time for performing the coordination after the initiation of the attack and before decamping. Another significant fact involves that the existence of similar belief for two sets of nodes does not imply those nodes are regular.

The regular nodes dominantly cooperate when it comes to communication thus raising the belief. Nevertheless, the cooperation shown by the malicious node is targeted to breach the regular node belief system. Therefore, the temporal analysis of simulation is performed by the system for extracting three crucial parameters – belief, uncertainty and malicious node probability.

Evaluating these three terms shall feature the distinction between malicious and regular nodes. Thus, it is highly reasonable to set up a dedicated channel for the communication of malicious nodes under the condition that the three parameters as mentioned above are computed parallelly by another task. From Fig. 2(i), it can be observed that the malicious node at cluster position CP1 can probably communicate with the surrounding attacker nodes CP7, CP6 and CP2. Likewise, after establishing the communication, any of them might extend to the particular neighboring attacker nodes. This phenomenon continues while the cluster ID is stored for avoiding C_{info} redundancy among them. To sum up, it means that the whole communication channel encapsulating every attacker node (with no repetition) shall be compromised as shown in Fig. 2(ii).
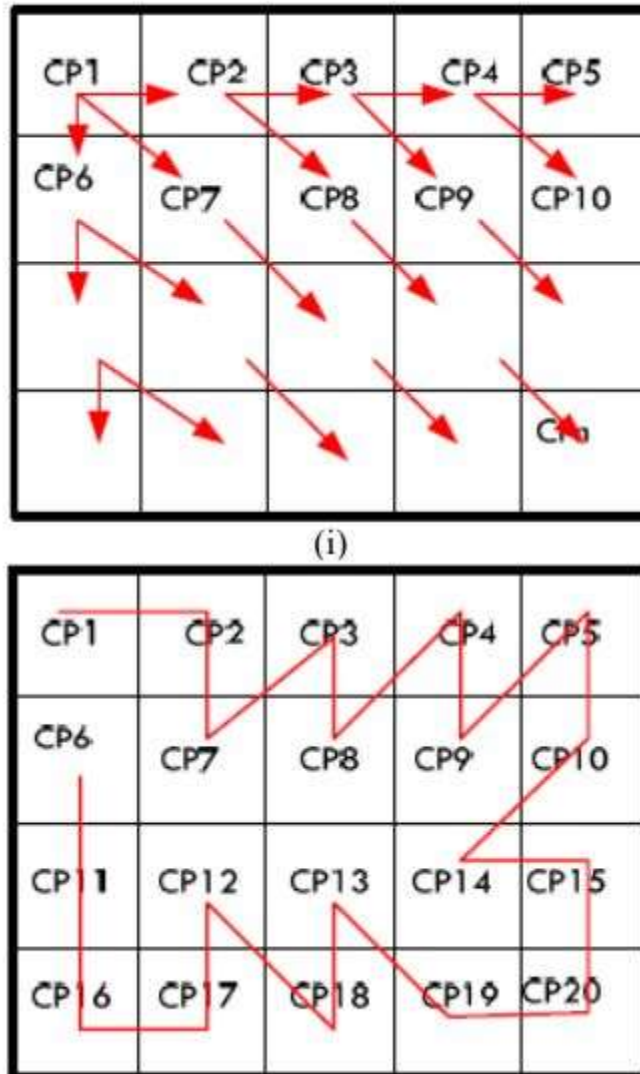
6231

Figure 2. Example depicting malicious node coordination

B. Dependencies and Assumptions

The core assumptions of the proposed framework are given below:

i. Malicious nodes can be rational regarding their targets.

ii. Malicious nodes are correctly modeled, i.e., they do not show any indications of selfishness in any game-stage.

iii. Nodes may trace the outgoing packets of their neighbors (network monitoring mechanism) at a one-hop distance through passive observation.

iv. Observation error may arise but with decidedly less probability.

v. An authentication scheme is assumed to exist, and that the identity is confined to the physical node that cannot be faked or changed in the time the node stays in the cluster.

vi. Malicious node is assumed to deport from the cluster where it carried out the attack; it shall also obliterate the entire history of transactions in that cluster with it thereby making the detection process really challenging.

vii. The trust of the mobile nodes cannot be monitored external to the cluster.

viii. Since the proposed study has been performed considering a multi-stage game, thus the time factor is supposed to be classified into slots, and every slot represents the present game stage progress.

6232

ix. Malicious nodes do not perform an attack in the initial game stages for maximizing their utility by decamping the regular node trust factor.

C. Payoff Formulation

For payoffs, the result of the players is presented in the numeric form. It evaluates the performance or utility of the player. The comprehensive procedure for the formulation of payoff is given below:

1. For a regular stranger node, the target shall acquire 'a' payoff value when it trusts, where a > 1.
2. For a malicious stranger node attacking the target successfully, it shall result in damage to the target equivalent to 'a'.
3. If the stranger is suspected by the target node, it shall cost 1.
4. If there is a genuine doubt, the target node shall attain 'b' amount of the response message, somewhere b lies between 0 and 1.
5. If the trust is not valuable, the aim shall lose 'b' total of payoff.
6. If stranger node is malicious but feigns to be standard as the game proceeds.
7. The stranger node is deemed as the sender, and the target node is considered as the receiver.

The payoffs measure the strategy of players in subsectionA. In the BS game model, C is dominated by a stranger's strategy D because if the end node selects the trust, then the payoff value is 3 while selecting D and 2 when selecting C. If the end node selects doubt, the node receives-1 for D as opposite to 0 for C.

Therefore, D is the better result. Likewise, end nodes elect the strategy of doubt dominating trust.

D. Evaluating the Payoffs

In the BS approach, payoffs stimulate the specific players who are performing misbehavior actions that search for the better result of the game.

It can represent cardinal or ordinal payoffs, and payoffs are calculated using a payoff matrix. The decision maker estimates the best outcomes. Dual players are performed in this game model, including Sn and Rn. The sender node selects an action from the set of action space for forwarding the information 'i' to the receiver. The receiver notices this message 'i' and replies to it by selecting an action from the action set. The receiver does not contain any private message, so it contains a solo type node information.

The recipient already knows the sender's personality. The receiver then acts, assigning payoffs according on the Sn's message type. The receiver responds to the sender with a node type. The expected payout includes the player's attitude toward a probable threat. Every participant gets a reward based on their own and their neighbours' activities.

Table II overviews the payoffs of regular as well as malicious nodes. Here, SM stands for 'signaling malicious,' and PS stands for'prefers to send' The predictable payoff is measured as a product probability of the type of node and the payoff of every action selected. If the estimated payoff is high, the matching action is elected as a receiver-action and a sender-action. The sender's predictable utility is a mixture of its payoffs to pure strategy by the receiver.

6233

Table II. Rewards for both good and bad nodes

Node Type		R Action	
Normal Node	Malicious Node	Co-operate	Decline
SM	SM	0, 0	0, 0
SM	PS	P, 0	p-1, p-1
PS	SM	P, p	P, 0
PS	PS	1, p	-1, p-1

Depending on the kind of receiver, the sender must pick just one action: either to cooperate

(C) or to deny (D) the message. The activities are C, D, and report because the receiver is

regarded as a typical node in the network. The decrease indicates that a node has discarded participation, while co-operation indicates that a node has made itself available for communication. The sender may engage in a simple dropping packet attack, which is equivalent to the mechanism used by regular nodes to reject packets. Normal nodes do not get any results from D, but sender nodes generate the reward value from the malicious node, and vice versa. The benefit SM is provided by the receiver if he chooses a report, and if the sender is malicious, normal nodes build PS from an effective C, where the gains PS and SM are rising for the cooperate and report, respectively. In addition, such nodes may pick (D) refuse, which results in no cost and zero gain even if the opponent decides to attack. While the receiver does not react to the message delivered by the sender, it does tell the surrounding nodes whether the information received from the sender is harmful or not. The receiver decides on the decline action depending on the BE strategy that has been applied.

The sender gives guidance on how to deliver the message. In response to the sender's communication, the receiver picks action C or D. Regardless, the optimal reaction from the recipient is to accept the communication regardless of the sender's categorization. Because the receiver's message set is never comprehended by strategy profiles C and D, this message is not captured.

V. IMPLEMENTATION AND RESULT

5.1 Implementation

In this section we have to explain about harsware and software configuration with proposed simulation parameters.

Table 1. Hardware and software configuration.

Component	Specification (per node)
CPU	2.10GHz
RAM	4
Hard disk storage	1TB

Table 2. Software configuration.

Component	Specification
OS	Windows 10
Virtual Machine	VM ware
Compiler	GCC
Simulator	NS2

Table 3. Proposed simulation parameters.

Parameter	Value	Parameter	Value
Power	20 dBm	Number of node	50,100,…,500
Numerology	1	Distance between nodes	10m
Bandwidth	100MHz	Maximum communication distance	60m
Scenario	UMa	Initial energy of each node	100J
Data Rate	2,4,8,16,32,64,128,256 Mbps	Minimum energy threshold of nodes	1J
No of Malicious Nodes	9,18,……,90	Speed	10m/s 20m/s 30m/s …
Moving Module	Constant Speed	Scheduler Algorithm	Round Robin

5.2 Result : In this section, we have explained about results generated by the NS2 simulator. Results are calculated with 5 parameters in each setup. Results are calculated in four different scenarios, like a number of nodes, mobility, energy, and a number of malicious nodes.

5.2.1 Performance metrics

1) Throughput

The throughput (TP) of a network is equal to the total of the data sent to the based station divided by the time it takes to simulate the network [33].

$$AT = (number\ of\ bytes\ received * 8/\ simulation\ time) * 1000kbps \qquad (1)$$

2) Average end-to-end delay

The average end-to-end delay (AED) is the total amount of time it takes for all data chunks to transit from the source nodes to the base station on average.

The term "end-to-end delay" refers to the time it takes a packet to transit from its point of origin to its point of destination [33].

$$e2edelay = \frac{\sum_{i=1}^{n}(R_i - S_i)}{n} \qquad (2)$$

6235

3) Packet delivery ratio

The PDR is the ratio of data packets transmitted to data packets received at a certain period of time [33].
According to mathematical definition, it is as follows:

$$PDR = \frac{number\ of\ packets\ recieved}{number\ of\ packets\ sent} * 100 \qquad (3)$$

4) Routing overhead
The amount of repetitions between all designing pathways and SDPs (or MEPs) is used to determine the effectiveness of the proposed routing algorithm in terms of optimization efficiency. The repetition ratio calculated using SDP has an effect on the degree of transmission delay. The MEP-based repetition ratio indicates the capacity of the sensor nodes to balance the remaining energy they have available.

5) Energy consumption
For each loop, we compute the total energy consumption to study the link between the longevity and other Key variables.

5.2.2 Network scenarios based on number of nodes
In this section figure 1,2,3,4,5 respectively throughput, average end to end delay, packet delivery ratio, routing overhead, and Energy consumption based on a number of nodes. All these parameters proposed-TAODV better respect to existing-paper_19and existing paper_21.
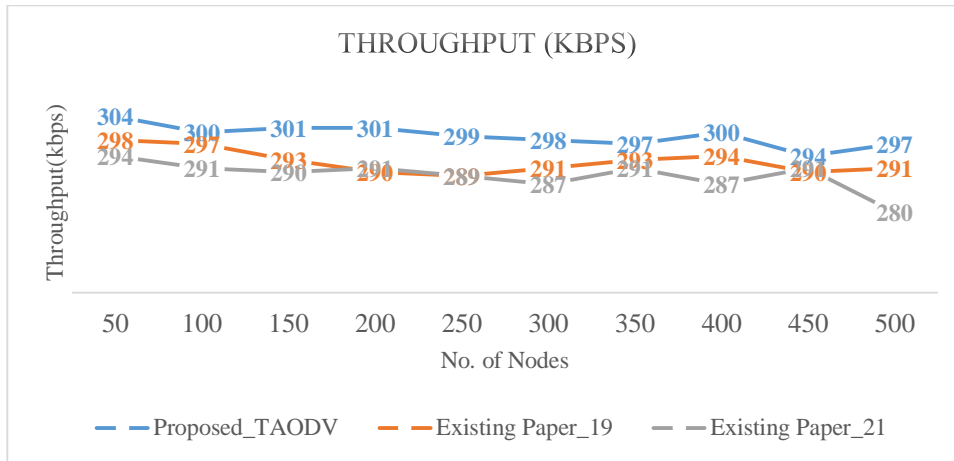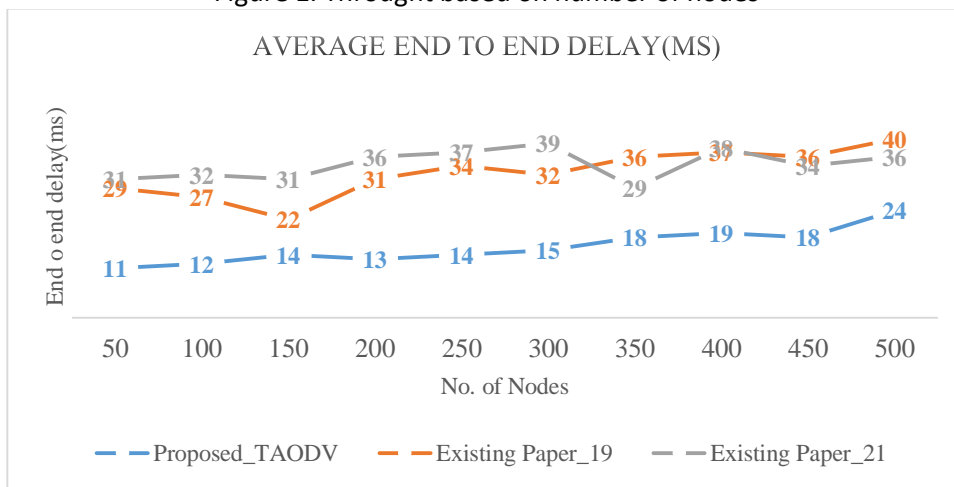
Figure 1. Throught based on number of nodes

Figure 2. Average end to end delay based on number of nodes
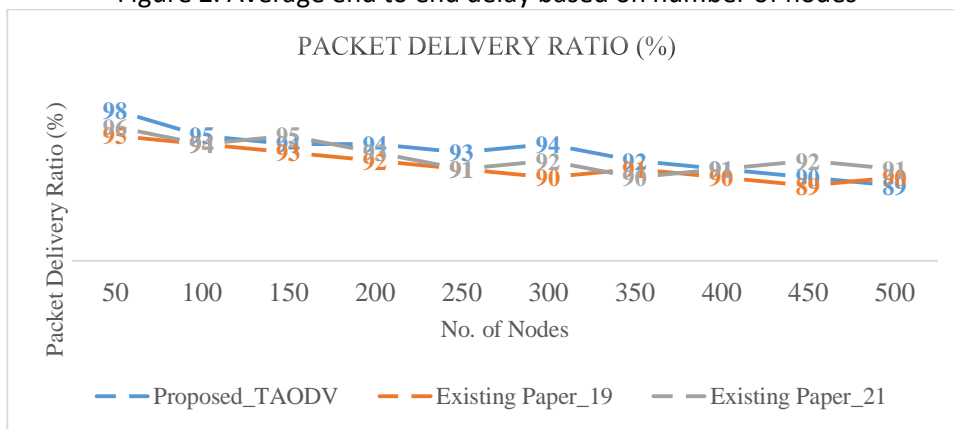

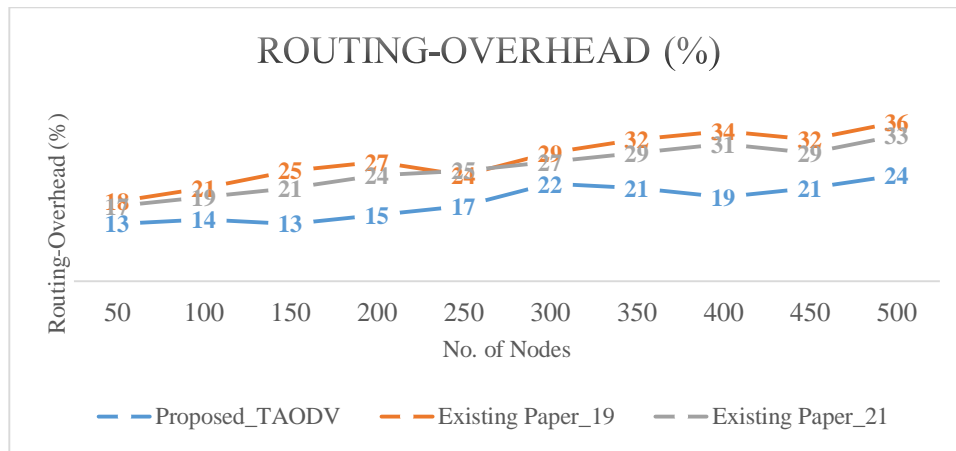Figure 3. Packet delivery ratio based on number of nodes

6236

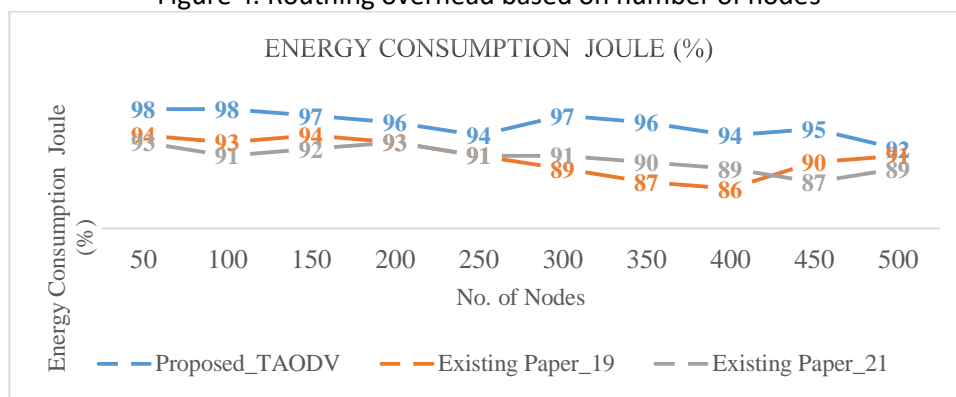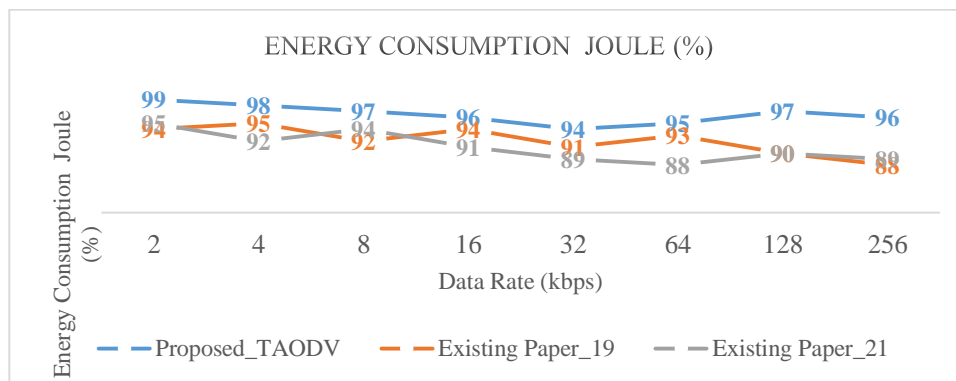Figure 4. Routning overhead based on number of nodes

Figure 5. Energy consumption based on number of nodes

5.2.3 Network scenarios based on data rate

In this section figure 1,2,3,4,5 respectively throughput, average end to end delay, packet delivery ratio, routing overhead, and Energy consumption based on data rate. All these parameters proposed-TAODV better respect to existing-paper_19and existing paper_21.
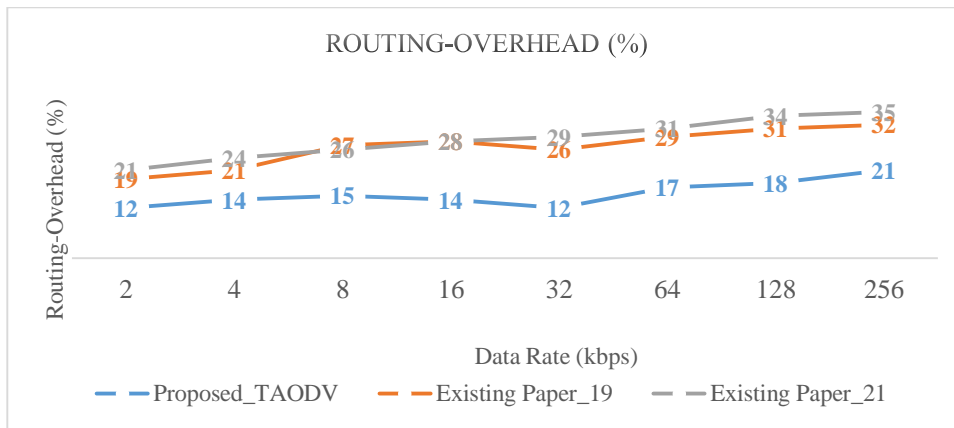
6237

Figure 6 Energy consumption based on data rate
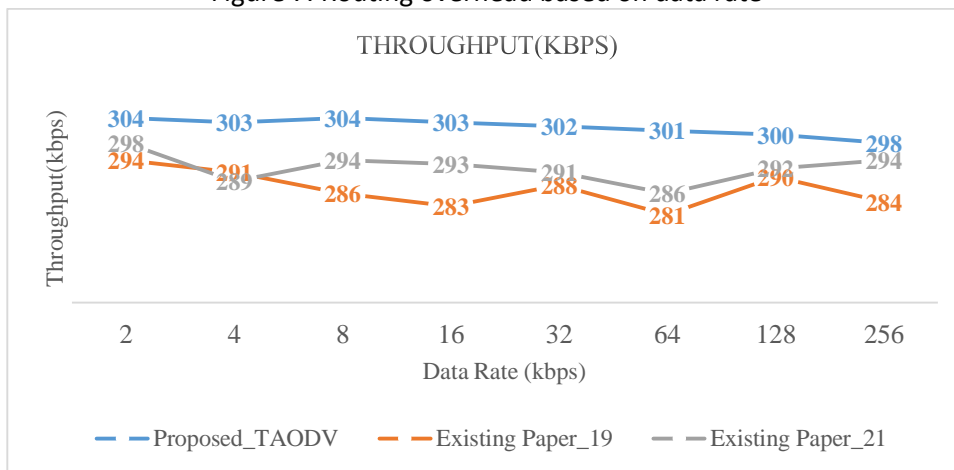
Figure 7. Routing overhead based on data rate
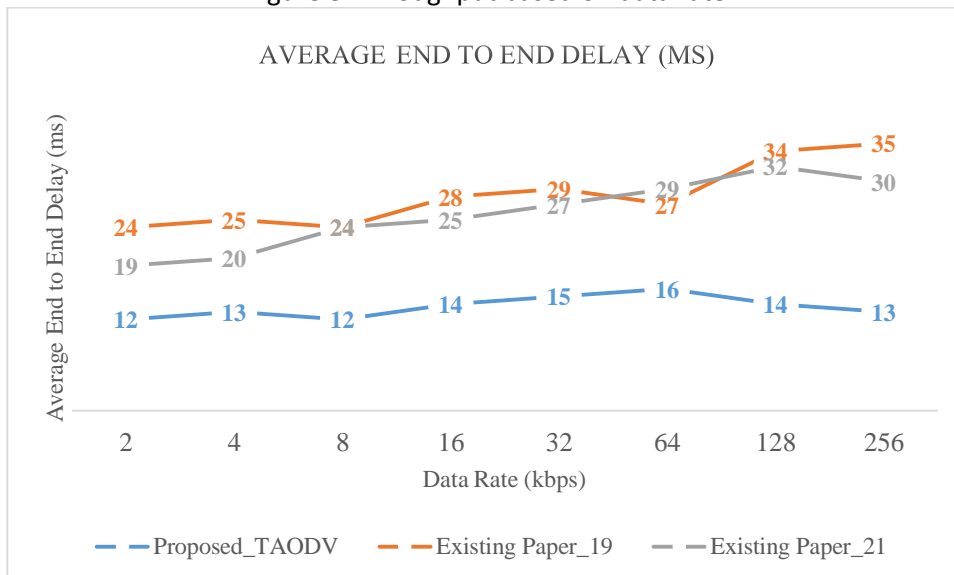
6238

Figure 8. Throughput based on data rate

Figure 9. Average end to end delay based on data rate

Neha Khandelwal et al/ Trust-based Secure IoT Architecture in Mobile Ad-hoc Network Against Malicious attacks
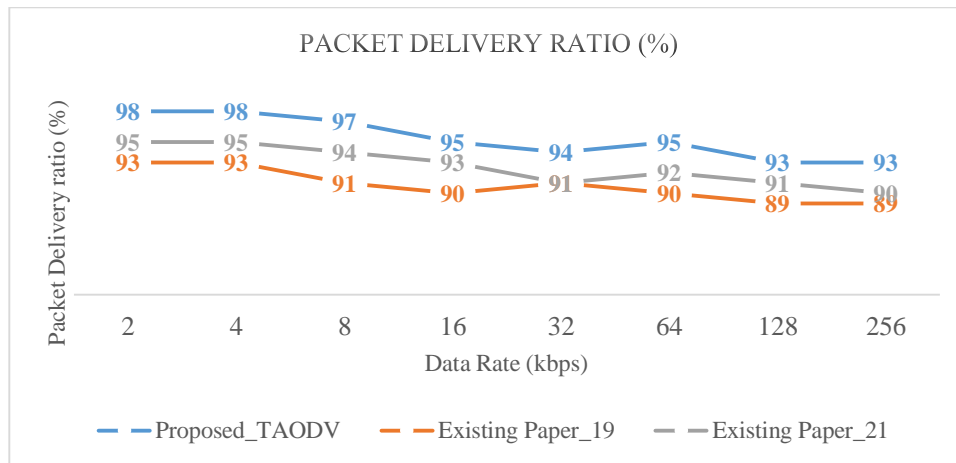

Figure 10. Packet delivery ratio based on data rate

5.2.4 Network scenarios based on node mobility (meter/second)

In this section figure 1,2,3,4,5 respectively throughput, average end to end delay, packet delivery ratio, routing overhead, and Energy consumption based on node mobility. All these parameters proposed-TAODV better respect to existing-paper_19and existing paper_21.
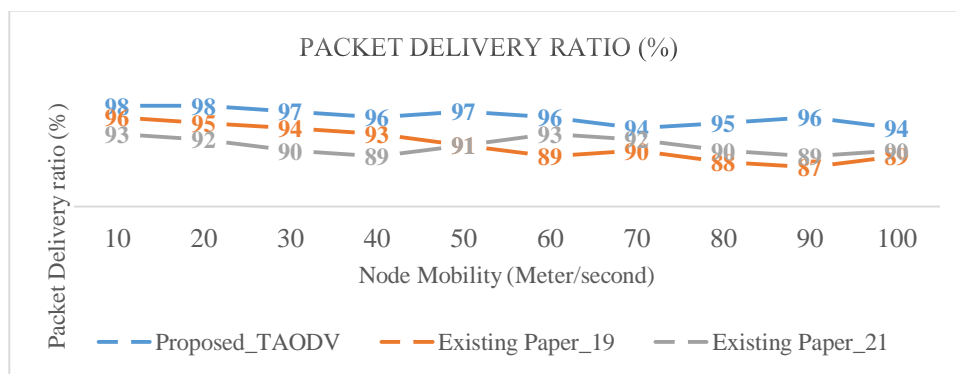

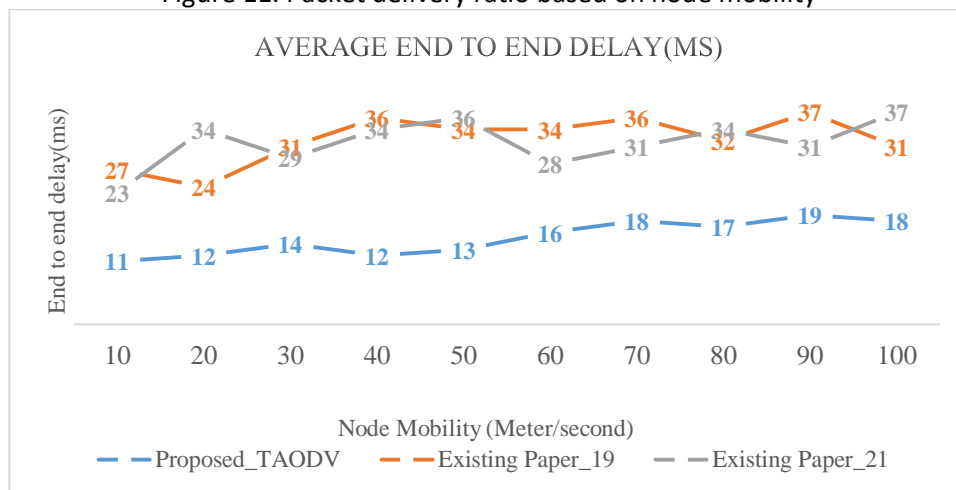Figure 11. Packet delivery ratio based on node mobility

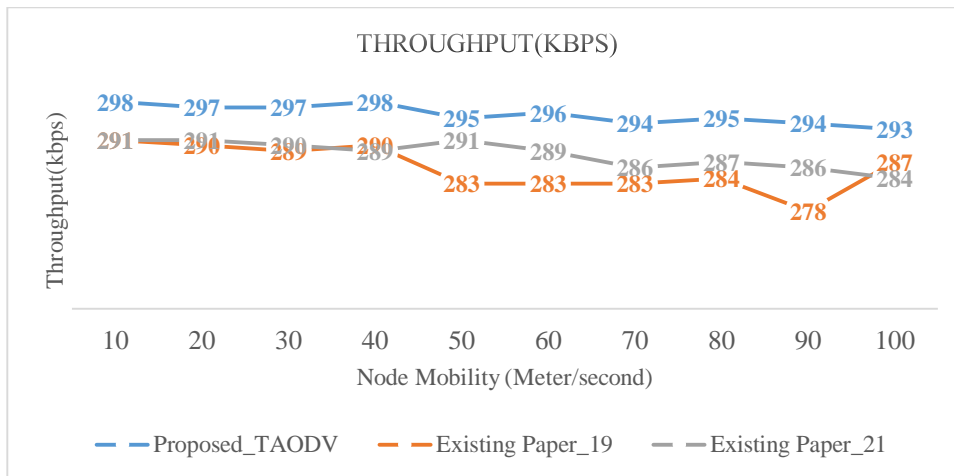Figure 12. Average end to end delay based on node mobility

6239

www.neuroquantology.com

Page 49

Neha Khandelwal et al/ Trust-based Secure IoT Architecture in Mobile Ad-hoc Network Against Malicious attacks

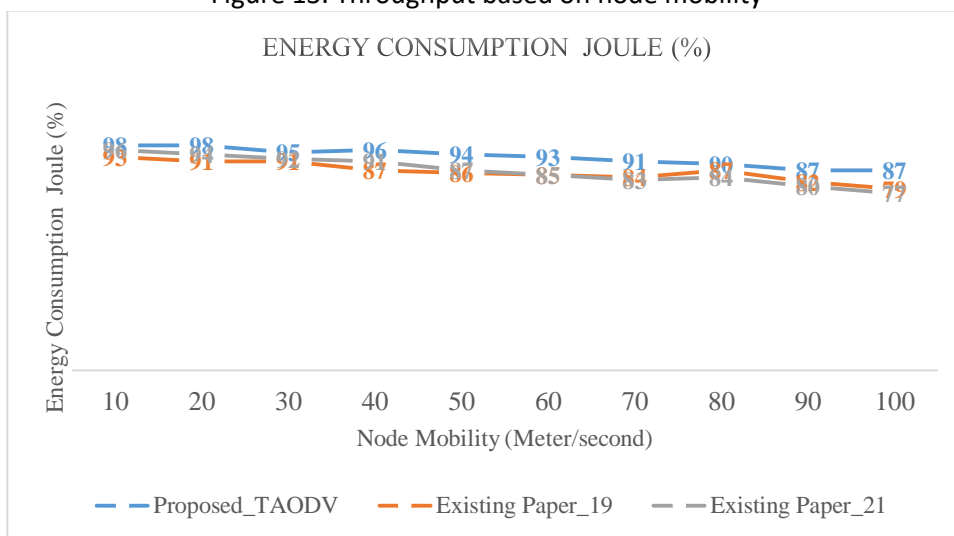Figure 13. Throughput based on node mobility
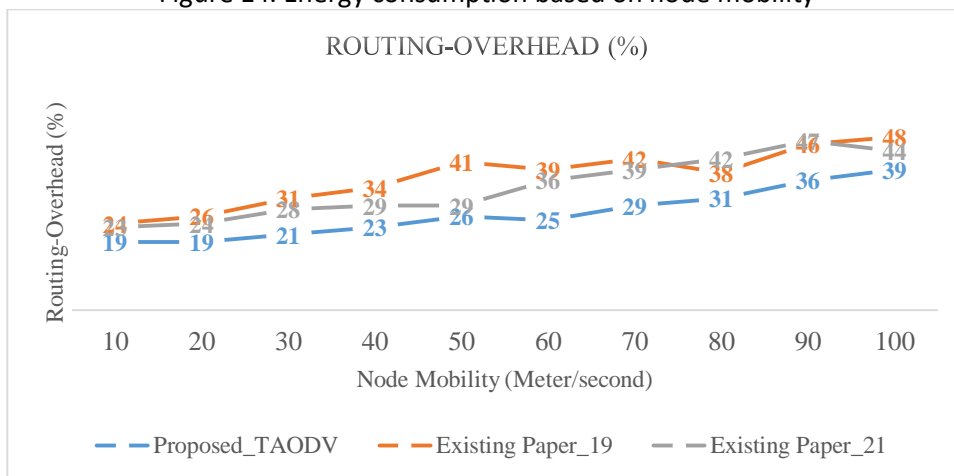

Figure 14. Energy consumption based on node mobility

6240

Figure 15. Routing overhead based on node mobility

5.2.5 Network scenarios based on number of malicious nodes

In this section figure 1,2,3,4,5 respectively throughput, average end to end delay, packet delivery ratio, routing overhead, and Energy consumption number of malicious nodes. All these parameters proposed-TAODV better respect to existing paper_19 and existing paper_21.
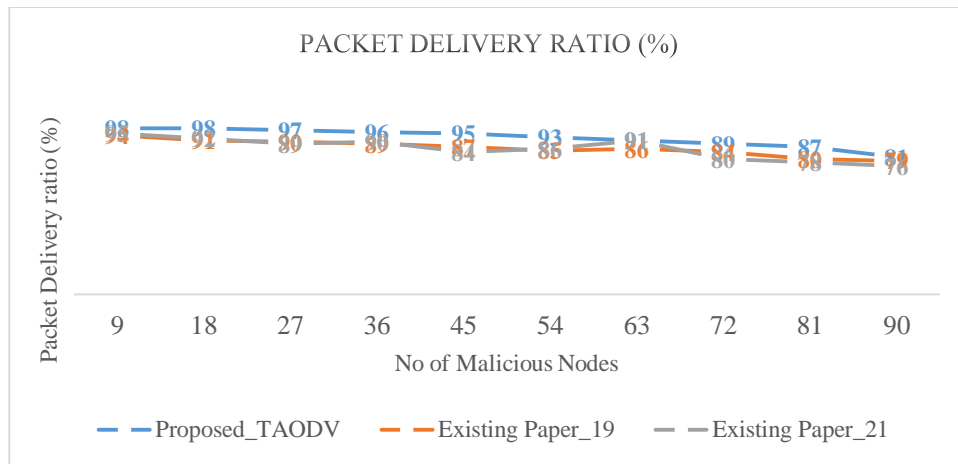

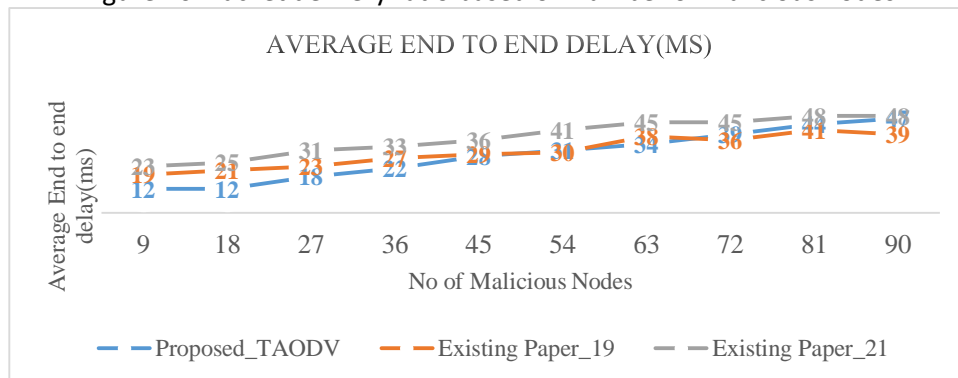Figure 16. Packet delivery ratio based on number of malicious nodes

Figure 17. Average end to end delay based on number of malicious nodes
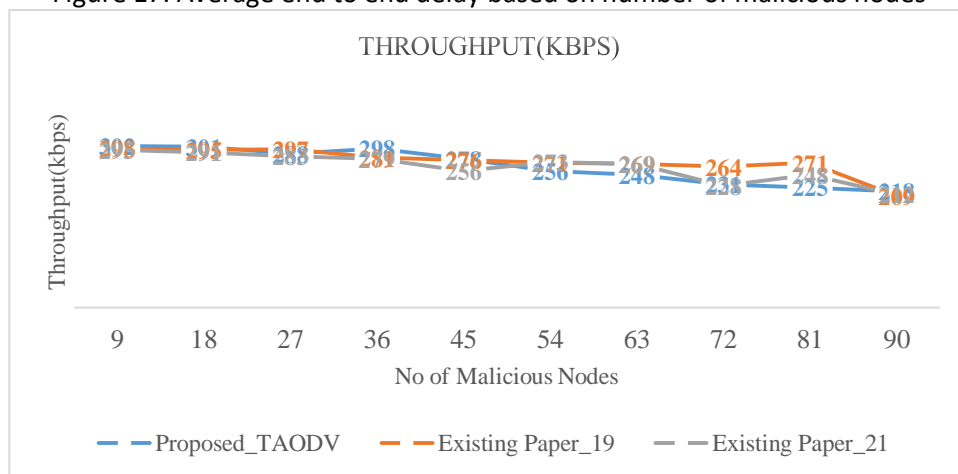

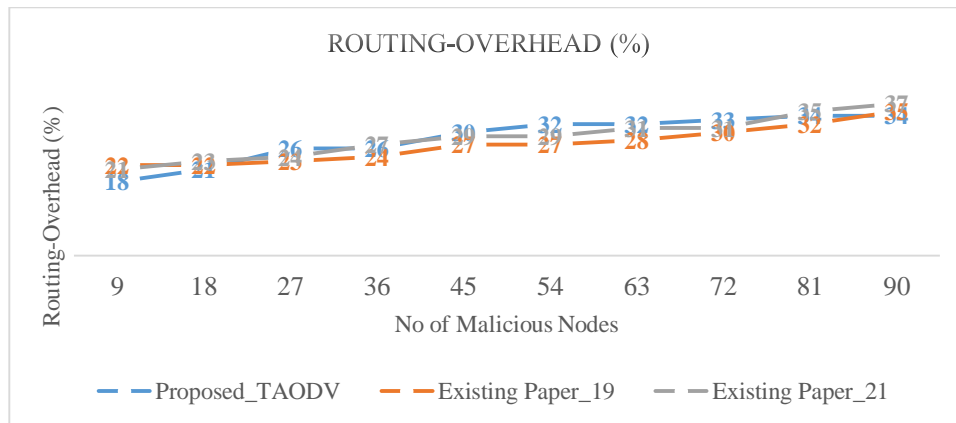Figure 18. Throughput based on number of malicious nodes

6241

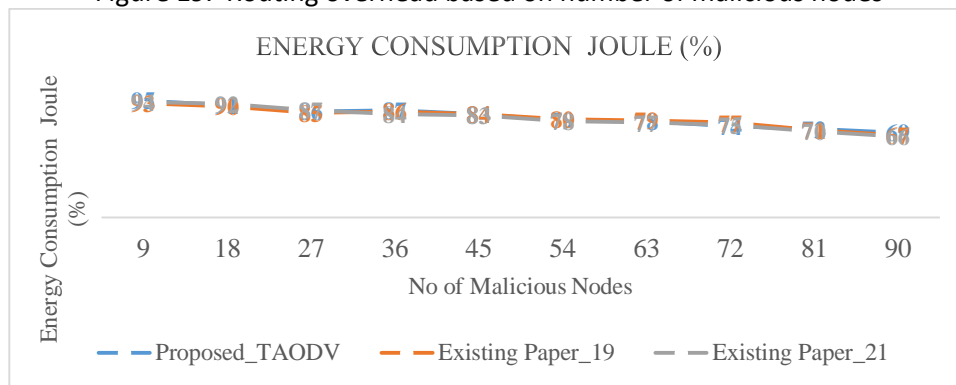Figure 19. Routing overhead based on number of malicious nodes

Figure 20 Energy consumption based on number of malicious nodes

VI. CONCLUSION

This study provides a Bayesian-Signaling (BS) game approach which finds out the malicious actions and behaviors in MANETs. It also provides a solution of the model and generates the threshold values which will be further considered for the designing of a secure routing protocol for MANETs. The BS game model is a type of sub-game which subsequently plays and is regarded as an optimum solution for the detection of malicious attacks. This system considered both regular and malicious nodes for the experimental analysis. If it is a malicious node, the co-operation among the nodes is quite less, and it can worsen the network's performance. Hence, the BS game model was adopted to protect the packet dropping attacks. The regular/normal node in the MANET continuously follows the belief revision process for self-information, then selects the probability to co-operate with its corresponding nodes and considers the BS decision rule to convey the nature of node. The proposed ECM-GT model also examined the strategies of nodes (regular and malicious nodes), and the motive was to diminish the malicious node utility and maximize the utility of regular node by applying Bayesian signaling approach. This system proved better than the existing system and can thus be applied for a safer and more reliable operation in micropayments in the ad-hoc wireless network.

6242

Reference

[1] C. Withanage, R. Ashok, C. Yuen, K. Otto, A comparison of the popular home automation technologies, in: Innovative Smart Grid Technologies-Asia (ISGT Asia), 2014 IEEE, IEEE, 2014, pp. 600–605.

[2] J. Zheng, M.J. Lee, A comprehensive performance study of ieee 802.15. 4, Sensor Netw. Oper. 4 (2006) 218–237.

[3] M. D. Sirajuddin, C. Rupa, and A. Prasad, "Advanced Congestion Control Techniques for MANET," Advances in Intelligent Systems and Computing, vol. 433, pp. 271–279, 2016.

[4] L. Femila and M. Marsaline Beno, "Optimizing transmission power and energy efficient routing protocol in MANETs," Wireless Personal Communications, vol. 106, no. 3, pp. 1041– 1056, 2019.

[5] B. Chen, J. Wan, L. Shu, L. Peng, M. Mukherjee, and B. Yin, "Smart factory of Industry 4.0: key technologies, application case, and challenges," Institute of Electrical and Electronics Engineers Access, vol. 6, 2018.

[6] H. Kathiriya, A. Pandya, V. Dubay, and A. Bavarva, "State of art: energy efficient protocols for self-powered wireless sensor network in IIoT to support industry 4.0," in Proceedings of the 2020 8th International Conference on Reliability, Infocom Technologies and Optimization (Trends and Future Directions) (ICRITO), pp. 1311–1314, Noida, India, June 2020.

[7] T. Li, J. Ma, and C. Sun, "SRDPV: secure route discovery and privacy-preserving verification in MANETs," Wireless Networks, vol. 25, no. 4, pp. 1731–1747, 2019.

[8] T. Singh, J. Singh, and S. Sharma, "Survey of secure routing protocols in MANET," International Journal of Mobile Network Design and Innovation, vol. 6, no. 3, pp. 142–155, 2016

[9] S. Hossain, M. S. Hussain, R. R. Ema, S. Dutta, S. Sarkar, and T. Islam, "Detecting Black hole attack by selecting appropriate routes for authentic message passing using SHA-3 and Diffie-Hellman algorithm in AODV and AOMDV routing protocols in MANET," in Proceedings of the ICCCNT, pp. 1–7, Kanpur, India, June 2019.

[10] S. Hossain, M. S. Hussain, R. R. Ema, S. Dutta, S. Sarkar, and T. Islam, "Detecting Black hole attack by selecting appropriate routes for authentic message passing using SHA-3 and DiffieHellman algorithm in AODV and AOMDV routing protocols in MANET," in Proceedings of the ICCCNT, pp. 1–7, Kanpur, India, June 2019.

[11] H. Moudni, M. Er-rouidi, H. Mouncif, and

[1] B. El Hadadi, "Secure routing protocols for mobile ad hoc networks," in Proceedings of the IT4OD, pp. 1–7, Fez, Morocco, March 2016.

[12] F. Abdel-Fattah, K. A. Farhan, F. H. Al-Tarawneh, and F. AlTamimi, "Security challenges and attacks in dynamic mobile ad hoc networks MANETs," in Proceedings of the JEEIT, pp. 28–33, Amman, Jordan, April 2019.

[13] W. Li, W. Meng, L. Kwok, H.H. Ip, PMFA: toward passive message fingerprint attacks on challenge-based collaborative intrusion detection networks, in: Network and System Security - 10th International Conference, NSS 2016, Taipei, Taiwan, September 28-30, 2016, Proceedings, 2016, pp. 433–449,

[14] W. Meng, X. Luo, W. Li, Y. Li, Design and evaluation of advanced collusion attacks on collaborative intrusion detection networks in practice, in: 2016 IEEE Trustcom/BigDataSE/ISPA, Tianjin, China, August 23-26, 2016, 2016, pp. 1061–1068

[15] W. Li, W. Meng, L.F. Kwok, Investigating the influence of special onoff attacks on challenge-based collaborative intrusion detection networks, Future Internet 10 (1) (2018) 6

[16] G. Rathee, S. Garg, G. Kaddoum and B. J. Choi, "Decision-Making Model for Securing IoT Devices in Smart Industries," in IEEE Transactions on Industrial Informatics, vol. 17, no. 6, pp. 4270-4278, June 2021, doi: 10.1109/TII.2020.3005252.

[17] J. Chen, C. Touati and Q. Zhu, "Optimal Secure Two-Layer IoT Network Design," in IEEE Transactions on Control of Network Systems, vol. 7, no. 1, pp. 398-409, March 2020, doi: 10.1109/TCNS.2019.2906893.

[18] S. Malani, J. Srinivas, A. K. Das, K. Srinathan and M. Jo, "Certificate-Based Anonymous Device Access Control Scheme for IoT Environment," in IEEE Internet of Things Journal, vol. 6, no. 6, pp. 9762-9773, Dec. 2019, doi: 10.1109/JIOT.2019.2931372.

[1] Mohammad Sirajuddin, Ch. Rupa ,

6243

9] Celestine Iwendi , and Cresantus Biamba , "TBSMR: A Trust-Based Secure Multipath Routing Protocol for Enhancing the QoS of the Mobile Ad Hoc Network" , Hindawi Security and Communication Networks Volume 2021, Article ID 5521713, 9 pages https://doi.org/10.1155/2021/5521713

[20] Jun Jiang, Yuhong Liu , "Secure IoT Routing: Selective Forwarding Attacks and Trust-based Defenses in RPL Network" , Networking and Internet Architecture (cs.NI) ,arXiv:2201.06937

[21] LiangLiu,ZuchaoMa,WeizhiMeng , "Detection of multiple-mix-attack malicious nodes using perceptron-based trust in IoT networks" , Future Generation Computer Systems , Volume 101, December 2019, Pages 865-879.

[22] Serin V.Simpson , G.Nagarajan , "A fuzzy based Co-Operative Blackmailing Attack detection scheme for Edge Computing nodes in MANET-IOT environment" , Future Generation Computer Systems Volume 125, December 2021, Pages 544-563.

[23] MohammedAmoon, TorkiAltameem , AymanAltameem , "RRAC: Role based reputed access control method for mitigating malicious impact in intelligent IoT platforms" , Computer Communications Volume 151, 1 February 2020, Pages 238-246

[24] Pallavi Kaliyar , Wafa BenJaballah , Mauro Conti , Chhagan Lal , "LiDL: Localization with early detection of sybil and wormhole attacks in IoT Networks " , Computers & SecurityVolume 94, July 2020, 101849

[25] Sowmya Kudvaa Shahriar Badshaa Shamik Senguptaa Hung Laa Ibrahim Khalilb Mohammed Atiquzzaman , "A scalable blockchain based trust management in VANET routing protocol ", Journal of Parallel and Distributed ComputingVolume 152, June 2021, Pages 144-156

[26] DiLu, Ruidong Han, Yue Wang, Yongzhi Wang, Xuewen Dong, Xindi Ma, TengLi, Jianfeng Ma,"A secured TPM integration

scheme towards smart embedded system based collaboration network " , Computers & SecurityVolume 97, October 2020, 101922.

[27] Deebak B D , Fadi Al-Turjman , "A Hybrid Secure Routing and Monitoring Mechanism in IoT-based Wireless Sensor Networks", Ad Hoc NetworksVolume 97, February 2020, 102022 , Ad Hoc Networks (2019), doi: https://doi.org/10.1016/j.adhoc.2019.102022

[28] Rajasoundaran, S., Kumar, S.V.N.S., Selvi, M. et al. Machine learning based volatile block chain construction for secure routing in decentralized military sensor networks. Wireless Netw 27, 4513–4534 (2021). https://doi-org.libproxy.viko.lt/10.1007/s11276-021-02748-2

[29] K. A. Awan, I. Ud Din, A. Almogren, M. Guizani and S. Khan, "StabTrust—A Stable and Centralized Trust-Based Clustering Mechanism for IoT Enabled Vehicular Ad-Hoc Networks," in IEEE Access, vol. 8, pp. 21159-21177, 2020, doi: 10.1109/ACCESS.2020.2968948.

[30] M.S. Abdalzaher, K. Seddik, M. Elsabrouty, O. Muta, H. Furukawa and A. Abdel-Rahman, "Game theory meets wireless sensor networks security requirements and threats mitigation: A Survey," Sensors, vol. 16, no. 7, p. 1003, 2016.

[31] A. Ilavendhan and K. Saruladha, "Comparative study of game theoretic approaches to mitigate network layer attacks in VANETs," ICT Express, vol. 4, no. 1, pp. 46-50, 2018.

[32] R. F. Olanrewaju, B. U. I. Khan, F. Anwar, R. N. Mir, M. Yaacob and T. Mehraj, "Bayesian Signaling Game Based Efficient Security Model for MANETs", in Lecture Notes in Networks and Systems series, K. Arai and R. Bhatia, Ed. Switzerland: Springer, Cham, 2019, pp. 1106-1122.

[33] TahaA,AlsaqourR,UddinM,AbdelhaqM,SabaT(2017)Energy efficient multipath routing protocol for mobilead-hoc network using

6244

the fitness function. IEEE access5:10369–
10381

6245

ANALYTICAL AND EXPERIMENTAL STUDYON BEHABIOUR OF DOUBLE SKIN HOLLOW CONCRETE FILLED STEEL SQUARE TUBE BEAM UNDER BENDING USING FEM

Goutam Varma[1], Dr. Arafat Rehman[2], Dr. Jyoti Yadav[3],

1- *Ph.D, Scholar*, *2-Assitant Professor Civil Engineering Department, SRK University, Bhopal*

3 Assistant Professor & Head Civil Engineering Department, SRK University, Bhopal

Abstract: The concrete filled steel tubular (CFST) beam is the most commonly used one. Owing to their structural benefits such as reduced cross section, high strength, improved fire resistance, greater apparent stiffness and excellent seismic resistant structural properties. For a variety of reasons such as fire, ageing, environmental degradation and overloading, the infrastructure concerned with concrete filled tubular and other metallic structures become structurally unsatisfactory. Therefore, actions like implementation of strengthening techniques with the new materials become essential to combat this problem. Due to their in-service and superior mechanical properties such as high strength and stiffness, double skin Hollow concrete filled steel tubular (DSHCFST) composites make them excellent material for repairing, upgrading and retrofitting of metallic structure. This paper, study has been carried out to investigate the suitability of Double skin Hollow concrete filled steel tubular (DSHCFST) for strengthening of concrete sections under flexure. A Finite Element Model (FEM) has been developed using ANSYS to analyse beam with concrete filled steel tube beam and the Experimental results study was carried out by applying two points loading. Thus the flexural behavior of both the results are compared and analysed.

Index Terms - Double skin hollow concrete filled steel tubular (DSHCFST), FEM, and ANSYS.

I. INTRODUCTION

The flexural behaviour of square Double skin Hollow concrete filled steel tubular (DSHCFST) and more recently, some research related to strengthening of CFST beam members using double tube composites have been reported. It is a rather simple and economical approach to meet the increased load carrying capacity for a structure. The external and internal bonding of two tube composites under increased load conditions reveals a reduced deflection and better enhancement in moment carrying capacity and increases ductility. Also use of double tube offers several advantages like bonding to curved or irregular surfaces and flexibility to orient in a desired direction for strengthening.

In this study, another part of investigation focused on the effectiveness of the Double skin Hollow concrete filled steel tubular (DSHCFST) composites under flexural loading and aimed to develop optimum hollowness ratio that can be used to make these structures and also to study the effect of increase in number of steel layers in enhancing the moment carrying capacity. Different types of tubes were introduced. Furthermore, to eliminate the galvanic corrosion between steel tube and CFRP, a thin layer of red oxide was introduced between steel and concrete.

Beams were tested under two point loading until failure to understand the influence of double tube in flexural behaviour of CFST beam members. Failure modes of each strengthened beams were observed and also the enhancement in moment carrying capacity and reduction in mid-span deflection were also addressed. Since the Finite Element Method has reached a state of maturity, numerical simulation is an alternative method to validate with the experimental results and understand the behavior of Double skin Hollow concrete filled steel tubular (DSHCFST) members. As a result, the present investigation also focused on modeling of Double skin Hollow concrete filled steel tubular (DSHCFST) strengthened beams using

ANSYS 16.0. On the basis of experimental observations, a three-dimensional finite element model was developed to predict the load–deformation behavior of Double skin Hollow concrete filled steel tubular (DSHCFST) members in which all the structural parameters and nonlinear properties of concrete, steel were included.

<div align="center">II. OBJECTIVE</div>

In previous works and available literatures the comparison between solid and hollow tube is not considered properly. Very less work is done for confinement of concrete by using two steel tubes to increase confinement; Very less work is done for CFST under flexural loading using two steel tubes. Hence the objectives of this study are

1. To make comparison between structural behaviour of solid and hollow tube under different loading.
2. To describe structural behavior of double skin hollow concrete filled steel tube under flexural loading.
3. To compare the analytical and experimental results of DSHS-CFST.

<div align="center">III. METHODOLOGY</div>

The concrete filled steel tubular beam can improve the flexural strength, Reduce cross section of the beam and more effective in RC beam, when compared concrete filled steel tube section. Reduced cross section, high strength, improved fire resistance, greater apparent stiffness and excellent seismic resistant structural properties like high ductility and energy absorption, the use of (DSHS-CFST) beams. The software ANSYS is used to analyze the concrete filled steel tubular beam using (DSHS-CFST) composites. Two types of investigation will be done in this study one is experimental and another is analytical study.

<div align="center">**Modeling and Analysis**</div>

Experimental Investigation

The objectives of this project are to assess the feasibility of strengthening of Double skin Hollow concrete filled steel tubular (DSHCFST) members subjected to flexural loading and to develop an adequate double tube for in-air applications. The materials used in the present investigation and their properties are briefly discussed below.

Mix Design

Mix design for M20 grade concrete by Indian Standard recommended of concrete mix design as per design code IS: 10262- 2009. The mix designs are considered the normal beam and CFST beams. Six concrete cubes were prepared mix proportion **1:2.21:4.02** and water-cement ratio 0.51. Cubes were cured in water and 28 days compressive strength was determine by digital compressive strength testing machine.

<div align="center">**Table 1: Mix Design of concrete**</div>

Water	Cement	Fine Aggregate	Coarse aggregate
160	380 kg	711 kg	1283 kg
0.42	1	1.87	3.38

<div align="center">**Compressive Strength Test**</div>

Cube of size 150x150x150 mm were cast. Three specimens were made and tested for 28 days.

Specimen No.	Compressivestrength(N/mm^2)
1	22.06
2	22.3
3	22.4
Average	22.3

Compressive Strength = load /area (N/mm²)
The compressive strength test results of three specimens. Average compressive strength of cube 22.3**(N/mm²)**.

Conventional Beam

Conventional beam is developed of length 1000 mm and cross section of the beam is 150 x 150 mm. Where the mix design of M20 are used concrete as per IS: 456-2000 and IS 10262-2009.The concrete are mixed with the mix ratio of **1:2.21:4.02**. Where all the side of the beam are moulded properly to prevent concrete from leakage. After mixing, the concrete is poured immediately inside the beam. Concrete is filled in three layers, and each layer is compacted well by using a tamping rod of standard size, so as to avoid entrapped air inside the concrete beam and honey combing effect on the sides. The test specimens after compaction were kept as such for a period of 24 hours. After that period of time the moulds were removed and the specimen are cured. The beam was tested under two point loading. Where the load applied is 50 tons.
 Hot rolled steel tube was used for square section are made of varying dimension and thickness. Yield strength of steel was 250N/mm². The required height of square hollow tubes was cut from 1m length hollow tubes. Inside portion of the hollow steel tubeswere thoroughly wire brushed to remove the rust and loose debris presented. After that period of time the moulds were removed and the specimens were kept in ordinary curing tank and allowed to cure for a period of 14 days.

TWO POINT BENDING TEST SETUP

The beam was tested under two point loading. Where the load applied on (DSHCFST) beam.

Experimental analysis

S.No	LOAD (kN)	DEFLECTION (mm)
1	0	0
2	10	1.7
3	25	4.9
4	30	7.2
5	40	16.4

The DSHCFST beam experimental test results are mentioned below:

Specimen name	Avg. Load Obtained Experimentally in KN	Load Obtained from K.Kwedaras equation in KN	Deflection in mm	Percentage deviation
DSHS-CFST 150x100	255.67	174.96	8.92	68.6
DSHS-CFST 150x75	227.33	166.82	8.80	73.38
DSHS-CFST 150x50	215.00	162.54	7.82	75.6
DSHS-CFST 125x25	160.33	102.21	9.66	63.75
DSHS-CFST 100x25	81.00	36.67	15.48	45.27
DSHS-CFST 75x25	29.33	14.39	16.81	49.06
Average Deviation				62.69

FEM analysis

The analytical investigation of DSHS-CFST beams using ANSYS software. The class focuses on geometry creation and optimization, attachingexisting geometry, setting up the finite element model, solving, and reviewing results.

Modeling of Rectangular Beam

Square beams are analysed using ANSYS Software. Where two point loading is applied up to failure for DSHS-CFST beam. Thebeam of 1000 mm length and cross section of inner tube variation **150 x 100 mm, 150x75mm, 150x50mm,** outer tube variation **125x25mm, 100x25mm, and 75x25mm** were developed.

150 x 100 mm DSHS-CFST
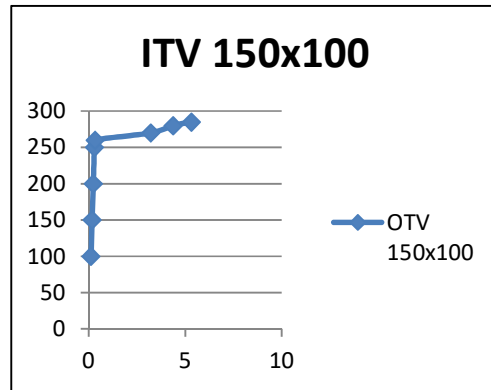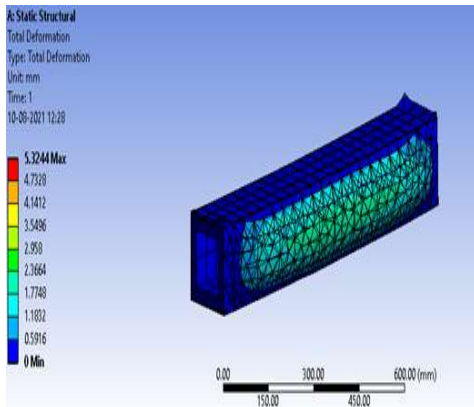
150x75mm DSHS-CFST beam
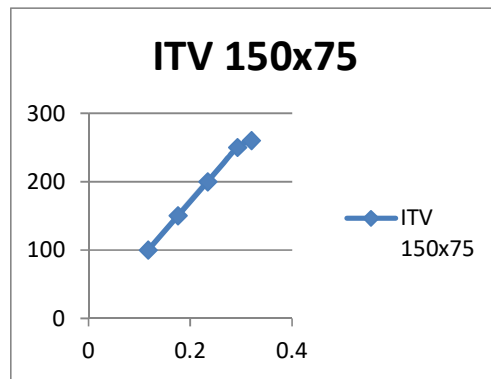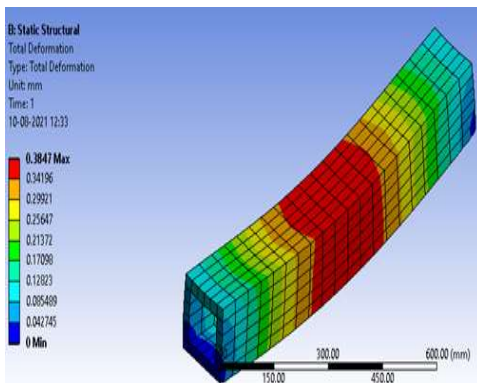
150x50mm DSHS-CFST beam.
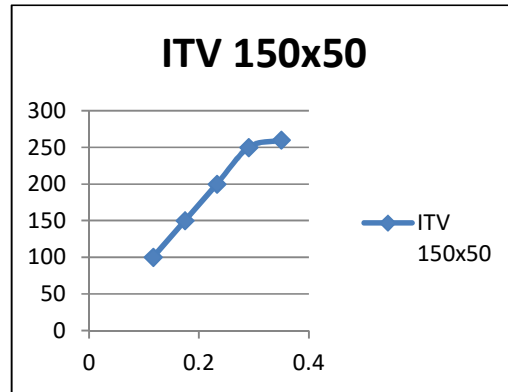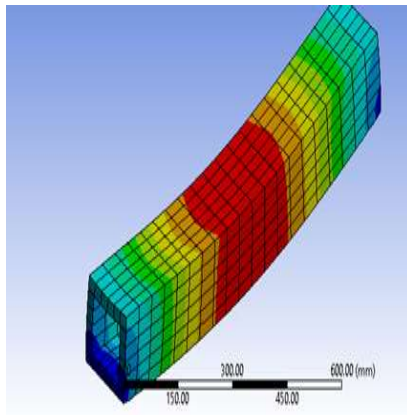
Outer thickness variation

150x25mm DSHS-CFST beam
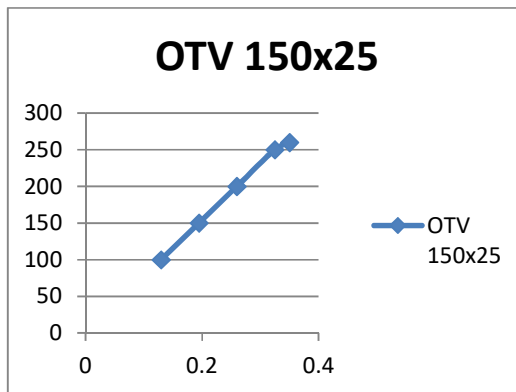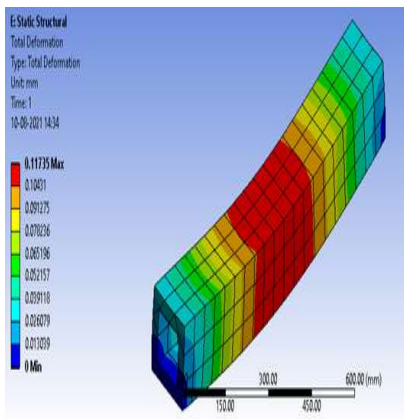
125x25mm DSHS-CFST beam
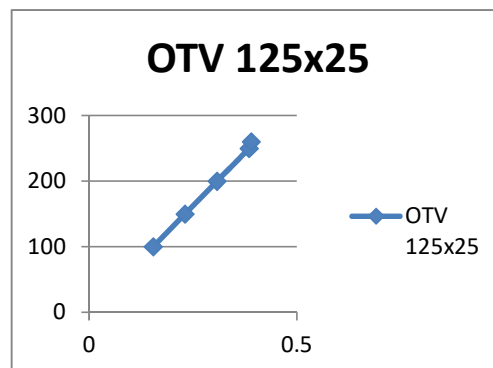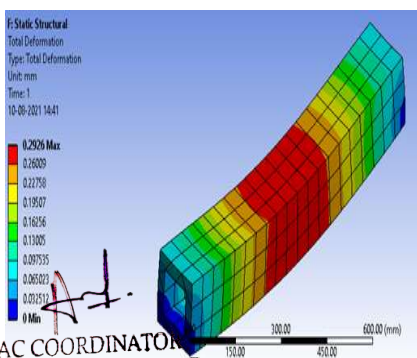
100x25mm DSHS-CFST beam
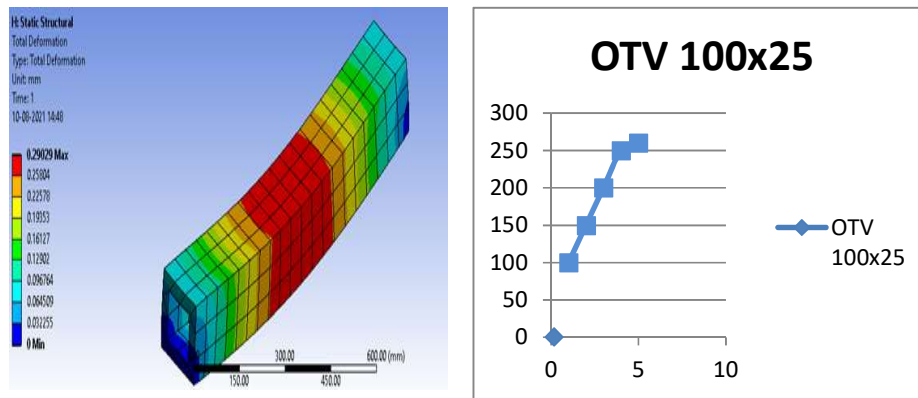
IV. RESULT

Experimental Result

The comparison of conventional, CFST beam and DSHS-CFST experimentally shows that the DSHS-CFST is more efficient than the conventional beam and CFST beam.

Analytical Result

The comparison of conventional, CFST beam and DSHS-CFST Analytically shows that the DSHS-CFST is more efficient than the conventional beam and CFST beam

V. CONCLUSION

In experimental and analytical results, the flexural strength is maximum at 50 KN for CFST Beams compared to the Normal beam.
Concrete filled double skin tubular beams were subjected to bending under two points loading, following conclusions had been drawn.

1. A series of experimental tests on square DSHS-CFST subjected to Flexure test. Enhancement in strength has been observed for DSCFST beams (square in square) due to the ductile nature of steel and Composite action between steel and concrete.

2. The flexural strength of DSHS-CFST beams increases with respect to the increase in the dimensions of inner tube, by keeping the outer steel tube dimension as constant and changing the inner steel tube dimensions.

3. The DSHS-CFST beam 150 x 100mm has attained more bending strength than 150 x 50mm beam.

4. The bending strength of DSHS-CFST beams is increased with respect to the increase in the dimension of outer tube, by keeping the inner steel tube dimension as constant and changing the outer steel tube dimensions.

5. The beam of inner steel tube 25mm and having outer steel tube of increasing dimensions (75mm, 100mm, and 125mm) has gets increasing in deflection.

The beams of outer steel tube 150mm and having inner steel tube of increasing dimensions (100mm, 75mm, 50,) has gets increasing in maximum load.

REFERENCES

[1] ShehdehGhannam "Flexural Strength Of Concrete-Filled Steel Tubular Beam With Partial Replacement Of Coarse Aggregate ByGranite" Volume 7, Issue 5, September-October 2016.

[2] NaveenaTreesa Joseph, JerisonScariah James, Priya Philip, "Flexural Performance of Concrete Filled Steel Tube Beams", Vol. 5 Issue07, July-2016.

[3] Salam Al-Obaidi, Thulfiqar Salim, Sadjad Amir Hemzah, "Flexural Behavior Of Concrete Filled Steel Tube Composite WithDifferent Concrete Compressive Strength" Volume 9, Issue 7, July 2018.

[4] Madiha Z.J. Ammari, Moayyad M. Al-Nasra, AbdelqaderNajmi, "Effective use of U-Link in Concrete Filled Steel Tubes Beams"Volume 2 Issue 4 ‖ April. 2013.

[5] Anjali M S, EapenSakaria, "Retrofitting of Concrete Filled Cold Formed Steel Tubular Beams with GFRP Sheets: ExperimentalInvestigation"Vol. 4, Issue 9, September 2015.

[6] Mr. Subhankar Debnath, Mr. G. Vimalanandan, Dr. S. Senthil Selvan, "Experimental Investigation And Finite Element Modeling Of Concrete Filled Steel Tube" Volume 119 No. 14 2018, 1317-1324.

[7] Audronis Kazimieras Kvedaras, GintasSauciuvėnas, ArunasKomka and Ela Jarmolajeva, "Analysis of behaviour for concrete-filledsteel tubular beams" jeju, korea, September 8-12-2018.

[8] N. Pannirselvam, V. Nagaradjane and K. Chandramouli, "Strength Behaviour Of Fibre Reinforced Polymer Strengthened Beam"VOL. 4, NO. 9, november 2009.

[9] Nadeem A. Siddiqui, "Experimental investigation of RC beams strengthened with externally bonded FRP composites" Received 1May 2009; In revised form 21 Oct 2009.

[10] Namasivayam Aravind, Amiya K. Samanta, D. K. Singha Roy and Joseph V. Thanikal, "Retrofitting Of Reinforced ConcreteBeams Using Fibre Reinforced Polymer (Frp) Composites – A Review" v.7, n.1, p.164-175,2013.

[11] Heeyoung Lee, Hoon Jang and Wonseok Chung, "Effect of Recycled Concrete on the Flexural Behavior of Concrete-Filled FRPTubes" Lee et al. Int J Concr Struct Mater (2019).

[12] HoussamToutanji, P.E., F.ASCE; Liangying Zhao; and Eugene Anselm, "Verifications of Design Equations of Beams ExternallyStrengthened with FRP Composites" Journal of Composites for Construction · June 2006.

[13] Muhaned A. Shallal, "Flexural Behavior of Concrete-Filled Steel Tubular" 978-1-5386-3540-7/18/31.00$©2018.

[14] Liang Huang, Chen Zhang, LiboYan, and BohumilKasal, "Flexural Behavior of U-shape FRP Profile-RC Composite Beams withInner GFRP Tube Confinement at Concrete Compression Zone"10 October 2017.

[15] Prathamesh S. Padwal, Dr. S. R. Parekar, "Experimental and Analytical Analysis of Concrete Filled Square and CircularTubes"Volume: 03 Issue: 12 | Dec -2016.

[16] Tusshar Goel, Aditya Kumar Tiwar, "Finite Element Analysis of Circular Concrete Filled Steel Tube: A review" Volume: 05 Issue:05 | May-2018.

[17] Vijay laxmi B. V, Manoj Kumar Chitawadagi, "Finite Element Analysis of Concrete Filled Steel Tube (CFT's) Subjected toFlexure" Volume 3, Issue 12 (July 2014).

[18] Ahmed A. M. AL-Shaar, and Mehmet TolgaGogus, "Performance of Retrofitted Self-Compacting Concrete-Filled Steel Tube BeamsUsing External Steel Plates" Volume 2018, Article ID 3284745, 18 pages.

[19] Khaja Mohiuddin, R Sankar, "Behavior Of Concrete-Filled Steel Tubular Beam With Partial Replacement Of Demolition Waste AsA Coarse Aggregate" Volume: 03 Issue: 12 | Dec -2016.

[20] C.C. Spyrakos, I.G. Raftoyiannis, L. Credali and J. Ussia, "Experimental and Analytical Study on Reinforced Concrete Beams inBending Strengthened with FRP"1874-8368/14,2014, Volume 8.

[21] Robert Sonnenscheina,, Katarina Gajdosovaa, Ivan Hollya, "FRP Composites and Their Using in the Construction of Bridges"Procedia Engineering 161 (2016).

[22] Robert Sonnenscheina, Katarina Gajdosovaa, Ivan Hollya, "FRP Composites and Their Using in the Construction of Bridges"Procedia Engineering 161 (2016).

An Experimental Study on the effects of Zycotherm on Marshall Properties of Warm Mix Asphalt

Kapil Kushwah[1], Dr. Arafat Rehman[2], Dr. Jyoti Yadav[3]

1 Ph.D Research Scholar, Department of Civil Engineering, SRK University, Bhopal

2 Supervisor & Assistant Professor, Department of Civil Engineering, SRK University, Bhopal

3 Assistant Professor & Head, Department of Civil Engineering, SRK University, Bhopal

Abstract: Abstract:- In this study bitumen was modified with Zycotherm additive to prepare Warm Mix Asphalt. Various standard tests were performed with neat bitumen and Zycotherm modified bitumen. The objective of the study was to know the effect of Zycotherm on the properties of bituminous mix. The effects of the Zycotherm Additive on Dense Bituminous Mix (Grade 1) ware tested by the Marshall Stability Test. Various properties such as Bulk Density, Volume of air voids, Voids in Mineral Aggregates, Voids Filled with Bitumen, Stability and Flow were determined from Marshall Stability Test. Comparisons were made between mixes prepared with base bitumen & Zycotherm modified bitumen at different temperatures. The additive dose was kept the same for all mixtures i.e. 0.1% by weight of bitumen. The results of the study concluded that the emissions were significantly reduced during the production of Warm Mix Asphalt mixtures (WMA) as compared to Hot Mix Asphalt mixture (HMA). The laboratory test results also concluded that Stability & Marshall properties were improved for the WMA mix by the addition of the additive.

Keywords: - Additive, Zycotherm, Hot Mix Asphalt, Warm Mix Asphalt, Marshall Stability, DBM.

1. INTRODUCTION

Flexible Pavement construction emits CO_2 and other greenhouse gases, which contributes to global warming. India is one of the largest emitters of CO2 and is working to reduce its emissions in the coming years. Most paved roads in India are made of hot mix asphalt (HMA), which consists of aggregate and asphalt binder. Hot Mix Asphalt refers to asphalt mixes that are traditionally made at high temperatures (150 to 180°C). HMA production necessitates a significant amount of energy, as well as a significant amount of CO_2 emissions.

With rising concerns about global warming and rising emissions, the asphalt industry is constantly working to reduce emissions by lowering the mixing and compaction temperatures of the asphalt mixture without compromising the mix's properties. The asphalt industry is making endless efforts to reduce its emissions by reducing the temperatures of mixing and compaction of asphalt mixes without affecting the mix properties. Rising fuel prices, global warming, and strict environmental regulations have led to an interest in Warm Mix Asphalt technology as a way to reduce energy consumption and emissions associated with conventional hot mix asphalt production.

Warm Mix Asphalt technology is a generic term used for variety of technologies that allow Hot Mix Asphalt (HMA) pavement material producers to reduce temperatures at which the material is mixed and placed on the road.

In recent years, the asphalt industry has explored the Warm Mix Asphalt technology as a way to reduce the mixing and compaction temperatures of asphalt mixtures. Warm Mix Asphalt is a mixture of asphalt mixed at lower temperatures than conventional hot asphalt. The mixing temperatures of the Warm Mix Asphalt range from 100 to 140° C (212 to 280 ° F) as compared to the mixing temperatures of 150 to 180 ° C (300 to 350 ° F) of Hot Mix Asphalt.
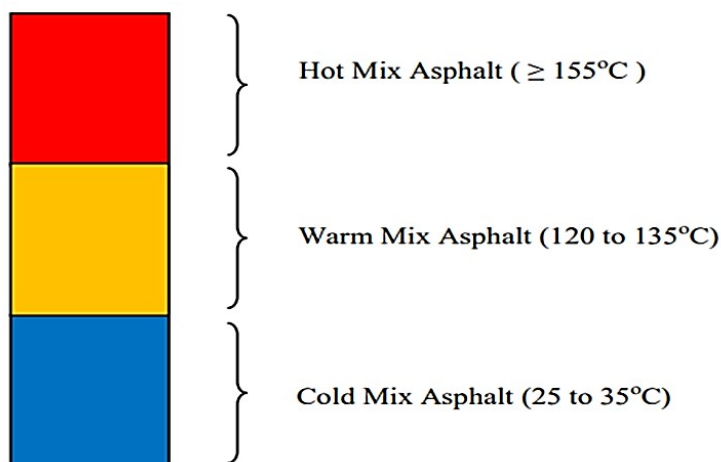
Figure 1 Typical Mixing Temperature Range of Different Bituminous Mixes

2. OBJECTIVE

The objective of this study to determine the effects of Zycotherm additive on DBM Mixes (Grade-1) prepared at different temperatures and their comparison with conventional HMA mixes. Mid-size gradation was adopted for both HMA and WMA mixes. The study included preparation and testing of laboratory specimens for Marshall Test of HMA mix at 155°C and WMA mix at temperature ranging from 100 to 140°C with additive dosage rate of 0.1% by weight of bitumen.

3. MATERIALS

3.1 Bitumen

Plain & Zycotherm modified bitumen of Viscosity Grade 30 (VG-30) was used for the preparation of specimens. The basic test results of the bitumen are tabulated in Table 1.

Table 1 Properties of Plain & Modified Bitumen

S.No.	Test	Results		Range as Per IS:73-2013
		Plain Bitumen	*Modified Bitumen*	
1	Penetration, at 25°C, (0.1mm)	55	61	Min. 45
2	Softening point (R&B), °C	48	49	Min. 47
3	Ductility (cm)	79	92	Min. 75 cm
4	Flash Point °C	250	280	Min. 225
5	Specific Gravity	1.01	1.02	0.97-1.02

3.2 Aggregates

The aggregates with desired strength, hardness & toughness were selected as such aggregates produce higher stability. The properties of bituminous mix very much depend on the aggregate size and their grain size distribution. The requirements of gradation for various layers of different bituminous courses has been specified by Ministry of Roads Transport & Highways (MoRTH 5th

revision). The different tests conducted on coarse aggregates to check the physical properties and their results are tabulated in Table 2.

Table 2 Properties of Coarse Aggregates

S.No.	Test	Results	Range as MoRTH
1.	Aggregate Impact Value, %	16.04	Max. 27%
2.	Aggregate Crushing Value, %	16.37	--
3.	Combined Flakiness & Elongation Index, %	22.33	Max. 35%
4.	Specific gravity	2.7	--
5.	Water Absorption, %	0.8	Max. 2%
6.	Los Angeles Abrasion Value, %	25.32	Max. 35%

3.3 Zycotherm

ZycoTherm is a Warm Mix Asphalt additive which is developed by Zydex Industries, Gujarat, India. It is an odour free chemical warm mix additive that offers lower production and compaction temperatures, while simultaneously enhancing the moisture resistance of pavements by serving as an antistrip. Due to its built-in antistrip mechanism it acts as an antistrip as well as a warm mix additive. Zycotherm is compatible with both modified & unmodified binders. For the study the additive dose was kept the same for all mixtures i.e. 0.1% by weight of bitumen.
The physical properties of Zycotherm are shown in Table 3.

Table 3 Properties of Zycotherm

S.No.	Property	
1.	Physical Form	Liquid
2.	Color	Pale Yellow
3.	Density	1010 kg/m^3
4.	Specific Gravity	1
5.	Viscosity	300 CP (25°C)
6.	Flash Point	>80°C
7.	Odor	No Odor
8.	Solubility in Water	Soluble in water
9.	pH	10 % Solution in water neutral or slightly acidic

4. METHODOLOGY

The bituminous mix for Dense Bituminous Macadam (DBM) Grade-1 was designed using Marshall Method of Mix Design to obtain Optimum Binder Content (OBC). The specifications of the basic outline for the design, construction & controls needed while laying Dense Bituminous Mixes in the base course, binder course and wearing course are covered by IRC:111 – 2009. The aggregate gradation of DBM Grade-1 is shown in Table 4.

Since the maximum size of aggregate is more than 26.5 mm in DBM Grading-1 the conventional Hot Mix Asphalt Specimens for DBM Grading-1 were prepared as per Modified Marshall Method of bituminous mix design. Total weight of specimen was taken as 4050 grams for preparation of Modified Marshall specimen for grading-1. Then required weight of aggregate of desired gradation were weighed and heated up to 175 to 190°C. Bitumen (virgin VG-30) was separately heated up to 121 to 125°C with the first

trial percentage of bitumen (say 3.5 % by weight of the mineral aggregates). The calculated amount of bitumen was mixed with aggregate till proper coating was achieved. The mix was placed in the mould (152.4mm diameter and 95.25mm thick) and compacted by giving 112 blows on each face. The mould was taken out and kept under normal temperature for 24 hours. The height and weight of the specimen were measured. It was immersed in a water bath kept at constant temperature of 60°C for 30 minutes and after that it was taken out for testing in the Marshall testing machine. The bitumen content was varied in the next trial by +0.5% and the above procedure was repeated for bitumen content upto 5.5%.

Table 4 Composition of DBM Layer (MoRTH 2013)

Grading	1	
Nominal aggregate size	37.5mm	
Layer Thickness	75-100mm	
IS Sieve (mm)	Cumulative % by weight of total aggregate passing	% Passing at Mid-point gradation
45	100	100
37.5	95-100	97.5
26.5	63-93	78
19	-	-
13.2	55-75	65
9.5	-	-
4.75	38-54	46
2.36	28-42	35
1.18	-	-
0.6	-	-
0.3	7-21	14
0.15	-	-
0.075	2-8	5
Bitumen content % by mass of total mix	Min 4.0	

For the determination of Optimum Binder Content, the average value of bitumen contents corresponding to maximum stability, maximum unit weight & 4% air voids were considered.

Warm Mix specimens were prepared similar to Hot Mix Asphalt Specimens. For DBM Grading-1, Warm Mix Modified Marshall specimens were prepared similar to Hot Mix Modified Marshall Specimens except that instead of virgin bitumen, modified bitumen was used as binder material and the mixing & compacting temperatures were varied from 100°C to 140°C. For each bitumen content & temperature three test specimens were prepared. The specifications for DBM Grade-1 as per MoRTH 5th Revision are given in Table 5.

Table 5 DBM Grade-1 Specifications (MoRTH 2013)

Mix Design Properties	Requirements for DBM Grade-1
Minimum Stability (KN at 60°C)	20.25 KN
Marshall Flow (mm)	3 mm (Min.)
Air Voids (%)	3-5%
Voids Filled with Bitumen VFB (%)	65-75%
Voids in Mineral Aggregates, VMA (%) (Min.)	10-12%
Marshall Quotient (Stability/Flow)	2-5

5. TEST RESULTS & DISCUSSION

The Modified Marshall Stability Test results of Hot Mix Asphalt specimens for DBM Grade-1 at 155°C are shown in Table 6. The test results of Warm Mix Asphalt specimens prepared with 0.1% Zycotherm for DBM Grade-1 at temperature ranging from 100°C to 140°C are shown in Table 7 to 11 respectively.

Table 6 Marshall Properties of Hot Mix Asphalt Specimens for DBM Grading-1 at 155°C

Property	Bitumen Content				
	3.5%	*4%*	*4.5%*	*5%*	*5.5%*
Bulk Density (g/cc)	2.37	2.39	2.44	2.39	2.36
Marshall Stability (KN)	18.45	20.13	23.54	21.64	20.18
Flow (mm)	3.48	3.93	4.31	4.86	5.13
Total Air Voids (%)	6.17	5.74	4.87	3.76	3.14
Voids Filled with Bitumen VFB (%)	60.15	68.65	74.79	80.15	84.26
Voids in Mineral Aggregates VMA (%)	14.65	14.06	13.69	12.95	12.14

Table 7 Marshall Properties of Warm Mix Asphalt Specimens with 0.1% Zycotherm for DBM Grading-1 at 100°C

Property	Bitumen Content with 0.1% Zycotherm				
	3.5%	*4%*	*4.5%*	*5%*	*5.5%*
Bulk Density (g/cc)	2.40	2.41	2.42	2.43	2.41
Marshall Stability (KN)	18.14	19.24	21.47	20.45	19.68
Flow (mm)	3.30	3.75	4.14	4.51	4.92
Total Air Voids (%)	6.51	5.89	5.12	4.45	3.95
Voids Filled with Bitumen VFB (%)	59.11	62.14	65.32	68.14	70.36
Voids in Mineral Aggregates VMA (%)	16.87	16.12	15.48	14.12	13.48

Table 8 Marshall Properties of Warm Mix Asphalt Specimens with 0.1% Zycotherm for DBM Grading-1 at 110°C

Property	Bitumen Content with 0.1% Zycotherm				
	3.5%	*4%*	*4.5%*	*5%*	*5.5%*
Bulk Density (g/cc)	2.42	2.44	2.45	2.46	2.44
Marshall Stability (KN)	20.16	22.24	24.15	23.46	22.71
Flow (mm)	3.80	4.12	4.52	4.89	5.12
Total Air Voids (%)	5.50	4.88	4.12	3.67	3.32
Voids Filled with Bitumen VFB (%)	61.17	64.85	67.59	73.49	76.14
Voids in Mineral Aggregates VMA (%)	16.12	15.74	14.84	13.51	12.86

Table 9 Marshall Properties of Warm Mix Asphalt Specimens with 0.1% Zycotherm for DBM Grading-1 at 120°C

Property	Bitumen Content with 0.1% Zycotherm				
	3.5%	4%	4.5%	5%	5.5%
Bulk Density (g/cc)	2.44	2.46	2.47	2.44	2.42
Marshall Stability (KN)	23.47	25.61	28.23	26.15	24.16
Flow (mm)	4.21	4.75	5.14	5.41	5.74
Total Air Voids (%)	4.92	4.52	4.13	3.96	3.41
Voids Filled with Bitumen VFB (%)	67.15	69.17	73.65	79.86	82.19
Voids in Mineral Aggregates VMA (%)	15.16	14.34	13.74	12.83	11.91

Table 10 Marshall Properties of Warm Mix Asphalt Specimens with 0.1% Zycotherm for DBM Grading-1 at 130°C

Property	Bitumen Content with 0.1% Zycotherm				
	3.5%	4%	4.5%	5%	5.5%
Bulk Density (g/cc)	2.44	2.45	2.46	2.47	2.45
Marshall Stability (KN)	22.32	23.47	25.17	24.19	23.49
Flow (mm)	4.61	4.96	5.34	5.96	6.31
Total Air Voids (%)	4.85	4.41	3.86	3.21	2.87
Voids Filled with Bitumen VFB (%)	70.16	73.54	77.15	80.65	83.24
Voids in Mineral Aggregates VMA (%)	14.32	13.64	12.73	12.21	11.14

Table 11 Marshall Properties of Warm Mix Asphalt Specimens with 0.1% Zycotherm for DBM Grading-1 at 140°C

Property	Bitumen Content with 0.1% Zycotherm				
	3.5%	4%	4.5%	5%	5.5%
Bulk Density (g/cc)	2.46	2.47	2.48	2.49	2.47
Marshall Stability (KN)	21.21	22.82	24.61	23.41	22.74
Flow (mm)	5.61	5.91	6.14	6.32	6.51
Total Air Voids (%)	5.17	4.87	4.21	3.91	2.89

Voids Filled with Bitumen VFB (%)	71.69	74.65	79.18	82.15	85.14
Voids in Mineral Aggregates VMA (%)	13.87	12.73	12.16	11.42	10.91

To obtain Optimum Binder Content (OBC) graphs were plotted between bitumen content & Marshall stability, density & air voids. The relationship between these Marshall Properties & bitumen content for DBM Grade-1 specimens prepared with neat bitumen at 155°C & WMA specimens prepared with 0.1% Zycotherm at temperature range 100°C to 140°C are shown in Fig. 2 to 4.

Figure 2 shows the variation in Marshal Stability for incremental bitumen content with Hot Mix Asphalt specimens prepared with neat bitumen and WMA mixes prepared with 0.1% Zycotherm for DBM grade-1 of layer thickness 75-100 mm. According to MORT&H specification, all the mixes of HMA and WMA satisfy the minimum stability criteria of 20.25 KN at bitumen content of 4% & above.

In accordance with figure 2, for binder content 4.5 %, HMA had stability of 23.54 KN, at the same binder content Warm Mix Asphalt specimens prepared with Zycotherm had maximum stability of 28.23 KN at 120°C. For binder content 5.50%, HMA has stability of 20.18 KN at 155°C, at the same bitumen content Warm Mix Asphalt specimens
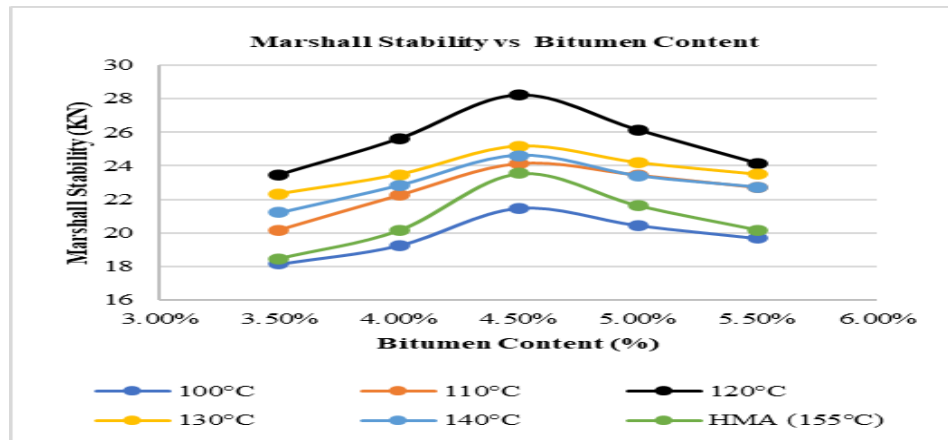
prepared with Zycotherm has maximum stability of 24.16 KN at 120°C. From the overall observation, it can be said that Warm Mix Asphalt specimens prepared with Zycotherm at 120°C is preferred as it has the higher stability at each bitumen content.

Figure 2 Marshall Stability Value vs Bitumen Content

Figure 3 shows the variation in Bulk Density for incremental bitumen content with HMA and WMA mixes for DBM grade-1 of layer thickness 75-100 mm. Bulk Densities are within the desired range. At the bitumen content 4.50% Bulk Density for all Warm Mix Asphalt Specimens is higher than HMA which indicates the higher rate of compaction.
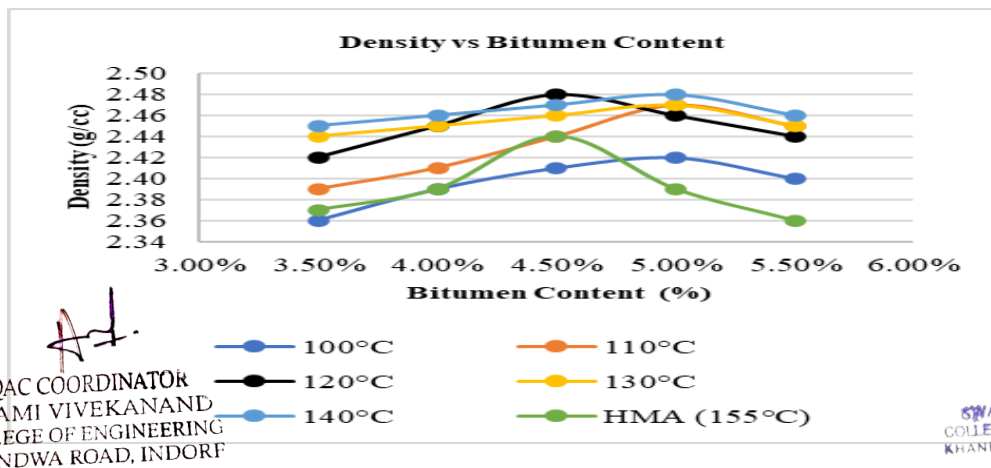
Figure 3 Bulk Density vs Bitumen Content

Even at 5.50% bitumen content the bulk densities of all Warm Mix Asphalt Specimens are higher than HMA. Considering the overall behaviour, Warm Mix Asphalt specimens prepared with Zycotherm shows the higher bulk density at the bitumen content of 4.50% and 5.50% but the bulk density gets reduced as the bitumen content increases.

Figure 4 shows the variation in air voids with respect to the incremental bitumen content at 0.5% incremental rate with HMA and WMA mixes for DBM grade-1 of layer thickness 75-100 mm. According to MORT&H specification, air voids should be 3% to 5 % of bituminous mixes.

In the present investigation for 3% air voids the bitumen content was found to be 5.80% for HMA mix. At the same time for 4% air voids, the bitumen content was found to be 4.80% for HMA mix & 4.50% for WMA specimens.

From the study it was found that WMA specimens prepared with Zycotherm is succeeded to perform with same compaction as of HMA mix, significantly the compaction effect at 4.50% bitumen content found to be same for both mixes. By this it was found that rearrangement of particle succeeds in WMA specimens prepared with Zycotherm at 4.50% bitumen content as same of HMA mix at slightly higher bitumen content of 4.6%.
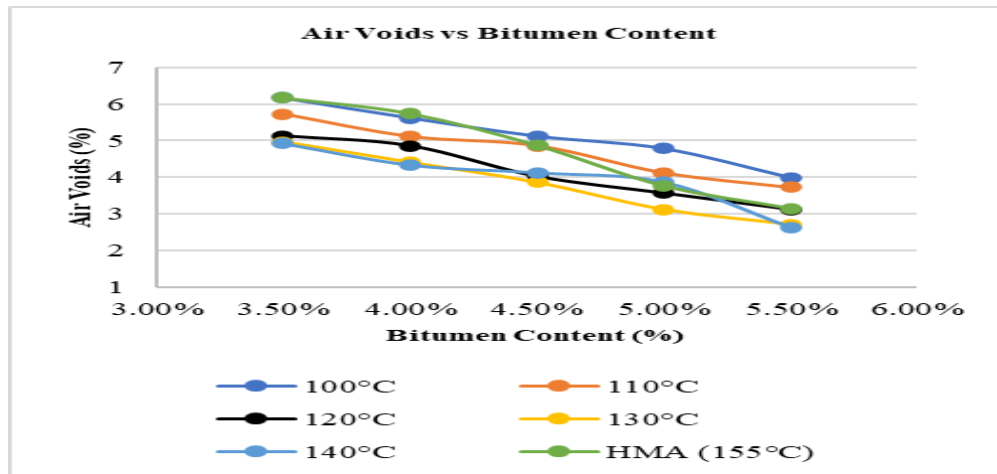
Figure 4 Bulk Density vs Bitumen Content

From the above figures the bitumen contents corresponding to maximum Marshall stability, bulk density and 4.0% air voids were obtained and the average of the three bitumen contents was calculated and considered as optimum bitumen content (OBC). OBC values of HMA at 155°C and WMA for DBM grade-1 at temperature range from 100°C-140°C is presented in Table 12.

Table 12 Optimum Binder Contents of HMA & WMA Specimens

Type of Specimen	Maximum Stability		Maximum Bulk Density (g/cc)		4% Air Voids	Average
	KN	OBC %	g/cc	OBC %	OBC %	OBC %
HMA 155°C	23.54	4.5%	2.44	4.5%	4.8%	4.60%
WMA 100°C	21.47	5%	2.42	5%	5.5%	5.17%
WMA 110°C	24.15	5%	2.47	5%	5.10%	5.03%
WMA 120°C	28.23	4.5%	2.48	4.5%	4.5%	4.5%
WMA 130°C	25.17	5%	2.47	5%	4.4%	4.80%
WMA 140°C	24.61	5%	2.48	5%	4.9%	4.97%

From the above table it can be stated that the OBC for HMA grade-1 specimens is 4.6% and for WMA specimens prepared with 0.1% Zycotherm the OBC values are different for different temperatures.

6. CONCLUSIONS

On the basis of the detailed study carried out on the effects of Zycotherm on the performance of bitumen & WMA specimens prepared at different temperatures and its comparison with the performance of HMA specimens prepared with neat bitumen the following conclusions are drawn:-

➢ The properties of modified bitumen shown in Table 1, satisfies the requirement of Viscosity value, Penetration value, softening point value and Ductility value as per the Requirement of IS 73-2013.
➢ Conventional test shows that Zycotherm additive increases penetration value of base bitumen and there was a slight increase in softening point of bitumen with addition of Zycotherm additive. Zycotherm additive tends to increase conventional properties of bitumen.
➢ The Marshall Stability value of HMA specimens produced at 155°C has good stability values. When compared with HMA specimens, the stability and Marshall Properties of WMA specimens prepared at 120°C for aggregate grading-1 were improved by the addition of Zycotherm at an additive dosage rate of 0.1% by weight of the binder.
➢ Zycotherm improved the bulk density of the mix by 2% for Grading-1. Hence 120˚C temperature with additives shows better and maximum bulk density.
➢ Zycotherm slightly reduced OBC of WMA specimens as compared to HMA specimens.
➢ Warm Mix Asphalt produced with 0.1% Zycotherm at 120°C can be used in place of conventional HMA for pavement construction.

REFERENCES

[1] Vinod D. Ninawe and Shashikant A. Deshmukh, "Laboratory Evaluation of Warm Mix Asphalt", International Journal of Advance Research in Science and Engineering, vol.6, pp. 259-268, July 2017.

[2] Tejash Gandhi, "Effects of Warm Asphalt Additives on Asphalt Binder and Mixture Properties" Ph.D Dissertation, The Graduate School of Clemson University, May 2008.

[3] Paltasingi Venkata Raju, M Udaya Sri, PMS Satish Kumar and Sumathi Misro, "Experimental Study on Bituminous Mixes by Using Zycotherm", International Journal of Scientific Development and Research, vol. 3, 71-83, January 2018.

[4] IS: 73 (2013), "Paving Bitumen – Specification", Bureau of Indian Standards, New Delhi.

[5] IS: 1203 (1978), "Methods for Testing Tar & Bituminous Materials: Determination of Penetration", Bureau of Indian Standards, New Delhi.

[6] IS: 1205 (1978), "Methods for Testing Tar & Bituminous Materials: Determination of Softening Point", Bureau of Indian Standards, New Delhi.

IQAC COORDINATOR
SWAMI VIVEKANAND
COLLEGE OF ENGINEERING
KHANDWA ROAD, INDORE

PRINCIPAL
SWAMI VIVEKANAND
COLLEGE OF ENGINEERING
KHANDWA ROAD, INDORE

[7]   IS: 1208(1978), "Methods for Testing Tar & Bituminous Materials: Determination of Ductility", Bureau of Indian Standards, New Delhi.

[8]   IS: 2386 (Part 1) – 1963 (Reaffirmed 2002), "Methods of Test for Aggregates for Concrete – Particle Size and Shape", Bureau of Indian Standards, New Delhi.

[9]   IS: 2386 (Part 3) – 1963 (Reaffirmed 2002), "Methods of Test for Aggregates for Concrete – Specific Gravity, Density, Voids, Absorption and Bulking", New Delhi.

[10]   IS: 2386 (Part 4) – 1963 (Reaffirmed 2002), "Methods of Test for Aggregates for Concrete – Mechanical Properties", Bureau of Indian Standards, New Delhi.

[11]   Ministry of Road Transport and Highways (2013), "Specifications for road and bridge works (Fifth Revision)", Indian Road Congress, New Delhi.

IQAC COORDINATOR
SWAMI VIVEKANAND
COLLEGE OF ENGINEERING
KHANDWA ROAD, INDORE

PRINCIPAL
SWAMI VIVEKANAND
COLLEGE OF ENGINEERING
KHANDWA ROAD, INDORE

A Review of Piston and its Function Using Tungsten Alloy

M.E. Scholar Sachin Prajapat, Dr. Pardeep Kumar Patil, Dr. Rahul Joshi, Mr. Vishal Wankhede
Swami vivekanand College of Engineering,
Indore, M.P. ,India

Abstract- Piston is the part of engine which converts heat and pressure energy liberated by fuel combustion into mechanical works. Engine piston is the most complex component among the automotives. This paper illustrate design procedure for a piston for 4 stroke petrol engine for hero splendor – pro bike and its analysis by its comparison with original piston dimensions used in bike. The design procedure involves determination of various piston dimensions using analytical method under maximum power condition. In this paper the combined effect of mechanical and load is taken into consideration while determining various dimensions. The basic data of the engine are taken from a located engine type of hero splendor –pro bike.

Keywords:- Pistons, Insulators, Strain,Force, Fluids.

I. INTRODUCTION

Today, the pistons designed by the suppliers based on load data determined by the engine performance targets. From this data the supplier estimates the temperatures of the piston and recommends a design that is suitable for the application. This procedure is successful for the design of the piston, but gives no knowledge of the thermal interaction between the piston and its surrounding parts. The current trend in car engine development is to make smaller engines with higher specie power outputs to meet the demands for lower fuel consumption and emissions. This leads to higher thermal loads on the engine and an increasing need to understand the heat balance of the complete engine in order to optimize the different engine parts and systems.

 A substantial part of the heat generated by the combustion is transported to the coolant through the piston and to the surrounding structure. It is therefore important to get an accurate description of these interactions. The goal of Volvo Cars future

Combustion engine development is to increase power and efficiency and decrease fuel consumption while still maintaining reliability and durability of the highest possible level. As such, it is necessary to have a complete image of the thermal effect and how this aects the engine properties.

II. FUNCTIONS OF PISTON

1. To reciprocate in the cylinder as a gas tight plug causing suction, Compression, expansion, and exhaust strokes.
2. To receive the thrust generated by the explosion of the gas in the cylinder And transmit it to the connecting rod.
3. To form a guide and bearing to the small end of the connecting rod and to take the side thrust due to obliquity of the rod.

Sachin Prajapat. International Journal of Science, Engineering and Technology, 2021, 9:1

International Journal of Science, Engineering and Technology

An Open Access Journal
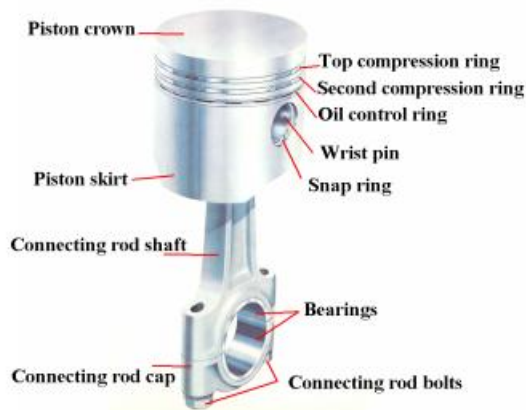
Fig 1. Piston Assemble Model.

III. PISTON RINGS

The piston rings are used to impart the necessary radial pressure to maintain the seal between the piston and the cylinder bore. These are usually made of grey cast iron or alloy cast iron because of their good wearing properties and also they retain spring characteristics even at high temperatures.

The piston rings are of the following two types:
1. Compression rings or pressure rings, and
2. Oil control rings or oil scraper.

The compression rings or pressure rings are inserted in the grooves at the top portion of the piston and may be three to seven in number. These rings also transfer heat from the piston to the cylinder liner and absorb some part of the piston fluctuation due to the side thrust.

The oil control rings or oil scrapers are provided below the compression rings. These rings provide proper lubrication to the liner by allowing sufficient oil to move up during upward stroke and at the same time scrap the lubricating oil from the surface of the liner in order to minimize the flow of the oil to the combustion chamber.

Table 1. Thermal and Mechanical Properties of Aluminum Alloys.

S.No	PARAMETERS	A2618
1	Elastic Modulus (GPa)	73.7
2	Ultimate Tensile Strength (MPa)	480
3	0.2% Yield Strength (MPa)	420
4	Poisson's Ratio	0.33
5	Thermal Conductivity (W/m/oC)	147
6	Coefficient of Thermal Expansion (1/K)	25.9 x 10-6
7	Density (Kg/m3	2767.9 9

3. Engine Specifications:

The engine used for this work is a single cylinder four stroke air cooled type Bajaj Kawasaki petrol engine.

Table 2. The engine specifications are given in Table.

PARAMETERS	VALUES
Engine Type	Four stroke engine
Induction	Air cooled type
Number of cylinders	Single cylinder
Bore	51 mm
Stroke	48.8 mm
Length of connecting rod	97.6 mm
Displacement volume	99.27 cm3
Compression ratio	8.4
Maximum power	6.03 KW at 7500 rpm
Maximum Torque	8.05 Nm at 5500 rpm
Number of revolutions/cycle	2

IV. ALLOY

Tungsten alloy

The name of "tungsten" is derived from the Swedish term meaning "heavy stone." Tungsten has been assigned the chemical symbol W after its German name wolfram. Tungsten, the metal with the highest

Sachin Prajapat. International Journal of Science, Engineering and Technology, 2021, 9:1

International Journal of Science, Engineering and Technology

An Open Access Journal

meting point (3422∘C), has many advantages, such as high temperature strength, high creep resistance and high thermal conductivity, high electric resistance, the lowest vapor pressure, and the lowest coefficient of thermal expansion.These properties make tungsten a premium candidate for high temperature applications like, for example, in fusion reactor.

Another important industrial property of tungsten is its high density of 19.3 g/cm3, which makes it an ideal material for shielding or collimating energetic α- and γ-radiation.

Fig 1. Tungsten Alloy.

The disadvantage of tungsten, however, is its inherent brittleness because tungsten has a transition from brittle to ductile fracture. Its treatment is realized at temperatures that are higher than brittleness limit. This temperature varies for commercially pure tungsten (99.95%) in the interval between 300 and 400∘C, in case of recrystallized tungsten around 500∘C. Undesirable mixtures such as oxygen, nitrogen, and carbon significantly influence mechanical and physical properties of pure tungsten. They mainly precipitate at the grain boundaries in the form of oxides, nitrides, and carbides.

V. LITERATURE REVIEW

Jihai Jiang, Kelong Wang [1] Due to their compact and simple design, axial piston pumps are widely used in hydraulic systems. The piston/cylinder lubricating interface is one of the most critical design elements in axial piston pumps, which fulfils the bearing and sealing function simultaneously. Also it is the main source of both friction and volumetric powerloss. In order to realize the optimal design of efficient and reliable axial piston pump, an accurate model of the tribological interface in axial piston pump is needed to save the cost and time in the design process.

Shengjun Wu, Zihao Cheng [2] Piston is the main component of the engine. In the engine work process, pistons need withstand both the instantaneous high temperature heat load and the mechanical load during the reciprocating process. The coupling between the thermal load and the mechanical load leads to the malfunction occurrence [2]of piston deformation, piston pin boss cracking, piston side wear, and top thermal cracking caused by the uneventemperature.

Jigui ZHENG, Ye DENG [3] Compact structure and high working efficiency are the characteristics of free Stirling linear generation device, whose power piston support components works in high frequency to produce elastic stiffness and to support the piston components.

Wu, Yi Zeng, Dongjian [4] The study of using DME as an alternative fuel on diesel engine started at early 90s. Experiments using DME as combustion fuel on all kinds of diesel engines done at Xi'anJiaotong University and Shanghai Internal Combustion Engine Research Institute show that DME can achieve high efficiency, ultra-low emission, gentle, nonsmoker combustion and meet the stringent Euro III and California ULEV standard

Shcherbachev Pavel [5] The article describes the electro-hydraulic rotary motion drive with separate control of piston groups. Proposed various schemes of construction of the drive. It is shown that the proposed actuator has a wide range of speeds, can work in tracking the position and speed of the output shaft. A nonlinear mathematical model of the drive is represented. The results of numerical simulation and experimental data are shown. The method of synthesis of a special control signal, which increases the efficiency of the drive is given.

O.F. Nikitin [6] This paper deals with the regulation of hydraulic parameters of movement of the output link (total stock) speed - load V = f (R) when using multiple cylinders, with a hard or serial connection rods. The required speed of movement is performed by connecting the required number of effective working areas of hydraulic cylinders. Change in the effective speed while maintaining the load may lead to changes in pressure in the cavity involved in the work of the hydraulic actuator.

Guo Feng, Zhao Chang-lu [7] This paper investigates the piston motion control strategies of a single piston hydraulic free-piston diesel engine, which is intended to be a power supply for hydraulic propulsion systems. The Cycle fuel mass is determined by engine displacement and load. A closed loop control method is used in fuel injection timing control strategy to make the position of bottom dead center steady possibly.

Isam Jasim Jaber and Ajeet Kumar Rai [8] In this present work a piston and piston ring are designed for a single cylinder four stroke petrol engine using. Complete design is imported to ANSYS 14.5 software then analysis is performed. Three different materials have been selected for structural and thermal analysis of piston. For piston ring two different materials are selected and structural and thermal analysis is performed using ANSYS 19 software. Results are shown and a comparison is made to find the most suited design.

Lokesh Singh, Suneer Singh Rawat [9] A piston is a component of reciprocating engines. Its purpose is to transfer force form expanding gas in the cylinder to the crank shaft via piston rod and a connecting rod. It is one of the most complex components of an automobile. In some engines the piston also acts as a valve by covering and uncovering ports in the cylinder wall. In present, work a three-dimensional solid model of piston including piston pin is designed with the help ANSYS software.

VI. CONCLUSION

Engine downsizing is the utilization of smaller engine in a vehicle that provides required power with the help of additional boosting device such as turbocharger. It reduces carbon emissions to large extent as compared to conventional internal combustion engine. It reduces the number of cylinders used in the engine as the desired level of power is achieved by additional boosting device. Thus, the requirement of piston diminishes without compromising with output of engine. Due to this factor, engine downsizing is anticipated to restrain the growth of the global automotive piston market.

Piston skirt may appear deformation at work, which usually causes crack on the upper end of piston head. Due to the deformation, the greatest stress concentration is caused on the upper end of piston, the situation becomes more serious when the

stiffness of the piston is not enough, and the crack generally appeared at the point A which may gradually extend and even cause splitting along the piston vertical. The stress distribution on the piston mainly depends on the deformation of piston.

Therefore,in order to reduce the stress concentration, the piston crown should have enough stiffness to reduce the deformation.

REFERENCES

[1] Alam, Tanwir & Ansari, Akhter. 2017. REVIEW ON ALUMINIUM AND ITS ALLOYS FOR AUTOMOTIVE APPLICATIONS. International Journal of Advanced Technology In Engineering and Science. 5. 278-294.

[2] Alturki, Eng. (2017). Four-Stroke and Two-Stroke Marine Engines Comparison and Application. International Journal of Engineering Research and Applications. 07. 49-56. 10.9790/9622-0704034956.

[3] Bansude, Sushilkumar. (2019). Two Stroke and Four Stroke Cycle Engine. 10.13140/ RG. 2.2.35540.86401.

[4] Bose, Animesh & Sadangi, Rajendra. (2012). A Review on Alloying in Tungsten Heavy Alloys. TMS Annual Meeting. 1. 455-465. 10.1002 /9781118 356074.ch59.

[5] Davis, V. & Shafee, S.M. & Ponnusamy, Baskar. (2015). Performance analysis of four stroke si engine with preheated intake air. 13. 1277-1284.

[6] Dillibabu,Surryaprakash&Mariappan, Ramajayam & Anand, J & Sundar, D & Dinesh, K. (2018). A REVIEW ON LATEST DEVELOPMENT OF ALUMINIUM ALLOY METAL MATRIX COMPOSITE THROUGH POWDER METALLURGY ROUTE.

[7] Hirsch, Juergen. (1997). Aluminium Alloys for Automotive Application. Materials Science ForumMATERSCIFORUM.242.3350.10.4028/www. scientific.net/MSF.242.33.

[8] Lingappa, Shashank & M S, Srinath & Amarendra, H J. (2017). Microstructural and mechanical investigation of aluminium alloy (Al 1050) melted by microwave hybrid heating. Materials Research Express. 4. 076504. 10.1088/2053-1591/aa7aaf.

[9] Mishra, Prakash. (2013). Modeling for Friction of Four Stroke Four Cylinder In - Line Petrol Engine. Tribology in Industry. 35. 237-245.

Optimization Issues of Power Quality & Improvement Using Soft Computing Technique

Neha Katiyar[1], Hemendra Khedekar[2], Manisha Gaur[3]

PG Student, Dept. of EE, Vindhya Institute of Technology & Science, Indore, India[1]

Assistant Professor, Dept. of EE, Swami Vivekanand College of Engineering, Indore, India[2]

Assistant Professor, Dept. of EE, Swami Vivekanand College of Engineering, Indore, India[3]

ABSTRACT :As the power demand has been increasing rapidly, power generation and transmission are being affected due to limited resources, environmental restrictions and other losses.soft computing the techniques of correcting the supply voltage sag, swell and interruption in a distributed system. At present, a wide range of very flexible controllers, which capitalize on newly available power electronics components, are emerging for custom power applications. Power electronic-based equipment aimed at enhancing the reliability and quality of power flows in low voltage distribution networks. A control algorithm is used for the extraction of the fundamental weighted value of active and reactive power components. Using digital signal processor the DSTATCOM is developed and its performance of DSTATCOM is found to be satisfactory for various types of loads.

KEYWORDS: D-Statcom, DVR, Voltage Dips, Swells, Power Quality.

I. INTRODUCTION

As the power demand has been increasing rapidly, power generation and transmission are being affected due to limited resources, environmental restrictions and other losses. The quality of available supply power has a direct economic impact on industrial and domestic sectors which affects the growth of any nation. This issue is more serious in electronic based systems. The level of harmonics and reactive power demand are popular parameters that specify the degree of distortion and reactive power demand at a particular bus of the utility.

This implies that some measures must be taken in order to achieve higher levels of Power Quality. The FACTS devices and Custom power devices are introduced to electrical system to improve the power quality of the electrical power. DVR, STATCOM/DSTATCOM, ACTIVE FILTERs, UPFC, UPQC etc are some of the devices used to improve the power quality of the voltage and current. With the help of these devices we are capable to reduce the problems related to power quality. Under the thesis work among the different custom power devices DSTATCOM has been used to improve the quality of power under different conditions.

the power system, the major power quality problems are poor load power factor, harmonic contents in loads, notching in load voltages, DC offset on load voltages, unbalanced loads, supply voltage distortion, voltage sag, & voltage swell. One of the most common power quality problems today is voltage sag. Voltage sag is a short time event during which a reduction in R.M.S. voltage magnitude occurs. It is often set only by two parameters, depth/magnitude and duration. The voltage dip magnitude is ranged from 10-90% of nominal voltage (which corresponds to 90-10% remaining voltage) and with aduration from half a cycle to 1 minute. In a three-phase system, the voltage sag is by nature a three-phase phenomenon which affects both the phase-to-ground and phase-to-phase voltages. The faults are single-phase or multiple-phase short-circuit, which leads to high currents[1].

The introduction of FACTS has given the new direction to the power system to solve the power quality problems. At present, a wide range of very flexible controllers are emerging for custom power applications. The FACTS controllers like SVC, TCSC, TCPST, STATCOM, SSSC, UPFC, etc. are mainly used controllers. Among these, the STATCOM is the most effective device. The STATCOMis a shunt device & based on VSC principle. The inverter circuit along with interface transformers/inductors is called a STATCOM.

II. VOLTAGE SOURCE CONVERTER (VSC) AND CUSTOM POWER DEVICES

A voltage-source converter is a power electronic device, which can generate a sinusoidal voltage with any required magnitude, frequency and phase angle. The VSC is used to either completely replace the voltage or to inject the 'Dip voltage'. The 'Dip voltage' is the difference between the nominal voltage and the actual. The converter is normally based on some kind of energy storage i.e. capacitor, which will supply the converter with a DC voltage.

The solid-state electronics in the converter is then switched to get the desired output voltage. Normally the VSC is not only used for voltage dip mitigation, but also for other power quality issues, e.g. flicker and harmonics.

A. Shunt voltage controller [Distribution Static Compensator (DSTATCOM)]

The D-STATCOM (Distribution Static Compensator) configuration consists of a VSC, a DC energy storage device; a coupling transformer connected in shunt with the ac system, and associated control circuits. Fig. 1
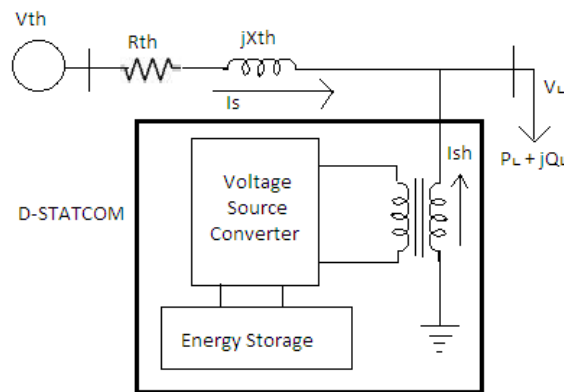

Figure 1 Schematic Dig. Of D-STATCO shows the basic configuration of D-STATCOM

Here, such device is employed to provide continuous voltageregulation using an indirectly controlled converter. Suitable adjustment of the phase and magnitude of the D-STATCOM output voltages allows effective control of active and reactive power exchanges between the D-STATCOM and the AC system. The VSC connected in shunt with the AC system provides a multifunctional topology which can be used for up to three quite distinct purposes:

a) Voltage regulation and compensation of reactive power
b) Correction of power factor
c) Elimination of current harmonics.

Figure 1 shows the shunt injected current I_{sh} corrects the voltage sag by adjusting the voltage drop across the system impedance Z_{th}. The value of I_{sh} can be controlled by adjusting the output voltage of the converter.

$$I_{sh} = I_L - I_s$$

It is mentioned that the effectiveness of the STATCOM in correcting voltage sag depends on the value of Z_{th} or fault level of the load bus. When the shunt injected current I_{sh} is kept in quadrature with V_L the desired voltage correction can be achieved without injecting any active power into the system. On the other hand, when the value of I_{sh} is minimized, the same voltage correction can be achieved with minimum apparent power injection into the system

B. Dynamic voltage restorer / regulator (DVR)

The Dynamic Voltage Restorer (DVR) is a series connected device analogous to a SSSC. The main function of a DVR is to eliminate or reduce voltage sags seen by sensitive loads such as semiconductor manufacturing plant or IT industry.. They have been designed to compensate three phase voltage sags up to 35% for duration of time less than half a second (depending on the requirement). If the voltage sag occurs only in one phase (caused by SLG faults) then the DVR may be designed to provide compensation for sags exceeding 50%. A DVR is connected in series with the feeder using a transformer. The low voltage winding is connected to the converter. A DVR with IGBT/IGCT devices

can be controlled to act as a series active filter to isolate the load from voltage harmonics on the source side. It is also possible to balance the voltage on the load side by injecting negative and/or zero sequence voltages in addition to harmonic voltages.
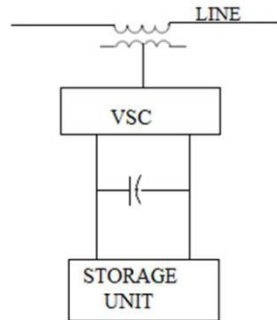

Figure 3: Basic configuration of DVR

C. UNIFIED POWER QUALITY CONDITIONER (UPQC)

Unified power quality conditioners are viable compensation devices that are used to ensure that delivered power meets all required standards and specifications at the point of installation.
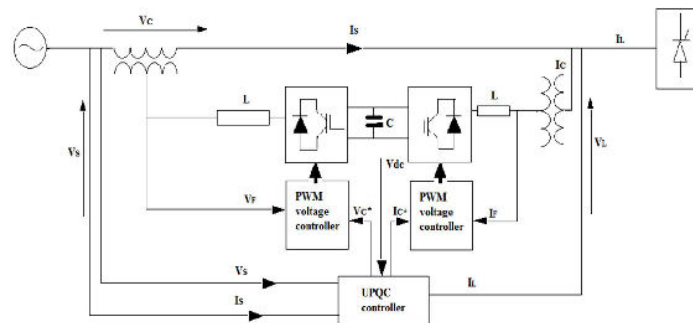

Figure 4: Basic Configuration of UPQC

The ideal UPQC can be represented as the combination of a voltage source converter (injecting shunt current) and a common DC link (connected to a DC capacitor).UPQC consist of combined series active power filter that compensates voltage harmonics of the power supply, and shunt active power filter that compensates harmonic currents of a non-linear load. This dual functionality makes the UPQC as one of the most suitable devices that could solve the problems of both consumers as well as of utility. UPQC, thus can help to improve voltage profile and hence the overall health of power distribution system

III.SYSTEM CONFIGURATION AND CONTROL ALGORITHM AND PROPOSE WORK

The performance of any custom power device depends very much upon the control algorithm used for the reference current estimation and gating pulse generation scheme. An implementation of a three phase distribution static compensator (DSTATCOM) using a control algorithm for its functions under nonlinear loads such as load balancing and reactive power compensation for power factor, and zero voltage regulation. The main advantage of this method is that it requires only waveforms of voltages and currents. A neural network with memory is used to identify the nonlinear load admittance. Once training is achieved, the neural network predicts the true harmonic current of the load when supplied with a clean sine wave. Feed forward back propagation (BP) artificial neural network (ANN) consists of various layers such as the input layer, hidden layer, and output layer. It is based on feed forward BP with a high ability to deal with complex nonlinear problems.
The BP control algorithm is also used to design the pattern classification model based on decision support system. The standard BP model has been used with the full connection of each node in the layers from input to the output layers.

Some applications of this algorithm are as to the identification of user faces, industrial processes, data analysis, mapping data, control of power quality improvement devices, etc. The control of power quality devices by neural network is a latest research area in the field of power engineering. The extraction of harmonic components decides the performance of compensating devices.

The BP algorithm which trained the sample can detect the signal of the power quality problem in real time. Its simulation study for harmonic detection is presented. The proposed control algorithm is used for harmonic suppression and load balancing in PFC and zero voltage regulation (ZVR) modes with dc voltage regulation of DSTATCOM. In this work, the proposed control algorithm on a DSTATCOM is implemented for the compensation of nonlinear loads.

A voltage source converter(VSC)-based DSTATCOM is connected to a three phase ac mains feeding three phase linear/nonlinear loads with internal grid impedance which is shown in Fig. 4
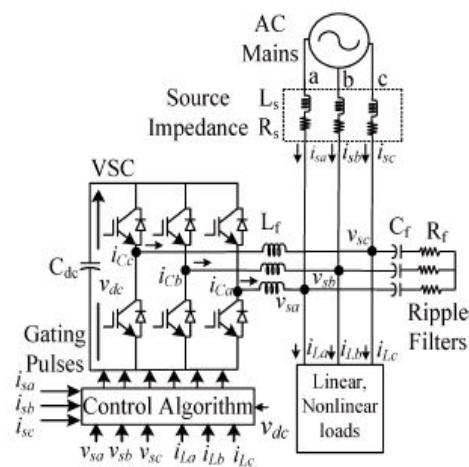

Figure 4 Schematic diagram of VSC-based DSTATCOM.

The performance of DSTATCOM depends upon the accuracy of harmonic current detection. For reducing ripple in compensating currents, the tuned values of interfacing inductors (L_f) are connected at the ac output of the VSC. A three phase series combination of capacitor (C_f) and a resistor (R_f) represents the shunt passive ripple filter which is connected at a point of common coupling (PCC) for reducing the high frequency switching noise of the VSC. The DSTATCOM currents (i_{cabc}) are injected as required compensating currents to cancel the reactive power components and harmonics of the load currents so that loading due to reactive power component/harmonics is reduced on the distribution system. In this algorithm, the phase PCC voltages, source current (i_{sa}, i_{sb}, i_{sc}) and (i_{La}, i_{Lb}, i_{Lc}) and dc bus voltage (V_{dc}) are required for the extraction of reference source currents. There are two primary modes for the operation of this algorithm: The first one is a feed forward, and the second is the BP of error or supervised learning.

A BP training algorithm is used to estimate the three phase weighted value of load active power current components (W_{ap}, W_{bp}, W_{cp}) and reactive power current components (W_{aq}, W_{bq}, W_{cq}) from polluted load currents using the feed forward and supervised principle. In this estimation, the input layer for three phases (a, b, and c) is expressed as

The detail application of this algorithm for the estimation of various control parameters is given as follows.

$$I_{lap} = W_O + i_{La}u_{ap} + i_{Lb}u_{bp+} + i_{Lc}u_{cp} \qquad (1)$$
$$I_{lbp} = W_O + i_{La}u_{ap} + i_{Lb}u_{bp+} + i_{Lc}u_{cp} \qquad (2)$$
$$I_{lcp} = W_O + i_{La}u_{ap} + i_{Lb}u_{bp+} + i_{Lc}u_{cp} \qquad (3)$$

Where Wo is the selected value of the initial weight and (u_{ap}, u_{bp}, u_{cp}) are the in-phase unit templates. In-phase unit templates are estimated using sensed PCC phase voltages (V_{sa}, V_{sb}, V_{sc}) It is the relation of the phase voltage and the amplitude of the PCC voltage (V_t). The amplitude of sensed PCC voltages is estimated as

$$V_t = \sqrt{2(v_{sa}^2 + v_{sb}^2 + v_{sc}^2)/3} \qquad (4)$$

Page 80

The in-phase unit templates of PCC voltages (u_{ap}, u_{bp}, u_{cp}) are estimated as

$$\mathbf{u_{ap}} = \frac{v_{sa}}{v_t} \, \mathbf{u_{bp}} = \frac{v_{sb}}{v_t} \, \mathbf{u_{cp}} = \frac{v_{sc}}{v_t} \; (5)$$

The extracted values of I_{Lap}, I_{Lbp}, I_{Lcp} are passed through a sigmoid function as an activation function, and the output signals Z_{ap}, Z_{bp}, Z_{cp} of the feedforward section are expressed as

$$z_{ap} = f\left(I_{lap}\right) \qquad (6)$$

$$z_{bp} = f\left(I_{lap}\right) \qquad (7)$$

$$z_{cp} = f\left(I_{lap}\right) (8)$$

The estimated values of Z_{ap}, Z_{bp}, Z_{cp} are fed to a hidden layer as input signals. The three phase outputs of this layer I_{Lap1}, I_{Lbp1}, I_{Lcp1} before the activation function are expressed as

$$I_{lap1} = w_{O1} + w_{ap}z_{ap} + w_{bp}w_{bp+} + w_{cp}u_{cp} \qquad (9)$$

$$\mathbf{I_{lap1} = w_{O1} + w_{ap}z_{ap} + w_{bp}w_{bp+} + w_{cp}u_{cp}} \qquad (10)$$
$$\mathbf{I_{lap1} = w_{O1} + w_{ap}z_{ap} + w_{bp}w_{bp+} + w_{cp}u_{cp}} \qquad (11)$$

Where (W_{01}, W_{ap}, W_{bp}, W_{cp}) are the selected value of the initial weight in the hidden layer and the updated values of three phase weights using the average weighted value (W_p) of the active power current component as a feedback signal, respectively. The updated weight of phase "a" active power current components of load current "W_{ap}" at the nth sampling instant is expressed as

$$\mathbf{w_{ap} = w_p(n) + \mu\{w_p(n) - w_{ap1}(n)\}f'(I_{ap1})z_{ap}(n)} \qquad \mathbf{(12)}$$

where (n) and (n) are `the average weighted value of the active power component of load currents and the updated weighted value of phase "a" at the nth sampling instant, respectively and $w_{ap1}(n)$ and $Z_{ap}(n)$ are the phase "a" fundamental weighted amplitude of the active power component of the load current and the output of the feed forward section of the algorithm at the nth instant, respectively. $f(I_{ap1})$ and μ are represented as the derivative of I_{ap1} components and the learning rate. Similarly, for phase "b" and phase "c," the updated weighted values of the active power current components of the load current are also expressed as same. The extracted values of I_{ap1}, I_{bp1}, and I_{cp1} are passed through a sigmoid function as an activation function to the estimation of the fundamental active components in terms of three phase weights w_{ap1}, w_{bp1}, and w_{cp1} as

$$z_{ap1} = f\left(I_{lap1}\right) \qquad (13)$$
$$z_{bp1} = f\left(I_{lap1}\right) \qquad (14)$$
$$z_{cp1} = f\left(I_{lap1}\right) \quad (15)$$

IV.CONCLUSION

Using this work, the investigation on the role of DSTATCOM is carried out to improve the power quality in distribution networks with static linear and nonlinear loads. PI controller is used with the device to enhance its performance. Test system is analyzed and results are presented in the previous chapter. DSTATCOM in the distribution networks under different fault conditions and it can be concluded that DSTATCOM effectively improves the power quality in distribution networks with static linear.A VSC-based DSTATCOM has been accepted as the most preferred solution for power quality improvement as PFC and to maintain rated PCC voltage. A three phase DSTATCOM has been implemented for the compensation of nonlinear loads us a BPT control algorithm to verify its effectiveness. The

proposed BPT control algorithm has been used for the extraction of reference source currents to generate the switching pulses for IGBTs of the VSC of DSTATCOM.

REFERENCES

[1] International Journal of Scientific and Research Publications, Volume 4, Issue 4, April 2014 ISSN 2250-3153.Roger C. Dugan, Mark F. McGranaghan and H. Wayne Beaty, Electrical Power, Systems Quality, Tata Mc Graw- Hill. Pages 1-8 and 39-80.

[2] Bhim Singh, AlkaAdya, A.P. Mittal, J.R.P Gupta, "Power Quality Enhancement with DSTATCOM for Small Isolated Alternator feeding Distribution System", conference on Power Electronics and Drive Systems, vol.1, pp. 274-279, 2005.

[3] Alexander Kusko, Sc.D., P.E., Marc T.Thompson, Ph.D., Power Quality in Electrical Systems, Tata McGraw-Hill publications, 2007.

[4] H.Nasiraghdam and A. Jalilian, "Balanced and Unbalanced Voltage Sag Mitigation Using DSTATCOM with Linear and Nonlinear Loads", Conference on World Academy of Science, Engineering and Technology, pp. 20–25, 2007.

[5] J. Sun, D. Czarkowski and Z. Zabar, "Voltage Flicker Mitigation Using PWM-Based Distribution STATCOM", Conference on Power Engineering Society Summer Meeting, Publication, vol.1 ,pp. 616 – 621,2002.

[6] Sung-Min, Woo Dae-Wook Kang, Woo-Chol Lee and Dong-Seok Hyun, "The Distribution STATCOM for Reducing the Effect of Voltage Sag and Swell", Conference on IECON'O1: The 27th Annual Conference of the IEEE Industrial Electronics Society Publication, vol.2, pp.1132 - 1137,2001.

[7] M. G. Molina, P. E. Mercado, "Control Design and Simulation of DSTATCOM with Energy Storage for Power Quality Improvements", Conference on IEEE PES Transmission and Distribution Conference and Exposition Latin America, Venezuela, pp.1 - 7, 2006.

[8] Pierre Giroux, Gilbert Sybille Hoang Le-Huy, "Modeling and Simulation of a Distribution STATCOM using Sirnulink's Power System Blockset", Conference on IECON 0l: The 27th Annual Conference of the IEEE Industrial Electronics Society, vol. 2, pp. 990 – 99, 2001.

[9] AfshinLashkarAra and Seyed Ali NabaviNiaki, "Comparison of The Facts Equipment Operation In Transmission And Distribution Systems" Conference on 17th Internationaln Conference on Electricity Distribution Barcelona, vol.2, pp.44,2003.

[10] Ben-Sheng Chen and Yuan-Yih Hsu, "An Analytical Approach to Harmonic Analysis and Controller Design of STATCOM", Conference on IEEE Transactions on Power Delivery, vol.22, 2007

IQAC COORDINATOR
SWAMI VIVEKANAND
COLLEGE OF ENGINEERING
KHANDWA ROAD, INDORE

PRINCIPAL
SWAMI VIVEKANAND
COLLEGE OF ENGINEERING
KHANDWA ROAD, INDORE

Significant of Smart Grid Technology in Power System

Sonal Baghel[1], Hemendra Khedekar[2], Manisha Gaur[3]

PG Student [POWER SYSTEM], Dept. of EE, Swami Vivekanand College of Engineering, Indore, India[1]

Assistant Professor (HOD), Dept. of EE, Swami Vivekanand College of Engineering, Indore, India[2]

Assistant Professor, Dept. of EE, Swami Vivekanand College of Engineering, Indore, India[3]

ABSTRACT: The Indian population are increasing day by day and energy demand are also increasing exponentially but the conventional energy sources are limited and exhaustible, not eco-friendly and more power loss in conventional Grid Technology, power supply also interrupted due to dependency on one source of energy.Today the time of new innovations in the field of technology because one of the primary needs for socio-economic development in any nation & all over the world is the provision of reliable electricity supply systems. The modernization of traditional Grid system is requirement of modern era because uninterrupted electricity is the basic need of development.

The main objective of my research work is to analyse the need of modernization of Grid technology by smart grid technology. To modernize the all Grid system first we proposed the small solar-wind On Grid Hybrid system. Using HOMER software for simulation & optimization of the Solar-Wind On-Grid hybrid system and cost analysis significant of smart grid, comparison between conventional & Smart Grid system. MATLAB software is used for simulation of modified boost converter for variable input.

KEYWORDS: Smart Grid, HOMER, Hybrid System, On-Grid, Smart Meter, MATLAB.

I.INTRODUCTION OF SMART GRID

Energy is the basic requirement to do any type of work without energy nothing possible in present. There are many types of energy in which one type of energy Electrical Energy, before generation of electrical energy all work based on mechanical system but after invention of electric power generation everything based on electric power.

India is a developing country, there are total 6, 38,596 villages in India, in which 5, 93,732 villages are inhabited. Out of 5, 93,732 villages, 5,127 villages are electrified only for some hours & rest 38605 villages are using kerosene lamp for lighting their houses.Rural areas receive only 5-10% of electricity to meet their demand. The total installed capacity for electricity generation in the country has increased from 16,271 MW as on 31.03.1971 to 370106 MW as on 31.03.2020. There has been increase in generating capacity of 18,654 MW over the last one year, which is 10% more than the capacity of last year. For full filling their demand, rural areas use renewable energy resources.

The adoption of SMART GRID Technology in India is the demand of modern era to compute at international level.

The "smart grid" is a term used to describe the rapid infrastructure replacement of the electrical wiring system in the United States. When the advanced system is completely implemented, it will allow for communication features across the grids that are not currently available--hence the term "smart"[1]. A "smart grid" is simply an advanced electrical distribution system that has the capability to balance electrical loads from diverse, and often intermittent, alternative energy generation sources. One key component of the "smart grid" is the capacity to store electrical energy; this allows the demand from consumers.

In this paper, we proposesthe solar-wind on grid hybrid system and using HOMER software analysed the modernization of grid technology by smart grid system.

II. SMART GRID ROAD MAP FOR INDIA

India has already established the India Smart Grid Task Force & India Smart Grid Forum to develop the framework and national policy. In this regard roadmap for future activities has already been released. Govt. of India has approved 14 pilot projects across the country for demonstration of different functionalities. Govt. of India has projected an outlay of about Rs. 9300 Cr for Smart Grid development during 12th plan period (2012-17).

POWERGRID has taken a leading initiative in developing Pondicherry as pilot smart grid project through collaborative efforts. Around 57 organizations have joined their hands for the project, where different attributes of Smart grid are being implemented in a holistic manner. "A Smart Grid is an electricity network that can intelligently integrate the actions of all users connected to it - generators, consumers and those that do both - in order to efficiently deliver sustainable, economic and secure electricity supplies."

## III. RENEWABLE ENERGY SOURCES

Now-a-days global warming is the most burning issue found in many of the climate summit. Many researchers, scientists are working their own relevant areas to reduce the Effective mitigation of climate effect due to global warming by using different techniques. Change will require deep reductions in greenhouse gas emissions.

Political and economic crisis, limitation of fossil reserves, environmental concerns, population and economic growth resulted in an increase in the use of renewable energy resources. However, the main problem of renewable energy is dependence of these sources to the weather conditions [35]. Therefore, there are oscillations in their outputs. To solve this problem, these generation units are used together. Therefore, there are oscillations in their outputs.

In the recent year, various combinations of renewable and non-renewable energy sources have been considered. Some of these combinations can be expressed as [14]:

➢ wind – solar – battery
➢ wind – micro turbine
➢ wind – solar – diesel
➢ wind – fuel cell
➢ solar – biomass

Wind and solar energy has become a common, because a requirement weather condition is available in many locations and technology needed to use this energy is provided [15].

IV. SIMULATION OF SOLAR-WIND HYBRID SYSTEM

The Hybrid Optimization Model for Electric Renewable (HOMER) software is used as a tool to carry out the research. The HOMER energy modelling software is a powerful tool for designing and analysing hybrid power systems. The proposed hybrid renewable energy system comprises of wind turbine and Photovoltaic (PV) array system.
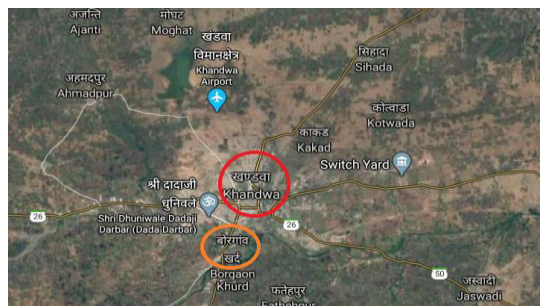
The solar-wind hybrid system design for village Borganw (MP).Village Borganw isolated from city khandwa, so many time villagers face power cut problem and electric bill problem also, therefore as a small project we study here for uninterrupted power supply and low cost availability of electric power.
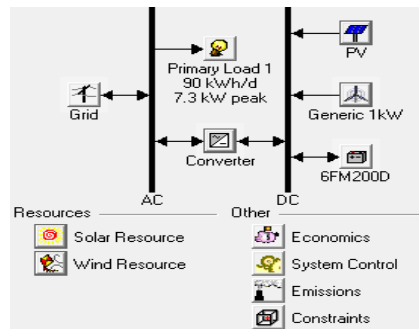
Fig. 1.1 Grid connected Solar-Wind Hybrid Model

In HOMER software first used component data input, software build a hybrid model after simulation software show the result as shown next chapter.

V. RESULT AND DISCUSSION

In optimization operation different combinations of the components are used and different feasible models are show as a result. In those results the best combination result is show in sensitivity process as shown in blue background.

Fig. 1.2 Simulation & Optimized result of Grid connected system

In grid-connected Hybrid system to fulfil the electric load 90 kWh/d, 10 kW PV array system, 10 kW wind turbine system and 10 kW grid connection are proposed for a feasible Hybrid system. The production of power by PV array is 17060 kWh/yr (43%), by Wind turbines 1648 kWh/yr (4%) and 20681 kWh/yr (53%) power required to purchase from grid to continuous supply. The total production of power is 39389 kWh/yr in which 32741 kWh/yr (87%) power is consumed by load and 4756 kWh/yr (14%) power is sale back to gird in excess power production situation.
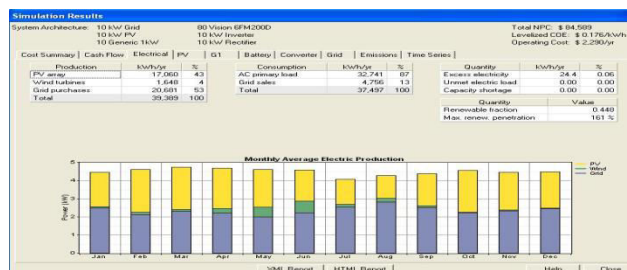
Fig. 1.3 Bar graph of electric production by hybrid system (On-Grid)

The results obtained for ON Grid (solar-wind) hybrid system, the optimized COE (cost of energy) is $ 0.176/(kWh)[Approx. 10.9 Rs/kWh] for above described load and designed system.
The total production of electricity is 39389 kWh/yr and unmet electric load and capacity shortage is 0% achieved as shown in figure. There is only 0.06% excess of electricity which can be saved and used by increasing further no of storage i.e. battery.

VI. CONCLUSION

The solar-wind hybrid system cost on installation year is high approximately Rs. 11/Unit but after installation year only operating and maintenance cost and grid sellback/purchase cost have to spend on the grid connected hybrid system therefore cost of energy per unit decrease up to Rs.4.22/Unit.

In "SMART GRID" system the cost of energy vary with variation in device cost variation and current data reading. Smart Grid technology calculates the cost of energy on the basis of current cost of devices and electricity charge calculated on real time consumption of energy.

In smart grid technology all system are operated according to requirements. Unlike conventional energy sources, renewable generations are highly intermittent and variable type. Large Scale Integration of renewable generation requires special balancing mechanism to deal with the uncertainty and variability to maintain grid stability & security.

REFERENCES

[1] Size Optimization of New Hybrid Stand-alone Renewable Energy System Considering a Reliability Index

[2] 'A hybrid solar-wind power generation system as an industrial resource for industrial technology students'- By Dr. Recayi Pecen, Dr. MD Salim, & Dr. Marc Timmerman

[3] Simulation of Closed Loop Controlled Boost Converter for Solar Installation Athimulam Kalirasu1, Subharensu Sekar Dash2

[4] http://homerenergy.com/software.html[accessed on 20.11.2020]

[5] Optimization of solar-wind hybrid system for distribution generation-Parita Dalwadi, V. Shrinet, C. R. Mehta and Pankit Shah

[6] Optimal Sizing and Operation Strategy of Hybrid Renewable Energy System Using HOMER Nurul Arina bte Abdull Razak,Muhammad Murtadha bin Othman, member, IEEE, Ismail Musirin, member, IEEE

[7] Simulation of Closed Loop Controlled Boost Converter for Solar Installation Athimulam Kalirasu1Subharensu Sekar Dash2

[8] MPSEB Head office Polo ground

[9] http://www.yhipower.com.au/main/data/vision/fmd_series/6FM200D.pdf [Accessed on 20.01.2020]

IQAC COORDINATOR
SWAMI VIVEKANAND
COLLEGE OF ENGINEERING
KHANDWA ROAD, INDORE

PRINCIPAL
SWAMI VIVEKANAND
COLLEGE OF ENGINEERING
KHANDWA ROAD, INDORE

Security Assessment of Authentication Protocols in Mobile Adhoc Networks

Megha Soni
Assistance Professor
SVCE, Indore India
meghasoni@svceindore.ac.in

Brijendra Kumar Joshi
Professor MCTE,
MCTE, Mhow India
brijendrajoshi@yahoo.com

Abstract—**Mobile Ad-hoc Networks can be easily targeted by different attacks such as Denial of Service, Wormhole and Man-in-the-Middle. A packet authentication is required in wireless communication to combat such attacks from outsider nodes. We have found out the parameters by which security of different protocols like HEAP, LHAP, TESLA, and Lu and Pooch's can be assessed. Also vulnerabilities of these protocols for different attacks have been discussed. To grade the performance of these authentication protocols, different parameters such as throughput, latency and packet delivery ratio have been used.**

Index Terms—HEAP, Authentication, Security, MANETs

I. INTRODUCTION

Mobile Ad-hoc Networks (MANETs) are getting noteworthy attention from industry and research area due to its versatile applications and security challenges. For example, in military applications, for infrastructure-less networks, MANETs are able to exchange strategic information and perform with high mobility. MANETs are also suitable for mobile conferencing in a big group of people. It can be quickly installed in emergencies like disaster management situations [1].

MANETs have to offer different levels of security in various applications for their successful utilization. However, due to absence of central authority and wireless links among nodes, they have much greater security issues than wired networks. An attacker can easily join or leave and snoop a network, as physical link is not required. Their aim is to disrupt the network, drop packets or inject fake packets. As a result, it is easy to launch Denial of Service (DoS) attack, Man-in-the-Middle attack and Wormhole attacks or imitate another node.

To improve MANET's security, different schemes such as secure routing using symmetric and asymmetric cryptography for key establishment and distribution have been proposed [2]. But, all these protocols are able to authenticate only control packets. If these are used for authentication of data packets, network overhead would increase. On the other hand, unauthenticated data packets make protocols vulnerable for different routing attacks, as it is essential to authenticate control and data packets both to provide guard against different attacks. Many authentication protocol like Hop-by-Hop Efficient Authentication Protocol (HEAP), Lightweight Hop-by-Hop Authentication Protocol (LHAP), Timed Efficient Stream Loss-tolerant Authentication (TESLA) and Lu and Pooch's algorithm have been designed to authenticate both types of packets.

II. AUTHENTICATION IN MANETS

In this process, an authentication protocol is used by authenticator to verify credentials presented by a supplicant. In this way supplicant's access privileges are established by the authenticator. Such an authentication protocol may also use a Trusted Third Party (TTP) during such a process. Here an supplicant is defined as an entity seeking access of protected resources through an authenticator, which is an entity that controls access to some resources. Further, it makes authentication decisions during the authentication process. A sequence of messages are exchanged between entities to identify each other. Here either supplicant or authenticator distribute secrets or allow secrets to be recognized. Further, an identifier that is used to authenticate a supplicant with high confidence is called a credential. Also, an entity trusted by both, supplicant and authenticator, is called TTP.

III. NEED OF AUTHENTICATION PROTOCOLS

Communication links in MANETs, in contrast to fixed networks, are open shared medium. As a result, communication between neighboring nodes is more vulnerable to attacks. In MANETs, due to constrained resources; limited battery power, small computational capacity and rapid changes in topography; both data packet delivery and authentication protocol used for routing need to be scalable and light weight. In MANETs, techniques such as asymmetric cryptography, being very intensive, are prohibitively insufficient due to associated computational complexity and message overhead. Contrastingly, symmetric cryptographic algorithms are fast; yet

complex in key maintenance, thus it creates difficulty in authentication of multicast and broadcast communication.

Need for efficient and large-scale data dissemination is driving popularity of broadcast communication. Ability of broadcast networks to distribute packets to multitude of receivers also frequently facilitates malicious users to impersonate as a sender and inject packets in a broadcast network. This gives rise to need for authentication protocol which will enable receivers to verify that a given received packet was indeed sent by the claimed sender.

Appending a Message Authentication Code (MAC); generated by use of a shared secret key; as usually deployed in point-to-point authentication mechanism; is actually insufficient to provide secure broadcast authentication. This is because any receiver with a secret key can forge data and function as a sender. To prevent such attacks, asymmetric cryptographic protocol becomes a natural choice. While its action of signing each data packet indeed provides secured broadcast authentication, it is associated with high overhead, time required to sign and verify as well as the consequent use of bandwidth.

There are many techniques which gradually reduce this overhead by using single signature over several packets; yet none of those offer complete satisfaction about their bandwidth deployed, scalability and processing time in network. And as against this, serious vulnerabilities against attacks; like DoS, replay attack, Man-in-the-Middle attack and Wormhole attack are possible If data packets are unauthenticated, loss of robustness to packets loss are observed. Serious attacks like DoS are possible If an attacker floods the receiver with bogus packets supposedly containing a signature while authentication deploying schemes amortize a digital signature over multiple data packets. The receiver gets overwhelmed while verifying bogus signatures as the signature verification being computationally costly.

Researchers have recognized that to protect against such attacks, it is important to authenticate both data as well as control packets; and have accordingly designed requisite authentication protocols.

IV. Authentication protocols

In TESLA [3], packets are not authenticated at every Hop; instead it uses end-to-end authentication in which packets are authenticated by final receiver, that too after a delay of several seconds. As a result, TESLA's throughput for mobile nodes is mediocre and suffers from long latency. Moreover, it also requires loose time synchronization between sender and receiver.

LHAP is built on principles of TESLA and it makes an attempt to overcome its drawbacks. Actually, LHAP was designed for MANETs and makes use of Hop-by-Hop authentication [4].

It deploys twin techniques of lightweight packet authentication and lightweight trust management and is consequently more efficient compared to traditional authentication algorithms. It is characterized by reduced number of public key operations as it makes use of TESLA for trust bootstrapping and maintaining trust relationships among a set of nodes. LHAP employs one-way hash chains in packet authentication technique.

Lu and Pooch's algorithm is based on LHAP. Even this algorithm uses Hop-by-Hop authentication and is known to be efficient like LHAP[5][6]. Yet, it uses only one key at every node instead of two as used by LHAP. Lu and Pooch's algorithm makes use of 'delayed key disclosure' like TESLA; resulting in network latency.

HEAP is independent of routing protocol used. It is suited for most applications, whether unicast, multicast or broadcast. It is very efficient protocol as it uses two keys and is based on modified HMAC algorithm [7].

In HEAP; as and when due to mobility, a given node's neighborhood alters; the said node shares the *Ikey* and a new *Okey* with each new neighbor. Even TESLA, LHAP and Lu function on similar lines. These keys need to expire after a certain amount of time and new keys should be generated, e.g. after every few hours is another requirement. This is one way to guard against crypt-analysis attacks by an adversary.

V. Security attacks on authentication protocols

Authentication Protocols in MANETs are prone to different types of attacks on their mechanism. Such attacks are mainly divided into two groups [4]; Outsider attack and Insider attack.

A. Outsider Attacks

Outsider attacks are defined as attacks from nodes which do not hold a valid certificate. Such attacks are further classified into two types.

1) Single Outsider Attack: This type of attack is possible when a valid node moves out of the range of other nodes for a period of time; and this transmitting node is not aware of the absence of node. Further, transmitting node happens to have disclosed its TESLA and TRAFFIC keys for the said time period and a malicious node now obtains these keys and uses the same to pretend a node from the network.

2) Collaborative Outsider Attack : Wormhole attack [8] is a type of collaborative outsider attack. It is launched by multiple attackers. These attackers form a private tunnel by which they communicate directly. For example, node A wants to send packets to node E but node P1 eavesdropped key messages and traffic packets of node A and forwards to P2 via

a wormhole tunnel. Then P2 can alter and rebroadcast to node E.

B. Insider attack

These attacks are launched by one or more nodes which are compromised and hold legal certificates. Insider attacks can be classified in to two types.

1) Single / Multiple Insider Attack : To increase the traffic inside the networks a compromised node may try to flood many traffic packets into the network. These attacks can be initiated by many compromised nodes which were legitimate previously.

2) Insider Clone Attack : When a compromised legitimate node shares its identity or private key with an outsider attacker node and both holding the same identity. It is less likely to detect an outsider node. The cloned nodes are mostly spread in different network areas. The collaborative attack by these nodes is called clone attack.

A few important attacks that affect authentication protocols are: Man-In-The Middle attack and DoS attack. In case of Man-In-The Middle, the attacker impersonates both sender as well as the receiver with respect to each other and without their knowledge of attack. In this attack, which is also called Bucket Brigade attack, the attacker is actively eavesdropping upon the link between the verifier and the prover and thereby intercepting all authentication messages being exchanged by the sender and the receiver in the network under attack [9].

In DoS attack, an attacker causes unnecessary communication delay in data reaching its destination or network traffic is dropped altogether or even redirected to another destination.

TABLE I.   ATTACKS ON PROTOCOLS

Name of Protocol	Attack		
	Man in Middle	*Wormhole*	*DoS*
Lu and Pooch's	No	No	Yes
TESLA	No	Yes	Yes
LHAP	Yes	Yes	Yes
HEAP	No	No	No

Source authentication schemes like TESLA having a upper bound limit on traffic rate but it can prevent some attacks on MANETs. In case of Hop-by-Hop authentication every node authenticates only neighborhood nodes in place of the sources of original traffic, compromised node is able to pretending itself as a valid forwarding node and transmits malicious traffic

inside the network. It does not offer strong source authentication,

TESLA, LHAP and Lu and Pooch's algorithm refer Table I are vulnerable to DoS attack and requires that all the nodes should be synchronized in time [7]. To prevent TESLA, LHAP and Lu algorithm from certain attacks, it is required that when a node moves from the range, one or two keys should be exchanged with all new neighbor nodes. The keys should be valid for fix time and after that it should expire and a new key should be generated for same time period.

To prevent "Man in-the-Middle" attacks from the TESLA it uses delayed key disclosure. LHAP is vulnerable to Wormhole and Man-in-the-Middle attacks refer Table I because periodic delayed key disclosure is not used in these algorithms [4].

HEAP offers some level of protection against insiders who try to forge packets and impersonate other insiders in order to incriminate them. Any packet transmitted by an outsider node should be immediately dropped by the receiving insider node at the first hop with a very high probability.

HEAP successfully guards against many outsider attacks refer Table I , such as DoS attack that attempt to flood the network, Wormhole attack, Man-in-the-Middle attack, and Flooding etc. [7].

VI.   SECURITY PARAMETERS

Security of any protocol can be assesed by following parameters-

- Protocol is based on source authentication or hop by hop authentication.

- Technique used for message broadcasting, weather protocol is multicast or unicast.

- Algorithm used for trust maintenance in authentication.

- No. of Keys used in trust bootstrapping.

- Condition of trust termination between two nodes.

- Use of symmetric cryptography (Digital Signature) in trust management.

- Delayed authentication with indexing in transmission.

- Delay time of key disclosure

- Use of varied delay in key disclosure

VII. PERFORMANCE PARAMETERS

The performance metrics employed to analyze different protocols are- Authentication Latency, Throughput, and Packet Delivery Ratio (PDR).

A. Authentication Latency

The latency in a packet authentication is due to MAC verification and delay key disclosure. The latency of MAC verification is less than one millisecond and it is due to computing one hash. The latency in packet authentication is mainly due to the key disclosure delay. The value of key disclosure delay is based on current traffic pattern and it is decided by the packet sender.

B. Throughput

Mean Throughput can be defined as the ratio of the number of packets successfully received by each node and total simulation time [10].

C. PDR

PDR is measured as the ratio of number of packets successfully received by each node and total number of packets sent [10].

Authors [7] have performed the simulation on GloMoSim v2.03. Following approximate values of Mean latency variation (Table II), PDR variation (Table III) and Throughput variation (Table IV) are found by the study of simulation results graph of TESLA, LHAP, Lu Pooch's algorithm and HEAP.

Mean latency of HEAP is very low as compared to other protocols.

In case of TESLA, LHAP and HEAP, the peak value of PDR (Table III) is reached approximately 85% at packet rate 20 packets/sec. Initially PDR remains constant up to 25 pkts/sec. As can be seen, at higher packet rates, PDR quickly reduces and tapers off to around 10%., as the throughput is a function of the product of the PDR and packet rate.

The peak value of throughput (Table IV) is reached at 25 packets/sec, because throughput is proportional to product of the PDR and packet rate. For high packet rate throughput falls sharply cutting with PDR but for packet rate more than 50 packets/sec. throughput is nearly constant and effect of low PDR is offset by the high packet rate.

The performance of Lu's algorithm is significantly poorer than all other algorithms in both PDR and throughput. It is due to caches of packets at first forwarding nodes. First forwarding node cached packets until it would not receive a key update packet.

TABLE I. Variation of Mean Latency

S.No.	Number of Hops	Protocol			
		LHAP	HEAP	TESLA	Lu Pooch's
1	1	1000	4	20000	2000
2	2	1000	10	20000	6000
3	3	1000	12	25000	9000
4	4	1000	14	30000	10000
5	5	1000	16	35000	11000

TABLE II. PDR (%) Variation

S.No.	Packet Rate (Pkts / sec)	Protocol			
		LHAP	HEAP	TESLA	Lu Pooch's
1	20	85	85	85	40
2	40	36	36	36	19
3	60	21	20	20	10
4	80	16	16	15	9
5	100	15	15	13	9

TABLE III. Variation of Throughput(bytes/s)

S.No.	Packet Rate (Pkts /sec)	Protocol			
		LHAP	HEAP	TESLA	Lu Pooch's
1	20	8800	8800	8800	4000
2	40	7200	7200	7200	3700
3	60	6800	6000	6800	3500
4	80	6900	6600	6500	3900
5	100	6900	6600	6300	4700

VIII. Conclusion

We compared the performance of HEAP, TESLA, LHAP and Lu and Pooch's algorithms and it is observed that TESLA is vulnerable to DoS attack and requires secure time synchronization of all the nodes. It introduces very large latencies of several seconds making it unsuitable for real time or QoS applications. LHAP is vulnerable to Wormhole and Man-in-the Middle attack. It also has very large memory requirements at every node. Lu's scheme has overall poor performance. In this scheme, throughput and PDR significantly degrade. It has extremely low memory requirements. HEAP is resistant to several outsider attacks such DoS, Wormhole, Replay. HEAP is suitable for use in MANETs for unicast, multicast or broadcast applications.

IQAC COORDINATOR
SWAMI VIVEKANAND
COLLEGE OF ENGINEERING
KHANDWA ROAD, INDORE

PRINCIPAL
SWAMI VIVEKANAND
COLLEGE OF ENGINEERING
KHANDWA ROAD, INDORE

IX. REFERENCES

[1]. Perkins, C. E. "Ad hoc Networking", Pearson Publication, India, 2008,

[2]. M. Soni, and B. K. Joshi, "Security Assessment of SAODV Protocols in Mobile Ad-hoc Networks", Proceeding of the International Symposium Data Science and Big Data Analytics (ISDB ACM-WIR 2018), Indore; 5-6 January 2018, pp. 347-355.

[3]. A. Perrig, R. Canetti, J. D. Tygar, and D. Song; "The TESLA Broadcast Authentication Protocol", Journal of Crypto Bytes, vol. 5, no. 2, Summer / Fall, 2002, pp. 2-13.

[4]. S. Zhu, S. Xu, S. Setia, and S. Jajodia, "LHAP: A Light-weight Hop-by-hop Authentication Protocol for Ad-Hoc Networks", Proceeding of 23rd IEEE International Conference on Distributed Computing Systems Workshops(ICDCSW03), Providence, USA, 19-22 May 2003, pp. 749.

[5]. Lu and U. W. Pooch, "A Lightweight Authentication Protocol for Mobile Ad Hoc Networks", Proceeding of the IEEE International Conference on Information Technology (ITCC'05), Las Vegas, USA, 4-6 April 2005, pp. 546-551.

[6]. Lu and U. W. Pooch, "A Lightweight Authentication Protocol for Mobile Ad Hoc Networks", International Journal of Information Technology, vol. 11, no. 2, 2005, pp. 119-135.

[7]. R. Akbani, T. Korkmaz and G.V.S. Raju; "HEAP: Hop-by-hop Efficient Authentication Protocol For Mobile Ad-hoc Networks", Proceeding of the Spring Simulation Multiconference, SpringSim 2007, Norfolk, Virginia, USA, 25-29 March 2007, pp. 157-165.

[8]. B. K. Joshi and M. Soni; "Security Assessment of AODV Protocol under Wormhole and DOS Attacks", Proceeding of the 2nd International IEEE Conference on Contemporary Computing and Informatics (IC3I2016), Noida , India, 14-17 December 2016, pp. 173-177.

[9]. N. Pari S, "Investigation of malicious nodes by security improvisation of routing in mobile ad hoc networks", PhD Dissertation, Anna University, Chennai 2014, pp. 111-112.

[10]. Megha Soni, and Brijendra Kumar Joshi; "Security Assessment of Routing Protocols in Mobile Ad-hoc Networks"; Proceeding of the International IEEE Conference on ICT in Business, Industry and Government (ICTIBIG2016) Indore; 18-19 November 2016, pp. 24.

[11]. M. Soni, and B. K. Joshi, "Security Assessment of DSDV Protocol in MANET", International Journal of Advance Computational Engineering and Networking (IJACEN), vol. 5, no, 9, September 2017, pp. 107-111.

AUTHORS PROFILE

Megha Soni doning PhD research work at Electronics and Telecommunication Department of MCTE, Mhow, DAVV University Indore, India. She has obtained BE in Electronics and Telecommunication Engineering from Govt Engg College, Sagar; M.E in Digital Communication from Davi Ahilya University Indore. She joined as an Assistant Professor in Electronics & Communication in Dec. 2005. Her research interest is in security assessment of routing and authentication protocols of Mobile Ad Hoc Networks.

Dr Brijendra Kumar Joshi is associated with as a Professor of Electronics &Telecommunication and Computer Engineering at Military College of Telecommunication Engineering, MHOW (MP), India. He has obtained BE in Electronics and Telecommunication Engineering from Govt Engg College, Jabalpur; ME in Computer Science and Engineering from IISc, Banglore, PhD in Electronics and Telecommunication Engineering from Rani Durgavati University, Jabalpur, and MTech in Digital Communication from MANIT, Bhopal. He has more than 34 years of teaching experience. His research interests are programming languages, compiler design, digital communications, mobile ad-hoc and wireless sensor networks, image processing, software engineering and formal methods. He has number of research publications to his credit. He has supervised six Ph D thesis and currently supervising nine research scholars. He has authored two books on Data Structures and Algorithms in C/C++ published by Tata McGraw-Hill, New Delhi.

IQAC COORDINATOR
SWAMI VIVEKANAND
COLLEGE OF ENGINEERING
KHANDWA ROAD, INDORE

PRINCIPAL
SWAMI VIVEKANAND
COLLEGE OF ENGINEERING
KHANDWA ROAD, INDORE

Development of Natural Fiber Composite and Characeristics

Geeta Dwivedi[1], Mr. Manoj Sharma[2], Mr. Vishal Wankhade[3], Dr. Rahul Joshi[4], Dr. Pradeep Kumar Patil [5]

Research Scholar[1], Swami Vivekanand College of Engineering, Indore, India

Assistant Professor[2&3], Swami Vivekanand College of Engineering, Indore, India

Associate Professor[4&5], Swami Vivekanand College of Engineering, Indore, India

Abstract : In past few years, composites are gaining considerable importance by their low cost, lighter weight, easy availability and are also ecofriendly as compared to synthetic fiber. These are the important attractive characteristics of composites that make them useful for almost all fields like engineering, medical etc. In this work naturally obtained FRC materials like sunn hemp and coconut fiber are used. The sunn hemp and coconut fiber are adopted as a natural Fiber and epoxy resin is applied as matrix to make the composite. The hand layup process is used to prepare the samples at normal temperature. The sunn hemp and coconut fiber are reinforced in the matrix at two different fibre percentage 3% and 5%. To avoid voids these samples are kept under pressure for 24 hr. Universal Testing Machine is used for to test the tensile strength and flexural rigidity as per the standard. The composites are analyzed in Hypermesh software. The results are compared with pure epoxy sample and it is analyzed that composite with coir Fiber gives more strength than pure composite. It is evaluated that tensile strength increases with rise in angle of orientation whereas flexural rigidity decreases.

IndexTerms - Sunn hemp, Coconut fiber, Composite, Hand layup, Universal Testing Machine.

I. INTRODUCTION

New material development mutates design and manufacturing processes. The availability of new materials enhances an existing design or process and also revolutionizes it entirely. In the modern society, materials came out as one of the most remarkable areas of research on a global level and in all disciplines. Whether they are a natural resource or a product of artificial substances, all the materials people use have an huge impact on the environment, economy, health, and finally, on the quality of life of people as end users. Some examples of new materials developed or been used in industries are Grapheme in Smartphone, Coatings harder than steel, Mindboggling Recycling and composites.

A material which is contains two or more materials at a microscopic scale and have chemically different phases which is Heterogeneous at a microscopic scale but statically homogeneous at macroscopic scale. The Constituent materials mixed together to form composite have significantly different properties.

One of the constituent reinforcements which provide strength to the matrix and the other is used to embed the reinforcing phase material which is called the matrix. It holds the reinforcements in one place. And this combination of matrix and reinforcements is called as the composite.

The reinforcement's are available in varieties like fibers, particles, or flakes. The reinforcement transfer's the strength to matrix. The matrix is a fluid like epoxy resin used to bind the fibers together. It behaves as a protection from environment. It is responsible for uniform distribution of load in the fibers which results in the development of same quantity of strain in the fiber. Matrix phase is comparatively light-weight and weak than reinforcement.

Tailored characteristics can be developed in the composites which make it useful in almost all areas.

The following conditions are needed to be fulfilled for a material to be a composite:

a) It can be manufactured both by naturally and/or artificially available composites.
b) It is composed phases which are set orderly which may be physical and/or chemical and segregated by a line
c) It has different characteristics from the components used separately.

II. Literature Review

Asim Shahzad et. al. He studies that Hemp fibers have properties that make them a suitable material to replace glass fibers as reinforcements in composite materials. Their main drawback is the uncertainty in their properties. Immeasurable research has been bring off on hemp fiber composites using thermoplastic, thermo sets, and biodegradable polymer matrices. These composites have express mechanical properties which, in some cases, excel even those of glass fiber composites. different fiber surface treatments have been explain to improve the hemp fiber/matrix interfacial bonding, brought improved mechanical properties. Another drawback of sunn hemp fiber composites, their moisture assimilation, can also be overcome by using fiber surface treatment process.

Kiran Rohit et. al. It is a review paper this review has provided a concise summary of the major material attributes of natural fiber composites. These includes: good specific – but different – properties of mechanical, environmental recommendation (renewable, biodegradable, low embodied energy, non-toxic), less cost, high water absorption rate, low durability and bio similarity. After inspect, the current literature present on natural fiber composite the particulate fiber such as coconut coir, Lantana camera, sisal have been already utilized. This developed in growing interest in natural lingo cellulosic materials and composites based on them. addition of wood flour in polyester improved the load bearing capacity (tensile strength) and the ability to withstand bending (flexural strength and modulus) but with the incorporation of met kaolin in wood flour polyester composite adequately decrease the tensile, flexural modulus and strength and increases the water absorption.

III. Objective

The objective of this research work is to determine a better option in the field of reinforcement material.

The first objective is to utilize the natural waste in the form reinforcing material; therefore coir fiber is taken. The second objective is to develop the composite material by using the coir rope which has been achieved successfully. The third objective is to use of fiber content variation to find out the better result in composite and also use a mixed fiber for compare all the result. After the manufacturing of composites mechanical properties like tensile strength and flexural rigidity were evaluated.

IV. Methodology
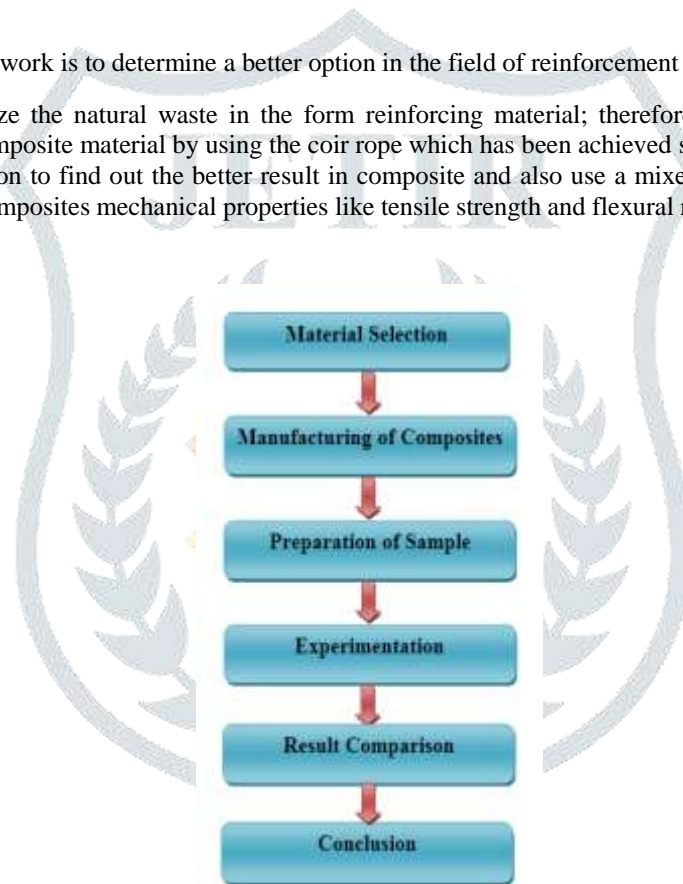
Fig 1 Methodology Flow Chart

V. Material Selection

Matrix phase: Epoxy resin is nominated as a matrix. It is a polymer matrix that is commonly used is having a thermal conductivity of 0.363W/mK .These resins have low molecular weight and available in viscous liquid form. Epoxy resin and hardener (Haksons clear coat epoxy resin and hardener). We have used this epoxy resin as matrix phase material because it is easily available, corrosive resistant, it has good strength and ability to transfer stress to reinforcement material without failure. As a result, various epoxy adhesives have been manufactured to satisfy.

Various demands based on the applications.Theyaresuitableforanyproductrequiringahighstrengthadhesiveandcan be used on a variety of materials. The density of this epoxy is 1.1gm/cc3 and the density of hardener is 0.98gm/cc^3.

Fig 2 Epoxy Resin used in matrix phase

Properties of Epoxy Adhesives

As used as a binding material, the epoxy material needs to withstand warmth, water, and it should be chemical resistant. It also needs to have a high level of adhesion on a variety of substance sand to be adaptable enough to be formed into various shapes. All these properties can be achieved by handling the situations by which the adhesives are being created. Epoxies are additionally sturdy and can withstand substantial burdens, making them astonishing basic glues. Epoxies come in possibly one-part or two-segment frameworks. The primary contrast between the frameworks is the distinction in relieving temperatures.

Properties of Hardener

- A hardener is a segment of particular sorts of blends. In certain blends a hardener is utilized basically to build the flexibility of the blend once it sets. In different blends a hardener is utilized as a curing agent. Hardener in various forms such as reactant or in the form of catalyst that occurs in the reaction during the process of mixing.
- Hardeners are quite often important to make an epoxy resin helpful for its planned reason. Without a hardener, epoxies don't accomplish anyplace close the noteworthy mechanical and chemical properties that they would be with the hardener. The right type of hardener must be chosen to guarantee the epoxy blend will meet the necessities of the application. Research ought to consistently be done on both the resin and the hardener to ensure the last epoxy blend will perform agreeably.
- Hardeners are utilized to fix epoxy resins. In any case, basically adding a hardener to an epoxy gum may not make the epoxy blend fix rapidly enough. If so an alternate hardener might be required. Additionally, hardeners with specific added substances can be utilized. This hardener added substances fill in as catalysts that accelerate the restoring procedure.

Reinforcement phase:

They can be particles, flakes, whiskers or sheets. Here we have used coir rope as reinforcement in the matrix material. Composites are fabricated by the means of coir rope at three different orientation angles namely 0°, 45° and 90°. Coir fiber rope strands are used for making of composites by arranging the strands of ropeside by side with no gap between them.Coir ropes are used as because they are light weight and their fibers possess fairly good strength.

Materials Used:

Coconut fiber

Coir is the naturally obtained fiber which is taken from the outer covering that is called as the coconut shell husk. These are non uni-cellular, hard & rigid array of natural fruit fiber. They are renewable and biodegradable in addition to that it has several properties such as good amount of strength, sufficient length, moisture regain capacity and high durability against solar radiations, salty water, microbes etc. They are modified into coir ropes .The thermal conductivity of coir rope is about 0.1036 W/mK and its density is 0.75 gm/cc^3. The specimen samples are prepared from this coir rope. Now here this coir rope strands are the main load carrying constituents which are acting as a reinforcing material for the composites.

Fig 3 Coconut Coir Fiber used in reinforcement phase

Sunn hemp

Sunn, (Crotalaria juncea), also called sunn hemp or Indian hemp, annual plant of the pea family (Fabaceae) and its fiber, one of the bast fiber group. The fiber is made into cordage, fishing nets, sacking fabrics, canvas, and rug yarns and is used to manufacture such paper products as cigarette and tissue papers. These Fibers are being procured for use as the composite Fiber due to its mechanical properties it possesses which are discussed herewith. It has a Fiber diameter of 48 μm, its apparent Density is 1.34 g/cm^3 , Its Ultimate tensile strength is 200-300 MPa, its Modulus is 2.68 GPa, and its Extension at breakage is 2.5-3.5% (Details Procured from Central research institute for jute and allied Fibers(ICAR), West Bengal.) all the sunn hemp long fiber arranged in a straight line and then cut them into small flakes about 1 cm. They are used for making samples of composite.

Fig. 4 Sunn Hemp Fibre used in reinforcement phase

Specimen Preparation

Specimens are made and have the following dimensions:

TEST	SCHEMATIC FIGURE		
Tensile strength	2.5 cm	29 cm	

3%SHFE   5%SHEF   3%CFE   5%CFE   3%SHCFE   5%SHCFE

Fig. 5 Specimen prepared with different combination of reinforcement and matrix material

Table 1 – Nomenclature of Specimen Prepared

Abbreviations Used	Details
3% SHFE	3% Of sunn hemp fiber epoxy composite
5% SHFE	5% Of sunn hemp fiber epoxy composite
3% CFE	3% Of coconut fiber epoxy composite
5% CFE	5% Of coconut fiber epoxy composite
3% SH-CFE	3% Of sunn hemp + coconut fiber epoxy composite
5% SH-CFE	5% Of sunn hemp+coconut fiber epoxy composite

Tensile test:

This test is one kind of mechanical test. It is also referred as tension testing. It's a basic material science check during which a specimen is put down in tension till failure occurs. By tensile test we determine the ultimate tensile strength value of the material, in this test a sample is typically pulled to its breaking point. A tensile test is used to knowhow a material will behave and also to find out the elongation within the material. Tensile tests are normally performed on UTM.

In this test, test piece ends are hold into the grips and are linked to a device that measures the load. If small load is applied, the deformation will be entirely elastic. However, when the value of the load increased further, the material is permanently deteriorated. Usually, this test is performed at normal temperature and the load is applied gradually.

Effect of Different fiber used in composite

The tensile strength represents the maximum stress which it can bear prior to its failure. UTM TUE-C-200 of load capacity 200 kN is used to test specimens as per ASTM D3039 standards.
It was found that the tensile strength value of the fiber epoxy composite is increased for all samples of fiber epoxy as compare to plain epoxy. The value of the tensile strength varies with the change of composite fiber and increases with the increase of fiber content.

The tensile strength for 5% CFE samples was found to be maximum.

Observation table of tensile strength of composite fiber at different % fiber contribution as shown in figure below:

Table 2 Observation Table of Tensile Strength for Different Fibre Composite

S.NO	NAME OF SPECIMEN	TENSILE STRENGTH
1.	3% SHFE	6.374 Mpa
2.	5% SHFE	19.005 Mpa
3.	3% CFE	18.906 Mpa
4.	5% CFE	21.536 Mpa
5.	3% SH-CFE(Hybrid)	9.292 Mpa
6.	5% SH-CFE(Hybrid)	18.833 Mpa
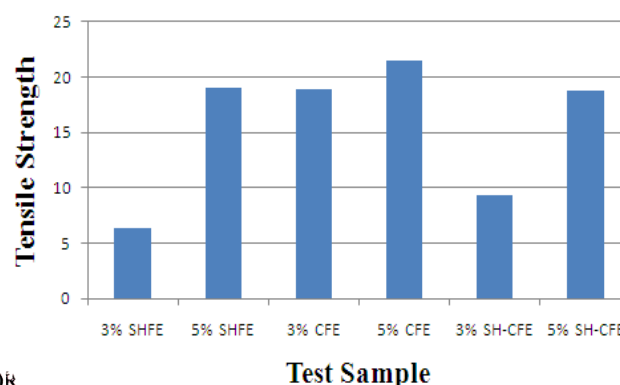
Fig. 6 Graph for tensile strength of different fiber composite

Graphical representation of Tensile Testing results of different composite fiber material on UTM Machine
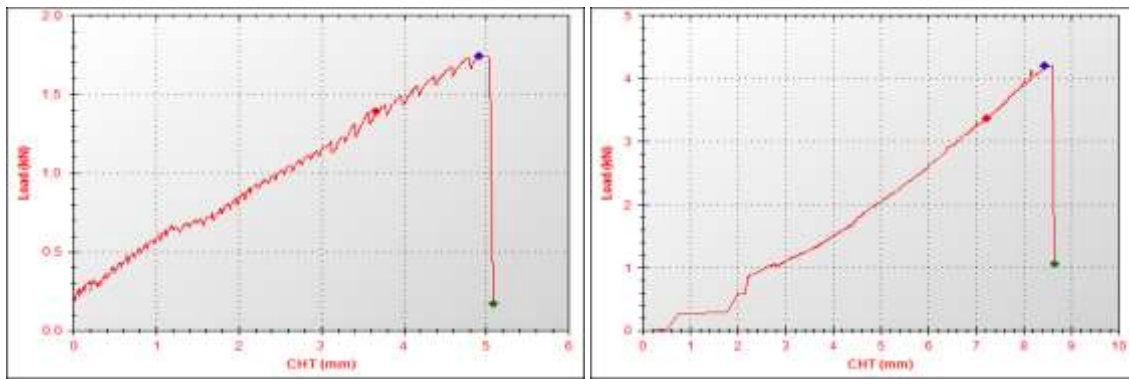
Fig.7 (3% SHFE & 5% SHFE)
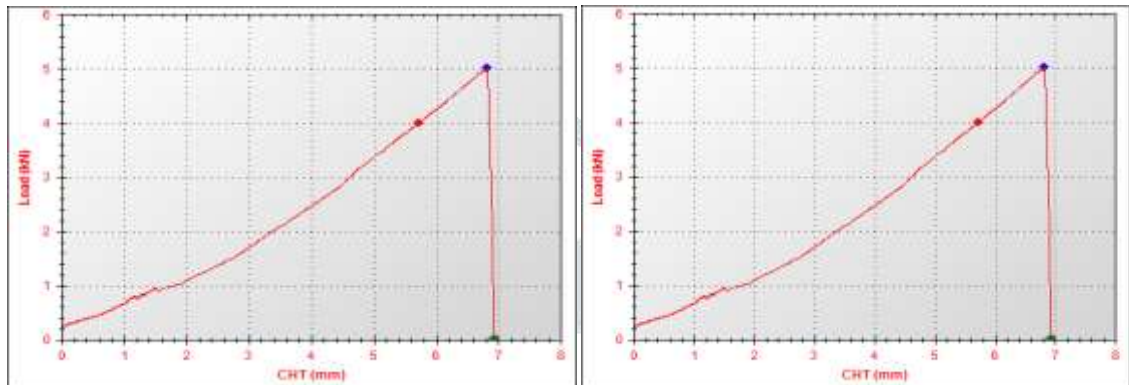
Fig. 8 (3% CFE & 5% CFE)
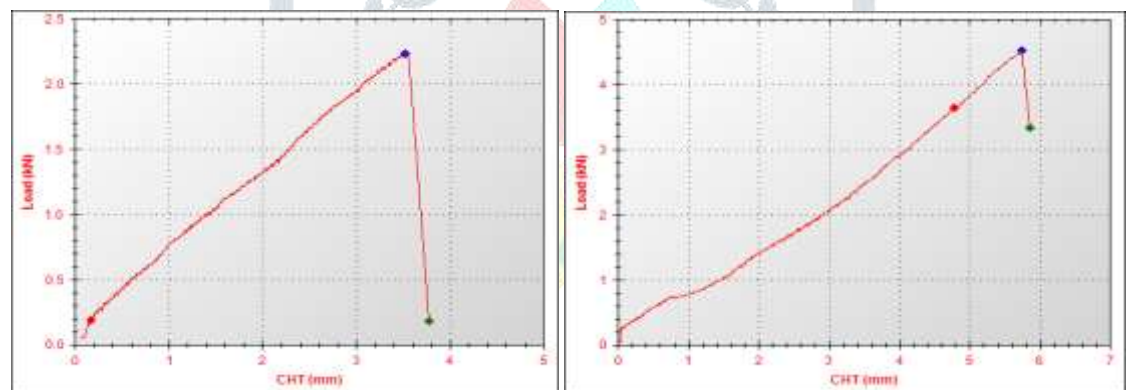
Fig.9 (3 % SH-CFE(Hybrid) & 5% SH-CFE(Hybrid))

Observation table of percentage of elongation of different fiber composite at different percentage of fiber contribution

Table 3 Observation Table of % Elongation of Coconut fiber, Sunn hemp fibre and Hybrid Fiber Composite

S.NO	NAME OF SPECIMEN	% ELONGATION
1.	3% SHFE	12.50%
2.	5% SHFE	2.50%
3.	3% CFE	5%
4.	5% CFE	3.75%
5.	3% SH-CFE(Hybrid)	3.7%
6.	5% SH-CFE(Hybrid)	2.50 %

IQAC COORDINATOR
SWAMI VIVEKANAND
COLLEGE OF ENGINEERING
KHANDWA ROAD, INDORE

PRINCIPAL
SWAMI VIVEKANAND
COLLEGE OF ENGINEERING
KHANDWA ROAD, INDORE

Page 97
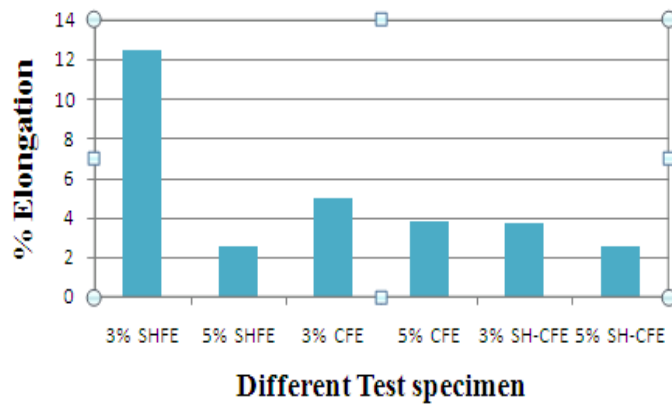
Fig. 10 Percentages of Elongation of Coconut fiber , Sunn hemp fibre and Hybrid Fiber Composite

Observation table of Impact Strength of different fibre composite at different % of fibre contribution as shown in figure below:

Table-4 Observation Table of Impact Strength of Coconut fiber, Sunn hemp fibre and Hybrid Fiber Composite

S.NO	NAME OF SPECIMEN	IMPACT RESULT
1.	3% SHFE	2.3 KJ
2.	5% SHFE	8.2 KJ
3.	3% CFE	9.2 KJ
4.	5% CFE	11.1 KJ
5.	3% SH-CFE(Hybrid)	5.1 KJ
6.	5% SH-CFE(Hybrid)	9.9 KJ
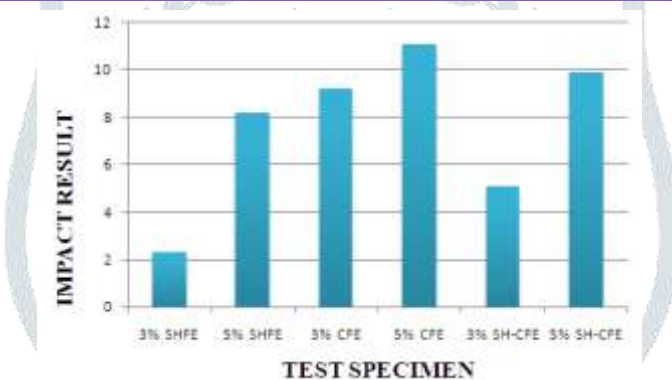
Fig. 11 Impact Strength of Coconut fiber, Sunn hemp fibre and Hybrid Fiber Composite

Comparison Graph of Impact Strength and Tensile Strength of different fiber composite at different % of fiber contribution as shown in figure below:
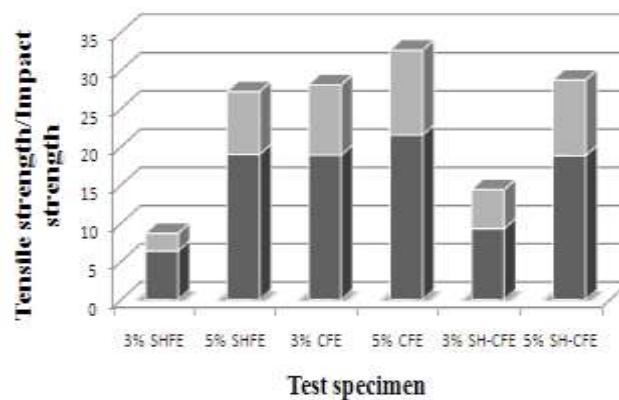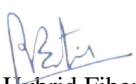
Fig. 12 Comparison Graph of Impact Strength and Tensile Strength for Coconut fiber, Sunn hemp fibre and Hybrid Fiber Composite

VI. CONCLUSION

Coir fiber epoxy samples were fruitfully made by utilizing coir fibers as reinforcement with epoxy resin as a matrix. By performing the tensile test using the Universal Testing Machine it was concluded that by increasing the fiber content, the tensile strength of FE-composites can be increased. The maximum value of tensile strength that was determined through the test was 5% CFE samples and if looking at the percentage elongation the maximum value is found out to be 3% for SHFE. If all the samples are compared, the fiber which has good tensile strength and less percentage elongation is the Coconut fiber than Sunn hemp and Hybrid composite samples. The conclusion is also shown in the following graph.
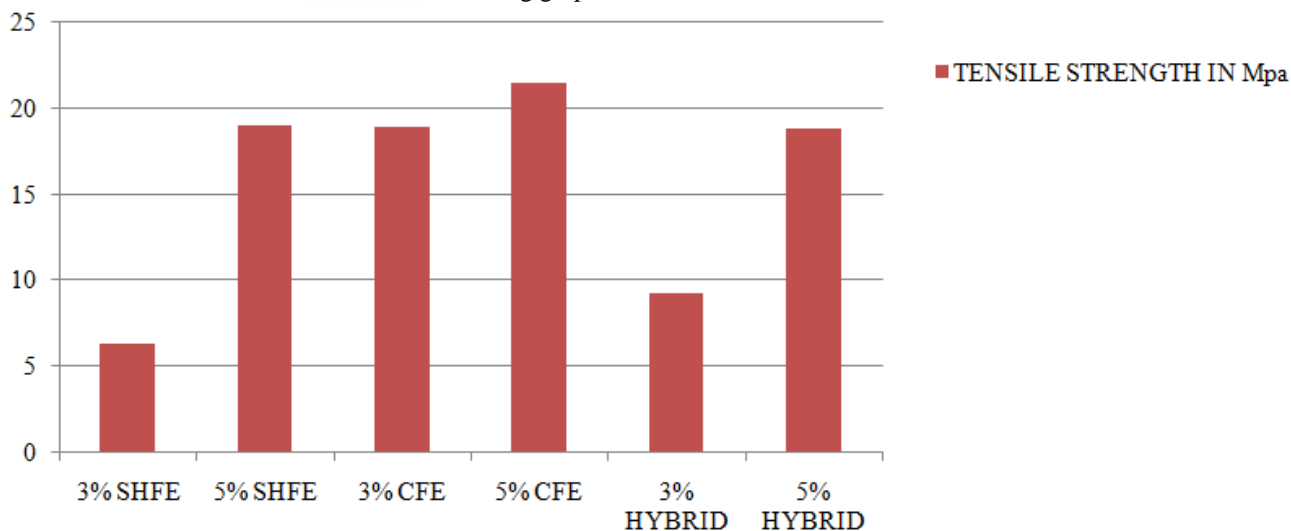
Therefore, it can be concluded that coconut fiber is a suitable material which can be used to replace the conventional materials for reinforcement purpose and this too is a demand of new era of material science. Coconut fiber have further advantages like easy availability, easy degradation etc. which make it more suitable as a better option in reinforcement purposes.

VII. REFERENCES

1.AsimShahzad ,"Hemp fibre and its composites ",Journal of Composite Materials published online 15 August 2011 ,DOI: 10.1177/0021998311413623

2.KiranRohit* and Savita Dixit," A Review - Future Aspect of Natural Fiber Reinforced Composite", Department of Chemistry, Polymers from Renewable Resources, Vol. 7, No. 2, 2016,Manit Bhopal, 462051, Madhya Pradesh, India

3.T. Prakash, "Processing and characterization of natural fiber reinforced polymer composites," Bachelor's Thesis, National Institute of Technology, Rourkela, 2009.

4.Wambua P., Ivens J., Verpoest I., Composite Science Technology, 63, 2003, 1259-64, Journal of Minerals and Materials Characterization and Engineering, Vol.11 No.4, April 20, 2012

5.D. Tama, M. Isler and M. J. Abreu, Evaluating the thermal comfort properties of Rize's traditional hemp fabric (Feretiko) using a thermal manikin, Materials Today: Proceedings, https://doi.org/10.1016/j.matpr.2019.10.063

6.L.Y. Mwaikambo, M.P. Ansell / Composites Science and Technology 63 (2003) 1297–1305

7.Yadvinder Singh a, Jujhar Singh" Fabrication and characterization of coir/carbonfiber reinforced epoxy based hybrid composite for helmet shells and sports-good applications: influence of fiber surface modifications on the mechanical, thermal and morphological properties"Journal of material research and technology 2020; 9(6): 15593-15603.

8.Schwarzova, I.; Stevulova, N.; Melichar, T. 2017. Hemp fibre reinforced composites

9.Andrea Parenti a , Giovanni Cappelli" SunnGro: A new crop model for the simulation of sunn hemp (Crotalaria juncea L.) grown under alternative management practices" Biomass and Bioenergy 146 (2021) 105975

10.Nilza G. Jústiz-Smith," Potential of Jamaican banana, coconut coir and bagasse fibres as composite materials" MATERIALS CHARACTERIZATION 59 (2008) 1273 – 1278.

Significant of Smart Grid Technology in on Grid & Off-Grid Solar-Wind Hybrid System

Surendra Kumar Patel[1], Swati Velaskar[2] , Hemendra Khedekar[3]

PG Student [Power Electronics], Dept. of EE, Vindhya Institute of Science & Technology, Indore, M.P., India[1]

Assistant Professor, Dept. of EE, Vindhya Institute of Science & Technology, Indore, M.P., India[2]

Assistant Professor, Dept. of EE, Swami Vivekanand College of Engineering, Indore, M.P., India[3]

ABSTRACT*: The electricity generation using solar-wind hybrid system is best in present era because all over worlds' countries are focused on installing eco-friendly power generation system. Present time old system is replaced by new Smart grid systems. The solar-wind hybrid system is best for electricity generation but when this system connects with on & off grid system a smart grid system required.
The main objective of my research work is to analyse the significant of smart grid system, it provide alternative energy source, save the energy. To analyse the comparison between old grid system and smart grid system, Use the HOMER software for simulation & optimization of the solar-wind hybrid system and cost analysis between grid-connected & off-grid. Smart Grid technology is better than old grid system, in modern era all system required smart technology.*

KEYWORDS: Smart Grid, HOMER, METLAB, On Grid-Off Grid, Hybrid System

I.INTRODUCTION

India is a developing country, there are total 6, 38,596 villages in India, in which 5, 93,732 villages are inhabited. Out of 5, 93,732 villages, 5,127 villages are electrified only for some hours & rest 38605 villages are using kerosene lamp for lighting their houses. India is not economically stable as it is a developing country. As the population increases day-by-day, so the demand of electricity increases simultaneously. All the electricity is supplied in cities, industries, mills and factories. The "smart grid" is a term used to describe the rapid infrastructure replacement of the electrical wiring system in the United States. When the advanced system is completely implemented, it will allow for communication features across the grids that are not currently available--hence the term "smart". A "smart Grid" is simply an advanced electrical distribution system that has the capability to balance electrical loads from diverse, and often intermittent, alternative energy generation sources. One key component of the "Smart Grid" is the capacity to store electrical energy; this allows the demand from consumers.

The first alternating current power grid system was installed in 1886 in Great Barrington, Massachusetts. At that time, the grid was a centralized unidirectional system of electric power transmission, electricity distribution, and demand-driven control.
In the 20th century local grids grew over time, and were eventually interconnected for economic and reliability reasons. By the 1960s, the electric grids of developed countries had become very large, mature and highly interconnected, with thousands of 'central' generation power stations delivering power to major load centres via high capacity power lines which were then branched and divided to provide power to smaller industrial and domestic users over the entire supply area.In the 21st century, some developing countries like China, India and Brazil were seen as pioneers of smart grid deployment. Since the early 21st century; opportunities to take advantage of improvements in electronic communication technology to resolve the limitations and costs of the electrical grid have become apparent.

Technological limitations on metering no longer force peak power prices to be averaged out and passed on to all consumers equally. In parallel, growing concerns over environmental damage from fossil-fired power stations has led to a desire to use large amounts of renewable energy.

II. LITERATURE SURVEY

Literature review has helped to attain the conceptual clarity and to frame my theoretical perspective. Smart Grid &Renewable Global Status Report provides a comprehensive and timely overview of renewable energy and energy policy development worldwide, World wind energy scenario, Global investment in renewable energy, Global demand for renewable energy.

Mag. Inż. Indrajeet Prasad ''Smart grid technology: Applications and controls'' is the base paper this paper given the ideas to compare the old grid system & Smart Grid system so we proposed solar-wind hybrid model used for it.

Z. Benhachani, B. Azoui, R. Abdessemed, M. Chabane–"Study the sizing and economic optimization of a stand-alone photovoltaic-wind hybrid system with storage batteries".

Two methods are developed. The first method is based on the average annual monthly values in which the size of photovoltaic (PV) and wind generators is determined from the average monthly contribution of each component.

III. DATA FEEDING IN HOMER

To analyse the significant of Smart Grid system in comparison with traditional grid system, we proposed a solar-wind hybrid system and for electric load select the village Umrikheda. The 24 hours data of electric load village umrikheda used for system design and these data feed in HOMER software as shown in fig. 1 below and wind data in fig.2 and solar data in fig.3 feed average month wise because the system is based on tradition model. In my thesis work this is the research point, what happen the data feed month wise and data feed present time wise.
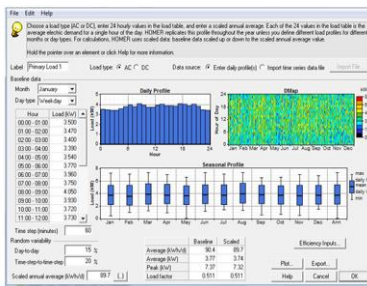
| Fig.1: Electric Load hourly | Fig.2: Wind data month wise | Fig.3: Solar data month wise |
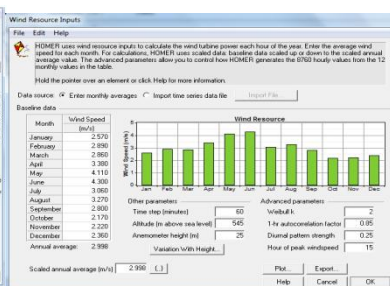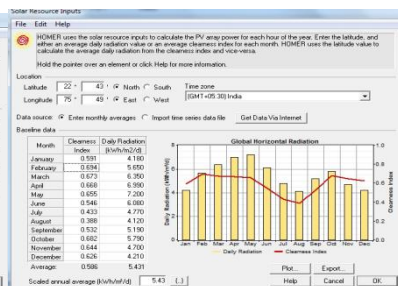
The data of electric load calculated on basis of 24 hours requirements and average data of solar-wind collected yearly month wise and these data feed in HOMER software for proposed model.

IV.PROPOSED SYSTEMOF ON-GRID& OFF-GRID

The generation, transmission and distribution of electric energy are based on traditional system but in present era. The time required changes in electrical system so that to analyse the significant of new technology like "Smart Grid". We survey the village Umrikheda, Indore for electric load collection there electric load fluctuate time to time and design an On-Grid & off-GridModel using HOMER software for village umrikheda.

Table: 1 Electric Load Hourly

TIME (HOURS)		1	2	3	4	5	6	7	8	9	10	11	12
KW	Jan to Dec	3.50	3.47	3.40	3.39	3.54	3.77	3.96	3.75	4.05	3.93	3.72	3.73
TIME (HOURS)	Jan to Dec	13	14	15	16	13	18	19	20	21	22	23	24
KW		3.93	4.03	3.85	3.87	3.81	4.08	4.04	3.89	4.03	3.80	3.46	3.40
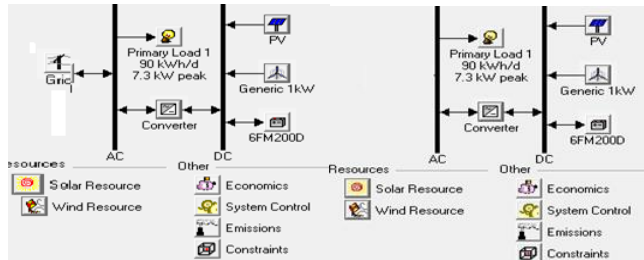
Fig.4 On-Grid Model   Fig.5 Off-Grid Model

The electric power requirement of village umrikheda is around 90 kWh/day for this load, we proposed asolar-wind hybrid system using HOMER software, to analyse thesignificant of new technology like Smart Grid. Smart Grid means the data of electric load, data of power generation, data of transmission and data of distribution in present old technology calculated month wise or year wise but in smart grid technic all data calculated on present time and data updating using all digital based devices. The data of electric load may be varying season to season in tradition technic.In tradition old grid system the load forecasting is major problem. We also analyse this problem in smart grid technic to solve the problems.

In faulty condition major problem is that to find the exact faulty location, according to load variation how the react the electrical device all thesis thinks. We have to analyse in smart grid system so proposed an on-grid and off-grid model. In both systemsthe system is better than other analysed in comparison with smart grid system.

V. SIMULATION RESULTS

The proposed solar-wind hybrid model simulates in HOMER software and generates the number of feasible combination of system with optimized result as shown in fig.6 on-grid and fig.7 off-grid. It is difficult manually to finalize the feasible combination of components, which are actually used in Installation of solar-wind hybrid system. We provide the number of different combinations to HOMER software, on the basis of different combination, HOMER calculate the solar radiation of whole year, wind speed and other devices prices.

Fig.:6 Simulations results of On-Grid   Fig.:7 Simulations results of Off-Grid

The HOMER software use the data feed by us and after simulation, display the number of feasible combination of solar-wind hybrid system and also suggest the optimized combination of system. The data in both hybrid model on-grid and off-grid feed on the basis of month wise collected data. The load demand data vary day to day but these are the traditional based hybrid system so we use month wise data. In Smart Grid system these data updated time to time using digital GPS based device.In both proposed systems on-grid and off-grid, we find the scope where data may be updated with real time, so we proposed these systems.
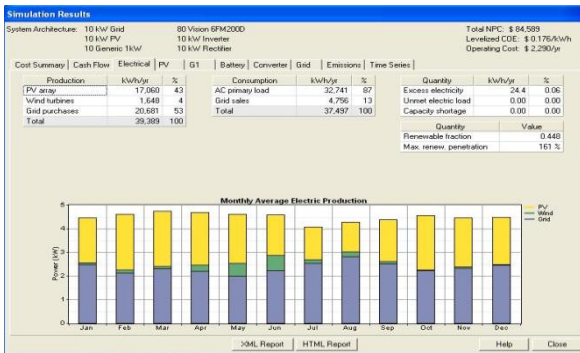
Fig.8 Renewable output power on-grid
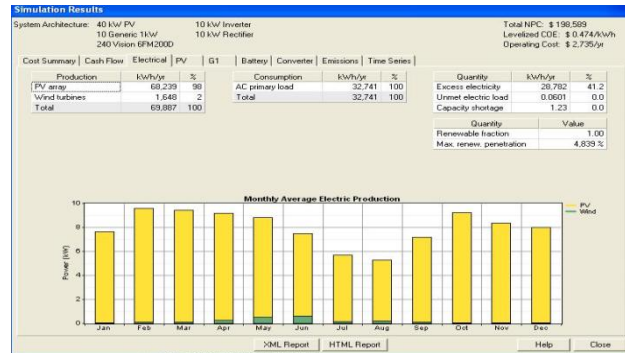
Fig.9 Renewable output power off-grid

In on-grid system 10 kW wind generator, 10 kW PV panels and 10 kW grid connections provided. The production of total renewable power output is 39389 kWh/yr. in which generation by solar 17060 kWh/yr. (43%), wind 1648 kWh/yr. (4%), and grid purchasing 20601 kWh/yr. (53%) in on grid hybrid system.

In off grid system 40 kW PV panels and 10 kW wind generator used. The production of total renewable power output in off-grid hybrid system is 69887 kWh/yr. in which generation by solar 68239 kWh/yr. (98%), wind 1648 kWh/yr. (2%) around 41% power is excess because the system off-grid system.

VI. CONCLUSION

The old grid system uses the fix tariff system and use the single source to supply electric power. As we proposed the solar-wind hybrid system based on old grid pattern in which all the data required are month wise or year wise according to these data, we analysed the electric power generation and distribution.
We conclude this the Smart Grid system is better than old grid system in all aspect like multi supply source instead of single source as in old grid system. The data used for analysis not month wise or year wise, whereas real time data used in Smart Grid system with the help of digital based devices. Smart Grid system provides the alternative source of energy that's why continues the supply and avoid the blackout situations.

VII. FUTURE SCOPE

The Smart Grid system technology is better than old grid technology in all respect, as multiple supply sources, real time data collection, and multiple supply tariff system. The coming era in electric power generation, transmission and distribution required the smart system. In future all devices will be converted in smart devices because smart technology not only help in power generation but also help in electric power saving.

REFERENCES

[1]   http://www.rgcetpdy.ac.in/Notes/EEE/IV%20YEAR/Smart%20Grid/Unit%201.pdf
[2]   https://www.ieee-pes.org/images/files/pdf/2012-pe-smart-grid-compendium.pdf
[3]   https://www.nist.gov/system/files/documents/smartgrid/Smart_Grid_Program_Review_ overview_-_arnold_-_draft1.pdf
[4]   Mag. Inż. Indrajeet Prasad ''Smart grid technology: Applications and controls''
[5]   Renewable global status report- 2018
[6]www.worldenergyoutlook.org/media/WEO2012_*Renewables.pdf*
[7]   www.cea.nic.in/reports/monthly/dpd_div_rep/village_electrification.pdf
[8]   http://www.ptlsolar.com/India/Energy-Scenario.asp
[9]   Source: www.mnre.gov.in/related-links/offgrid/small-wind
[10] Book- Rai, G.D; Non-conventional energy sources, 4 ed. Khanna publication New Delhi, 2006.
[11] www.mnre.gov.in/solar-mission/jnnsm/introduction
[12] India Wind Energy Outlook 201
[13]http://www.cea.nic.in/reports/articles/god/renewable_energy.pdf
[14] http://www.mnre.gov.in/schemes/offgrid/remote-village-electrification
[15] http://www.ushdev.com/windmill-power-activities.php

AN ANALYTICAL STUDY OF MARSHALL PROPERTIES OF WARM MIX ASPHALT USING DIFFERENT TYPES OF BITUMINOUS ADDITIVES

Kapil Kushwah

Ph.D, Scholar,
Department of Civil Engineering
SRK University, Bhopal, Madhya Pradesh, India

Dr. Pankaj Singh

Singhpankaj627@gmail.com
HOD & Associate Professor
Civil Engineering Department, SRK University, Bhopal

Abstract –The specific objectives of the research project are determining the performance of warm mix asphalt prepared with different types of bituminous additives with respect to hot mix asphalt in terms of Engineering Properties such as Marshall Characteristics & investigate the effects of varying temperatures on mixes in terms of Marshall Properties also to decide the best additive & best mix parameters such as temperature for the preparation of warm mix and optimum binder content. The main objective of work is to work out Marshall Properties of Warm Mix Asphalt Mixes prepared with different types of additives at different temperature ranges specified for Warm Mix Asphalt & Comparing the Marshall Properties of Warm Mix Asphalt specimens prepared using different types of bitumen additives with each other & with Hot Mix Asphalt Specimen (prepared using virgin bitumen only) as well. Present studies developed to the investigation made through special researchers within the discipline of financial and safe road construction design. The studies afford the precis of different research work & conclude with identified gaps in the research in addition to recognize the object of required work.

*Key Words***: Warm Mix Asphalt, Marshall properties, IRC, Bituminous, etc.**

I. INTRODUCTION

The quality of roads dictates the economy of a country and hence the quality of our life's. Roads are vital for the transport of the goods and passengers. Over time, roads have emerged as the predominant mode for passenger transport. The share of roads in passenger traffic (billion passenger kilometer or bpkm) in total passenger traffic carried by rail and roads together has increased from 32 per cent in 1951 to about 90 per cent in 2011 (GoI -2014).

National Transport Development Policy Committee (NTDPC) has estimated that the modal share of rail and road in the total freight traffic will be 35:65 in the 12th Plan (2016-17), 39:61 in the 13th (2021-22), 45:55 in the 14th (2026-27) and 50:50 in the 15th Plan (2031-32). With elasticity at 1.2, total freight traffic is expected to grow at 9.7 per cent per annum to reach over 13,000 BTKM in 2031-32 from about 2,000 BTKM in 2011-12. Total passenger traffic is expected to grow at about 15 per cent per annum to reach 168,875 bpkm in 2031-32 from 10,375 bpkm in 2011-12. Growth in road passenger traffic is expected to be around 15.4 per cent per annum. (NTDPC -2014).

"The year 2018-19 was declared by the Ministry of Road Transport & Highways as the YEAR OF CONSTRUCTION. The construction of highways involves huge amount of the investment and mainly the highway project cost is associated with the pavement construction".

Due to increasing demand in highway construction, scientists and researchers are constantly trying to improve the performance of bituminous pavement. Increased number of vehicles in recent years have exposed road surfaces to high traffic resulting in deformation of pavements due to excessive stress. (Prasad, 2012)

Pavement deforms due to insufficient stability, improper compaction, and insufficient strength. Therefore, stability should be high enough to handle traffic sufficiently, low stability causes unravelling and flow of the road surface. One of the most important properties of bitumen mixture is its ability to resist shoving and rutting under traffic.

The important highways in India are built by Dense Bituminous Macadam (DBM) or Bituminous Concrete (BC). (Gupta & Agrawal, 2017) Dense Bituminous Macadam is mainly used as binder course for roads having much higher number of heavy commercial vehicles. In DBM mix there is a wide scope of varying the gradation to obtain the good mix without affecting the durability of pavement.

There are three principal bituminous mix design methods in general use. They are Marshall Method, Hveem Method and Superpave Method. Normally Marshall Mix design method is adopted for mix design of Dense Graded Bituminous Macadam, (DBM).

II. SIGNIFICANCE OF RESEARCH & CONTRIBUTION OF RESEARCHERS

In the past, a lot of work has been done in European countries to produce asphalt mixes at lower temperatures without significantly affecting the quality of the mixes. The research papers published in various journals gives an idea about a few properties of asphalt mix such as aging of binder, temperature susceptibility, tensile strength ratio etc. But there is not much information is available about the stability value, flow value & optimum binder content etc. (Marshall Properties). It is difficult to state currently which WMA technologies or additives are most suitable for India. The situation is very dynamic as more and more new technologies are being developed at the time of this writing. Since the environmental conditions, equipment's, standards, and work practices, are different, a thorough investigation of warm asphalt is necessary before it is implemented in the India.

Construction sector is considered as one of the major sources for economic growth and development of a country. In India, it forms the second largest economic activity which includes roadways, railways, water transport, ports, urban infrastructure etc. Out of them, road construction is a predominant segment which plays an important role in the growth of country's economy. (Sahoo et.al. 2015)

Roads in India have expanded both in terms of capacity and dimensions. Today, India is having the second largest road network in the world, with over 5.89 million km of roadways spread across the country.

The total road length increased from about 400,000 km to 4.7 million km between 1951 and 2011. Surfaced roads increased from 157,000 km to around 2.5 million km. Road density in India is now nearly 1.42 km per sq km, which compares favorably with many countries. Surfaced road length accounted for 54 per cent of total road length in 2011, compared with 39 per cent in 1951. (NTDPC,2014)

Currently, majority of the Indian roads are paved with Hot Mix Asphalt (HMA), which consists of aggregates and bitumen mixed at high temperature, approximately150-170°C. The production and placement of HMA pavements has evolved over the last 130 years and recognized as a high-quality engineered paving material to produce good quality pavement. During all these years, the production of HMA has modernized from manual hand mixing and placement with rakes and shovels to computerized plants feeding, placement, and compaction equipment that track location and material quality.

The main concern with the production of HMA is, it requires large amount of energy and releases enormous amount of emissions into the environment. (Choudhary & Julaganti, 2014)
Production of one lakh tons of HMA in a year using batch mix plant requires about 6.5 to 7.5 lakh liters of fuel and releases about 20 tons of carbon monoxide (CO), 0.7 tons of volatile organic compounds (VOC), 0.3 tons of sulfur oxides, 1.3 tons of nitrogen oxides and about 0.45 tons of total hazardous air pollutants into the atmosphere (USEPA Report, 2000).

So, the road construction industry is looking for an alternate material or a technology that reduces the amount of energy required to produce the HMA, to combine energy savings and environmental benefits. Warm Mix Asphalt (WMA) technology is one of the solutions.

A. Warm Mix Asphalt Technology
Warm mix asphalt technology is identified as an asphalt mix technology that allows a temperature reduction in the range of 20 to 55°C lower than typical hot mix asphalt by reducing the viscosity of the asphalt binder at a certain temperature range. By this way, aggregate could be fully coated at a lower temperature by the reduced viscosity asphalt binder. (Kristjansdottir, 2006)

The technique of WMA was first invented by Professor Csanyi at Iowa State University in 1956. He found out that the foaming asphalt could be possible for use as soil binder. (Button JW, 2007)

This invention was then modified by adding cold water instead of steam in asphalt, and it was patented by Mobil Oil Australia in 1968. This invention was later licensed to Conoco Inc. to promote foamed asphalt in United States, and further develop the product as a base stabilizer for both laboratory and field evaluation. (Kristjansdottir O, 2006)

Since 1970s, researchers have been trying to investigate a new method to reduce asphalt mixture production temperature. This method was later termed as Warm Mix Asphalt (WMA) (Zettler R.,2006)

The concept of WMA was proposed first time in the German Bitumen Forum in 1997 and then has been widely developed in Europe after these countries signed the Kyoto Agreement on greenhouse gas reduction (Newcomb, 2007).

In 2007, the Federal Highway Administration's International Technology Scanning Program organized a U.S. expert team to visit four European countries to evaluate the feasibility of WMA in U.S. After the trip, the scan team suggested that the WMA technology can be recommended for use in the United States (D'Angelo, 2008).

Prowell et al. (2011) and Bonaquist (2011) presented the detailed description about the asphalt plant modifications and the mixing process, and that stepped up the WMA paving technology in the USA. The total market share of WMA mixture in the USA was 22% in 2012 (Hansen and Copeland, 2013). NAPA conducted a survey under the contract of FHWA, found that 114 million tons of WMA were produced in 2014. Higher prices of asphalt and aggregates led Europe (Koenders et al. 2000), South Africa (Jenkins et al. 2002; Jenkins et al. 1999), Australia (AAPA 2001) and India (Behl et al. 2013) to examine the benefits and performance of WMA.

In 2009, the first trial section of WMA was laid as per Indian Road Congress (IRC) specifications over a 500-meter section of road at Bawana industrial area by the Delhi State Infrastructure Development Corporation (DSIDC) in India (Behl et al. 2013). The Indian Institute of Technology (Madras, Roorkee, Guwahati) and Central Road Research Institute (CRRI) have started the preliminary research on the effects of WMA on Indian mixes (Gandhi 2014). CRRI and IRC jointly developed an additive to produce an asphalt mixture at a temperature lower than HMA and which can compact the asphalt mixture at a temperature as low as 90°C. However, the performance of this new material is still in evolution (Behl and Chandra 2017).

P.S Kandhal in 2014 formulated the draft specifications for the introduction of the WMA mixtures into India, based on that IRC issued interim guidelines for the production and construction of WMA pavements (IRC SP:101- 2014).

B. IMPACT OF WMA
Kristjansdottir et. al (2007) concluded that Several WMA technologies are gaining traction in the United States and abroad as evidenced by the increasing number of demonstration projects. These technologies are typically promoted based on lower emissions, reduced energy consumption & reduced viscosity.

Kandhal (2010) in his research paper described the WMA technologies developed to this date in Europe and the US, such as synthetic zeolite, Sasobit, Evotherm, WAM Foam, LEA, Rediset WMX, REVIX, and Double Green Barrel together with their laboratory evaluation. All the WMA technologies described in the paper together with the findings of their laboratory evaluation by the National Center for Asphalt Technology. He recommended to conduct field trials of WMA in India especially by the Border Roads Organization in remote places far away from hot mix plant and/or located on high altitude with colder climate. He also recommended to encourage introduction of WMA in lieu of HMA in response to the need for greenhouse gas reduction and earn carbon credits for India under the Kyoto Protocol.

Lekha et al. (2018) reviewed the performance of additives in Warm Mix Asphalt and concluded that WMA is gaining popularity primarily due to its proven benefits in various aspects (safer working conditions, longer paving sessions, lower plant wear

and cost-effectiveness) without compromising on the mechanical performance of the asphalt mixture. The main aim of their review paper was to explain different technologies used in the manufacturing of WMA to evaluate the performance of different additives, which are best suitable for the Indian conditions. They further concluded that the foaming-based additives and organic-based additives both are uneconomical as they incur extra production cost. Whereas the organic additives are economical than the foaming-based additives because the plant modification cost is less and can be blend directly into the asphalt mixture. More research should focus on the mix design procedure and long-term performance. It is still a juggernaut subject since the field test sections are at the initial phase. Most of the WMA additives are commercial products and has their own aids.

Khan & Chandra (2012) studied the effect of warm mix additives on mixing, laying and compaction temperatures of warm mix binders. Sasobit & Evotherm were used as additive in their study. Different Warm Mix Binders were prepared by mixing different doses of additives. The different doses of sasobit used in this study were 0.5%, 1.0%, 1.5% and 2.0%, by weight of the binder. The different doses of Evotherm were 0.2%, 0.4% and 0.6%, by weight of the binder. The variation of their viscosity with temperature was then studied. The Brookfield viscometer was used for this purpose. They concluded that the viscosity of the bituminous binders varies exponentially with the temperature and linearly with respect to the dose of Warm Mix additives and the mixing temperature can be reduced by 20ºC to 25ºC while laying and compaction temperature can be reduced by 10ºC to 15ºC by using these additives.

Choudhary and Julaganti (2014) presented a comprehensive literature review paper on various WMA technologies across the globe and advantages associated with WMA technologies & concluded that WMA technology is an environment friendly technology that allows a reduction in mixing and compaction temperature of asphalt mixes either through lowering of viscosity of asphalt binders or by increasing the workability at lower temperatures without compromising the quality or properties of the mix. It also offers many other advantages like cost savings, energy savings, cutting of natural resources requirement, etc.
They further concluded that significant amount of efforts in terms of studies, research & proper implantation is required to adopt WMA on Indian roads.

In their review paper on Warm Mix Asphalt technologies Monu et. al. (2015) identified the following gaps:
- The evaluation is newer; most of the studies have been done abroad need to make more in this country.
- No specific considerations have been given to different grades of binder.
- There are limited studies which are based on SUPERPAVE classification method which is not prevailing in India
- Specific studies are needed to evaluate the properties of the surface and base course.

The study carried out by Kumar and Chandra (2016) on history and development of warm mix asphalt in different countries including advantage and disadvantage of warm mix asphalt concluded that Warm mix asphalt (WMA) technology, has developed in Europe, and is gaining strong interest worldwide. WMA is gaining popularity worldwide mainly due to reduction in emission and fuel consumption when compared with conventional HMA.
They also reviewed the warm mix asphalt in India & found that the major research in India is going on organic and chemical warm mix additives because these additives do not require major modification in the plant because the additive can be blended with bitumen.

Srikanth & et. al. (2018) presented a review paper about various trends, merits & de-merits, technical aspects, various temperatures of additives while adding with binders, various live examples where this technology implemented, mix design, performance tests on WMA. Based upon the literature review it was concluded that Warm Mix Asphalt Technology has many advantages and for disadvantages, there are solutions to reduce its negative effect. It's an alternative way for HMA in metropolitan cities. WMA exhibiting same positive results of HMA (Approx.). Due to lower mixing temperature, it reduces the aging of binder that results in resistance towards thermal and fatigue cracks. WMA has good compatibility with waste & recycling materials like RAP, various plastic polymers, replaceable materials with aggregates and with binders so it is a user-friendly technology. As environmental, economic, health benefits of WMA compared with HMA have much better results that result in US, UK, Germany, Canada, and India etc. can adopt this technology in their public transportation infrastructure.
There is no evidence of reduction of CO in case of WMA; there is a reduction of 36% of total organic matter (Prowell et al. 2014). In India Organic & chemical additive are better because for using they not required huge modifications of existing HMA plants (Prowell et al. 2011).

C. EFFECT OF BITUMINOUS ADDITIVES ON MARSHALL PROPERTIES OF WARM MIX ASPHALT

Renugadevi. A (2014) evaluated Marshall Properties of Warm Mix Asphalt using Sasobit. Dense Graded Macadam (DBM) grading-2 was designed & tested using Marshall method of mix design. WMA mixes at different temperatures (115 to 155°C) were prepared with various dosages (0 to 5% by weight of binder) of organic additive (Sasobit). Marshall properties these WMA mixes were compared with Marshall properties of HMA.

It was concluded that the mixing can be done successfully at lower temperature of 135°C as compared to conventional mix at 155°C. Thus, the production temperature can be reduced by 30°C. Stability and Density of mix were improved with addition of Sasobit. Flow, Voids Filled with Bitumen (VFB) of Warm Mix Asphalt increased with increase in temperature at optimum content of Sasobit. Air voids and Voids in Mineral Aggregates (VMA) of WMA with Sasobit decreased as compared to conventional HMA. Optimal amount of Sasobit was found to be 2% by weight of bitumen.

Kumar & Vadraj (2014) evaluated the laboratory performance of warm mix asphalt mixtures with Sasobit for Dense bituminous macadam (DBM) Grade-2. After the determination of gradation, Marshall stability tests were conducted to determine the volumetric properties of the specimens. HMA specimens were prepared at 160°C & Marshall stability tests were conducted with varying percentage of binder content to determine the optimum binder content (OBC) for HMA. Tests were also conducted for WMA to determine its volumetric properties with different dosages of Sasobit (from 1.5 to 2.5% by weight of bitumen) as additive at OBC for different mixing temperatures (120°C, 130°C, 140°C). The OBC was found to be 5% for HMA at 160°C. From the test results it was concluded that the maximum stability for 60/70 grade bitumen was achieved at 130°C temperature with 2% dosage rate. Among 120°,130°, 140°C temperature, the 130°C temperature demonstrated better and maximum stability. There was an increase in stability up

to 25% at 130°C for 60/70 grade bitumen after adding Sasobit to the mix. Hence the warm mix additive of 2% Sasobit at 130°C temperature can be used as an alternative for HMA.

The potential to reduce the amount of optimum bitumen content by addition of sasobit was carried out by Frag Ahmed Ma Kridan et. al. (2011) by laboratory research. Two types of mixes were produced by Marshall method procedure to achieve this. The first was control mix with unmodified bitumen 80/100 penetration. The other was mixed with modified same bitumen penetration with sasobit additive in concentration 2 % identified as saso mix. The mixes were produced at 155°C & 135°C respectively. The volumetric properties Bulk density (Gmb), Air voids in compacted mix (AV), voids filled with bitumen (VFA) as well as Marshall stability and flow were within investigated to determine the effect of sasobit additive on the amount of optimum bitumen content. The specimens showed significant reduction in air voids by adding the sasobit additive on the mix in most cases. The results also showed somewhat decrease in stability whereas slight increase regarding flow parameter values in saso cases in all bitumen content as well as slight increase in VFA while no clear trend in term of Gmm.

The optimum bitumen content was 4.82 % and 4.78% for control mix and sasobit modified mixes respectively, which means that the addition of sasobit additive on the mix by using Marshall Method revealed very slight reduction in optimum bitumen content. The performance of warm mix asphalt mixture by incorporating sasobit additive was evaluated by Gunti & Jalegar (2017).

The essential objective of the study was to develop WMA using Sasobit additive and to assess the effects of additive on the properties of binder and mixture. the mixing temperature was found by conducting viscosity test of binder in Brookfield viscometer at various temperature for different percentages of Sasobit. Viscosity of VG-30 with 1%, 2% & 3% percentage of Sasobit is measured at 110°C, 120°C and 130°C to produce WMA. It is Compared without Sasobit additive at various temperatures. To evaluate the best combination additive percentages in mixing temperature and bitumen, warm DBM mixtures were prepared with VG-30 with various percentages of additive content at 110°C, 120°C, 130°C and 140°C temperature.

D. WARM MIX ASPHALT FIELD STUDIES

Behl & et. al. (2013) evaluated the field performance of warm-mix asphalt pavements in India. The field performance of two pavements constructed using an IRC accredited surfactant based chemical warm-mix technology (Evotherm) were evaluated in the study. The two pavements evaluated in this study were produced and placed at a significantly lower temperature relative to the control hot-mix sections. Both the pavements were evaluated after considerable exposure to weather elements and traffic. Methods like Benkelman beam deflection, bump integrator value, and Marshall stability, resilient modulus and static creep test on field cores were used to evaluate the performance of the WMA sections in comparison to the control hot-mix sections. The results of the   study indicate that despite the several monsoons and heavy traffic both pavements were exposed to, the performance of the warm-mix sections was equal or better compared to the control hot-mix sections. Due to the improved densities achieved at the site, and due to the reduced oxidation of the bitumen as a result of the lower production and placement temperatures, the performance of the warm-mix seemed to be improved in terms of permanent deformation and resilient modulus.

Based on this study of two pavements where the field performance was monitored for a duration ranging from 13 - 31 months, the following can be concluded about the short-term field performance of warm mixes relative to the control hot mixes:

- Visual inspections reveal that the warm mix sections are equally comparable to the control hot mix sections and there were not visible cracks and deformations in both the sections in both the project sites.
- The Benkelman beam deflection values of the warm mix as well as the hot mix sections were found to be identical, indicating similar performance and ability to maintain structural adequacy.
- The roughness values of the warm mix and the hot mix sections were also found to be similar, indicating equal performance of the warm mix section. Additionally, all values were found to be well within the limitations as mentioned in the Indian Road Congress codes.
- The Marshall stability test results, resilient modulus test results and the static creep test results all indicate that the compatibility and constructability benefits associated with the warm mix asphalts render pavements that are stiffer and denser and therefore better able to resist distortion, displacement, rutting and shearing stresses when subjected to heavy static and dynamic loads.
- Since density is the most important aspect associated with the performance of a pavement, it can be concluded that the compatibility and constructability benefits of warm mix asphalts allow the contractors to easily achieve the required densities during construction and therefore construct pavements that can perform better in the long run.

III. GAP IN RESEARCH REVIEW AND OBJECTIVE OF NEW RESEARCH

Based on the survey of available literature following gaps in the research are identifying.

- Several researches have been conducted to evaluate the performance of Warm Mix Asphalt Mixes as compared to Hot Mix Asphalt Mixes. Most of them are carried outside India. India has a limited level of experience in WMA. The need of today is to evaluate and analyse this technology to extract the various benefits associated with it. Some trail stretches are also constructed using WMA in India and some WMA technologies or WMA additives are accredited by IRC for trials in India.
- A few researches have also been carried out in India using WMA Additives. But most of them have only evaluated the Marshall Properties of either Bituminous Concrete (BC) Grading 1 & 2 or Dense Bituminous Macadam (DBM) Grading-2. Also, the reduced temperature range involved in these researches is very limited.

- Most of the researchers compared the Marshall & other Properties of Warm Mix Asphalt with Hot Mix Asphalt for DBM Grading-2. Only a few have compared the properties for DBM Grading-1. Considering the research and exploration of WMA in India, the technology is still in its infancy stages.

Based on above-mentioned gaps following the objectives of the research are being investigated:

- Numerous researches have been conducted in Europe & U.S. to assess the properties of WMA mixes. Aging of binder, temperature susceptibility, tensile strength ratio etc. are some of the properties of WMA mixes which have been compared with the properties of Hot Mix Asphalt. The mix design of both WMA & HMA is based on Superpave method. In India, presently the bituminous mixes are designed based on empirical laboratory procedures i.e. Marshall method of mix design. Hence, there is a scope to evaluate the Marshall properties of WMA mixes.
- Determining the performance of warm mix asphalt prepared with different types of bituminous additives with respect to hot mix asphalt in terms of Engineering Properties such as Marshall Characteristics.
- To investigate and study the effects of varying temperatures on mixes in terms of Marshall Properties.
- To decide the best additive & best mix parameters such as temperature for the preparation of warm mix and optimum binder content.

IV. CONCLUSION

1. From the research, we understand approximately the contribution of different researches inside the area of the Marshall properties of WMA mixes a gap in the research and objective of the studies to be carried out.
2. These contributions help to visualize the hassle faced by way of road construction from a new perspective.
3. By evaluating the overall performance of warm mix asphalt prepared with different types of bituminous additives with respect to hot mix asphalt in terms of Engineering Properties such as Marshall Characteristics its enhanced financial element may be completed.
4. which shall result in the path of the layout of secure stronger and greater comparatively cheap design.

REFERENCES

1. Renugadevi. A, "Evaluation of Marshall Properties of Warm Mix Asphalt using Sasobit", International Journal of Engineering Sciences & Research, Volume-3, Issue-12, December 2014. PP 421-428

2. Shaleha I. Vahora1 and C. B. Mishra2 "Investigating the Performance of Warm Mix Additives", International Journal of Current Engineering and Technology, Volume-7, Number-.3, June-2017. PP 1011-1015

3. Manjunath K. R1, Dheeraj Kumar N2, Thippeswamy G. S3 "Performance and Evaluation on Marshall Stability Properties of Warm Mix Asphalt Using Evotherm and Cecabase Rt®-A Chemical Additive" International Journal of Engineering Trends and Technology (IJETT) – Volume 12 Number 8 - Jun 2014. PP 406-410

4. Rohith N.1, J. Ranjitha 2 "A Study on Marshall Stability Properties of Warm Mix Asphalt Using Zycotherm A Chemical Additive", International Journal of Engineering Research & Technology (IJERT), Volume-2, Issue-7, July-2013. PP 808-813

5. Raveesh J1, Manjunath SM 2 "Laboratory Evaluation of WMA with Zycotherm Warm Mix Additive", International Journal for Research in Applied Science & Engineering Technology (IJRASET), Volume-5 Issue 7, July 2017. PP 327-330

6. Vinod D. Ninawe1, Shashikant A. Deshmukh2 "Laboratory Evaluation of Warm Mix Asphalt", International Journal of Advance Research in Science and Engineering, Volume- 6, Issue-7, July-2017 PP 259-268.

7. Mitul Patel1, Vikas Patel2, Devendra K. Patel3, Prof. Mishra4 "Evaluating Properties of VG 30 Paving Mix with and Without Warm Mix Additive", International Journal of Innovative Research in Science, Engineering and Technology, Volume- 3, Issue 6, June 2014. PP 13895-13898

8. Jayaprakash B1, Maneeth P D2, Brijbhushan S3 "Laboratory Investigation of Conventional Asphalt Mix Using Shell Thiopave for Indian Roads", Journal of Engineering Research and Applications, Volume - 5, Issue 2 (Part 3), February 2015, PP 67-76.

9. Harpreet Singh1, Tanuj Chopra2, Neena Garg3, Maninder Singh4 "Effect of Zycotherm Additive on Performance of Neat Bitumen and Bituminous Concrete Mixes", International Journal of Civil Engineering and Technology (IJCIET), Volume-8, Issue 8, August 2017, PP 232-238

10. Nazimuddin M. Wasiuddin1, Selvaratnam Selvamohan2, Musharraf M. Zaman3, and Marie Louise Thérèse Anne Guegan4 "Comparative Laboratory Study of Sasobit and Aspha-Min Additives in Warm-Mix Asphalt", Transport Research Record: Journal of the Transportation Research Board, Volume 1998 Issue 1, January 2007, PP 82-88

11. Martinsh Zaumanis1, Viktors Haritonovs2 "Research on Properties of Warm Mix Asphalt", Scientific Journal of Riga Technical University, Construction Science, Volume-11, Number-1, 2010, PP 77-84

12. Ambika Behl1, Gajendra Kumara2, Girish Sharma3, Dr.P.K. Jain3 "Evaluation of field performance of warm-mix asphalt pavements in India", Procedia - Social and Behavioral Sciences, 2nd Conference of Transportation Research Group of India (2nd CTRG) Volume 104, 2 December 2013, Pages 158-167

"Load Frequency Control of Two Area System with the help of Intelligent Controller Gain Optimizer"

Mr. Deepak Patidar[1], Mr. Pawan Pandey[2]

[1] M. Tech Scholar in Power System, MIT, Indore (M.P). E-mail: (er.depakpatidar86@gmail.com)

[2] Assistant Professor & head in Electrical & Electronics Dept. MIT, Indore (M.P). E-mail: (pawanpandey@mitindore.co.in)

Abstract —Load Frequency Control (LFC) are used to regulate and control the output frequency signal of the electric generated power within an area in response to changes in system loads. The gain constants in the case of conventional controllers remain same throughout, for changes in the load value. However, Load cannot be the same throughout, load deviates from time to time. To get rid of these disadvantages related to conventional controllers, a lot many schemes have been put forth in literature. This work presents a new design of various types of load frequency controllers based on different types of Artificial Intelligent (AI) optimization techniques such as Fuzzy logic, ANN tuner for a single area power system. The performance of the controller under study shows an enhancement in the frequency deviation signal as well as the peak overshoot and settling time for the frequency output signal. The performance of the proposed scheme is validated using MATLAB/ SIMULINK tools.

KEYWORDS: *LFC, ANN, ANFIS, PI, Fuzzy, Multi- Area Power System.*

I. INTRODUCTION

As the loading in a power system is not constant so the controllers for the system must be aimed to provide quality service in the power system. The power flow and frequency in an interconnected system is well regulated by AGC. The main purpose of the AGC is to retain the system frequency constant and almost inert to any disturbances. Generally two things are being controlled in AGC i.e. voltage and frequency. Both have separate control loops and independent of each other.

Apart from controlling the frequency the secondary majors is to maintain a zero steady state error and to ensure optimal transient behavior within the interconnected Areas. The objective is to design a controller to apprehend preferred power flow and frequency in single Area power system.

The input mechanical power is utilized to control the frequency of the generators and the variation in the frequency and tie-line power are detected, which is the extent of the alteration in rotor angle. A decently outlined power framework ought to have the capacity to give the satisfactory levels of power quality by keeping the frequency and voltage size inside middle of as far as possible.

II. LITERATURE REVIEW

[1] In this paper presented that Grids face a new and important challenge: the oncoming mass penetration of plug-in Electrical Vehicles (EVs). Nevertheless, the architectures of transmission and distribution grids are still focused on traditional design and operational rules. Consequently, it is necessary to predict the adequate solutions for the problems which are going to rise to the electrical and production grids as well as the effect on their commercial operation as a result of the gradual integration of EVs into the network. [2] This paper discussed that in renewable penetrated power systems, frequency instability arises due to the volatile nature of renewable energy sources (RES) and load disturbances. The traditional load frequency control (LFC) strategy from conventional power sources (CPS) alone unable to control the frequency deviations caused by the aforementioned disturbances. Therefore, it is essential to modify the structure of LFC, to handle the disturbances caused by the RES and load. [3] This paper discussed that the rapid development of technology used in electric vehicles, and in particular their penetration in electricity networks, is a major challenge for the area of electric power systems. The utilization of battery capacity of the interconnected vehicles can bring significant benefits to the network via the Vehicle to Grid (V2G) operation. [4] In this paper the use of the proportional integral (PI) algorithm incorporated with the fuzzy logic technique has been proposed as advanced gain scheduling load frequency control (GLFC) in two-area power systems. The proposed controller comprises two-level control systems, such that it consists of a pure integral compensator, which is connected, in parallel with a PI controller. However, and based on load demand, the PI parameters are updated online by means of fuzzy logic rules. With this control technique, it becomes possible to eliminate steady state errors as well as to maintain

good transient responses. The task of keeping a stable and overall satisfactory mode of operation in interconnected electric power systems is the main goal of any control strategy. [5] This study aims to develop a Load Frequency Control (LFC) for a single area power system using a fuzzy logic tuned PI controller. A deviation of frequency value from the standard (±0.5Hz) arises when real power generation fails to supply demand along with network losses. Various LFC studies have been done exploiting control strategies ranging from classical control schemes to soft analysis techniques. [6] This paper discussed in this paper the Artificial Neural Network (ANN) Controller for load frequency control of Multi area power system is presented. The performances of ANN Controller and conventional PI controllers are compared for Single area and Multi area power system with non-reheat turbines. [7] This paper discussed a control scheme of ANN based proportional integral-derivative (PID) controller is developed here to maintain the system frequency at nominal value. Due to some complication of modern industrial system, the conventional PID controller is not capable to meet our requirement. Neural network is have great capability in solving complex, nonlinear mathematical problems. This paper introduces the design of neuro-PID controller model to improve the response and performance of conventional PID controller. [8] In this paper, a hybrid combination of Neuro and Fuzzy is proposed as a controller to solve the Automatic Generation Control (AGC) problem in a restructured power system that operates under deregulation pedestal on the bilateral policy. In each control area, the effects of the possible contracts are treated as a set of new input signal in a modified traditional dynamical model. The prominent advantage of this strategy is its high insensitivity to large load changes and disturbances in the presence of plant parameter discrepancy and system nonlinearities. [9] This paper discussed that Load frequency control (LFC) is required for reliable operation of a large interconnected power system. The main work of load frequency control is to regulate the power output of the generator within a specified area with respect to change in the system frequency and tie-line power; such as to maintain the scheduled system frequency and power interchange with other areas in a prescribe limits. In this paper, study of LFC system for single area. [10] This paper discussed while the number of internal combustion vehicles is stagnating, and is even expected to decrease in a few decades, the amount of electric vehicles is predicted to increase. Most of the electric cars are designed for daily urban use, thus in the near future, bigger cities might have some ten percentage of electric cars running on their streets during the day.

III. LOAD FREQUENCY CONTROL

With many loads linked to a system in a power system, speed and frequency vary with the characteristics of the governor with variations in loads. No need to modify the setting of the generator if maintaining of constant frequency is not needed. When constant frequency is needed the turbine speed can be adjusted by varying the governor characteristic.

Let both generating stations are interconnected through a tie line. If load varies at X or Y & A generation has to maintain the constant frequency, at that time it is known as Flat Frequency Regulation.

- Secondly, where both X & Y have to maintain the constant frequency. It is known as parallel frequency regulation.
- Thirdly where frequency maintenance is done of a certain Area by its own generator & keeping constant the tie-line loading. It is called flat tie-line loading control.
- In Selective Frequency control, individually system handles the variation in load itself & without interfering, beyond its limits, the maintenance of the other one in that group.

In Tie-line Load-bias, control all systems in the interconnection help in maintaining frequency no matter where the variation is created. It has a principal load frequency controller & a tie line plotter determining input power on the tie for proper control of frequency.

IV. METHODOLOGY

- ANN

Machine learning technique is not new to the field of science and technology. It has been utilize by various fields to solve complex algorithmic problems. With its excellent development, it has found its way in the field of electrical engineering also. It has been widely used for load forecasting, stability analysis, in solving economic load dispatch etc. to name a few of them. Due its strong learning ability, expert systems are easily overtaking digital techniques. Techniques like ANN, ANFIS etc, which are different forms of machine learning, prove to be very reliable along with providing fast results.

The ANN has advanced methods such as optimal control adaptive control, multi-variable control and different approaches such as microprocessor based controllers and digital signal processing have been investigated or under investigation.

- **ANFIS**

ANFIS stands for Adaptive Neuro-Fuzzy Inference System. The ANFIS controller combines the advantages of fuzzy controller as well as quick response and adaptability nature of ANN Fundamentally, ANFIS is about taking a fuzzy inference system (FIS) and tuning it with a back propagation algorithm based on some collection of input-output data. This allows your fuzzy systems to learn. A network structure facilitates the computation of the gradient vector for parameters in a fuzzy inference system. Once the gradient vector is obtained, a number of optimization routines is applied to reduce an error measure (usually defined by the sum of the squared difference

between actual and desired outputs). This process is called learning by example in the neural network literature.

- Some Constraints are as follows:-

Since ANFIS is much more complex than the fuzzy inference systems discussed so far, all the available fuzzy inference system options cannot be used. Specifically, ANFIS only supports Sugeno systems subject to the following constraints:

- First, order Sugeno-type systems.
- Single output derived by weighted average defuzzification.
- Unity weight for each rule.

An error occurs if your FIS matrix for ANFIS learning does not comply with these constraints. Moreover, ANFIS is highly specialized for speed and cannot accept all the customization options that basic fuzzy inference allows, that is, one cannot make own membership functions and defuzzification functions; that to make do with the ones provided.

The fuzzy inference system that has been considered is a model that maps:

- – Input characteristics to input membership functions,
- – Input membership function to rules,
- – Rules to a set of output characteristics,
- – Output characteristics to output membership functions, and
- – The output membership function to a single-valued output, or
- – A decision associated with the output.

The inputs are ACE and Change in ACE. We have studied above the Fuzzy rule base and formed the rules. Two linguistic variables of the inputs and 2 linguistic variables of the output using the NeuroFuzzyAnalyzer toolbox. The membership functions used are
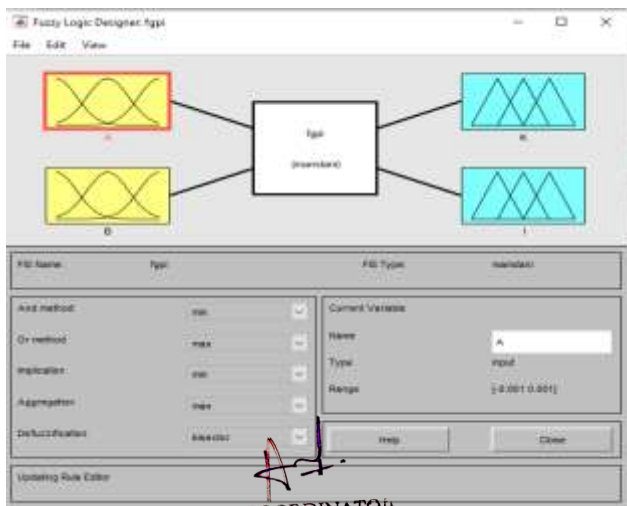
Fig 1 Fuzzy Logic Designer

V. RESULT

In this section ANN, based PI tuner controller results are discussed. Below figure 2 shows the Simulink model for it. The ANN model is trained and tested with neural network toolbox in MATLAB only. The model is prepared with data collected from PID model simulation. Input data consist of ACE and change in ACE and output data consist of Proportional gain and integral gain value. 85% of data is used for training 5% for validation and 10% for testing. The overall regression has a value of more than 0.9 that is considered as good value for any training. Post development of model in neural network toolbox, its Simulink model is prepared from same GUI.
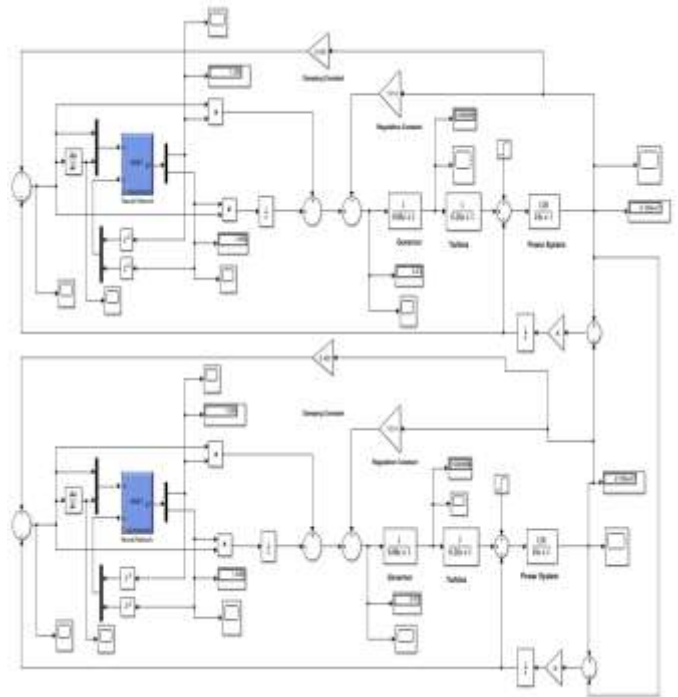
Fig 2 Simulink model of LFC using ANN-PI controller

The above fig 2 shows the Simulink model for load frequency control using ANN-PI controller.
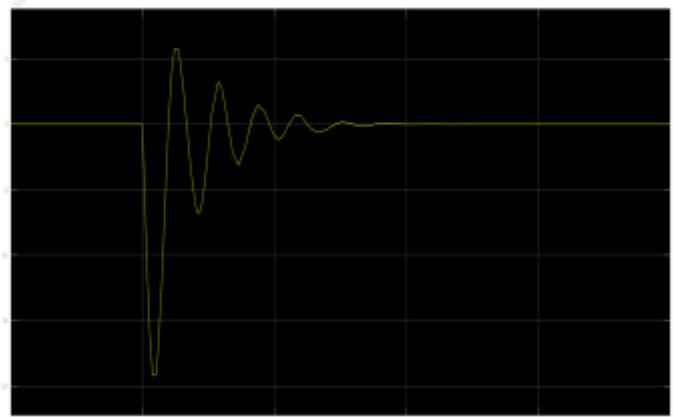
Fig 3 Change in frequency *(Δf)* response for ANN-PI controller.

Figure 3 displays the output signal of Change in frequency response of DC motor using ANN-PI controller.

Fig 4 Simulink model of LFC using ANFIS controller

The above figure 4 shows the Simulink model for load frequency control using ANFIS controller. The output signal from controller block after subtracting from frequency regulator value is supplied to Governor Block. The output from this block is then provided to turbine block. The output of this block, after subtracting change in power value is supplied to power system block to regulate output power so that frequency is maintained at constant value.
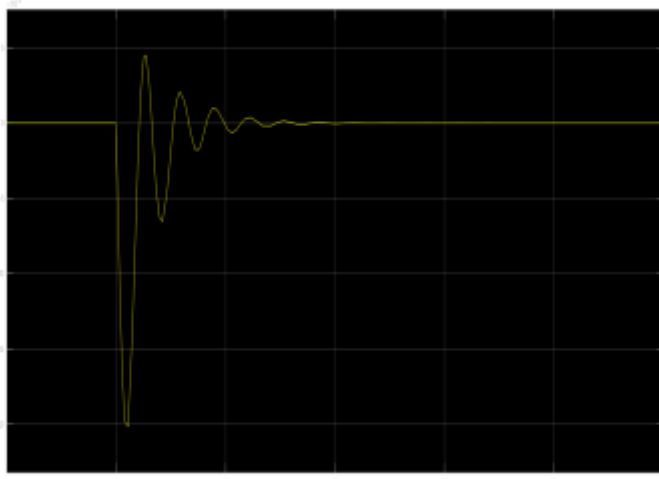
Fig 5 Change in frequency *(Δf)* response for ANFIS controller.

Figure 5 displays the output signal of Change in frequency response using ANFIS controller.

Table 1 shows the value of LFC response parameters for ANN and ANFIS controller. Based on this parameters the comparison between two controllers will be done to check there performance.

Table 1

Parameters	ANN	ANFIS
Rise Time (Sec):	1.9877e-05	3.7420e-05
Settling Time (Sec):	11.9946	10.5160
Settling Min (Hz):	-0.0192	0.0202
Settling Max (Hz):	0.0058	0.0045
Overshoot:	8.8382e+06	1.4082e+06
Undershoot:	2.6515e+06	3.1419e+05
Peak (Hz):	0.0192	0.0202
Peak Time (Sec):	5.3776	5.5464

VI. CONCLUSION

The performance of the controllers under study are tested and validated using MATLAB/SIMULINK tools. On comparison, it is found that ANFIS has minimum settling time and minimum percentage overshoot out of the two. The simulation results proof that the new techniques is succeeded to improve the controller performance.

REFRENCES

[1] Anestis G. Anastasiadis, Georgios P. Kondylis, Apostolos Polyzakis, Georgios Vokas, "*Effects of Increased Electric Vehicles into a Distribution Network*", Technologies and Materials for Renewable Energy, Environment and Sustainability, TMREES18, Athens, Greece, PP 586–593, Energy Procedia 157, ScienceDirect, 2019.
DOI: 10.1016/j.egypro.2018.11.223

[2] Anil Annamraju and Srikanth Nandiraju, "*Coordinated control of conventional power sources and PHEVs using jaya algorithm optimized PID controller for frequency control of a renewable penetrated power system*", Protection and Control of Modern Power Systems, Spinger open, 2019.
DOI: https://doi.org/10.1186/s41601-019-0144-2

[3] Neofytos Neofytou, Konstantinos Blazakis, Yiannis Katsigiannis, and Georgios Stavrakakis, "*Modeling Vehicles to Grid as a Source of Distributed Frequency Regulation in Isolated Grids with Significant RES Penetration*", Energies 2019, volume 12, mdpi journals, 2019.
DOI: 10.3390/en12040720

[4] Tawfiq Hussein and Awad Shamekh, "*Design of PI Fuzzy Logic Gain Scheduling Load Frequency Control in Two-Area Power Systems*", Designs 2019, Volume 3, Edition 26, mdpi journals, 2019.
DOI: 10.3390/designs3020026

[5] T. Mohammed, J. Momoh and A. Shukla, "*Single area load frequency control using fuzzy-tuned PI controller*," *2017 North American Power Symposium (NAPS)*, Morgantown, WV, pp. 1-6, IEEE, 2017.
DOI: 10.1109/NAPS.2017.8107352.

[6] S. Jennathu Beevi1, R. Jayashree, S. Shameer Kasim, "*ANN Controller For Load Frequency Control*", International Journal for Research in Applied Science & Engineering Technology (IJRASET), Volume 4 Issue I, 2016.

[7] V. S. Sundaram and T. Jayabarathi, "*Load Frequency Control using PID tuned ANN controller in power system*," *2011 1st International Conference on Electrical Energy Systems*, Newport Beach, CA, pp. 269-274, 2011.
DOI: 10.1109/ICEES.2011.5725341.

[8] S. Baghya Shree, N. Kamaraj, "*Hybrid Neuro Fuzzy approach for automatic generation control in restructured power system*", Electrical Power and Energy Systems 74, pp. 274–285, Elsevier, 2016.
DOI: http://dx.doi.org/10.1016/j.ijepes.2015.05.029

[9] D. K. Sambariya and Vivek Nath, "*Load Frequency Control Using Fuzzy Logic Based Controller for Multi-area Power System*", British Journal of Mathematics & Computer Science", 13(5), PP. 1-19, SCIENCEDOMAIN international, 2016.
DOI: 10.9734/BJMCS/2016/22899

[10] G. Chun-lin, W. Li, W. Dan, Q. Wen-bo and X. Xiang-ning, "*Impact of electric vehicle charging on power grid*," International Conference on Electrical and Control Engineering, Yichang, 2011, pp. 2270-2274, IEEE, 2011.
DOI: 10.1109/ICECENG.2011.6057167.

[11] S. K. Jain, A. Bhargava and R. K. Pal, "*Three area power system load frequency control using fuzzy logic controller*," 2015 International Conference on Computer, Communication and Control (IC4), Indore, pp. 1-6, IEEE, 2015.
DOI: 10.1109/IC4.2015.7375614.

[12] H. Shayeghi, H. A. Shayanfar, "*Application of ANN Technique for Interconnected Power System Load Frequency Control*", 2015 International Conference on Computer, Communication and Control (IC4), 2015.

[13] S. K. Jain, A. Bhargava and R. K. Pal, "*Three area power system load frequency control using fuzzy logic controller*," 2015 International Conference on Computer, Communication and Control (IC4), Indore, 2015, pp. 1-6, IEEE, 2015.
DOI: 10.1109/IC4.2015.7375614.

[14] Poonam Rani, Mr. Ramavtar Jaswal, "*Automatic load frequency control of multi area power system using ANN controller and Genetic algorithm*", International Journal of

Engineering Trends and Technology (IJETT) – Volume 4 Issue 9, 2013.

[15] David B. Richardson, "*Electric vehicles and the electric grid: A review of modeling approaches, Impacts, and renewable energy integration*", Renewable and Sustainable Energy Reviews 19, pp 247–254, Elsevier, 2013.
DOI: http://dx.doi.org/10.1016/j.rser.2012.11.042

[16] K. A. Ellithy, K.A. El-Metwally, "*Design of Decentralized Fuzzy Logic Load Frequency Controller*", I.J. Intelligent Systems and Applications, MECS volume 2, pp 66-75, 2012.
DOI: 10.5815/ijisa.2012.02.08

[17] S. Prakash and S. K. Sinha, "*Four area Load Frequency Control of interconnected hydro-thermal power system by Intelligent PID control technique*," 2012 Students Conference on Engineering and Systems, Allahabad, Uttar Pradesh, pp. 1-6, IEEE, 2012.
DOI: 10.1109/SCES.2012.6199090.

[18] V. S. Sundaram and T. Jayabarathi, "*Load Frequency Control using PID tuned ANN controller in power system*," 2011 1st International Conference on Electrical Energy Systems, Newport Beach, CA, pp. 269-274, IEEE 2011.
DOI: 10.1109/ICEES.2011.5725341.

[19] G. Chun-lin, W. Li, W. Dan, Q. Wen-bo and X. Xiang-ning, "*Impact of electric vehicle charging on power grid*," 2011 International Conference on Electrical and Control Engineering, Yichang, 2011, pp. 2270-2274,IEEE, 2011.
DOI: 10.1109/ICECENG.2011.6057167.

[20] Surya Prakash, S K Sinha, "*Artificial Intelligent & PI in Load Frequency Control of Interconnected Power system*", International Journal of Computer Science & Emerging Technologies, Volume 1, Issue 4, 2010.

[21] A. Salami, S. Jadid, N. Ramezani, "*The Effect of load frequency controller on load pickup during restoration*", in: 1st International Power and Energy Conference, PECON 2006, pp. 225–228, 2006.

[22] D.K. Sambariya, V. Nath, *"Load frequency control using fuzzy logic based controller for multi-area power system*", Brit. J. Math. Comput. Sci., PP 1–19, 2016.

[23] Mohamed M. Ismail, M.A. Moustafa Hassan, "*Artificial intelligence based load frequency controllers for different multi areas power*", Int. J. Control Autom. Syst. 1, 2012.

[24] V. Nath, D.K. Sambariya, "*Application of NARMA L2 controller for load frequency control of multi-area power system*", in: IEEE Proceeding of 10th International Conference on Intelligent Systems and Control (ISCO 2016), vol. 2, pp. 352–358, 2016.

[25] Emre Ozkop, Ismail H. Altas, Adel M. Sharaf, "*Load frequency control in four area power systems using fuzzy logic PI controller*", in: 16th National Power Systems Conference, 15th– 17th December, 2010.

[26] Sukhwinder Singh Dhillona, Jagdeep Singh Latherb, Sanjay Marwahac, "*Multi area load frequency control using particle swarm optimization and fuzzy rules*", in: 3rd International Conference on Recent Trends in Computing (ICRTC), pp. 460–472, 2015.

[27] Surya Prakash, Sunil Kumar Sinha, *"Four area Load Frequency Control of interconnected hydro-thermal power system by Intelligent PID control technique*", 2012.

[28] S. Priyadharshini, P. Vanitha, *"Four area interconnected system on load frequency control using firefly algorithm"*, Int. J. Adv. Res. Electric. Electron. Eng. 3 , ISSN_NO: 2321-4775, 2014.

IQAC COORDINATOR
SWAMI VIVEKANAND
COLLEGE OF ENGINEERING
KHANDWA ROAD, INDORE

PRINCIPAL
SWAMI VIVEKANAND
COLLEGE OF ENGINEERING
KHANDWA ROAD, INDORE

Relative Study of Inconsistent Size P&O based Maximum Power Point Tracking (MPPT) for PV systems

Lokesh Nimole [1], Prof. Hemendra Khedekar[2]

Student, Swami Vivekanand College of Engineering, Indore (M.P.) India[1]

H.O.D., Dept. of EX, Swami Vivekanand College of Engineering, Indore (M.P.) India [2]

ABSTRACT: Maximum Power Point Tracking (MPPT) techniques are used in photovoltaic (PV) systems to maximize the output power of the photovoltaic field, incessantly monitoring the Maximum Power Point (MPP) that depends on the temperature of the panels and the radiation circumstances. The MPPT problem has been addressed in dissimilar ways in the literature, but, especially for low-cost implementations, the algorithm for tracking the point of maximum disturbed and observed power (P&O) is the method most used for its ease of use. implementation. A disadvantage of P&O is that, in a stable state, the operating point fluctuates around the MPP resulting in the waste of a certain amount of available energy; Furthermore, it is known that the P&O algorithm can be confused throughout those time intervals characterized by rapidly evolving atmospheric conditions. This paper shows that, The performance of the developed model is tested under different Load conditions. Our Proposed PV model controlling a motor and battery with control architecture. Rapid Time is reduced from 10-20 second to 0.05 second. Using PID controller along with MPPT algorithm produce stable power with less transient time and also improve quality of supply for sensitive industries.

KEYWORDS : Maximum power point tracking (MPPT), photovoltaic (PV) systems, Perturbation   and Observation (P & O)

I.INTRODUCTION

Renewable energy is energy that is collected from non- depleting resources, which are naturally replenished, such as sunlight, wind, tidal waves. This energy consumption is sub-divided as 8.9% from traditional biomass, 4.2% as heat energy,3.9% hydroelectricity and 2.2% is electricity from solar energy, wind, geothermal, and biomass. Globally fund invested in renewable technologies is more than US$286 billion in 2015, with China and the United States diverting funds heavily in wind, hydro, solar and bio fuels. Universally, about 7.7 million jobs linked with the renewable energy industries, with solar photo voltaic' being the largest employer. As of 2015 globally, about half of all new electricity capacity installed was renewable.

Different type of renewal energy sources

A). Wind power: Air pressures used to run wind turbines. Modern wind turbines range from around 600 kW to 5 MW, however turbines with rated output of 1.5–3 MW have become the most common for commercial use. The largest generator capacity of a single installed wind turbine reached 7.5 MW in 2015.

B). Hydro power: hydropower generated 16.6% of the world total electricity and 70% of all renewable electricity till 2015. Since water is about eight hundred times denser than air, even a slow flowing stream of water, or light sea swell, can yield considerable amounts of energy. There are many forms of water energy.

C). Solar energy: Solar energy, radiated light and heat from the sun, is harvested using a range of various technologies such as solar heating, photovoltaic cell, concentrated solar power (CSP), concentrator photovoltaic (CPV), solar architecture and artificial photo synthesis.
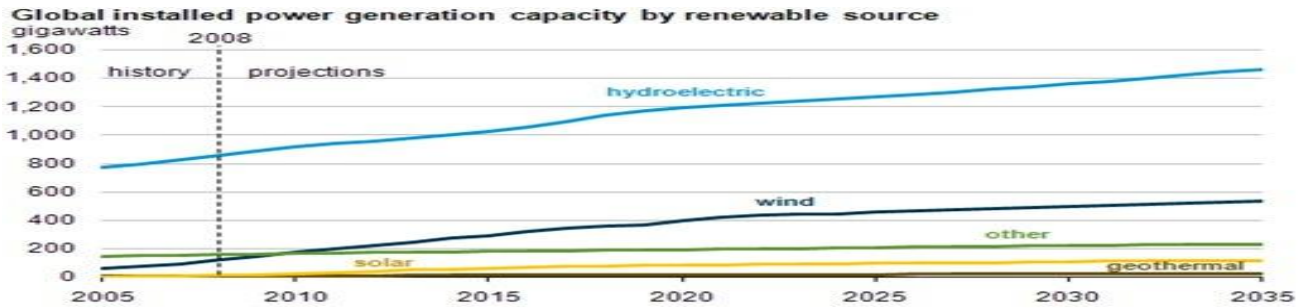
Fig. 1: - Comparison Power generation in different source.

Materials used in PV cell

The materials used in Photovoltaic (PV) cells are as follows:

a) Single crystal silicon:

Single crystal silicon cells are most commonly used in the Photovoltaic (PV) industry. The main procedure for producing single-crystal silicon is the C Zochralski (CZ) method. High-purity polycrystalline is melted in a quartz crucible. A single-crystal silicon seed is dipped into this molten mass of polycrystalline. As the seed is pulled slowly from the melt, a single-crystal ingot is designed. The ingots are then sawed into thin wafers about 200-400 micrometers thick (1 micrometer = 1/1,000,000 meter). The thin wafers are then refined, doped, coated, interconnected and assembled into modules and arrays.

b) Polycrystalline silicon:

Consisting of small grains of single-crystal silicon, polycrystalline Photovoltaic (PV) cells are less energy efficient than single-crystalline silicon Photovoltaic (PV) cells. The grain boundaries in polycrystalline silicon hinder the flow of electrons and reduce the power output of the cell. A common approach to produce polycrystalline silicon Photovoltaic (PV) cells is to slice thin wafers from blocks of cast polycrystalline silicon. Another more advanced approach is the "ribbon growth" method in which silicon is grown directly as thin ribbons or sheets with the approach thickness for making Photovoltaic (PV) cells.

II. PROBLEMS IDENTIFICATIONS

As is clear from the review of the related literature a lot of problems like Power quality (voltage sag, voltage swell, Transients) are identified and studied. The photo voltaic system convert sunlight to direct current. The solar array is formed by connecting individual solar panel system together. The output current of solar array depends on the ambient temperature, solar radiation, the size and configuration of the PV array. In general, the larger area photo voltaic panels will generate more energy, and smaller photo voltaic panels generate less energy. From the simulation result, the PID controller has shown the better performance than other MPPT techniques. In study of literature we observed that if we did not use PID controller with MPPT then output power was low. It gets improved when we apply the PID controller along with MPPT complete control architecture and getting the output power is increased. After Appling MPPT and PID controller the output results of the current, voltages and power get improved. Previous Test results indicate that diesel generator can compensate PV power reduction relatively fast. The proposed method could be used to levelling PV output power fluctuation and reduce the frequency deviations and maintain resilience on the grid. "The three test results indicate that diesel generator can compensate for the rise and fall in solar active power in a relatively rapid time (10 to 20 seconds) and maintain the stability of grid frequency".

III.OBJECTIVES

This thesis presents the MATLAB SIMULINK model of PV Grid with the control strategy needed for the improvement of power Quality at distribution end. The major objectives are as follows:

1. To analyse the effect of non-linear loads, linear loads and Motor loads on Distribution system.

2. To study, Design and simulate PV based power generation with battery controller.

3. To study and Present a systematic approach for designing PV Grid with various islanding faulty (LL-G) loads.

4. Modelling of Indirect Current Control (vector control method) and VSC (Voltage source converter) theory.
5. To Study and Simulation of controllers like PID-PI And (Battery) Hysteresis controller.

IV.PERTURBATION AND OBSERVATION (P & O) METHOD

The P & O algorithm, as shown below in, operates by increasing or decreasing the array terminal voltage, or current, at regular intervals and then comparing the PV output power with that of the previous sample point. If the PV array operating voltage changes and power increases (dP/dV, PV > 0), the control system adjusts the PV array operating point in that direction; otherwise the operating point is moved in the opposite direction. At each perturbation point, the algorithm continues to operate in the same manner. The main advantage of this approach is the simplicity of the technique. Furthermore, previous knowledge of the PV panel characteristics is not required. In its simplest form, this method generally exhibits good performance provided the solar irradiation does not vary too quickly. At steady state, the operating point oscillates around the MPP voltage and usually fluctuates lightly. For this reason, the perturbation frequency should be low enough so

➢ **P&O method Principle**

In P&O method, the MPPT algorithm is based on the calculation of the PV output power and the power change by sampling both the PV current and voltage. The tracker operates by periodically increment or decrement the solar array voltage. If a given perturbation leads to an increase (decrease) in the output power of the PV, then the subsequent perturbation is generated in the same (opposite) direction. So, the duty cycle of the dc chopper is changed and the process is repeated until the maximum power point has been reached. Actually, the system oscillates about the MPP. Reducing the perturbation step size can minimize the oscillation. However, small step size slows down the MPPT. To solve this problem, a variable perturbation size that gets smaller towards the MPP.

However, the P&O method can fail under rapidly changing atmospheric conditions. Several research activities have been carried out to improve the traditional Hill-climbing and P&O Methods.

Block Diagram of Perturb and Observe (P&O) method:-
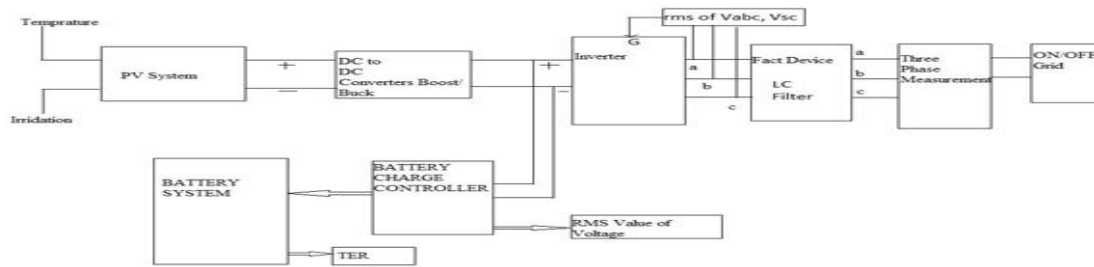
Fig. 2:-Block Diagram of Perturb and Observe (P&O)

➢ **Perturb and Observe (P&O) method has the disadvantage**

The classic perturbs and observe (P & O) method has the disadvantage of poor efficiency at low irradiation. For this reason, alternative solutions have been proposed. Combine a constant voltage (CV) algorithm with a modified P & O method to track the MPP with high efficiency under both low and high solar irradiation conditions. The algorithm operates by increasing the duty cycle until the PV output voltage is close to the open circuit voltage of the panel (VOC), this is then using the initial conditions for the MPP tracker. The algorithm then evaluates the current output; if the current is higher than (0.7 A) the algorithm adopts the P&O method; if it is lower it converts to the CV method. Simulation results demonstrate that overall greater energy can be extracted from the PV panel; efficiency levels of 95% to99% are quoted over a wide irradiation range. However, there is complication of combining the two methods.

The P & O method is also prone to erratic behavior under rapidly variation in light levels. This may result in slow, or incorrect, MPP tracking. Introduced a modified P&O (MP&O) method to solve this problem. The method adds an irradiance-changing estimate process in every perturb process to measure the amount of power variation caused by the change of conditions. Results show improved performance over the conventional P & O method. However, MP&O has a slow tracking speed which is approximately half of the conventional P & O method.

Model of PV cell:
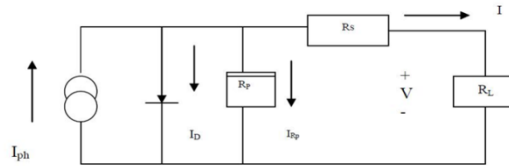
Fig. 3:- Equivalent circuit

An ideal solar cell is modeled by a current source in parallel with a diode. But no solar cell is ideal and therefore shunt and series resistances is added to the model as shown in the equivalent diagram shown in fig.

Here R_S= intrinsic series resistance whose value is very small and

R_P= equivalent shunt resistance has very high value.

$I = I_{ph} - I_d - IR_{sh}$

$$I = I_{ph} - I_0 \left(e^{\frac{q(v+IR_s)}{aKT}} - 1 \right) - \left(\frac{V + IR_s}{R_{sh}} \right)$$

I = Cell current,

I_{ph}=photon current,

I_0= Reverse saturation Current of diode at T,

V = voltage across diode,

V_T= Thermal voltage,

K =Boltzmann constant,

T = Temperature in Kelvin,

q =Charge of an electron in coulombs

a=diode ideality factor, normally between 1 and 2

Structure of grid connection system

➢ This focuses on the overall design of a Photovoltaic (PV) system interfaced with a grid/stiff grid or utility.

➢ The description of each of the components of the Photovoltaic (PV) system, namely the Photovoltaic (PV) module, the boost converter, the inverter, and the grid. This description helps to understand the functionality of each component of the system, leading to its detailed mathematical design, the results of which are shown in the following chapters.

➢ A Glimpse of the architecture of the two-stage Photovoltaic (PV) system connected to a grid is shown in fig. 4. It is followed with sections describing the Photovoltaic (PV) cell, the MPPT controller, the DC-DC converter, the DC-AC converter, and finally the phase lock loop PLL.

➢ A parallel RLC load is connected to the system. P and Q represent the active and the reactive power, respectively, that is delivered from the Photovoltaic (PV) system to the grid, at Point of Common Connection (PCC). In different control aspects involved in a Photovoltaic (PV) system. Phase Locked Loop (PLL) is used to extract the phase angle (θ) and frequency (ω) at PCC. The current controller is used to control the AC side inverter currents. A DC-link voltage controller is used to maintain the Photovoltaic (PV) array voltage (V_{dc}or V_{pv}) at the reference value $V_{dcref\ which}$ is given by the MPPT controller.

Interfacing of the PV Array with Boost Converter

The Photovoltaic (PV) array has been interfaced with the boost converter using a controlled voltage source as shown in the circuit diagram below.
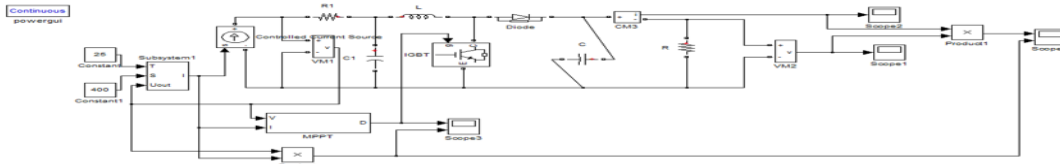
Fig.4 :- Simulink model of PV array with the boost converter

The detailed internal circuit of the Photovoltaic (PV) array showing the design is given below:
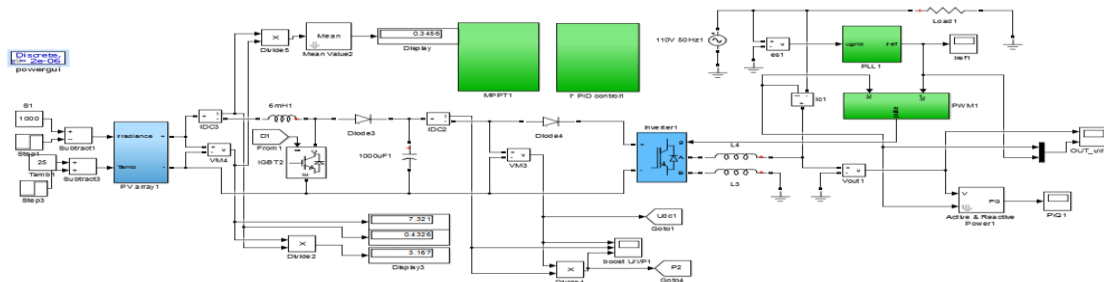
Fig. 5 :-   Modeling of MPPT with PID controller.
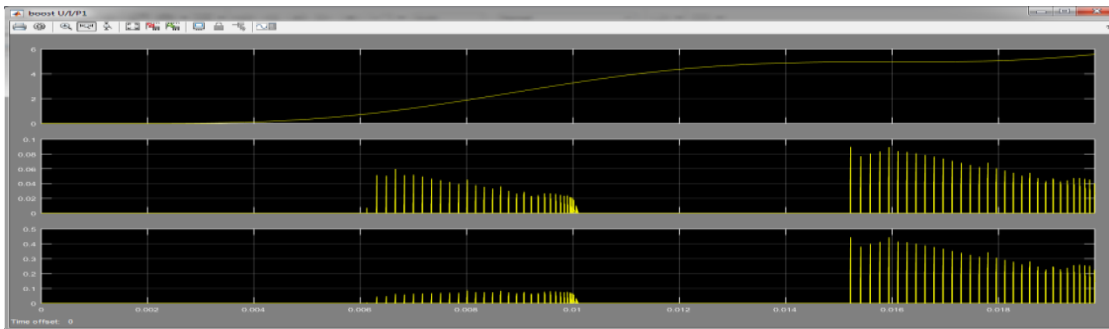
Fig.6:- Voltage, current and power variations.
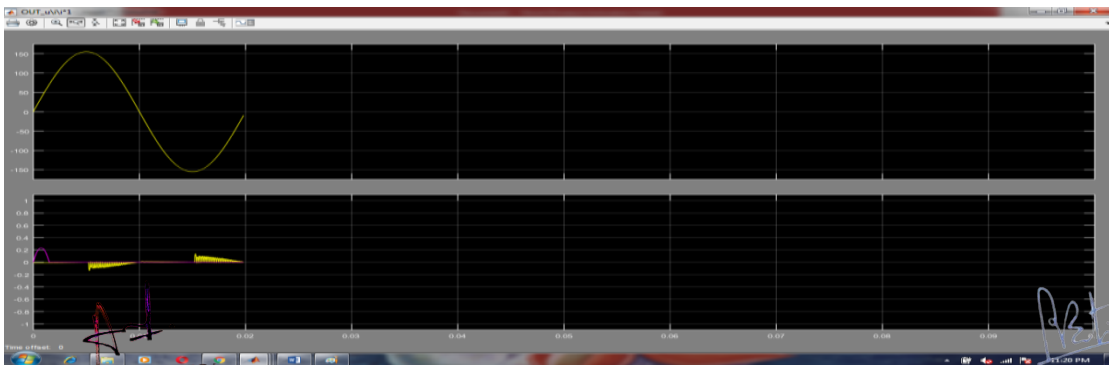
Fig. 7:- Single phase voltage and power.
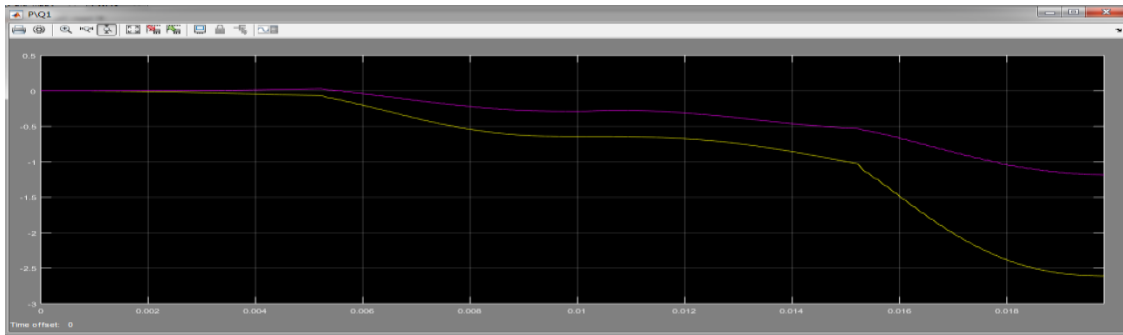
Fig.8 :- Active power deviations.
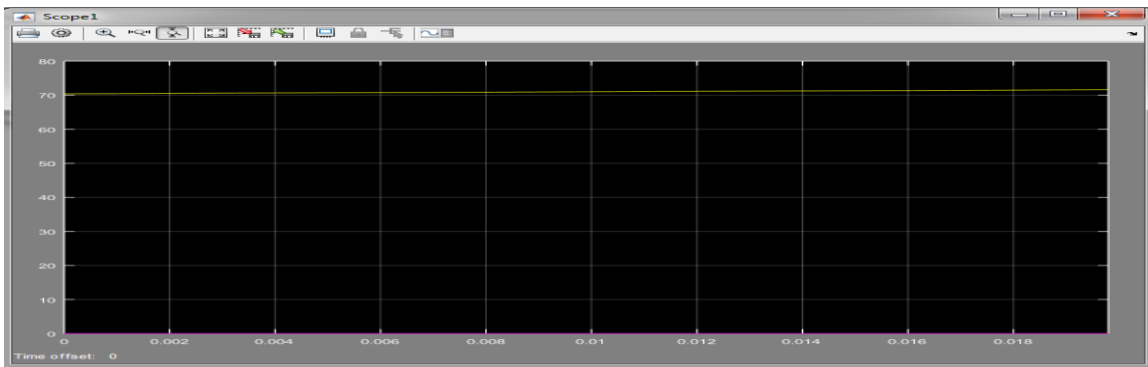
Fig . 9:- MPPT reference power.

PARAMETERS TABLE

1. without boost converter PV output:

Irms	0.3456A
V_{pv}	0.4326V
P_{pv}	3.167Watt
Temperature	25^0C
Irridation	1000

2. With Boost converter output:

Irms	0.3456A
V_{Total}	150V(With Exponential Increase)
PQ	-2.61Watt,-1.183
Kp	0.00001
Ki	0.000015
Kd	0.000015

IQAC COORDINATOR
SWAMI VIVEKANAND
COLLEGE OF ENGINEERING
KHANDWA ROAD, INDORE

PRINCIPAL
SWAMI VIVEKANAND
COLLEGE OF ENGINEERING
KHANDWA ROAD, INDORE

V.CONCLUSIONS

The Performance of the developed model is tested under different Load conditions.

➢   Our Proposed PV model controlling a motor and battery with control architecture.
➢   Rapid Time is reduced from 10-20 second to 0.05 second.
➢   Using PID controller along with MPPT algorithm produce stable power with less transient time and also improve quality of supply for sensitive industries.
➢   Results of Perturb and observe algorithm produce good result mean to say able to obtain maximum power point in comparison with other algorithms.
➢   Our model using FACTS devices and PLL system improve voltage stability and minimizes Harmonics.
➢   Our model present best controlling Techniques for small to high load systems.

REFERENCES

1. S. Liu and R. A. Dougal, "Dynamic multiphysics model for solar array," IEEE Trans. Energy Conv., vol. 17, no. 2, pp. 285–294, Jun. 2002.

[2] K. H. Hussein, I. Muta, T. Hshino, and M. Osakada, "Maximum photovoltaic power tracking: an algorithm for rapidly changing atmospheric conditions," Proc. Inst. Elect. Eng., vol. 142, no. 1, pp. 59–64, Jan. 1995.

[3] M. Veerachary, T. Senjyu, and K. Uezato, "Voltage-based maximum power point tracking control of PV system," IEEE Trans. Aerosp. Electron. Syst., vol. 38, no. 1, pp. 262–270, Jan. 2002.

[4] K. K. Tse, M. T. Ho, H. S.-H. Chung, and S. Y. Hui, "A novel maximum power point tracker for PV panels using switching frequency modulation," IEEE Trans. Power Electron., vol. 17, no. 6, pp. 980–989, Nov. 2002.

[5] P. Midya, P. Krein, R. Turnbull, R. Reppa, and J. Kimball, "Dynamic maximum power point tracker for photovoltaic applications," in Proc. 27th Annu. IEEE Power Electronics Specialists Conf., vol. 2, Jun. 1996, pp. 1710–1716.

[6] E. Koutroulis, K. Kalaitzakis, and N. C. Voulgaris, "Development of a microcontroller-based, photovoltaic maximum power point tracking control system," IEEE Trans. Power Electron., vol. 16, no. 1, pp. 46–54, Jan. 2001.

[7] T. Noguchi, S. Togashi, and R. Nakamoto, "Short-current pulse-based maximum-power-point tracking method for multiple photovoltaic-andconverter module system," IEEE Trans. Ind. Electron., vol. 49, no. 1, pp. 217–223, Feb. 2002.

[8] Santos J.L., Antunes F., Chehab A. and Cruz C.C., "A Maximum Power Point Tracker for PV systems using a high performance boost converter", Science Direct. Solar Energy 80, 2006, pp.772-778. [9] N. Pandirajan and R. Muthu, "Mathematical Modelling of Photovoltaic Module with Simulink", in Proceedings of the International Conference on Electrical Energy Systems (ICEES'11), Jan 2011.

[10] "Neural network in maximum power point tracker for PV systems", Science Direct Electric Power Systems Research, July 2010, pp.43-50

[11] S Samal, P K Hota and P K Barik, "Comparitive analysis of MPPT algorithms for maximum power extraction from PV systems", in Recent Advances and Innovations in Electrical Engineering (RAIEE 2014), VSSUT, Burla, 2014

[12] Abdelsalam, Ahmed K., Ahmed M. Massoud, Shehab Ahmed, and Prasad N. Enjeti, "High- Performance Adaptive Perturb and Observe MPPT Technique for Photovoltaic-Based Microgrids", IEEE Transactions on Power Electronics, 2011

[13] Abhishek Sakhare, Asad Davari, Ali Feliachi, "Fuzzy Logic Control of fuel cell for stand alone and grid connection", Journal of Power Sources, 2004

[14] Christopher A. Otiento, George N. Nyakoe, Cyrus W. Wekesa, "A Neural Fuzzy Based Maximum Power Point Tracker for a Photovoltaic system", IEEE Africon, September 2009.

EXPERIMENTAL STUDY OF DOUBLE SKINND CONCRETE FILLED STEELTUBULAR STRUCTURES IN BENDING

Goutam Varma[1], Dr. Pankaj Singh[2], Mayur Singi[3], Kapil Kushwah[4]

[1,3,4]Research Scholar S.R.K. University Civil Engineering
[2]Professor S.R.K. University Civil Engineering

---***---

ABSTRACT - Concrete-filled twofold skin rounded (DSCFST) shafts comprise of two concentric steel tubes; the void between them is loaded up with cement. Favorable circumstances of CFDST over completely concrete filled steel tubes (CFST) incorporate increment in segment modulus, better damping, lighter weight; cyclic stacking. In these paper mechanical properties, for example, Compressive quality shapes and Split rigidity of barrels were tried for M20 grade Concrete. Diverse DSCFST pillars fluctuating internal and external measurements with relating thicknesses were created. Bowing test is performed and contrasted and hypothetical qualities. The shafts are demonstrated great execution in pliable and twisting.

Key words: Double Skin Concrete Filled steel Tubes (DSCFST), Composite Beams, Bending Test, Compressive Strength, Split Tensile Strength.

1. INTRODUCTION

Double Skin Concrete Filled steel Tubes (DSCFST) are composite auxiliary individuals, which comprises of solid which is filled between the voids of inward and external steel tubes. The utilization of cement filled steel tubes (CFST) ends up well known in the previous couple of decades. DSCFST have been utilized in skyscraper wharfs to diminish oneself weight and expansive vitality retention limit against earth shudder stacking. The DSCFST part having empty cross-segment are lighter in weight, contrasted with cement filled steel tubes. In this paper, the trial investigation of twenty four examples of DSCFST bars were tried under two point stacking test technique. Skyscraper composite structures prompt huge development as CFST sections, which bring distinctive financial advantages. Beforehand CFSTs ponders concentrated on joined hub flexural Response or axial. However, recently, CFST elements were used as a main girder of a railway bridge. The behavior of CFST for its flexure has studied experimentally. Experimental work on (DSCFST) members which are subjecting to fire, static loading, cyclic loading and the durability were also studied in the past few years. The changing behavior of sub structural elements due to impact load becomes important because of the increase in accidental impacts. Research work is going on the dynamic response of reinforced concrete and steel structures

2. EXPERIMENTAL STUDY

Compressive strength: The cubes of size 150 mm X 150mm X 150 mm are used for calculating the compressive strength. Concrete cubes were casted with M20 grade of concrete. The compressive strength of cubes for 7, 14, and 28 days were tested. The specimens are tested by compression testing machine. Load should be applied gradually until the specimens fails. Table 1 gives values for compressive strength of cubes. The Compressive strength of cubes Vs Number of days graph has plotted on Figure 1.

Table 1 Compressive strength of cubes

S.No	No. of days	Compressive Strength (N/mm²)
1	7	15.92
2	14	20.24
3	28	24.57
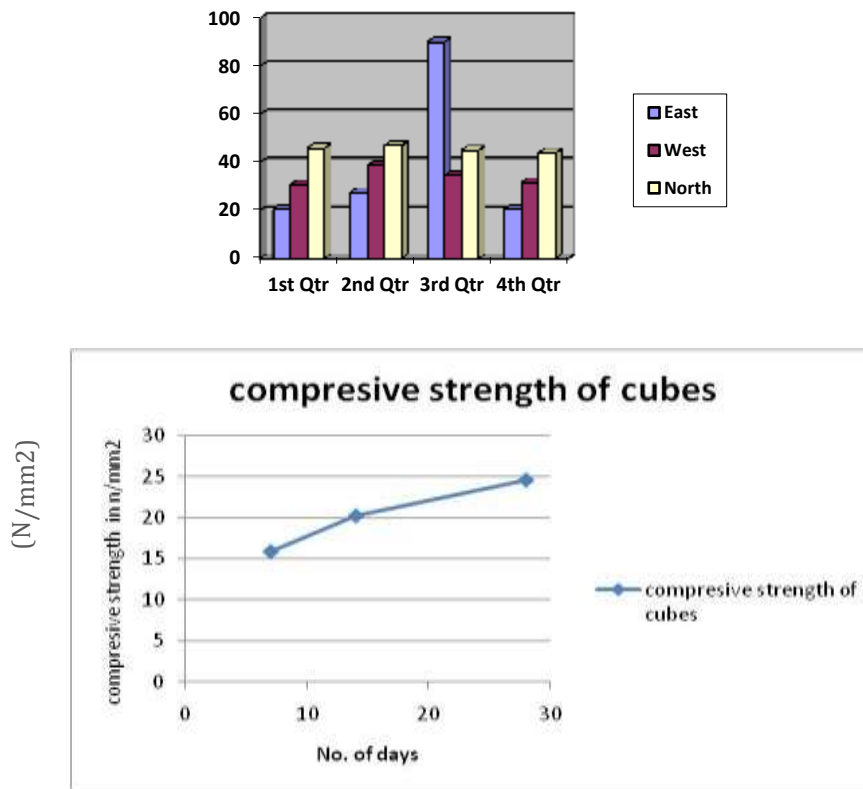
Figure 1 Compressive strength of cubes

2.1. Split tensile strength

The Cylinders of dimensions 300mm X 150mm are used for calculating the split tensile strength. Concrete cylinders were casted with M20 grade of concrete. The split tensile strength of cylinders for 7, 14, and 28 days were tested. The load is applied continuously without slip. Note down the breaking load (P) and the results were tabulated in Table 2. The Split tensile strength of cylinders Vs Number of days

Figure 2

Table 2 Split tensile strength of cylinder

S.No	No. of days	Split tensile strength (N/mm²)
1	7	2.58
2	14	2.96
3	28	2.94

IQAC COORDINATOR
SWAMI VIVEKANAND
COLLEGE OF ENGINEERING
KHANDWA ROAD, INDORE

PRINCIPAL
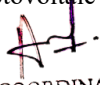SWAMI VIVEKANAND
COLLEGE OF ENGINEERING
KHANDWA ROAD, INDORE
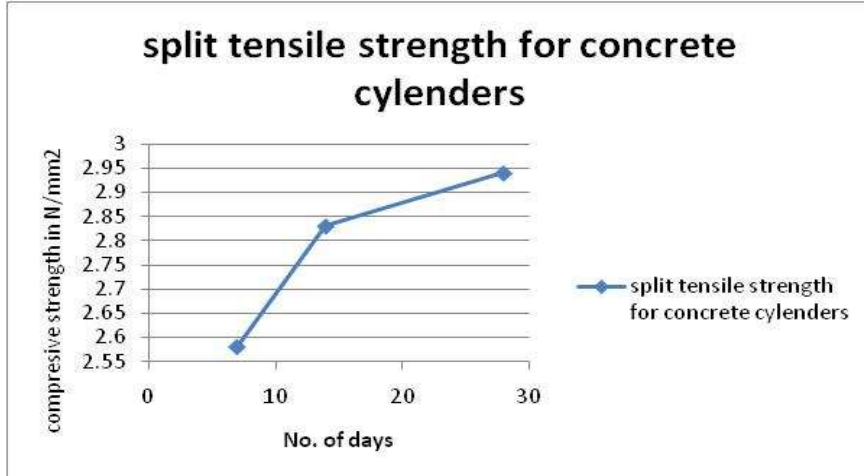
3. FLEXURAL STRENGTH

3.1. Specimen fabrication

The specimen's outer width varies from 75mm to 150mm and inner width varies from 25mm to 100mm respectively. Both outer and inner steel tubes having thickness varies from 1.2mm to 3mm. A steel plate was welded to one end of the empty steel tube to prevent deterioration of concrete. The beams were casted such that voids between inner and outer steel tubes were filled with concrete. All specimens were cured for room temperature for 28 days. The cross section details of the square DSCFST specimens are listed in Table

Table 3 Cross section details of CFDST beams

S.No	Type of specimen	Bo.o (mm)	To (mm)	Bi.o (mm)	Ti (mm)	Hollow ratio (C)
1	S in S	150	2.5	25	1.2	0.690
2	S in S	150	2.5	50	1.2	0.517
3	S in S	150	2.5	75	2	0.345
4	S in S	150	2.5	100	2	0.172
5	S in S	50	1.2	25	1.2	0.210
6	S in S	75	2	25	1.2	0.260
7	S in S	100	2	25	1.2	0.352
8	S in S	125	3	25	1.2	0.525

S in S   - Square in Square

L   - Length

Bo.o   - Breadth of outer steel tube outer side

Bi.o   - Breadth of inner steel tube outer side

To   - Thickness of outer tube

Ti   - Thickness of inner tube

Hollow ratio = C

Page 125

4. LOADING FRAME

Beams were tested for a span of 1500mm, which is subjected to two points loading and overhang support distance is maintained at 100mm on both sides. The deflection is noted at a distance of L/3 from each end. Each beam was tested for its maximum load and load Vs mid-span deflection graph is plotted. The beams are attaining its original shape after completing the experimental work due to its ductile nature of steel. The experimental set up for DSCFSTbeam.

5. RESULTS AND DISCUSSIONS

The Experimental and theoretical results are tabulated below and the graphs are drawn below.
The experimental results are tabulated below in Table 4.

Table 4 Dimensions of beams with maximum load and maximum deflection

S.No	Beam size (mm x mm)	Thickness of outer steel (mm)	Thickness of inner steel (mm)	Hollow ratio (C)	B_i / B_0 ___	Max load (kN)	Ave. Max Load (kN)	Max deflection (L/2) (mm)	Ave. Max deflection (L/2) (mm)	Max deflection (L/3) (mm)	Ave. Max deflection (L/3) (mm)
1	150 X 100	2.5	2	0.690	0.67	256	255.67	8.11	8.92	7.25	8.35
2						249		5.49		9.43	
3						262		9.22		9	
4	150 X 75	2.5	2	0.517	0.50	226	227.33	8.7	8.80	7.5	7.81
5						230		9.2		8.04	
6						226		9.65		8.8	
7	150 X 50	2.5	1.2	0.345	0.33	230	215.00	7.99	7.82	6.4	6.52
8						205		7.77		7.78	
9						210		7.7		6.17	
10	125 X 25	3	1.2	0.210	0.20	160	160.33	12.06	9.66	10.1	8.07
11						164		7.1		8.7	
12						157		8.21		7	
13	100 X 25	2	1.2	0.260	0.25	98	81.00	15.55	15.48	13.25	13.02
14						80		8.2		15.6	
15						65		15.3		12.4	
16	75 X 25	2	1.2	0.352	0.33	32	29.33	17.21	16.81	15.2	14.78
17						25		7.2		16.23	
18						31		17		14.99	

The comparison of Experimental maximum load and Theoretical maximum load is shown in Table 5

Table 5 Comparison of results for experimental and theoretical values

S.No	Size of beam	Theoretical value (kN)	Experimental value (kN)	Ratio (Exp/The)
1	150 X 100	174.96	255.67	1.461305
2	150 X 75	166.82	227.33	1.362726
3	150 X 50	162.54	215.00	1.322751
5	125 X 25	102.21	160.33	1.568633
6	100 X 25	36.67	81.00	2.20889
7	75 X 25	14.39	29.33	2.038221

6. LOAD VS. DEFLECTION

The beam of outer steel tube 150mm and varying inner steel tube dimensions (100mm, 75mm, 50mm,) has gets increasing in maximum load respectively. The Load Vs Deflection graph for DSCFST beams of outer tube 150mm and varying inner tube (100mm, 75mm, 50mm) is shown in Figure
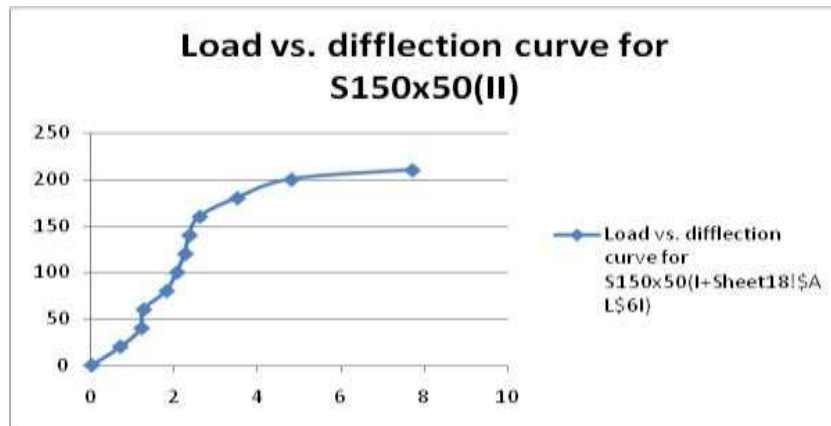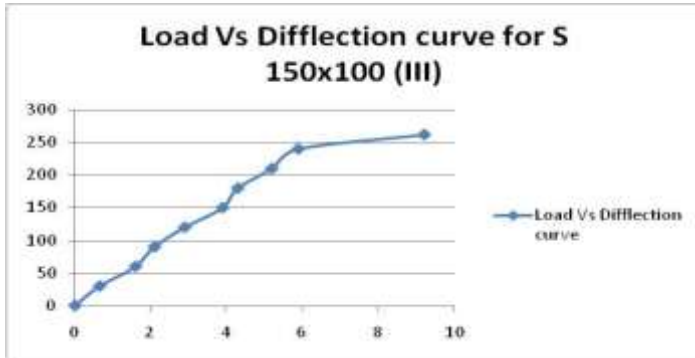
The Load Vs Deflection graph for DSCFST beams of inner tube 25mm and varying outer tube (125mm, 100mm, 75mm) is shown in Figure below.
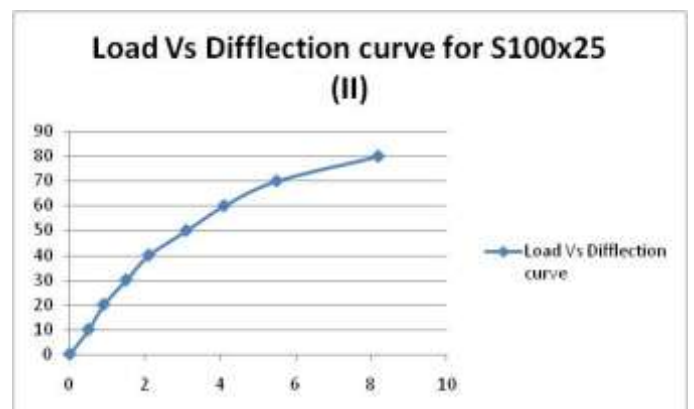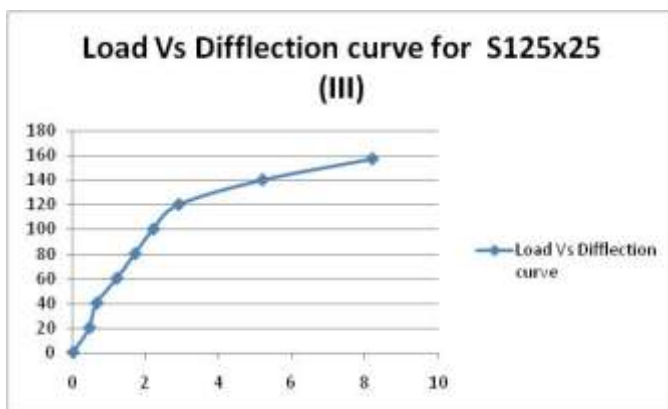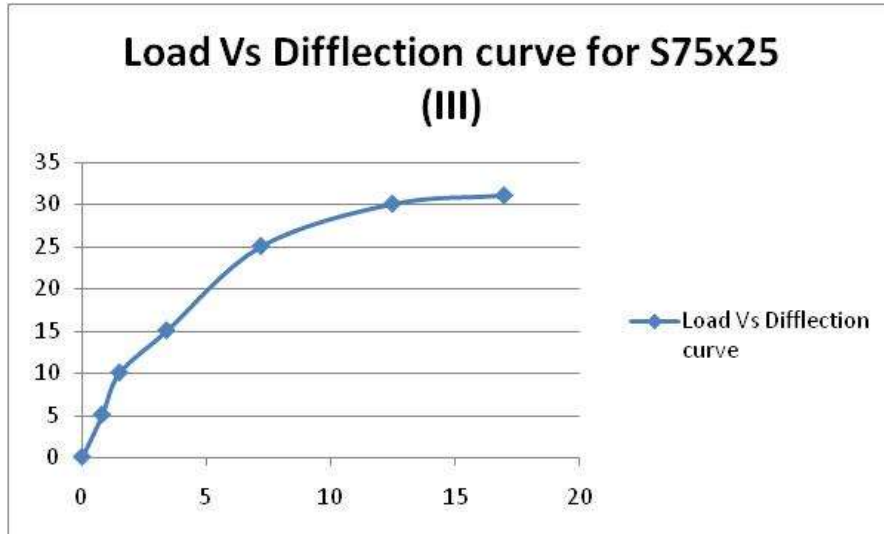
CONCLUSIONS

Concrete filled double skin tubular beams were subjected to bending under two points loading, following conclusions had been drawn.

1. A series of experimental tests on square DSCFST subjected to Flexure test. Enhancement in strength has been observed for DSCFST beams (square in square) due to the ductile nature of steel and Composite action between steel and concrete.

2. The flexural strength of DSCFST beams increases with respect to the increase in the dimensions of inner tube, by keeping the outer steel tube dimension as constant and changing the inner steel tube dimensions.

3. The DSCFST beam 150 x 100mm has attained more bending strength than 150 x 50mm beam.

4. The bending strength of DSCFST beams is increased with respect to the increase in the dimension of outer tube, by keeping the inner steel tube dimension as constant and changing the outer steel tube dimensions.

5. The beam of inner steel tube 25mm and having outer steel tube of increasing dimensions   (75mm, 100mm, and 125mm) has gets increasing in deflection.

   The beams of outer steel tube 150mm and having inner steel tube of increasing dimensions (100mm, 75mm, 50,) has gets increasing in maximum load.

REFERENCES

[1]   Ju Chen, Jun Wang, Fang Xie Wei-liang Jin Behavior of thin-walled dodecagonal section double skin concrete-filled steel tubes under bending Thin-Walled Structures98(2016)293– 300

[2]   Kojiro Uenaka, Hiroaki Kitoh Mechanical behavior of concrete filled double skin tubular circular deep beams Thin-Walled Structures 49 (2011) 256–263

[3]   Kojiro Uenaka CFDST stub columns having outer circular and inner square sections under compression Journal of Constructional Steel Research 120 (2016) 1–7

[4]   Lin-Hai Hana, Hong Huangc, Zhong Taoc, Xiao-Ling Zhaod Concrete-filled double skin steel tubular (CFDST) beam–columns subjected to cyclic bending Engineering Structures 28 (2006) 1698–1714

[5]   Xiao-Ling Zhao, Raphael Grzebieta Strength and ductility of concrete filled double skin (SHS inner and SHS outer) tubes Thin-Walled Structures 40 (2002) 199–213

Page 128

[6]   M.F. Hassanein, O.F. Kharoob , L. Gardner Behaviour and design of square concrete-filled double skin tubular columns with inner circular tubes Engineering Structures 100 (2015) 410–424

[7]   Jiho Moon, Charles W. Roeder , Dawn E. Lehman , Hak-Eun Lee Analytical modeling of bending of circular concrete-filled steel tubes Engineering Structures 42 (2012) 349–361

[8]   Raed Abendeh, HeshamS. Ahmada, Yasser M. Hunaiti Experimental studies on the behavior of concrete-filled steel tubes incorporating crumb rubber Journal of

STUDY AND PARAMETRIC OPTIMIZATION OF GAS METAL ARC WELDING PROCESS (GMAW) PROCESS

[1]Shweta S. Adayprabhu, [2] Vishal Wankhade, [3] Dr.Pradeep Patil,

[1]ME Student, [2] Assistant Professor, [3]Assossiate Professor
[123] Mechanical Engineering Department, Swami Vivekanand College of Engineering, Indore, India.

Abstract: Welding is widely used by metalworkers in fabrication, maintenance and repair of parts and structures. The arc welding process is a remarkably complex operation involving extremely high temperatures, which produce severe distortions and high levels of residual stresses. These extreme phenomena tend to reduce strength of the structure, which becomes vulnerable to fracture, buckling, corrosion and other type of failures. In gas shielded arc welding, an inert gas is used as a covering shield around the arc to prevent the atmosphere from the contaminating the weld. For the same Taguchi methods are applied to reform the objectives of the study. All these targets are achieved by making an experimental setup.

IndexTerms - **arc welding, fracture, buckling, inert gas, taguchi method.**

I. INTRODUCTION

The arc welding process is an extremely multifaceted process, needs high temperatures, which results in severe distortions and lasting stresses. These extreme phenomena tend to reduce the strength of a structure, which becomes vulnerable to fracture, buckling, corrosion and other type of failures. The primary goal of any welding operation is to make a weld having the same properties as the base metal. The only way to produce such a weld is to protect the molten puddle from atmosphere. In a gas shielded arc welding process, an inert gas is used for covering shield around the arc to prevent the atmosphere from contaminating the weld. Gas shielding makes it possible to weld metals that are otherwise impartial or difficult to weld by eliminating atmospheric contamination of the molten puddle. In order to weld all kinds of ferrous / nonferrous metals of all thickness, Gas shielded AW is most useful. In general, the controlling factors are the metal types you are using for joining, cost involved, nature of the products you are fabricat8ing, and the techniques used to fabricate them.

II. LITERATURE SURVEY

Chunlin Dong et.al performed Preliminary study on the mechanism of Arc Welding with the activated flux type 304 austenitic stainless steel with different S content. Individual flux compound such as TiO_2, Cr_2O_3, SiO_2, ZrO_2 is used it is found that Weld Penetration depth dramatically increase in presence of some individual Oxides. It is found that fluid flow appear n outward direction in case of ZrO_2.

M Tanaka et.al study Arc constriction and observed during A-TIG welding and this is caused by changes within the arc plasma for the distribution of metal vapors from the weld pool, accompanied by variation in the size and the surface temperature of the weld pool. The constriction of either the arc or the arc root does not play a central role as the deep penetration mechanism during A-TIG welding but cannot be ignored as an auxiliary factor for deep penetration, as seen in high S stainless steel helium TIG welding.

Ugur Esmel et.al study has concentrated on the application of Taguchi method coupled with Grey relation analysis for solving multi criteria optimization problem in the field of tungsten inert gas welding process. Experimental results have shown that the tensile load, heat affected zone and penetration, area of penetration, heat affected zone, bead width and bead height of the weld bead in the TIG welding of stainless steel are greatly improved by using Grey relation analysis in combination with Taguchi method.

III. PROBLEM FORMULATION & OBJECTIVES

The present work "optimization of ATIG Welding process parameter for enhancement of weld penetration" has been undertaken keeping in consideration the following problem.

Inadequate weld bead dimensions such as shallow depth of penetration may contribute to failure of a welded structure since penetration determines the stress carrying capacity of a weld joint.

To avoid such occurrences the input or welding process variables which influence the weld bead penetration must therefore be properly selected and optimized to obtain an acceptable weld bead penetration and hence a high quality joint.

Objective of dissertation work is;
1. Comparative study of coated uncoated sample.
2. Find out the most effective parameter by Taguchi Method.
3. Enhancement of weld Penetration.
4. Study the effect on tensile strength on welded sample.

Page 130

IV. METHODOLOGY


```
┌─────────────────────────────────────────────┐
│     Basics of welding and its requirements    │
└─────────────────────────────────────────────┘
                      ⇩
┌─────────────────────────────────────────────┐
│              Details of TIG welding           │
└─────────────────────────────────────────────┘
                      ⇩
┌─────────────────────────────────────────────┐
│             Problems in TIG welding           │
└─────────────────────────────────────────────┘
                      ⇩
┌─────────────────────────────────────────────┐
│              Objectives of research           │
└─────────────────────────────────────────────┘
                      ⇩
┌─────────────────────────────────────────────┐
│      ATIG Welding and their evaluation criteria│
└─────────────────────────────────────────────┘
                      ⇩
┌─────────────────────────────────────────────┐
│   Details of Taguchi experimental design technique│
└─────────────────────────────────────────────┘
                      ⇩
┌─────────────────────────────────────────────┐
│              Data analysis procedure          │
└─────────────────────────────────────────────┘
                      ⇩
┌─────────────────────────────────────────────┐
│  Experimental investigation showing effect of various│
│        parameters on weld penetration         │
└─────────────────────────────────────────────┘
                      ⇩
┌─────────────────────────────────────────────┐
│   Result, discussion, future scope and applications│
└─────────────────────────────────────────────┘
```

Figure : Methodology

V. SYSTEM DEVELOPMENT

For studying the effects of Welding Process parameters on the weld penetration in the TIG welding heat source is most commonly required. Heat source produces the electric arc which generates the heat for melting the metals and to form the weld for particular purpose which is to be continuous supplied either by direct current or by the alternating electric current. This TIG welding machine has fallowing technical specifications,

1. Input power   18.4 KVA
2. Current range   20A-400 A
3. Duty cycle   60%
4. Weight   43 Kg
5. Input supply   380-440 V
6. Efficiency at full load   89%
7. Power factor   0.95
8. Ambient Temperature   40 degree C

Machine Tool Features:
1. Advanced soft switching inverter Technology and high efficiency.
2. Digital display of current and precise present function.
3. High power factor.

Page 131

4. High Switching frequency, hence low volume and weight.
5. 2/4 Track functions in TIG.
6. Adjustable Down slope function in TIG.
7. Can be used with extended welding cable in MMA.
8. Basic outfits Power source, Remote socket for Torch trigger.
9. Optional TIG welding, Argon regulator, water circulating system, wired remote controller.

AISI304 Steel materials plates are used, having large scale application in process industry. Sample of 100mm×70mm×5mm size has been used as a work piece material and bead on welding is done for present experiments. The SS304 sheet was changed into the desired work pieces sizes by shearing operation application. After shearing the work pieces are straighten by holding them in a press. The burr from the cut edges of the work pieces is removed by manual filing.

Activated flux can increase the joint penetration, mainly because the surfactant (surface-active element) in the molten pool switches the surface tension gradient, and consequently reverses the Marangoni convection pattern, resulting in a deep-penetration weld. To clear this concept, the following studies are used for flux powder.

The SS304 sheet is converted in to the desired 100mm×70mm×5mm size by using shearing operation. After shearing the work pieces are straighten by holding them in a press. The burr from the cut edges of the work pieces is removed by manual filing the plate surface was ground using 400 grit (silicon carbide) flexible abrasive paper to remove the impurities, and then clean the surface with acetone . The different types of flux powders were mixed with acetone for obtaining paint-like consistency. A brush to apply the mixture over joints of the surface to be welded. The coating density of flux powder application was 4.3 mg/cm2.

Table: List of Specimen Plate for Welding

Sr.No	1	2	3	4	5	6
Sample	TiO2 Coated	Cr2O3 Coated	Al2O3 Coated	Uncoated	CaO Coated	SiO2 Coated
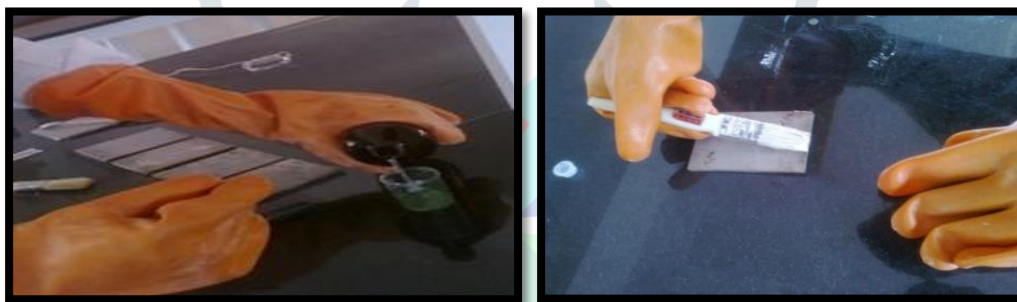
Figure : Preparations and Application of Activated Flux Powder

Figure : Activated Flux Powder Coated Sample

The primary goals of designed experiments are to:
- Determine the variables and there magnitude that influences the response.
- Determine levels of these variables.
- Determine how to manipulate these variables to control the response.

Experimental design is used to
i) Improve process by increasing its performance and eliminate troubles.

    ii) Establish statistical control of a process variable that is to identify the variables to control the process.

    iii) Improve the existing product or develop a new product.

Page 132

Guidelines for designing of an experiment are :
- Recognition and statement of the problem
- Selection of the response of the problem
- Choice of the factors, levels and ranges
- Performing the experiments
- Statistical analysis of the data
- Conclusions and recommendations

Generally, the steps 2 & 3 are usually performed simultaneously, or in the reverse step.

Requirements for Experimentation,
- Materials – stainless steel
  Shearing saw
- Chemical – HCL,H2SO4,Aceton
- Activated flux powder
- Metallurgical Microscope with photographs attachment
- Optical emission Spectrometer for chemical analysis
- Digital weight m/c, Vernier calliper, micrometer and height gauge.
- Stopwatch
- Stirrer and beakers
- Rubber gloves, goggles, plastic bags, jars, plastic trays
- ATIG Welding machine.

Table: List of Fixed Process Parameters

Sr. No.	Fixed Parameters	Level at which it is fixed
1	Welding current (A)	200
2	Gas flow rate(LPM)	15
3	Welding speed (second)	60
4	Torch angle	60 degree
5	Nozzle tip to work piece distance	3 mm
6	Work Piece size	100 mm × 70 mm × 5mm

Table: Preliminary Test Results of Various Activated Flux Powder

Activated Flux Powder	Weld penetration(mm)
Uncoated	2.0
Cr2O3 Coated	4.10
TiO2 Coated	2.70
Al2O3 Coated	2.20
CaO Coated	2.50
SiO2 Coated	3.00

Table: Effect of Welding Current on Weld Penetration

Sr.No	Welding current(A)	Weld penetration in mm
1	150	2.5
2	200	3.1
3	250	4.1
4	300	5.0

IQAC COORDINATOR
SWAMI VIVEKANAND
COLLEGE OF ENGINEERING
KHANDWA ROAD, INDORE

PRINCIPAL
SWAMI VIVEKANAND
COLLEGE OF ENGINEERING
KHANDWA ROAD, INDORE
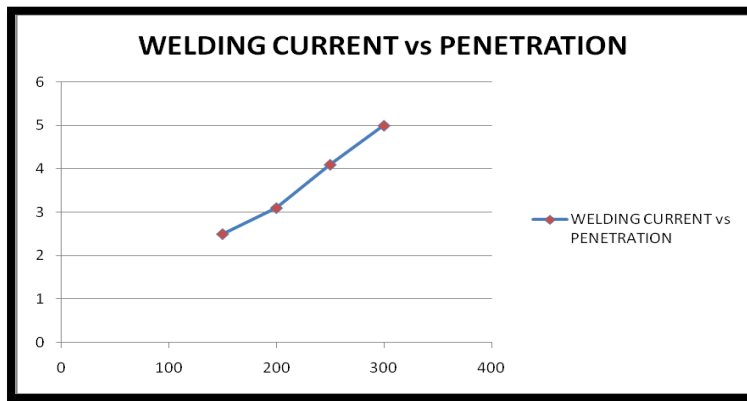
Figure: Graph Effect of Welding Current on Weld Penetration

Table: Effect of Welding Current on Weld Penetration

Sr.No	Gas flow rate(LPM)	Weld penetration in mm
1	5	3
2	10	3.5
3	15	5.0
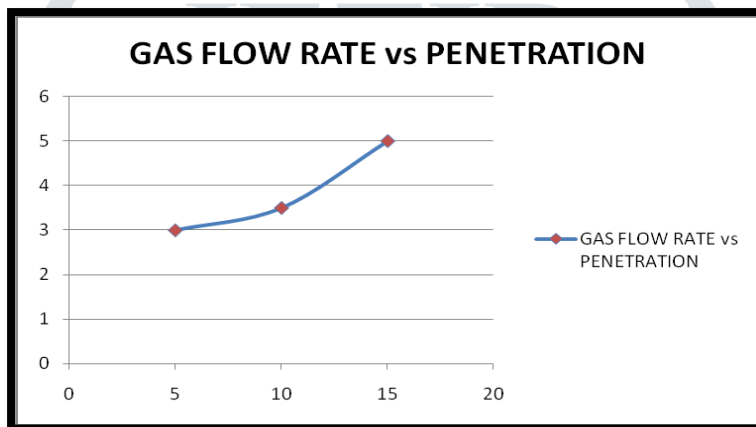
Figure: Graph Effect of Welding Gas Flow Rate on Weld Penetration

Table 5.9: Effect of Welding Speed on Weld Penetration

Sr. No	Welding speed	Weld penetration in mm
1	6.66	3
2	3.33	3.5
3	1.66	5.0
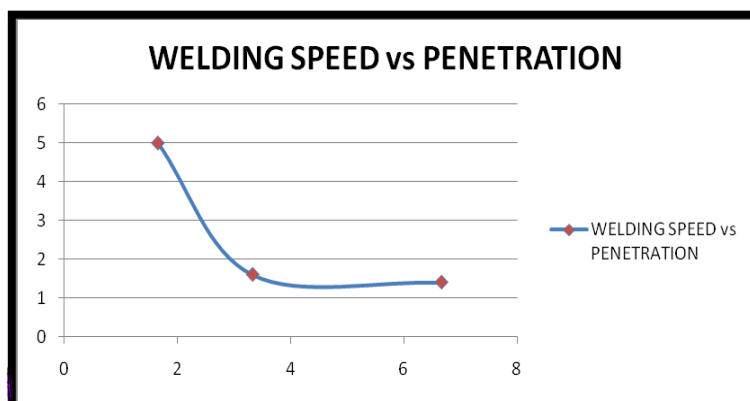
Figure: Graph Effect of Welding speed on Weld Penetration

IQAC COORDINATOR
SWAMI VIVEKANAND
COLLEGE OF ENGINEERING
KHANDWA ROAD, INDORE

PRINCIPAL
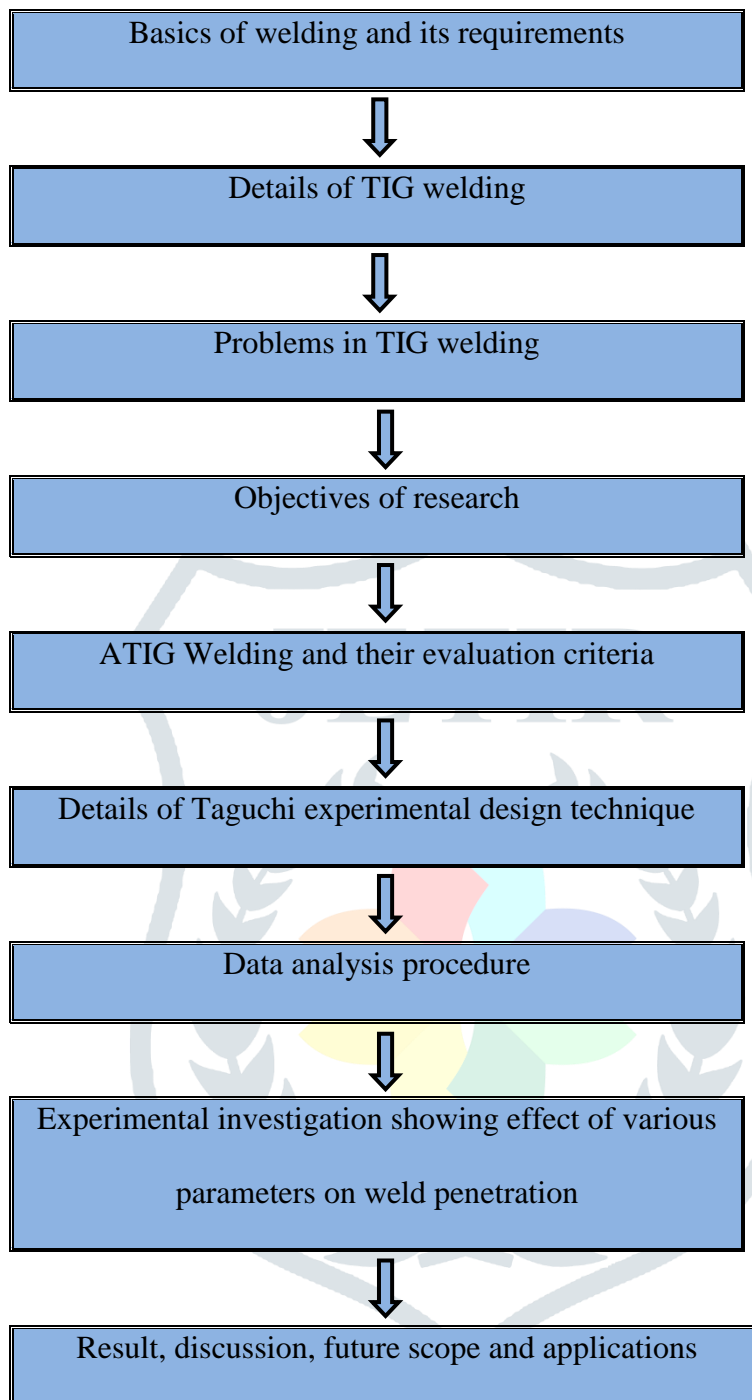SWAMI VIVEKANAND
COLLEGE OF ENGINEERING
KHANDWA ROAD, INDORE

Page 134

Table: Effect of Torch Angle on Weld Penetration

Sr.No.	Torch Angle in degree	Weld penetration in mm
1	60	5
2	75	3
3	90	1.6
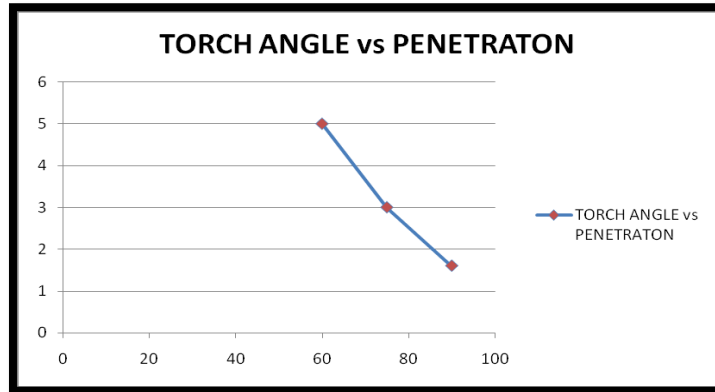
Figure: Graph Effect of Torch angle on Weld Penetration

VI. PERFORMANCE ANALYSIS
Design of Experiments
I) Purpose of Experimentation

The purpose of the product or the process development is to improve the performance characteristics of the product or the process relative to the customer needs and the expectations. The purpose of experimentation should be to understand how to reduce and control variation of a product or process; subsequently, decision must be made concerning which parameters affect the performance of a product or process. The loss function quantifies the need to understand which design factors influence the average and variation of a performance characteristic of a product or process. By properly adjusting the average and reducing variation, the product or process losses can be minimized.

II) Basis of Experimentation
This approach is based on the use of orthogonal array (Taguchi) to conduct small, highly fractional factorial experiments up to larger, full factorial experiments. The orthogonal array is basically used to design an experiment, but it's the most flexible in accommodating a variety of situations and also is easier for statistically oriented people to execute on the normal practical basis.

III) Definition of Design of Experiment
The designed experiment is continuous result of the two or the more factors (parameters) for their ability to affect the resultant average or variability of particular product or process characteristics. To get this in an very effective and statistically exact manner, the levels of the factors are managed in a proper manner, the results of this particular test combination is observed to be, and the complete set of results is analyzed to determine the influential factors and preferred levels, and whether increases or decreases of those levels will potentially lead to further improvement. It is important to note that this is an iterative process; the first round through the DOE process will many times lead to subsequent round of experimentation.
The DOE process is divided into three main phases which encompass all experimentation approaches. The three phases are:
1. Planning Phase
2. The conducting phase
3. The analysis phase
Steps in Experimental Design and Analysis
I)   Selection of orthogonal array (OA)
II)   Assignment of parameters and interaction to the OA
III)   Selection of outer array
IV)   Experimentation and data collection
V)   Data analysis
VI)   Parameter design strategy

IQAC COORDINATOR
SWAMI VIVEKANAND
COLLEGE OF ENGINEERING
KHANDWA ROAD, INDORE

PRINCIPAL
SWAMI VIVEKANAND
COLLEGE OF ENGINEERING
KHANDWA ROAD, INDORE

Page 135

Sr. no.	Welding Current(Amp)	Gas flow rate(LPM)	Welding speed(mm/s)	Weld Penetration(mm)
1	150	10	6.66	1.6
2	150	12.5	3.33	2.5
3	150	15	1.66	2.7
4	175	10	3.33	3.0
5	175	12.5	1.66	5.0
6	175	15	6.66	3.0
7	200	10	1.66	2.5
8	200	12.5	6.66	2.5
9	200	15	3.33	2.0

VII. CONCLUSION

The best result for welding penetration by the Taguchi Method is given as below;

According to Taguchi methods, an attempt is made to determine set of values of process variable at their selected levels.

Predicted optimum value of the welding penetration 4.89 mm but the actual value for the welding penetration is 5.00 mm at the conditions of confidence interval as shown in table where conclusions are according to the Taguchi method.

Table 7.1: Predicted Value Vs Actual Value of Welding Penetration

Response	Predicted Value	Actual Value
The welding Penetration Set for the optimum value of the process parameters are as below, 1. Welding Current 175 Amp 2. Gas flow rate 12.5 LPM 3. Welding Speed 1.66 mm/sec	4.89 mm	5.0 mm

Adding advantage to welding Penetration is that one additional test is performed which analyze the tensile strength. The standard value of tensile strength for 5mm AISI304 Plate is in the range of 540 to 750 N/mm2 and when the Specimen is welded with Cr2O3 Coating. Optimum Parameter in addition of full Weld Penetration the tensile strength obtained to be 707 N/mm2 which is supposed to be within the Standard range of Tensile strength.

VIII. APPLICATIONS

The major constraints of the TIG welding for the austenitic stainless steels are because of the limited thickness of the material which can be welded in a single pass, the poor tolerance to cast variations and the low productivity. The thickness of austenitic stainless steel that has to be welded in single pass is normally limited to 3 mm with argon as the shielding gas. Therefore, improvements in weld penetration have long been sought in austenitic stainless steel welds produced by TIG welding process because TIG welding result in high quality welds besides providing for exact control of the heat input and the low cost of the equipment. A novel variant of the TIG welding process called A-TIG is known to overcome the limitations. This process includes applying a thin coating of the activated flux on the joint before welding. The Cr2O3 activated flux has been used in the present work for enhancing the penetration during autogenously TIG welding of type 304LN steels. The use of activated flux produced a significant increase in penetration of 5.0 mm in single pass TIG welding of 304LN as compared to 1.2mm penetration of uncoated 304LN Steel plate.

IX. FUTURE SCOPE

A Penetration Enhancing Activating Flux (PEAF) in paste form for autogenously TIG welding of austenitic stainless steels adapted for ready application with a brush on top weld surface prior to conducting autogenously TIG welding to favor single weld pass, of austenitic stainless steels of AISI 304LN and AISI 316LN varieties with weld bead penetration up to a section thickness of 12 mm. Importantly, the (PEAF) paste based TIG welding of the invention achieves an increase in weld bead penetration of about 300% over the conventional TIG process without activating flux. The PEAF paste based TIG welding also favors higher productivity and high quality apart from being cost-effective due to fewer requirements of consumables and controlled heat input to arrest deformation, making it extensively acceptable for the variety of industrial applications for welding of the austenitic stainless steel.

X. REFRENCES

[1] Uger Esme, "Effect of Bead Geometry on the Quality of TIG Welded Joints", PhD Thesis.

[2] N.B. Mostafa , M.N. Khajavi, "Optimisation of welding parameters for weld penetration in FCAW", journal of Achievements in Materials volume 16 issue 1-2,may-june 2006.

Page 136

[3]   ASME International Handbook Committee, Metals Handbook, J.R Davis, Second Edition, 1998.

[4]   Reference Book Introduction to Welding

[5]   Kuang-Hung Tseng* and Kuan-Lung Chen, "Comparisons Between TiO2- and SiO2-Flux Assisted TIG Welding Processes", Journal of Nanoscience and Nanotechnology Vol. 12,2012,pp.6359–6367

[6]   Hsuan-Liang Lin & Tong-Min Wu , "Effects of Activating Flux on Weld Bead Geometry of Inconel 718 Alloy TIG Welds", Materials and Manufacturing Processes, 2712, 1457-1461,2012

[7]   M Tanaka, "Effects of Surface Active Elements on Weld Pool Formation Using TIG Arcs", Welding International, 1911, 870-876,2005

[8]   H Hirata & K Ogawa, "Effect of Aluminium Content on Penetration Shape of Stainless Steel in TIG arc Welding. Effect of Chemical Composition on Weldability in Fabrication of High-Alloyed Steel" (3rd report), Welding

[9]   R.-I.Hsieh, Y.-T.Pan, and H.-Y.Liou "The Study of Minor Elements and Shielding Gas on Penetration in TIG Welding of Type 304 Stainless Steel" ASM International JMEPEG 868-74 1999

[10] A. K. Pandey, m. I. Khan, k. M. Moeed, "Optimization of Resistance Spot Welding Parameters Using Taguchi Method", International Journal of Engineering Science and Technology,Vol. 5 No.02 February 2013,pp.234-241

[11] Uğur Eşme, "Application of Taguchi Method For The Optimization of Resistance Spot Welding"

[12] S.V.Sapakal[1], M.T.Telsang[2], "Parametric Optimization of Mig Welding Using Taguchi Design Method", Ijaers Vol. I Issue IVJuly-Sept., 201228-30

[13] S. P. Tewari et. al., "Effect of Welding Parameters On The Weldability of Material", International Journal of Engineering Science and Technology.

[14] R Sudhakarana, V Vel-Muruganb and PS Sivasakthivelc, "Effect of Process Parameters on Depth of Penetration in Gas Tungsten Arc Welded (GTAW) 202 Grade Stainless"

[15] Ugur Esme1, "Optimization of Weld Bead Geometry In Tig Welding Process Using Grey Relation Analysis And Taguchi Method", Materials and technology, MTAEC9, 43(3)143(2009)

[16] S. P. Gadewar et.al, "Experimental Investigation of Weld Characteristic for a Single Pass TIG Welding with ss304", International Journal of Engineering Science and Technology. Vol. 2(8), 2010, pp.3676-3686.

[17] Kuang-Hung Tseng1,Wei-Chuan Wang1,"Study of Silica-Titania Mixed Flux Assisted TIG Welding Process", Advanced Materials Research Vols. 291-294 2011 pp 949-953

[18] H. Y. Huang, S. W. Shyu2, K. H. Tseng3 and C. P. Chou4,Science and Technology of Welding and Joining,VOL 10 NO 5 573,2005

[19] Chunlin Dong,Y Fegzhu, "Preliminary study on the Mechansim of Arc Welding with the activating flux", Joining and welding research,vol.1,2004,pp.271-278

[20] G.Taguchi, Y.wu, "Off-line Quality Control", Central Japan Quality control association, Nagaya ,Japan,1979.

[21] D.C. Montgomery, "Probability and Statistics in Engg and management science",3rd edition, Willey Publication,1990.

[22] Influence of Gas Mixtures in GMAW of Modified 409M Ferritic Stainless Steel. Details are given on the effects shielding gas mixtures have on bead geometry, microstructure, and mechanical properties. By M. Mukherjee et al. Published 04/2015.

IQAC COORDINATOR
SWAMI VIVEKANAND
COLLEGE OF ENGINEERING
KHANDWA ROAD, INDORE

PRINCIPAL
SWAMI VIVEKANAND
COLLEGE OF ENGINEERING
KHANDWA ROAD, INDORE

Design and Analysis of Crane hook with different cross section and materials by Computational and Analytical method

[1]Mukesh Sonava, [2]Vishal Wankhade
[1]P.G. Scholar [2]Assistant Professor
[1,2]Swami Vivekanand College of Engineering, Indore.

Abstract : Modern technological period can't be imagined without several material handling equipment. Crane Hooks are highly liable components that are typically used for hold material in industries. Crane hook is the curved bar used for lifting loads in cranes. In order to reduce structure failure of crane hook, induced stress in crane hook is analysed properly. Stress analysis is considered an important factor in the design of structures like crane hook under its loading condition. In present work Crane hook is designed as per ISO 7597:2013 standard in Creo-parametric 4.0 by taking different cross-section area (Rectangular, Circular, Trapezoidal and T-Section) after that the designed hook is import in Hypermesh for analysis by taking four different types of materials (Structural steel, Aluminium Alloy, AISI 1040, ASTM Grade 60 steel) and applying three different loads (2KN, 5KN and 10KN). The outcome of the analysis presented that the Trapezoidal cross-section hook with ASTM Grade 60 material is found to be the best suitable hook from the above all arrangement of cross-section, loads and materials. After analytical verification the analysis concluded that there is only 0.334% dissimilarity between resultant stresses in analytical result and the Hypermesh result.

IndexTerms - **Creo4.0, Hypermesh, Trapezoidal, Circular, T-Section, Rectangular, FOS, material.**

I. INTRODUCTION

Crane Hooks are most responsible components that are used for industrial purposes. It is generally a hoisting fixture designed to engage a ring or link of a lifting chain or the pin of a shackle or cable socket and it must follow both health and safety guidelines. It is used to lift heavy loads in industries like marine industry, transportation etc. it is mainly used for lifting heavy loads and transporting them to other places. It uses one or more simple machines to create mechanical advantage and moves the load beyond the normal capability of a human. The following information helps us to select the crane hook: Capacity (tonnage). Material (carbon, alloy or bronze).Shank diameter, Shank length, Throat opening.

The FEM is one of numerical method for solving problems which are defined by partial differential equations or can be formulated as functional minimization. The present work is carried out by using HyperMesh. HyperMesh is Universal finite element pre- and postprocessor. HyperMesh is at the top as in the performance of finite element pre-processor and post-processor for major finite element solvers, which permits engineers to analyse design situations in a highly interactive and visual environment. HyperMesh's user-interface learning is easy and provision of the direct use of CAD geometry and current finite element models, providing strong interoperability and efficiency. An innovative automation tool in HyperMesh allows its users to improve meshes from a set of quality criteria, alter current meshes through morphing, and create mid-surfaces from models of variable thickness.

The present research of crane hook is according to ISO 7597:2013 standard. Firstly, the computational method is used for analysis of designed hook and then the optimized result is validated by analytical method.

II. THEORETICAL FRAMEWORK

Crane hook is designed as per ISO 7597:2013 standard in Creo parametric 4.0 by taking different cross-section (Rectangular, Circular, Trapezoidal and T-Section) after that the designed hook is import in Hypermesh for analysis by taking four different materials (Structural steel, Aluminum Alloy, AISI 1040, ASTM Grade 60 steel). The hook is analysed by applying three different loads (2KN, 5KN and 10KN). The stresses, displacement and factor of safety of the all combination is find out.

The further stage of analysis we take the trapezoidal cross-section hook for verifying the analysis by Analytical method and the variation between resultant stresses in analytical result and the HyperMesh result is tabulated. In further stage of the research we find out the fatigue life of the optimized hook and the result will be concluded as the result of the research. The hook design as per standard are show below in **Fig.1**

Page 138
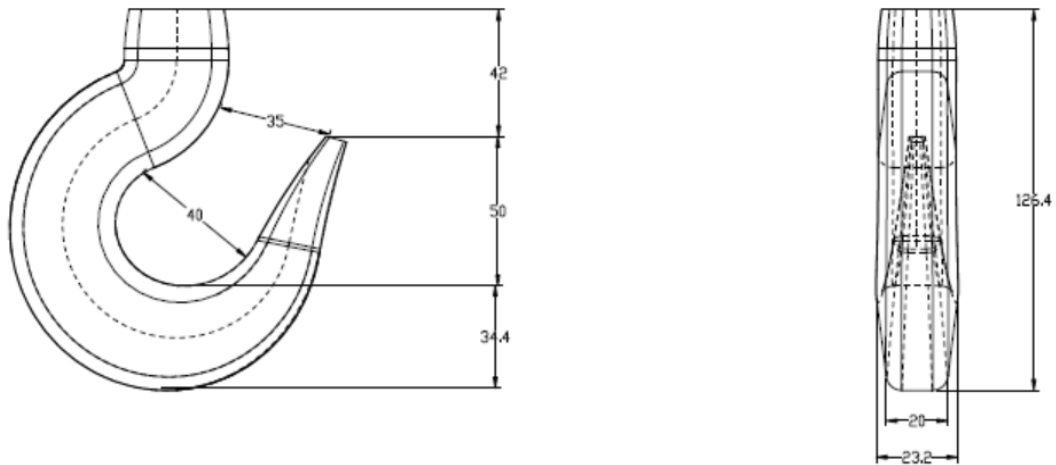
Fig.1 2D view of crane hook with Trapezoidal cross-section

III. COMPUTATIONAL MODELLING

3.1 Design of Hook in Creo

Design the hook with four different cross-sections namely Circular, Rectangular, Trapezoidal and T-Section in Creo 4.0 and import the design in Hypermesh for further analysis

[a]   [b]

Fig.2 Design of hook with [a] Circular and [b] Rectangular cross-section

[c]   [d]

Fig.3 Design of hook with [c] Trapezoidal and [d] T-section cross-section

Page 139

3.2 Meshing of hook

The design of crane hook by taking different cross-section and the dimensions of hook as per standard and when we import the design in Hypermesh the **Fig.4** shows the meshing of hook in Hypermesh. Following are the meshing details of trapezoidal and T-section. Rectangular and circular section has also same meshing

Element Type: Hex
Element Size: 3mm

[e]   [f]
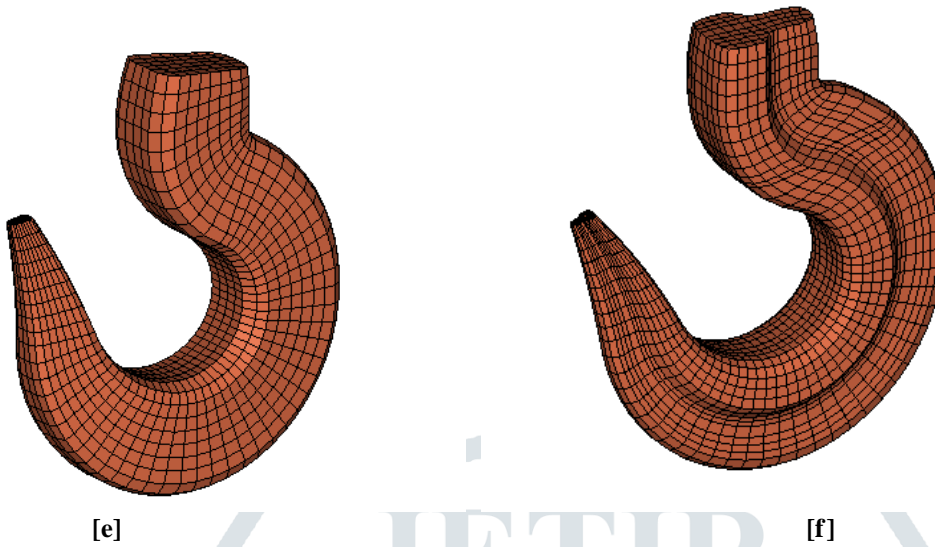
Fig.4 Meshed model with [e] Trapezoidal and [f] T-section in Hypermesh

3.3 Hypermesh analysis and Results

We performed test on different cross-section of crane hook for different loads and materials

Pre Processor   : Hypermesh
Solver   : Optistruct
Result Viewed   : Hyper View
Types of Analysis Performed   : Displacement and Von Mises Stresses
Force Applied   : 2KN, 5KN, 10KN
Materials   : Structural Steel, Aluminum Alloy, AISI 1040, ASTM grade 60
Cross-section   : Circular, Rectangular, Trapezoidal, T-Section

Following are some analysis result obtained by Hypermesh Analysis.

[g]   [h]
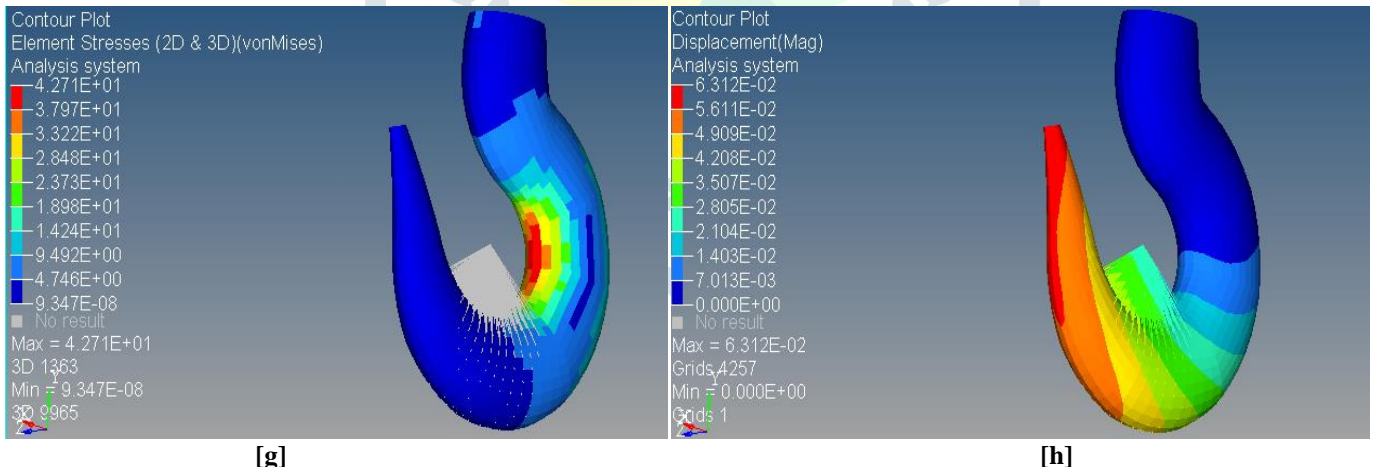
Fig.5 Hypermesh analysis shows[g] Vonmises stresses and [h]displacement in Circular cross-section with ASTM grade 60 material and 2KN load

Page 140

[i]   **[j]**
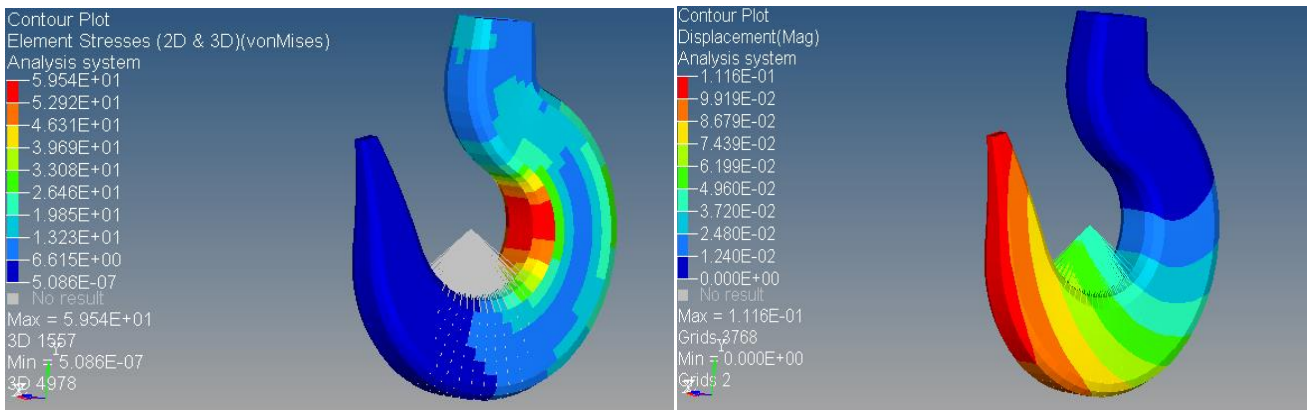
Fig.6 Hypermesh analysis shows[i] Vonmises stresses and [j]displacement in Rectangular cross-section with ASTM grade 60 material and 5KN load

[k]   **[l]**
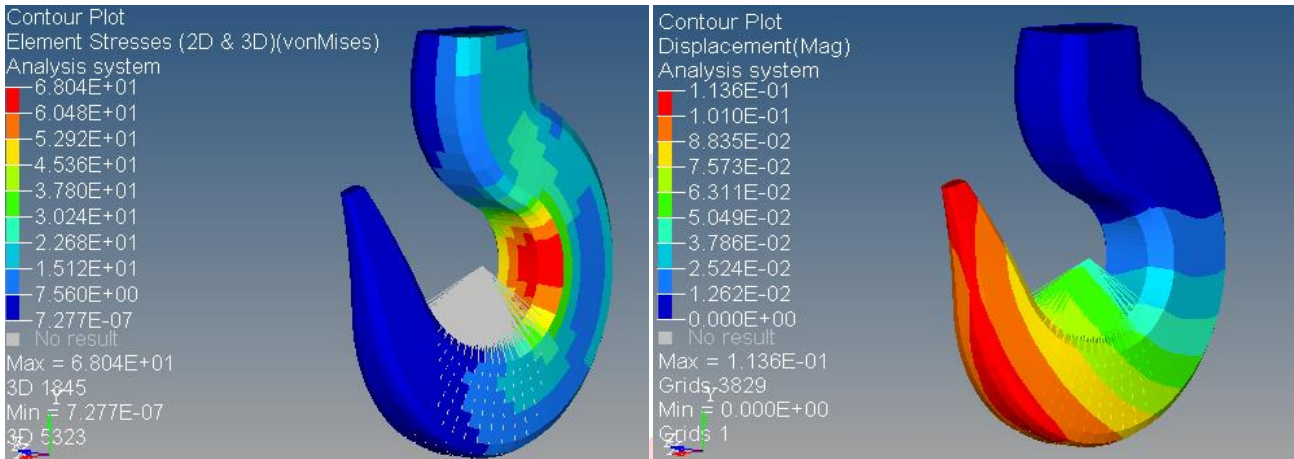
Fig.7 Hypermesh analysis shows[k] Vonmises stresses and [l]displacement in Trapezoidal cross-section with ASTM grade 60 material and 5KN load

[m]   **[n]**
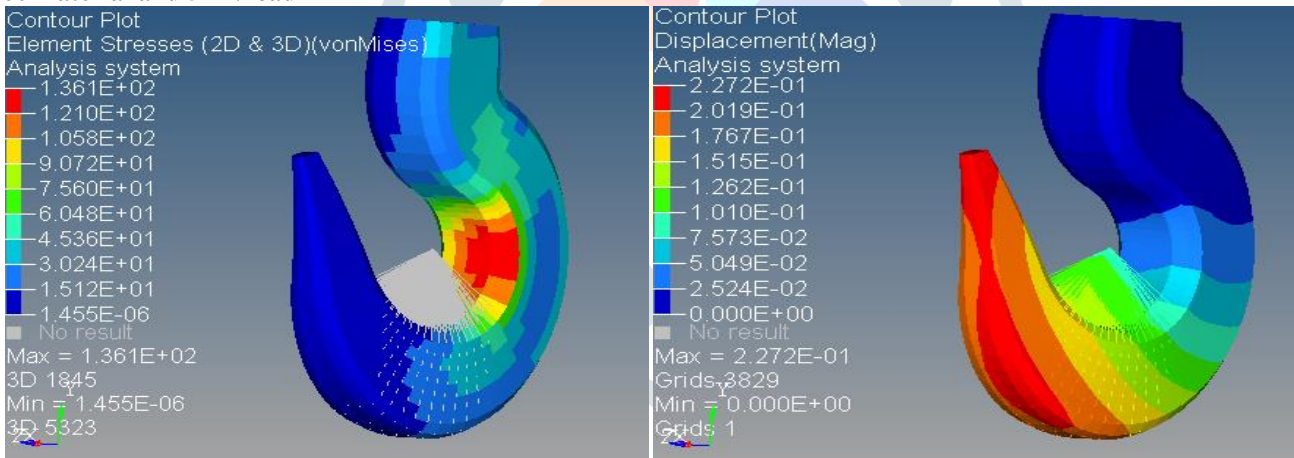
Fig.8 Hypermesh analysis shows[k] Vonmises stresses and [l]displacement in Trapezoidal cross-section with ASTM grade 60 materials and 5KN load

IV. ANALYTICAL ANALYSIS

Bending of Curve beam formula for finding the maximum bending stress at inside fibre

$$\sigma_{bi} = \frac{M \, y_i}{A.e.R_i}$$

Where,

M is bending moment acting at the given section about the centroidal axis

y_i is the distance from the neutral axis to the inside fibre

A is the area of cross-section

e is the distance from the centroidal axis to the neutral axis = $R-R_n$

R_i is the radius of curvature of the inside fibre

R_i =20 mm

R_o =54.4mm

IQAC COORDINATOR
SWAMI VIVEKANAND
COLLEGE OF ENGINEERING
KHANDWA ROAD, INDORE

PRINCIPAL
SWAMI VIVEKANAND
COLLEGE OF ENGINEERING
KHANDWA ROAD, INDORE

Page 141
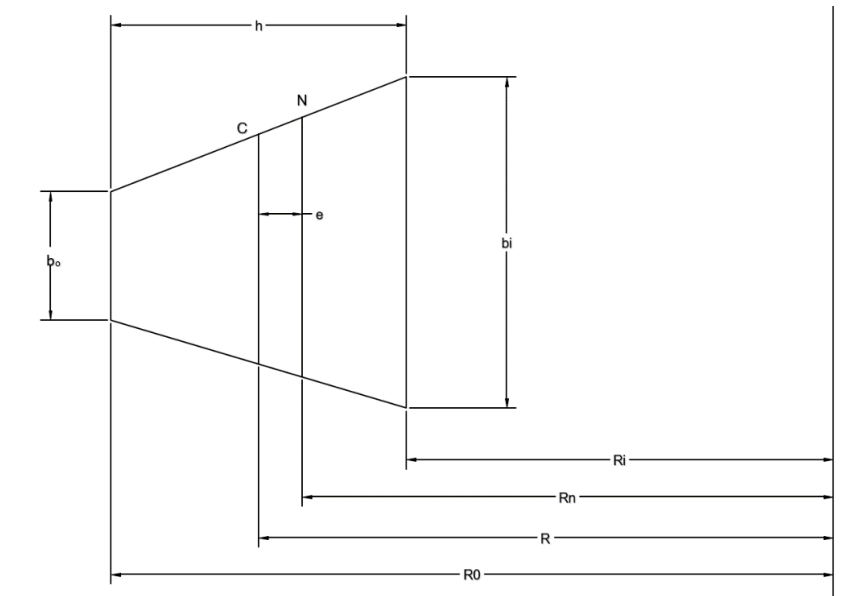
Fig.9 Trapezoidal Cross-section geometric relations

The Formula for finding the Radius of curvature of the neutral axis is given as

$$R_n = \frac{\frac{(b_i+b_o)h}{2}}{\left(\frac{b_iR_o-b_oR_i}{h}\right)\log_e\left(\frac{R_o}{R_i}\right)-(b_i-b_o)} = 33.9655 \text{ mm}$$

The Formula for finding Radius of curvature of centroidal axis is given as

$$R = R_i + \frac{h(b_i+2b_o)}{3(b_i+b_o)} = 36.7753 \text{ mm}$$

Formula for finding the Distance between the load and the centroidal axis

$$x = R = 36.7753 \text{ mm}$$

Formula for finding the Area of Trapezoidal section

$$A = \frac{1}{2}(b_i+b_o)h = 743.04 \text{ mm}^2$$

Formula for finding the distance from the neutral axis to the inside fibre

$$y_i = R_n - R_i = 13.9655 \text{ mm}$$

Formula for finding the distance from the neutral axis to the inside fibre

$$y_o = R_o - R_n = 20.2345 \text{ mm}$$

Formula for finding the distance between the centroidal axis and neutral axis

$$e = R - R_n = 2.80977 \text{ mm}$$

We will find out the stresses for different load by putting load values as 2KN, 5KN and 10KN .Here we discuss 10KN load

4.1 Finding stress for 10KN load

Direct tensile load W= 10000 N

The direct tensile stress is given by

$$\sigma_t = \frac{W}{A} = 13.45822$$

Bending moment about the centroidal axis

$$M = W \times x = 367753 \text{ N-mm}$$

Maximum bending stress at the inside fibre

$$\sigma_{bi} = \frac{M\,y_i}{A.e.R_i} = 122.998 \text{ N/mm}^2$$

Maximum bending stress at outside fibre

$$\sigma_{bo} = \frac{M\,y_o}{A.e.R_o} = 65.5188 \text{ N/mm}^2$$

The Resultant stress at the inside fibre

$$\sigma = \sigma_t + \sigma_{bi} = 13.45822 + 122.998 = 136.45622 \text{ N/mm}^2 \text{(Tensile)}$$

The Resultant stress at the outside fibre

$$\sigma = \sigma_t + \sigma_{bo} = 13.45822 - 122.998 = -109.53978 \text{N/mm}^2 \text{ (Compressive)}$$

4.2 Analytical Result

The maximum stress for 2KN, 5KN and 10KN load for trapezoidal section are as follow

Table 4.1: Show analytical stress Results

S.No.	Load	Maximum Stress
1	2 KN	27.2912 N/mm^2
2	5 KN	68.228 N/mm^2
3	10 KN	136.45622 N/mm^2

V. **DISCUSSION AND CONCLUSION**

The main results of the tests and studies carried out can be summarized as follows:

The crane hook with Trapezoidal cross-section is found to be best optimized cross-section in comparison with all other cross-section (Rectangular, Circular and T-section).

The ASTM grade 60 steel is found to be best material in comparison with all other materials (Structural steel, Aluminum Alloy, AISI 1040)

The crane hook with trapezoidal cross-section and ASTM grade 60 steel material is found to be best suited for all combination and the design in tested in different load 2KN. 5KN and 10KN and it can bear all the loads and the stress induced is less than the permissible values. The designed hook has factor of safety 3 when loaded on 10KN.

The Analytical method is applied for the verification of computational method and the comparison of stresses of the both methods are tabulated below

Table 5.1: Show Comparative results between Analytical method and Computational method

S.No.	Load	Analytical Result Maximum Stress	Computational Stresses	Percentage deviation of results
1	2 KN	27.2912 N/mm^2	27.22 N/ mm^2	0.3%
2	5 KN	68.228 N/mm^2	68 N/ mm^2	0.3%
3	10 KN	136.45622 N/mm^2	136 N/ mm^2	0.3%

REFERENCES

[1] M. CunetyFetvaci, Ismail Gerdemeli, A.BurakErdil. 2006 .Finite element modeling and static stress analysis of simple crane hooks. Trends in the development of machinery and associated technology10, 797-800.

[2] A. Sloboda; P. Honarmandi.2007. Generalized Elasticity Method for Curved Beam Stress Analysis: Analytical and Numerical Comparisons for a Lifting Hook Mechanics Based Design of Structures and Machines

[3] Y. Torres, J.M. Gallardo, J. Dominguez, F.J. Jimenez E.2008. Brittle fracture of crane hook.2008.J-GATE Engineering journals

[4] Jiancheng Liu, PhD, Ashland O Brown.2008. Enhancing Machine Design Course through Introducing Design and Analysis Projects American Society for Engineering Education.

[5] C. OktayAzeloglu, Onur Alpay.2009. Investigation Stress of a Lifting Hook with Different Methods, Verification of The Stress Distribution with Photo Elasticity Experiments Electronic Journal of Machine Technologies, Vol. 6, No: 4, (71-79).

[6] Yu Huali, H.L. and Huang Xieqing.2009. Structural- strength of Hook Ultimate load by Finite Element Method international multi conference of engineers and computer scientists (IMECS), HONKONG.

[7] ApichitManee-ngam*, PenyaratSaisirirat, PatpimolSuwankan.2017. Hook Design Loading by The Optimization Method With Weighted Factors Rating Method. International Conference on Alternative Energy in Developing Countries and Emerging Economies 2017 AEDCEE, 25-26 May 2017, Bangkok, Thailand ELSEVIER

IQAC COORDINATOR
SWAMI VIVEKANAND
COLLEGE OF ENGINEERING
KHANDWA ROAD, INDORF

PRINCIPAL
SWAMI VIVEKANAND
COLLEGE OF ENGINEERING
KHANDWA ROAD, INDORE

Page 143

REVIEW ARTICLE

UWB antenna and MIMO antennas with bandwidth, band-notched, and isolation properties for high-speed data rate wireless communication: A review

Rohit Yadav[1] | Leeladhar Malviya[2] (iD)

[1]Department of Electronics and Telecommunication, Swami Vivekanand College of Engineering, Indore, India

[2]Department of Electronics and Telecommunication, Shri G. S. Institute of Technology and Science, Indore, India

Correspondence
Leeladhar Malviya, Department of Electronics and Telecommunication, Shri G. S. Institute of Technology and Science, Indore, India.
Email: ldmalviya@gmail.com

Abstract

The prospective of ultrawide band (UWB) technology is enormous due to its remarkable advantages such as the capability of providing high-speed data rates at short transmission distances with low power dissipation. The swift growth in wireless communication systems has made UWB an exceptional technology to replace the conventional wireless technologies in today's use. UWB bandwidth (3.1-10.6 GHz) covers most of the communication applications. High frequency of operation with high level of miniaturization has enhanced the interest in designing high performance antennas. There is a growing demand for small and low cost UWB antennas that are able to provide satisfactory performance in both time and frequency domains. The trend in recent wireless systems, including UWB based systems, are to build small, low-profile integrated circuits so as to be compatible with portable wireless devices. Transformation of UWB in MIMO achieved high data rate and solved the problem of multipath propagation. The main reason for writing this review is to investigate various UWB methods and band rejection approaches on a single platform. Some of the isolation enhancement approaches are also included in article due to the requirement in MIMO antennas.

KEYWORDS
isolation, MIMO, notch, returnloss, UWB

1 | INTRODUCTION

The UWB technology provides the real wireless freedom with existing long-range radio technologies such as Wi-Fi, wireless local area network (WLAN), worldwide interoperability for microwave access (WiMAX), and other cellular wide area communications by replacing short-wired links. UWB offers the desirable cost-effective, power-efficient, high bandwidth solutions for transmitting multiple digital video and audio streams among the short-range devices. UWB is a new technology which has substantial development

potential in elementary areas like communication, automotive, localization services, security, imaging, and sensors. The growing number of media-intensive devices in the wireless personal area networks (WPANs) such as PCs, digital camcorders, digital cameras, high-definition TVs (HDTVs), gaming systems, office devices such as cordless connection to peripherals, notebook, printer, personnel digital assistant (PDA), fax machine, mouse, keyboard need a high bandwidth wireless solutions for easy connection and media exchange. UWB radio is predicted as one of the

most promising technologies for above-mentioned applications, due to its several advantages.

A lot of research has been done to develop UWB low noise amplifiers (LNAs), mixers and entire front-ends but not that much to develop UWB antennas. Recently, academic and industrial communities have realized the tradeoffs between antenna design and transceiver complexity. In general, the transceiver complexity has been increased, with the introduction of advanced wireless transmission techniques. In order to enhance the performance of transceiver without sacrificing its costly architecture, advanced antenna design should be used. Also, the complexity of the overall transceiver is reduced.

Some design issues are associated with the UWB antennas. First issue is to design an antenna with wide impedance bandwidth and with high radiation efficiency. Second is the size that affects the gain and bandwidth. Therefore, the size of the antenna is considered as one of the critical issues in UWB system design. Third is the transmitted power level of UWB signals, which is strictly limited in order for UWB devices to peacefully coexist with other wireless systems. Fourth issue is to achieve the desired performance at adequate transmission range using limited transmitted power. Fifth is to design UWB waveform that efficiently utilizes the bandwidth and power allowed by the Federal Communications Commission (FCC) spectral mask. Moreover, to ensure that the transmitted power level satisfies the spectral mask, adequate characterization and optimization of transmission techniques (eg, adaptive power control, duty cycle optimization) may be required.

The power consumption or the maximum power available to the antenna as a part of UWB system is of the order of 0.5 mW because of the spreading of the energy of the UWB signals over a large frequency band, according to the FCC spectral mask shown in Figure 1.

UWB can be recognized as impulse, carrier-free, baseband, time domain, nonsinusoidal, orthogonal function, and large-relative bandwidth radio signals. UWB antenna has

three-century long history (nineteenth century, twentieth century, twenty-one century) where broadband and UWB antennas originated in the starting period of radio in spark gap days with the idea of same frequency tuning at transmitter and receiver.[1-4]

The transmission and reception of signals were thought by some pioneered engineers, who showed the way to next generation wireless communication. Heinrich hertz designed parabolic cylinder, which was characterized as UWB.[5] Later, Lodge in year 1897,[6] Bose,[7] and Yagi-Uda in year 1926[8] tried their best to design antennas. An antenna system for the broadcast band was presented in 1936. This antenna was an improvement over broadband antennas, and was replaced by single vertical radiator.[9-11]

Levy designed a loop antenna,[12] and research was continued on omnidirectional antenna.[13,14] Grieg and Engelmann introduced microstrip antenna in year 1952.[15] The controlling of surface wave propagation on dielectric sheet was introduced by Fubini in year 1955.[16] The size requirement of transmitting and receiving antenna was comparatively small. Carver and Mink showed multiple solutions for rectangular and circular patch antennas.[17-19]

Specially, designers tried to develop small antennas for portable communication systems such as antennas for portable telephones,[20] direct broadcast from satellite,[21] and dual-band planar inverted F-antenna (DB-PIFA) for hand held portable telephones.[22-28] According to Howell "Microstrip antennas consist of a planar resonant radiating element parallel to, but separated, from a ground plane by a thin dielectric substrate," resonant frequency for the rectangular or square and circular antennas is given by Equations (1) and (2), respectively.[29]

$$f_{rr} = \frac{c}{2d(\varepsilon_r)^{1/2}} \tag{1}$$

$$f_{rc} = \frac{1.841c}{2\pi a(\varepsilon_r)^{1/2}} \tag{2}$$

where c is the velocity of light, d is the distance from the feed point to the opposite side, and a is the radius of antenna element, ε_r is the dielectric constant.

In this communication era, technology can provide us with many wide services such as fast internet access, video telephony, and enhanced video/music downloads, as well as digital voice services. For such services, high data rate is required.[30] UWB technology is a promising technology with wide bandwidth, high data rate wireless transmission, high capacity, and low power consumption. After the allocation of unlicensed frequency band of 3.1 to 10.6 GHz by FCC in 2002, UWB technology got hike in interest.[31]
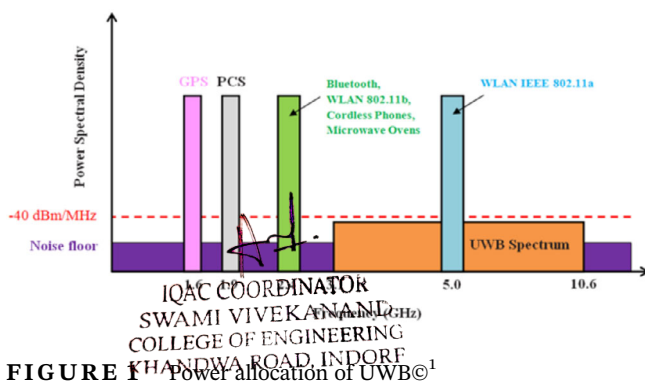
FIGURE 1 Power allocation of UWB©[1]

UWB technology is not efficient to face fading issues alone.[32] To enhance spectral efficiency and link reliability, multiple-input-multiple-output (MIMO) is used.[33] Most of the researchers have combined the features of both the technologies and introduced UWB-MIMO antenna for improving the performance of communication system. These communication systems have restriction of size, so it is a challenge to implement UWB-MIMO Antenna system. Due to restriction of size, MIMO antenna is implemented in smaller area, which leads to the problem of mutual coupling, and improved isolation is necessary to overcome multipath fading. The compact and portable devices are in demand for the wireless applications such as WLAN/WiMAX and long term evolution (LTE), etc.[34]

Figure 2 shows the flow chart of development of study on requirement of various UWB antennas and notch band characteristics.

2 | UWB AND UWB MIMO ANTENNAS FOR BANDWIDTH ENHANCEMENT

In this section, various designs of UWB and UWB MIMO antennas are discussed for bandwidth enhancement.

2.1 | UWB antennas for bandwidth enhancement

On FR-4 epoxy dielectric substrate (relative permittivity of 4.4, and loss tangent $\tan \delta = 0.025$) with an overall size of $19 \times 21 \times 1.6$ mm^3, a UWB antenna with time domain analysis was carried out to measure the pulse handling capability and fidelity factors. FR-4 dielectric substrate is a cheap, easily available, and mostly used material in antenna designs. FR-4 has easy transmission and reception capabilities. In this design, fidelity factor was measured, which is known as the degree of similarity or correlation between the transmitted and received pulses. The gain in the design varied from 0.84 to 1.76 dBi, and efficiency varied from 84% to 95%. The design is shown in Figure 3. Fidelity factor can be obtained using the following Equation (3).[35]

$$F = \max \left| \frac{\int_{-\infty}^{\infty} s_t(t) s_r(t+\tau) dt}{\sqrt{\left(\int_{-\infty}^{\infty} s_t(t)^2 dt\right)\left(\int_{-\infty}^{\infty} s_r(t)^2 dt\right)}} \right| \tag{3}$$

where $s_t(t)$ and $s_r(t)$ are transmitted and received signals, and τ is the delay.

A coplanar waveguide-fed H-tree fractal antenna was designed to cover WLAN, WIMAX, RFID, C-band, HiperLAN, and UWB applications. Increasing the number of iterations allows obtaining multiband and broadband behavior, and is shown in Figure 4. Fractal structure uses the concept "the Hausdorff dimension" which is defined by Equation (4).[36]
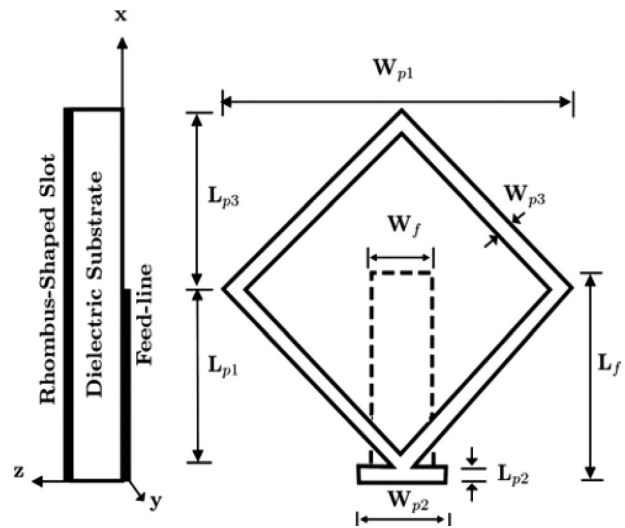
FIGURE 3 UWB antenna©[34]
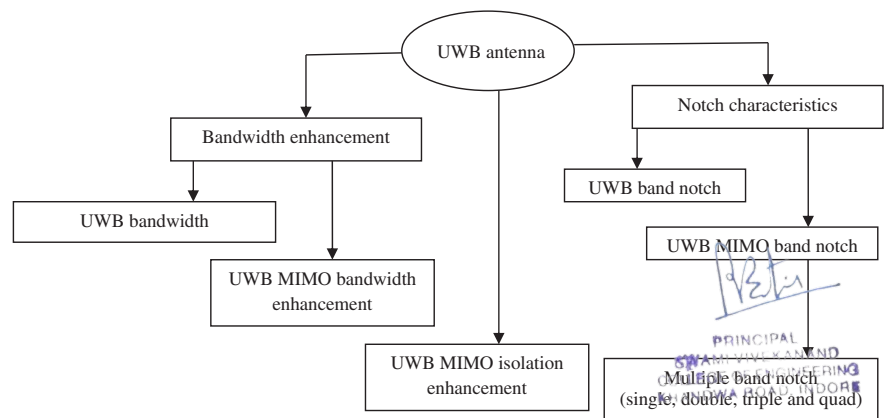
FIGURE 2 Flow chart on UWB antennas
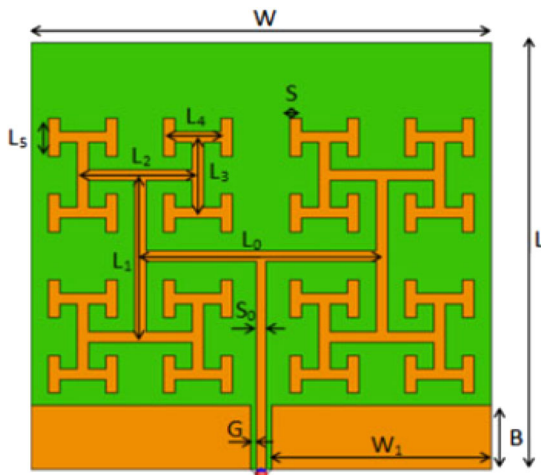
FIGURE 4 Geometry of the H-tree fractal antenna©[35]
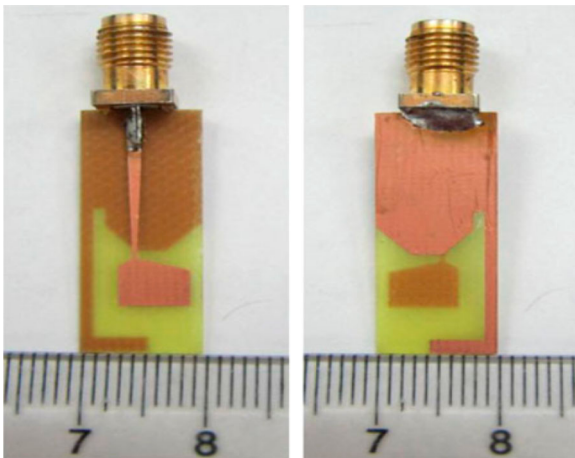
FIGURE 5 Fabricated antenna©[36]

$$d = \frac{\ln(n)}{\ln(R)} \quad (4)$$

where fractal is formed of "*n*" copies whose size has been reduced by a factor of "*R*."

An antenna was fabricated on FR-4 substrate of size $26 \times 10 \times 0.8$ mm^3, as shown in Figure 5. This system provides extended band from 3.1 to 12 GHz frequency, by using extended stub from ground. When the stub is extended, the cut off frequency gets reduced. The current distribution around the radiator is opposite in the direction of current in ground and stub. The designed antenna exhibited gain in 2 to 5 dBi range.[37]

An antenna design uses the conventional square patch and is modified by adding circle on edge and vertex of patch as well as defected ground structure is used with parasitic rectangular shape. Due to this modification antenna, system covers the UWB band with higher
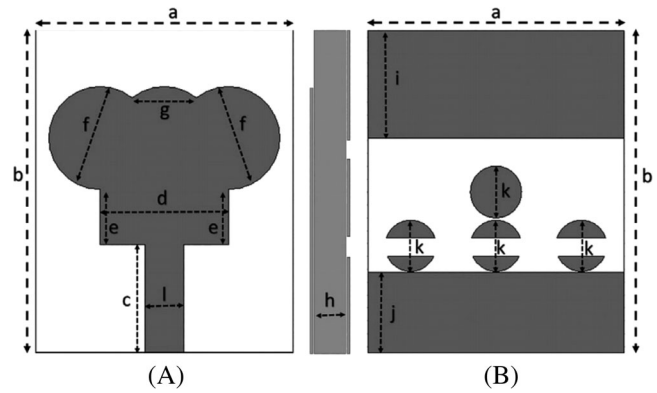
FIGURE 6 Antenna design: A, front view and B, back view©[37]

frequency range 3.1 to 20 GHz. The antenna system occupies $20 \times 25 \times 1.5$ mm^3 on FR-4 substrate shown in Figure 6. The design provides gain of 5.2 dBi and 85% efficiency.[38]

A modified circular patch antenna is constructed to cover 2.5 to 12.2 GHz. Modification is done by using extra circular patch and rectangular patch. These are added as main patches. This technique helps to design an antenna to cover 4.6 to 12.2 GHz range. An extra rectangular parasitic element is constructed on radiating side, and ground is made defected to cover lower frequency band. The peak gain in design is 3.5 dBi and radiation efficiency of 73.5% is achieved. The antenna is shown in Figure 7.[39]

The above discussed single element antennas are used for the UWB antennas only for wide band analysis.

2.2 | UWB MIMO antennas for bandwidth enhancement

The FCC allocated UWB frequency band to fulfill the UWB criterion and for various kinds of antenna designs. An antenna was designed for polarimetric UWB radar and UWB-MIMO on 40×40 mm^2 area. The impulse radiating response did not distort the radiating pulse in this design. The gain in copolarization was 4.0 dBi.[40] In a portable MIMO/diversity application, a tree shaped structure was designed on the ground plane to enhance isolation. The design occupied the size of 35×40 mm^2 on Taconic ORCER RF-35 dielectric substrate (tan $\delta = 0.0018$). The variation of gain was within 3.1 dBi in whole UWB band.[41] Similarly, the tree shaped antenna design utilized dielectric resonator antenna (DRA) for UWB band. The Rogers TMMI dielectric substrate (tan $\delta = 0.0022$) of 60×60 mm^2 with 2.65 permittivity, and DRA with 9.8 permittivity were used to cover 3.95 to 10.4 GHz frequency band. Radiation efficiency in this design was 98%.[42]

FIGURE 7 Antenna design: A, front view and B, back view©[38]

(A)　　　　　　　(B)

(A)　　　　　　　(B)
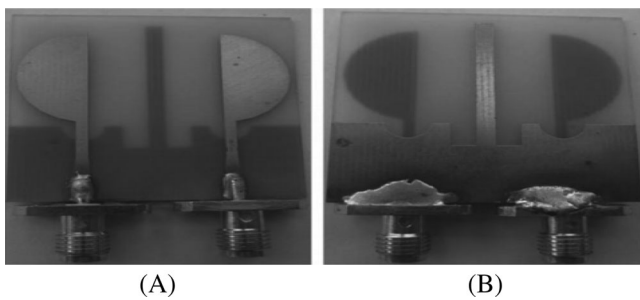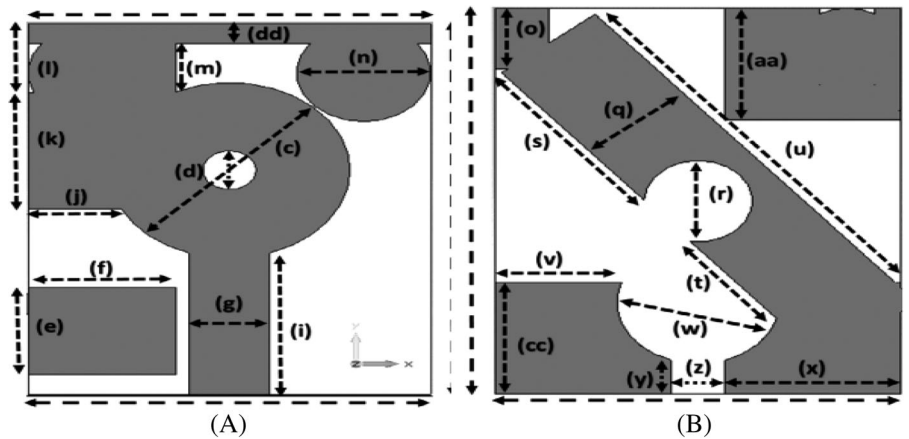
FIGURE 8 Half circular disc antenna: A, front view and B, back view©[43]

A UWB antenna was placed on substrate to make tree shaped DRA. Two planar monopoles with microstrip line were printed on one side of substrate, which occupied substrate size of $40 \times 26 \times 0.8$ mm^3 for portable devices.[43] By halving circular disc of 8.8 mm radius, feeding port is adjusted to 3 mm. Dual semi-circle slot in ground plane was designed for adjusting impedance bandwidth, and stub was also used to improve isolation. For the antenna size of 36×36 mm^2, UWB band was achieved. The antenna gain of about 6.9 dBi, with variations of less than 3.1 dBi in frequency band was achieved in design. The design is shown in Figure 8.[44]

A linearly tapered and slotted ground with two orthogonal microstrip feed line and a floating fork shaped decoupling structure were used to design an antenna of size $32 \times 32 \times 1.6$ mm^{3}for UWB-MIMO. It covered 3.1 to 12.0 GHz frequency range. For enhancement of isolation, a fork shape was considered. The isolation in whole frequency band was 15.0 dB. The design is shown in Figure 9.[45]

A design consists of two identical U-shaped monopole antenna elements for UWB communication was designed on $26 \times 31 \times 0.79$ mm^3 size on Rogers substrate (R04003). It covered 3.1 to 10.6 GHz frequency band. The staircase structure, which was symmetrical to two bottom corner of radiating element, was used for bandwidth enhancement.
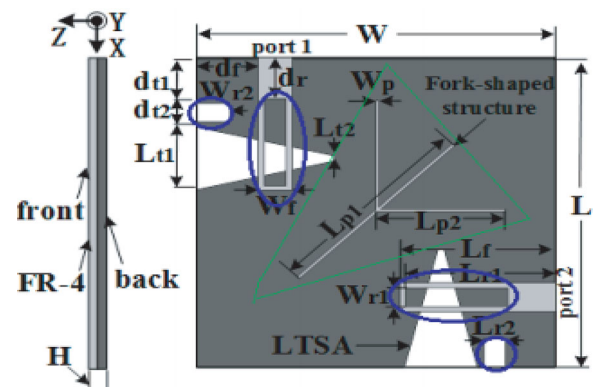
FIGURE 9 Two port UWB-MIMO antenna©[44]

The gain in this design was −2.0 to 5.8 dBi, and efficiency was 95% across the band. The design is shown in Figure 10. The monopole antenna was designed using lower resonance frequency, and is given by Equation (5).[46]

$$F_{rl} = \frac{144}{L_g + L_1 + g + \frac{w}{2\pi\sqrt{1+\varepsilon_r}} + \frac{w_1}{2\pi\sqrt{1+\varepsilon_r}}} \quad (5)$$

where F_{rl} is lower resonant frequency, L_g is length of ground, L_1 is length of radiating patch, g is gap between ground and patch, w is width of whole antenna, ε_r is relative permeability, and w_1 is width of radiating patch.

A UWB MIMO antenna with two L-shaped slots and a narrow slot on ground was designed to jointly cover the wide-band. The antenna system of size $32 \times 32 \times 0.8$ mm^3 was used to achieve 1.7 to 4.2 dBi gain, and more than 60% radiation efficiency in UWB band. The design is shown in Figure 11.[47]

A quasi-self-complementary antenna (QSCA) element consists of half circular conductor patch on one side of the substrate and a slot in shape of half circular with complement on the other side on RO4350 substrate ($\varepsilon_r = 3.5$, $tan\ \delta = 0.004$, $h = 1.6$ mm), occupied
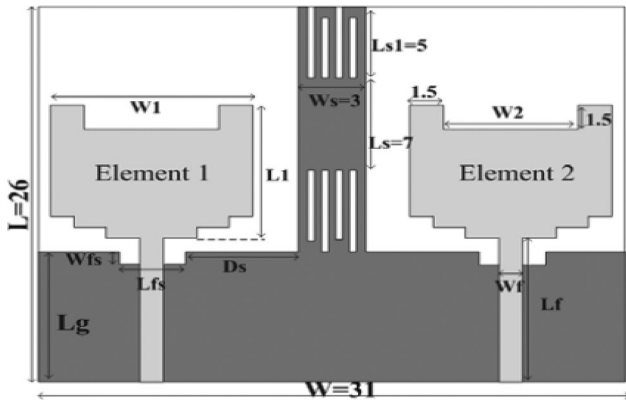
FIGURE 10 U-shaped with staircase MIMO antenna©[45]
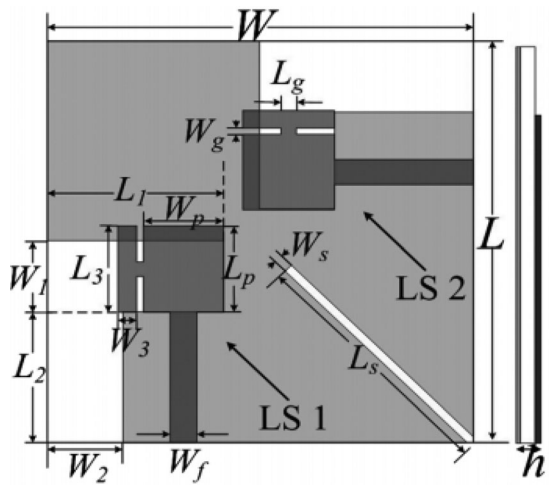
FIGURE 11 UWB MIMO antenna©[46]

21×38 mm². QSCA has the ability to achieve the wide bandwidth in compact size. The efficiency in design was above 70%, and the peak gain was 1.3 to 4.2 dBi across UWB band. The design is shown in Figure 12.[48]

Researchers and academicians contributed to cover 3G as well as lower frequency range combined with the UWB frequency range. A G-shaped antenna was designed on 8×8 mm² size, and used slot loading technique. The design covered 2.2 to 13.3 GHz frequency range for the mobile communication. The antenna gain was 2.44 to 4.78 dBi, and efficiency was 30% to 60% in whole band. Isolation between the elements is maintained using T-shaped isolating structure. The design is shown in Figure 13.[49]

A diversity antenna of size $46 \times 32.6 \times 1.6$ mm³ was designed on FR-4 substrate, where triangular shaped elements were used. Antenna covered frequency band of 1.9 to 16.7 GHz. Triangular shape acted as a monopole antenna, and resonated at 4.0 GHz. The frequency of resonant is given by Equation (6). The diversity gain was close to 10 dB in design. The design is given in Figure 14.[50]
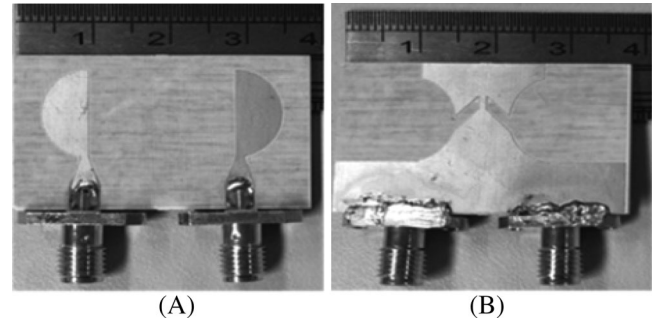
FIGURE 12 QSCA UWB MIMO: A, top view and B, bottom view©[47]

$$f_r = \frac{c}{4h} \tag{6}$$

where c is speed of light in free space and h is monopole height, also $h = L_2 + g$ (where L_2 is length of triangle shape and g is gap between ground and patch).

A rectangular patch monopole with glass shaped slot and CPW feed was designed to cover 2.8 GHz to 14.0 GHz frequency range. It was loaded with spiral shaped slots in ground plane. Antenna size on FR-4 substrate ($\varepsilon_r = 4.4$, and tan $\delta = 0.025$) was $40 \times 40 \times 1.58$ mm³, and the patch size was 21×19 mm². The gain in the design was 4 to 5 dBi, and efficiency was more than 75% over the operating band. Lower edge frequency can be calculated by printed rectangular monopole. Antenna used extra slot of spiral to add extra resonance frequency, and is given by Equation (7). The design is shown in Figure 15.[51]

$$F_l(\text{GHz}) = \frac{0.24 X 300}{l + s + \frac{w}{2\pi}} \tag{7}$$

where F_l is lower edge frequency, l is length of patch, s is separation between patch and ground, and w is width of the patch.

Similarly, f_l can also be obtained in terms of l_{sp} (length of spiral slot), and is given by Equation (8). Equation (9) is used to find the value of l_{sp}.

$$f_l = \frac{c_0}{2l_{sp}} \tag{8}$$

$$l_{sp} = 2 X 2\pi \left(R_s + w_s + \frac{g_s}{2} \right) \tag{9}$$

where R_s is radius of spiral, w_s is width of spiral, and g_s is gap between turns.

An UWB antenna was designed for wireless application with triple band notched function. It covered 2.49 to 19.41 GHz frequency band and occupied $20 \times 20 \times 0.787$ mm³ (or $0.28\lambda \times 0.28\lambda$, where λ is the first

FIGURE 13 UWB antenna: A, overall view; B, expanded view; and C, T-shaped isolator©[48]

(A)

(B)

(C)
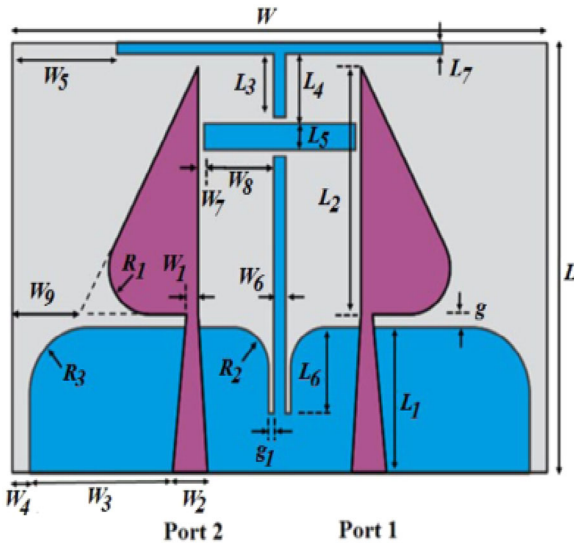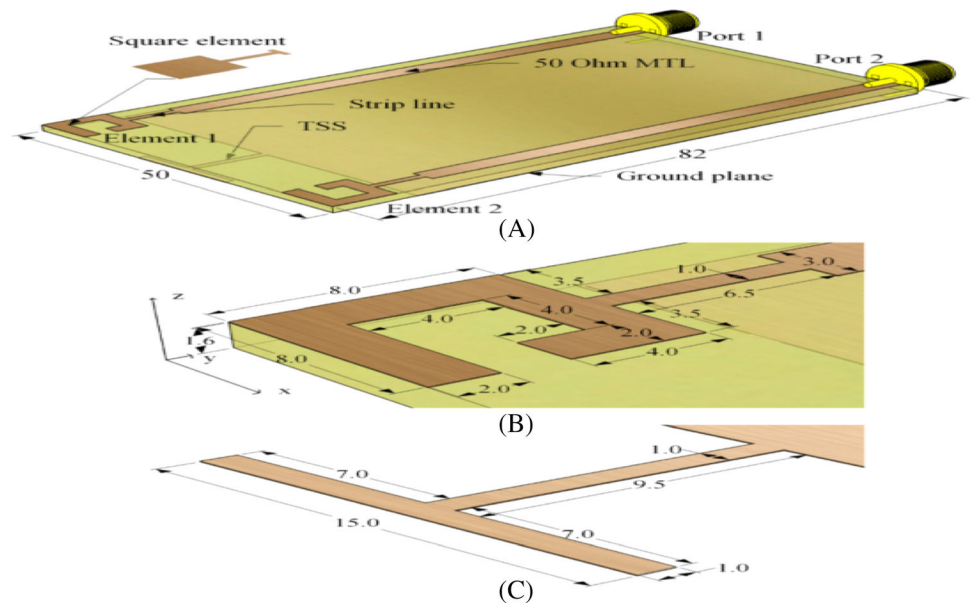
FIGURE 14 Triangular shaped MIMO antenna©[49]

FIGURE 15 Wide-band antenna©[50]

resonant frequency at 4.2 GHz). It was fed with 50 Ω microstrip line. The design has 5.98 dBi maximum gain and 85% efficiency across the band.[52] Two identical rectangular shaped patches were etched on FR-4 substrate for MIMO application. The antenna occupied space of $30 \times 30 \times 0.8$ mm^3 to cover 2.85 to 11.9 GHz frequency range. The efficiency of design was more than 80% in whole band.[53]

An antenna with slant polarization ($\pm 45°$) was designed for dual polarization to improve lower frequency (2.34 GHz) and upper frequency (12 GHz) on FR-4 substrate of size $76.43 \times 52.25 \times 1.6$ mm^3. The antenna consisted of V-shaped stepped rectangular slot on ground plane. The presented sots in antenna

resonate in lower frequency. The antenna covered 2.25 to 12.0 GHz. The design achieved simulated gain in the range 3.0 to 5.0 dBi. Stepped rectangular slot and feed line were used to enhance ultrawide impedance bandwidth. The efficiency in the band was above 50%. The design is shown in Figure 16.[54]

A UWB-MIMO antenna was fabricated using two monopoles placed side by side on Rogers TMM4 (tan $\delta = 0.002$) laminates. It occupied 23×39.8 mm^2 area and covered 2.5 to 12.0 GHz frequency range. The monopoles were fabricated with straight edges and arc feeding sections. A U-shaped slot was added in radiator to match wideband characteristics. This radiator was placed in 90° with other radiator (ie, orthogonal polarization). The gain in design varied from 2.4 to 5.1 dBi for port 1 in frequency range 2.5 to 12.0 GHz, while for port 2, it was 2.5 to 5.3 dBi. The isolation between ports was greater than 21.0 dB, and the efficiency was more than 82% in band.[55]

A typical semi-circular monopole antenna with 50 Ω CPW feed transmission line was designed on FR-4

Top Side (Ground-Slot)   Bottom Side (Microstrip Feed)

Top view   Bottom view
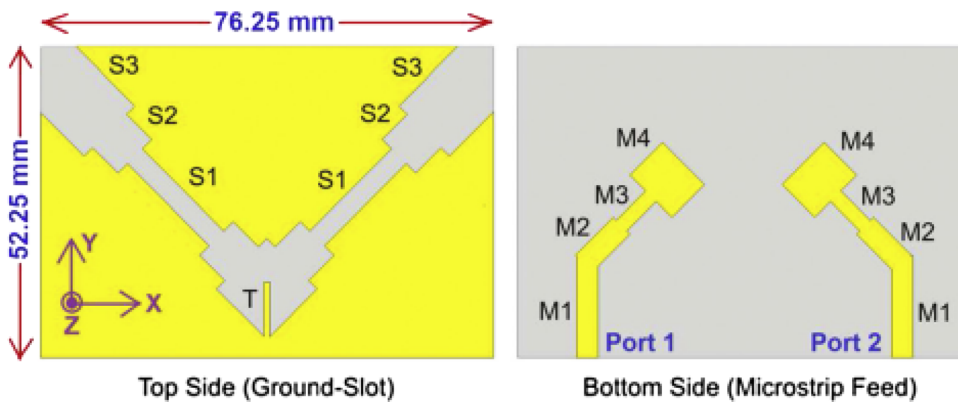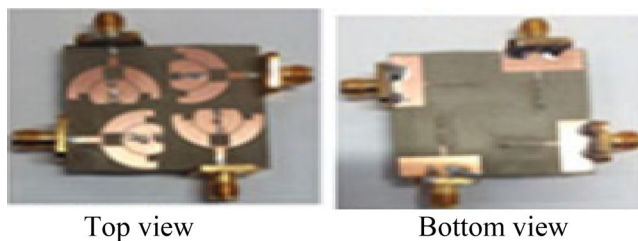
FIGURE 17 4-Element UWB-MIMO antenna©[56]

substrate. By reducing diffraction edges, edges are converted into smooth round curve to cover lower frequency till 2.2 GHz. This antenna showed UWB characteristics in the range 2.2 to 10.6 GHz. The gain in band was 3.0 dBi, and the efficiency was approximately 95%.[56]

Similarly, four element MIMO antenna is shown in Figure 17. The antenna occupied $38 \times 38 \times 0.762$ mm^3 and covered 3.0 to 15 GHz frequency band. The ground plane and disc is shorted by using holes and thin strip. This technique improves matching at lower frequency band. A rectangular slot is used for impedance matching on higher side. The gain in design varied from 0.5 to 5.0 dBi over the UWB range, and efficiency varied between 66% and 85%. The achieved isolation between antenna elements is ≥ 20 dB for UWB application.[57]

A broadband microstrip-to-slot line transition with circular stubs was applied to feed the antenna. The J-shaped slots were inserted on the ground plane of the antenna to create a new resonance in the low frequency region, thereby miniaturizing the antenna. The design covered 2.99 to 10.87 GHz, having front-to-back ratio (FBR) > 8.7 dB. The gain in the range was 3.2 to 7.3 dBi.[58]

All the above-discussed antennas are multi-element MIMO antennas and are used for bandwidth enhancement using UWB technique.

3 | UWB ANTENNAS AND UWB MIMO ANTENNAS WITH NOTCH FILTERS

In this section, various designs of UWB antennas and UWB MIMO antennas with notch filters are discussed for single, dual, three, and quad notches.

3.1 | UWB antennas with notches

Above discussed UWB-SISO and UWB-MIMO antennas were for bandwidth enhancement. There are several existing communication systems operating below 10.6 GHz in the same UWB frequency band and may cause interference with the UWB systems such as IEEE 802.11a WLAN system or HIPERLAN/2 wireless system. These systems may operate at 5.15 to 5.825 GHz, which may cause interference with a UWB system. To avoid the interference with the existing wireless systems, a filter with bandstop characteristics may be integrated with UWB antennas to achieve a notch function at the interfering frequency band. Many researchers have contributed for such antenna system. Few antenna designs are represented here as a review of these works. There are single band and multiband notch characteristics are available in literature.

For band notched characteristics for WLAN band, and uplink and downlink of X-band satellite communication system, an antenna was designed on $26 \times 30 \times 1.6$ mm^3 size to cover 3.15 to 10.63 GHz with VSWR<2 on FR-4 substrate. For the dual notch characteristics, tapered edge ground was used; also three rectangular slots were cut on the ground. The length of the slot at the 5.18 to 5.82 GHz for the notch band is obtained using Equation (10). There is always a difference between the calculated and practical length of the slots due to the coupling effect. Radiation efficiency is very low and gain is zero at notched band. The design is shown in Figure 18.[59]
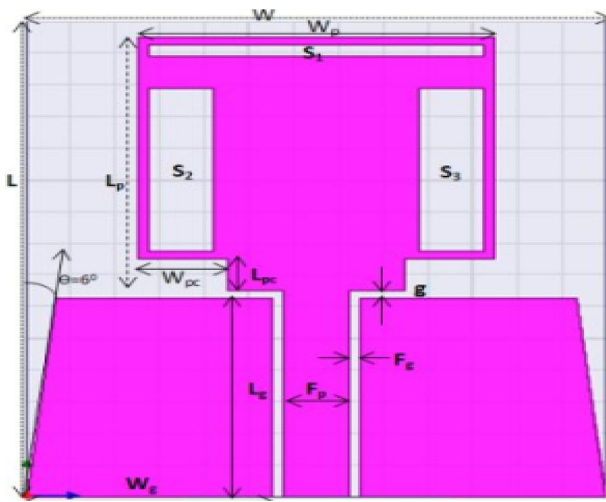
FIGURE 18 UWB dual notch antenna©[58]

FIGURE 19 Flower shaped UWB antenna©[59]

$$L = \frac{C}{2f\sqrt{\frac{\varepsilon_r + 1}{2}}} \qquad (10)$$

where L is length of slot, ε_r is relative permeability, and f is frequency.

A reconfigurable UWB flower shaped antenna was designed on FR-4 substrate of size 50×42 mm^2. Flower shaped antenna dimension is optimized to achieve UWB characteristics and a variable capacitor is formed using varactor diode in the range 0.3 pF to 1.4 pF to cover notch frequency band. At $C = 0.8$ pF, varactor diode based antenna showed the notch characteristics for WLAN band, and for $C = 0.7$ pF, it showed notch characteristics for WiMAX frequency band. The antenna design is shown in Figure 19.[60]

A CPW fed switchable UWB antenna was designed on Rogers RO4003 (tan $\delta = 0.0021$) substrate of size 24×30.5 mm^2. This antenna acted as an antenna filter with adjustable notched frequency bands in UWB frequency range. Rejection of frequency and shift can be done by using variable capacitors in the range 0.1 to 0.4 pf. The rejection band can be achieved by varying values from 3.1 to 2.9 GHz and 7.0 to 5.8 GHz, respectively. The antenna advocates the tunability for desired frequency band, just by changing the value of the capacitor, without any alteration in the basic structure of the antenna. The antenna geometry is shown in Figure 20.[61]

A V-shaped slit and a split ring shaped slit were introduced in antenna geometry to get notch characteristics for the 5.15 to 5.825 GHz and 3.4 to 3.7 GHz bands respectively to avoid the interference. The antenna occupied the area of 75×10 mm on FR-4 substrate and is shown in Figure 21. The gap loading is used with semicircular strip and bow-tie shaped patch are used in design.

FIGURE 20 UWB antenna: A, notched geometry and B, fabricated antenna©[60]

The antenna in mounted vertically on ground plane to cover 2.75 to 14.66 GHz. Less than 0 dB gain is obtained in notch band and the overall gain is maintained at 2.0 dBi in design.[62]

In view of more interference with the UWB, some researchers and academicians also worked on higher band notch characteristics such as, the triangular structure showed only a notch band at WiMAX (3.45-3.80 GHz), and by using rectangular, circular and fractal slot, dual notch band is accessible. With rectangular slot, notches are at 2.8 to 3.45 GHz and 5.6 to 6.3 GHz. This antenna was designed for Wi-Fi and Bluetooth applications, which occupied $50 \times 50 \times 1.6$ mm^3 size on FR-4 substrate. The designed antenna covered 2.0 to 11.0 GHz frequency range with triple band notch characteristics at 2.0, 3.5, and 5.8 GHz (PCS, WiMAX, WLAN). The gain in band is between -3.5 and -6.5 dBi, and the efficiency is around 10% for 2.05 GHz. At the second notch frequency, the antenna efficiency is reduced to 45% at 3.5 GHz, and for third notch, the efficiency is 65%. The design is shown in Figure 22.[63]
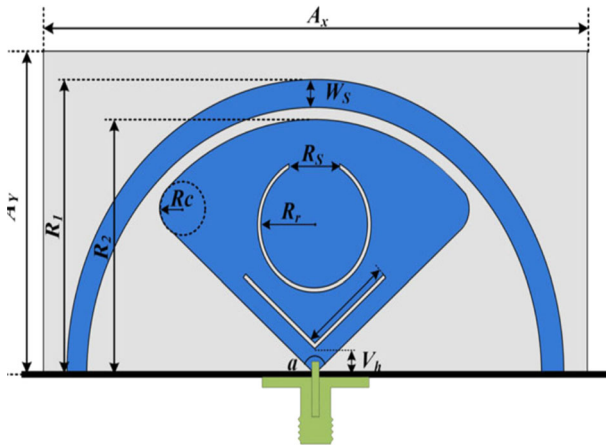
FIGURE 21 UWB antenna©[61]

FIGURE 22 Triple notch band antenna©[62]

Two round shaped slots of half wavelength were used for the band rejection of WiMAX (3.3-3.7 GHz) and WLAN (5.15-5.85 GHz), as well as a pair of C-shaped slots were also etched in ground plane to get a third notch in X-band satellite communication (7.1-7.76 GHz). The gain in design was almost stable over UWB, except at notch bands. At notch bands, very sharp gain suppression occurred up to 7.0 dB, which clearly confirms the band rejection capability of designed antenna. The size of the antenna was 31×22 mm^2 on FR-4 dielectric substrate. The design is shown in Figure 23.[64]

An antenna of size $28 \times 28 \times 0.8$ mm^3 was designed to operate in UWB band with three notches. Antenna consists of a rectangular patch with H-shaped slot, a defected ground structure (DGS) having two rectangular slots, as well as PIN diode is used to control the electrical length of radiating patch. This methodology is responsible for WiMAX band (3.2-3.75 GHz) notching characteristics.

FIGURE 23 UWB-notched antenna: A, front view and B, bottom view©[63]

Two C-shaped arms and two L-shaped slots on the ground plane are used for WLAN (5.05-5.9 GHz) and ITU band (8.0-8.45 GHz) rejection. Bands can be rejected further and can be controlled if two PIN diodes are placed on the slot between the C-shaped arm and patch. Antenna achieves better than 75% efficiency in operating band and this antenna is 25% efficient in notch band. The antenna structure is shown in Figure 24.[65]

The antenna size of UWB can be minimized by choosing appropriate patch size. An antenna having elliptical radiating patch with two inverted L-shaped stub occupied 12×19 mm^2 on FR-4 substrate, and is shown in Figure 25. Two stubs introduce notch band for WiMAX and WLAN band. The CSRR controls the current distribution for desired band and works as band stop filter for X-band downlink satellite communication system. The antenna showed the gain in stop band below 0 dBi, and 3.18 dBi maximum in desired band.[66]

For designing UWB with a band notch capability, the SRR and CSRR are the novel methods. Basically, SRR and CSRR generate strong magnetic and electric coupling from LC resonant and can be used for bandpass and bandstop filter applications. When SRR is placed on bottom plane, it creates magnetic coupling with antenna patch, resulted in LC resonant from magnetic coupling, that is, magnetic LC resonant. On the other side, on radiating patch, CSRR is loaded, which generates electric LC resonant. The antenna rejected the WiMAX (3.3-3.7 GHz), IEEE802.11a/n (5.15-5.825 GHz), and ITU (8.025-8.4 GHz) frequency bands. Overall size on FR-4 substrate was 32×34 mm^2, and the radiation efficiency was greater than 70% in the band. The antenna diagram is shown in Figure 26.[67]

All the above-discussed antennas are the UWB single element antennas and are used for elimination of the undesired frequency band due to the interference in communication channel.

FIGURE 24 UWB-notched antenna: A, top view and B, bottom view©[64]

(A)   (B)

(A)   (B)
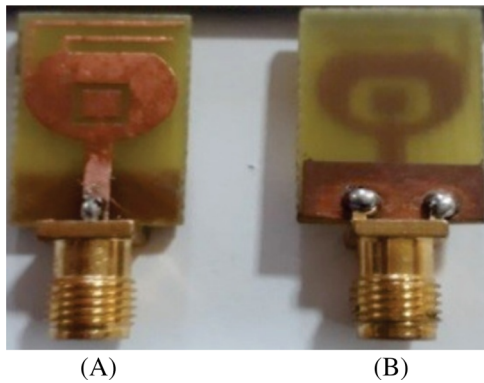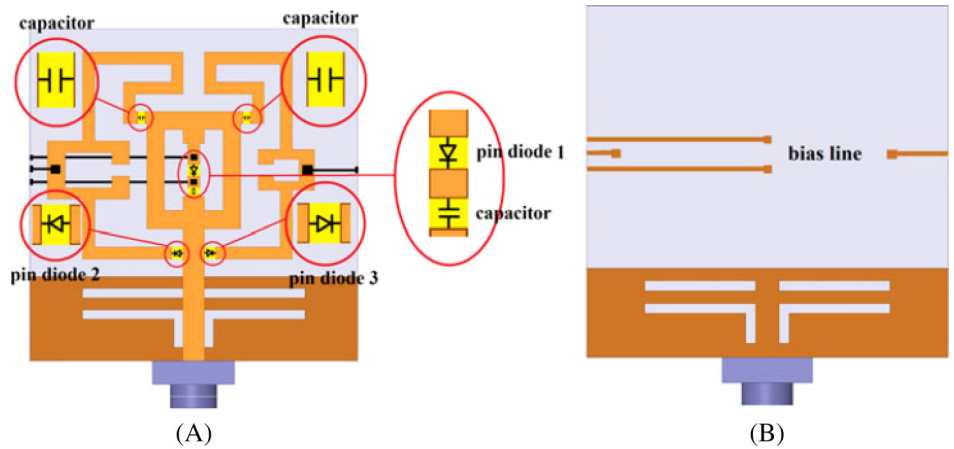
FIGURE 25 UWB-notched antenna: A, top view and B, bottom view©[65]

FIGURE 27 Notch band antenna©[67]

(A)   (B)
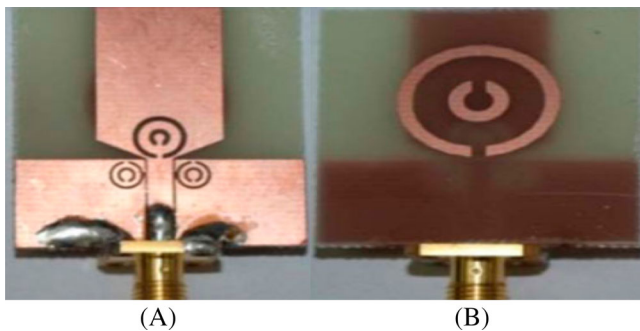
FIGURE 26 SRR-CSRR based UWB antenna: A, top view and B, bottom view©[66]

3.2 | UWB MIMO antennas with notches (single, dual, three, and quad)

A compact UWB MIMO antenna, which consisted of two half-circular slot antennas as radiators, was designed on 33×26 mm^2 size. It covered the frequency range 3.0 to 11.0 GHz with rejection of WLAN band at 5.2 GHz. A T-shaped slot was introduced to reject WLAN frequency

band from 5.15 to 5.35 GHz to remove interference in UWB operation. The T-shaped open slot was provided in the zone to concentrate the current. It disturbs the current distribution thus provides the band notch characteristics. The gain varied from 1.0 to 6.0 dBi, and isolation was more than 15 dB in band. The design is shown in Figure 27.[68]

Two split ring resonators were etched on radiator for achieving band notched characteristics at 5.5 GHz band. A quarter circular slot and one rectangular stub were etched in design. Rectangular stub is placed at 45° to control the direction of current. The isolation was enhanced in presented −10 dB impedance band. The center notched frequency in design was achieved at 5.5 GHz with −2.91 dB return loss. The gain in band was less than 3.0 dBi.[69]An asymmetric CPW strip fed UWB-MIMO antenna of size $50 \times 28 \times 1.6$ mm^3 was designed. The antenna consisted of semi-elliptical path radiator with asymmetric ground plane. The design covered 2.8 to 11.5 GHz frequency range. It also showed the band notch behavior for WiMAX (3.3-3.9 GHz) band by using a simple folded stub in patch radiator. The isolation was better
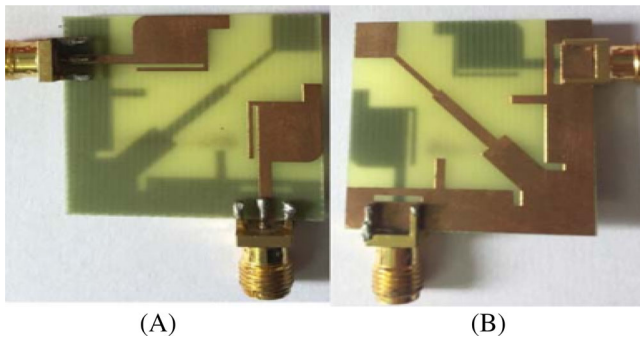
FIGURE 28 UWB notched MIMO: A, top view and B, bottom view©[70]

FIGURE 29 MIMO with offset©[72]

than −16.0 dB in band.[70] An open circuited stub was added at the edge of each radiator of a UWB antenna to cover frequency range of 3.08 to 10.98 GHz. The length of the stub was chosen as $\lambda_g/4$, where λ_g is the guided wavelength at the notch frequency. The notched frequency band is 4.98 to 5.96 GHz. The peak gain in applicable band is 5.0 dB with less than 3.0 dB variation, isolation level is ≥20 dB, and efficiency is >90%. The design is shown in Figure 28.[71]

An antenna was fabricated on FR-4 of size 44 × 44 × 1.6 mm³, and used step-shaped slot to obtain notch band from 5.10 to 5.95 GHz. The antenna gain in design ranges from 2.4 to 4.0 dBi, and efficiency was more than 70%.[72] A MIMO antenna design for UWB application was designed with 38.5 × 38.5 × 1.6 mm³ on FR-4. By using two offset microstrip fed antenna elements, 3.08 to 11.8 GHz band was covered. The pair of open-ended slits etched on the ground was employed to generate band-notched function. The notched band was controlled by adjusting the lengths of the slits. The notched frequency band was 5.03 to 5.97 GHz. The gain ranges from 1.4 to 3.6 dBi throughout the entire band, except the notched point, where it drops to −4.5 dBi. The isolation in band was better than 15 dB, and efficiency was above 75%. The design is shown in Figure 29.[73]

A MIMO antenna utilizes the concept of wideband characteristics, and is fabricated on FR-4 of size 29 × 38 mm². For the wideband performance and stable radiation performance Minkowski fractal geometry is used on the ground plane, below the feed line. The isolation in band is better than 21.5 dB, and is achieved by two ground stubs and a rectangular slot in the ground plane. The band notched characteristics in WLAN can be achieved by elliptical split-ring resonator (ESRR), and is imbedded in radiator. The notch length (L_n) of an ESRR slot of major axis length (L_{ma}), minor axis length (L_{mi}), and width (w) are calculated using Equations (11)–(13):
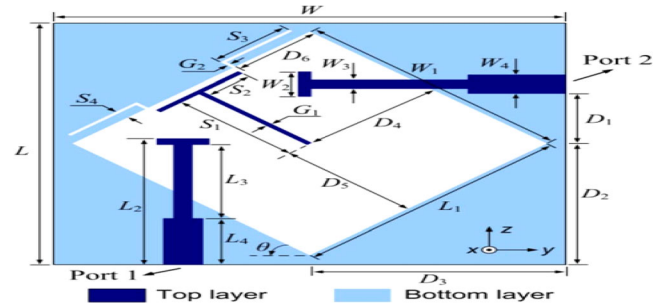
$$L_n = K\pi(0.5L_{mi} - w) \approx \frac{\lambda_g}{2} \approx \frac{c}{2f_{\text{notch}}\sqrt{\varepsilon_{eff}}} \quad (11)$$

$$K = 3(1+k) - \sqrt{(3+k)(1+3k)} \quad (12)$$

$$k = \frac{L_{ma}}{L_{mi}} \quad (13)$$

where λ_g is guided wavelength, and k is the axial ratio of the ellipse.

A UWB antenna of size 18 × 18 mm² on FR-4 substrate was designed for switchable band-notch characteristics for cognitive radio applications. The antenna consists of rectangular shaped radiating element and rectangular shaped parasitic elements on the ground plane to achieve the band-notch in WLAN band. Antenna showed spectrum sensing in cognitive radio and switchable band-notch with filtering characteristic for reconfigurable operation in the frequency band of 3.2 to 10.8 GHz. The position of PIN diode between two parasitic elements is selected for switchable band notch characteristics. The antenna system achieved 2.5 dBi gain and better than 70% efficiency.[75]

A wideband MIMO antenna was constructed on FR-4 of size 47 × 25.7 mm² by using U-shaped slot. A $\lambda/8$ distance was kept between two radiating elements. The purpose of U-shaped slot was to obtain band notch characteristics for 4.59 to 6.0 GHz, and another U-shape was created on feeding line to achieve second notch band from 8.92 to 9.9 GHz. The gain in the design was varied from 2.0 to 5.45 dBi across entire band and efficiency was 72%. In a design, first notch band covered 4.59 to 6.0 GHz, and second notch-band covered 8.92 to 9.9 GHz, which is the short range RADAR band. For the enhancement of isolation, both radiating elements are kept $\lambda/8$ wavelength apart.[76]

Another antenna was designed to generate dual notched bands with incorporated complementary split ring resonator (CSRR) within the radiator. The outer and the inner split rings generated notches at 3.5 GHz and 5.7 GHz, respectively. Theoretically, by changing the outer and the
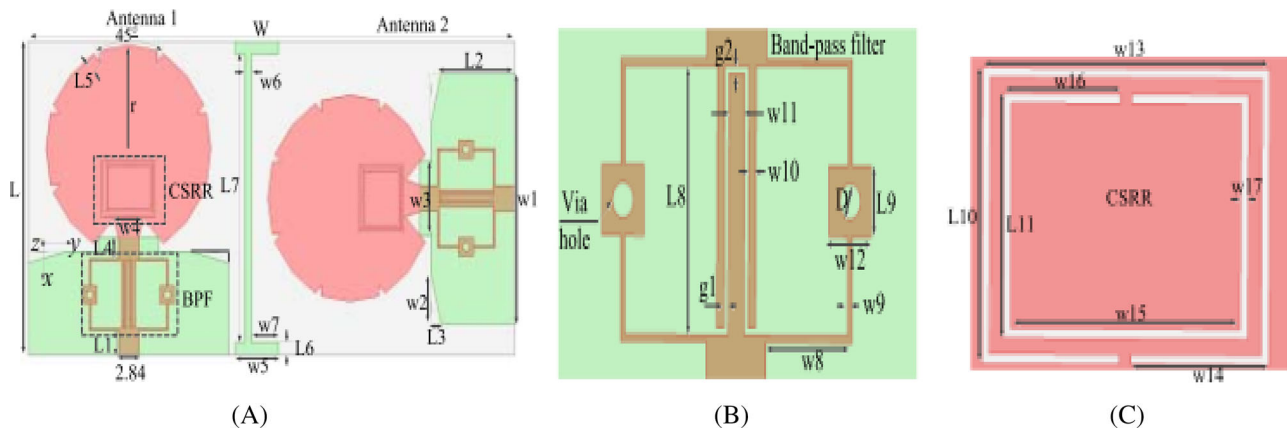
FIGURE 30 UWB notched MIMO: A, antenna; B, band pass filter; and C, CSRR©[76]
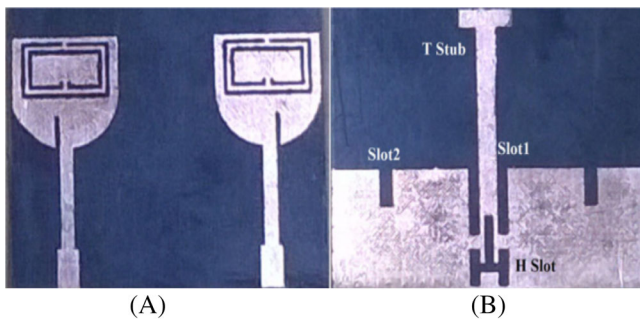
FIGURE 31 CSRR and stub based UWB notch antenna: A, front and B, back©[78]
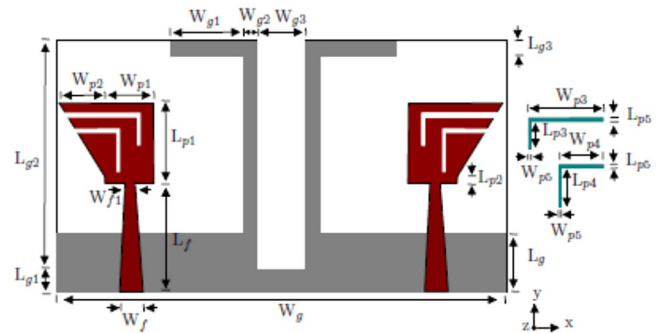
FIGURE 32 UWB MIMO antenna design©[81]

inner sizes of the CSRR, various dual notched bands can be achieved. The peak gain ranges from 1.7 to 4.2 dB in design. The design is shown in Figure 30.[77]

Similarly, two inverted L-shaped strips in the fork-shaped patches were used to obtain band rejection of WiMAX from 4.51 to 5.7 GHz and by switching diodes to ON and OFF positions. The band rejection of WLAN at 5.0 to 5.7 GHz was achieved. The gain of single notch is 0 dBi, and dual notch band is −6.0 dBi.[78]

An antenna consisted of two identical cup-shaped monopole radiators to achieve UWB characteristics. They shared common ground with rectangular slots and a ground stub to achieve better isolation. For the notched characteristics at WiMAX (3.4-3.6 GHz) and WLAN (5.725-5.825 GHz), CSRR was etched on both the antenna elements. The rectangular slots in both the radiators next to feed lines were etched out in order to achieve impedance matching. For further matching, two rectangular slots were made in the ground plane under the feed lines. Isolation is greater than 20 dB in entire band. The design is shown in Figure 31.[79]

To cover the frequency range 2.9 to 11.6 GHz, an antenna of size 26 × 26 mm was fabricated on Taconic RF-35 substrate (tan δ = 0.0018) of 0.762 mm thickness.

It was designed using dual port Vivaldi antenna. Two split ring resonators (SRRs) were placed near microstrip line to achieve dual notch characteristics in 5.3 to 5.8 GHz and 7.85 to 8.55 GHz bands. The antenna achieved less than 0 dB gains in notch bands.[80]

A dual band rejection in the band of 5.1 to 5.8 GHz (WLAN) and 6.7 to 7.1 GHz (IEEE INSAT/Super-Extended C-band) were achieved by using two inverted J-shaped slit in radiating patch. J-shaped slit forms quarter guided wavelength resonator, due to this current density can be controlled to get band notch characteristics. The antenna occupied the substrate size of $26 \times 15 \times 1.6$ mm^{3}.[81]

A combination of rectangular, triangular shapes and tapered microstrip line is used to from antenna radiator to cover 2.9 to 20 GHz frequency range. The design is shown in Figure 32. To avoid interference in WLAN band (5.09-5.8 GHz) and IEEE INSAT/Super-Extended C-band (6.3-7.27 GHz), the antenna is modified into dual band notch antenna using two L-shaped slits. The gain drops in the bandstop range are −10 db and −8 db for 5.45 GHz and 6.6 GHz, respectively. The gain in remaining bands is 0 to 7 dBi.[82]

A pair of C-shaped slots were introduced on the radiating elements to perform band notched functions from 5.15
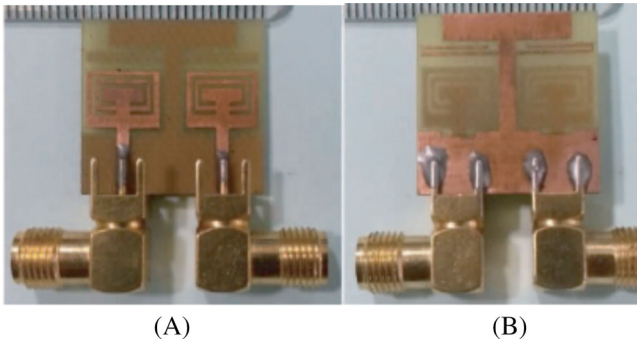
FIGURE 33 UWB MIMO: A, top view and B, bottom view©[82]

to 6.0 GHz (WLAN) and 7.8 to 8.4 GHz (X-band satellite communication), respectively. To create a third notched band from 3.3 to 3.7 GHz (WiMAX), a pair of U-shaped strips are joined to the ground plane. Peak gain in band varies from 2.0 to 5.0 dBi, isolation is higher than 25 dB, and efficiency is above 80%. The size of the antenna is $18 \times 21 \times 0.8$ mm^3 on FR-4 dielectric substrate. The design is shown in Figure 33.[83]

A triple-mode stepped impedance resonators consisted of two half-wavelength stepped impedance resonators (SIRs) and two short-circuited stubs. Since the resonator is symmetrical to the plane, the odd-even-mode method is implemented. For odd-mode excitation, the equivalent circuit is one-quarter wavelength with one end grounded. The f_{ino} is the center frequency of the notch band and is given in Equation (14).[84]

$$f_{ino} = \frac{c}{4L_1\sqrt{\varepsilon_{eff}}} \quad (14)$$

Triple band-notch characteristics at WiMAX (3.30-3.80 GHz), WLAN (IEEE802.11a/h/j/n 5.15-5.35 GHz, 5.25-5.35 GHz, 5.47-5.725 GHz, 5.725-5.825 GHz), and in X-band downlink satellite communication (7.25-7.75 GHz) were obtained by using inverted T-shaped stub, C-shaped slot, and pair of L-shaped slots in ground plane. Such type of shape/slot changes the current distribution and antenna impedance. Due to which current reflected back to input port, so such band notch characteristics can be achieved. The antenna represented these characteristics with gain of 3.96 to 10.98 dBi, and occupied $20 \times 20 \times 0.5$ mm^3 space on silicon substrate. Radiating patch is constructed in circular shape of radius R, and is given by Equation (15).[85]

$$R = \frac{F}{\sqrt{1 + \frac{2h_{si}}{\pi\varepsilon_r F}\left[ln\left\{\frac{\pi F}{2h_{si}}\right\} + 1.7726\right]}} \quad (15)$$

The effective radius is given by Equation (16), and F by Equation (17).

$$R_e = R\sqrt{1 + \frac{2h_{si}}{\pi\varepsilon_r R}\left[ln\left\{\frac{\pi R}{2h_{si}}\right\} + 1.7726\right]} \quad (16)$$

and

$$F = \frac{8.791 \times 10^2}{f_r\sqrt{\varepsilon_r}} \quad (17)$$

where h_{is} is the height of silicon substrate, ε_r is relative permittivity of the substrate; f_r is resonant frequency in GHz, and F is constant (depending on permittivity and resonant frequency).

Star shaped radiator and a defected rectangular ground plane is used to achieve UWB characteristics in 2.63 to 13.02 GHz frequency range. Antenna occupied size of $25 \times 20 \times 1.6$ mm^3 on FR-4 substrate which is shown in Figure 31. The capacitive loaded loop (CLL) structure near to the radiator is attached for band notched characteristics at WLAN band (5.1-5.9 GHz). One I-shaped strip is attached at lower rectangular slot, and L-shaped strip is added to upper rectangular slot of the ground plane to achieve the band-notched characteristics at WiMAX (2.94-3.7 GHz) and ITU bands (7.4-8.7 GHz). These shapes provide mechanism to concentrate surface current around the edges so that antenna structure is able to produce notch band characteristics.[86]

A reconfigurable antenna of size 24.0×12.0 mm^2 was fabricated on RT/Duroid 5880 substrate. By the use of PIN diodes instead of the switches connected with parallel microstrip line and the ground, reconfigurable function is achieved. Adjusting the position of the PIN diodes, notched frequency of the antenna can be changed. By adjusting the PIN diode, notch characteristics in the frequency band was 3.3 to 5.5 GHz which covers WiMAX (3.2-3.75 GHz) and WLAN (5.05-5.9 GHz) bands. The antenna covered 3.1 to 11.0 GHz frequency range, and achieved 3.5 dBi steady gain and more than 80% efficiency.[87]

A square shaped patch with rectangular defected ground plane was used to construct an UWB antenna. In this design, four elements are placed orthogonally. The antenna design occupied $39 \times 39 \times 1.6$ mm^3 on FR-4 substrate. To avoid interference, band notch characteristics are achieved by utilizing combination of H and L shaped slots on radiating patch and U-shaped slot in ground plane. The notch bands of 3.3 to 3.7 GHz (WiMAX), 5.15 to 5.875 GHz (WLAN), and 7.1 to 7.9 GHz (X-band) are achieved in design. The antenna system provides gain in the range 1.40 to 4.60 dBi, ECC less than 0.5, and efficiency of greater than −3.0 dB.[88]

An antenna occupied 30×30 mm^2 size on 1.6 mm thick RO4003 substrate using semicircle shaped radiating

element. To achieve the band notch characteristics, rectangular strip and hook shaped slots were used. The gain of less than −3.0 dBi was achieved in notch bands.[89]

An antenna of size 24.0×30.0 mm^2 on FR-4 substrate was fabricated with circular radiator. The V-shaped slot was used for impedance matching as well as to prevent interference with existing communication system. This consisted of a pair of interrogation-shaped slotted structure, a complementary SRR slot on the tuning stub, and two narrow open-circuited stubs at the edge of the aperture. These are employed to generate notch bands with central frequencies of 3.6 GHz, 5.3 GHz, and 5.9 GHz, respectively. Here, the average circumferential length of slotted ring considered less than half wavelength at resonant. The current distribution at 8.0 GHz frequency was concentrated along semi-circle shape, and at lower frequencies 3.5 GHz, 5.2 GHz, and 5.9 GHz, current concentrated around the slit. These currents showed the destructive interference for the surface current, so antenna did not respond over these frequencies.[90]

Microstrip UWB bandpass filter showed the functionality of quad notched-bands. The filter was constructed by a multimode resonator (MMR), which constituted from two modified stepped impedance stubs (SISs) to generate six resonant modes. Five of which were within the UWB passband, whereas, the sixth mode was used to extend the upper stop band of the filter. The UWB antenna occupied the size of 8.0×9.83 mm^2. MMR technique was used to develop the UWB filter in combination with SIS. In this antenna, two modified U shaped SIS; consists of low-impedance transmission lines with two tapped high-impedance lines were used to produce three resonant modes. To create band notch effect, microstrip lines and other feed-lines are combined. The combined effect produces UWB band pass filter (BPF). The achieved quad notched bands are 5.2 GHz and 5.8 GHz WLAN bands, 6.8 GHz radio frequency identification and 8.0 GHz X-band. The antenna design is shown in Figure 34.[91]

In a design, UWB-MIMO occupied 22.0×28.0 mm^2 on Rogers RO4003C substrate for quad-band notched characteristics in 3.25 to 3.6 GHz, 5.05 to 5.48 GHz, 5.6 to 6.0 GHz, and 7.8 to 8.4 GHz to suppress interference from WiMAX, lower and upper WLAN, and uplink of X-band satellite communication systems respectively. Each radiating element consists of a rectangular radiator with a beveled edge to get wider impedance bandwidth. On the other side of the antenna, a partial ground plane with a T-shaped stub, two inverted L-shaped slots, an inverted L-shaped meander slot, and a C-shaped stub were used to filter 3.4 GHz WiMAX, 5.3 GHz lower

FIGURE 34 Quad notched band UWB BPF©[90]

WLAN, 5.8 GHz upper WLAN, and 8.0 GHz X-band. The antenna exhibited more than 70% total efficiency.[92]

By inserting two L-shaped slots, CSRR and C-shaped stubs, four notched bands were achieved at 3.25 to 3.9 GHz, 5.11 to 5.35 GHz, 5.5 to 6.06 GHz, and 7.18 to 7.88 GHz frequencies to filter WiMAX, lower WLAN, upper WLAN, and X-band. Meanwhile, the isolation is obviously enhanced with three metal strips on the ground plane. Results indicated that the antenna covered UWB frequency band of 3.1 to 10.6 GHz except four rejected bands. The isolation was better than 18.0 dB, and efficiency was above 75% in band. The size of the antenna is 30.0×45.0 mm^2 on FR-4 dielectric substrate. The design is shown in Figure 35.[93]

A quad band notch UWB antenna was designed on 38×20 mm^2 using 0.508 mm thick Rogers 4350B substrate (tan $\delta = 0.0037$). A circular shape is utilized for this antenna system and stepped impedance resonator in quad mode is coupled to microstrip line. The stepped impedance resonator is arranged in two half wavelength SIR with two short circuited stubs. The structure helped to achieve quad-band notch characteristics for 5.2 GHz, 5.8 GHz, 7.6 GHz, and 8.2 GHz frequencies.[94]

The UWB BPF antenna was designed on Roger RT/duroid 5880 substrate of size $37 \times 21 \times 0.787$ mm^3. BPF characteristics were generated by modified multimode resonator based BPF, which is attached with radiating patch, and DGS based LPF which is etched on ground plane. The gain of the UWB filtering antenna varied in the range 2.52 to 5.3 dBi.[95]

Variety of notch characteristics is the outcome of the different structures of the UWB antenna designs and presented with all the possible aspects in above section. These notch structures are the requirements for the band elimination in lower and higher frequency bands.

FIGURE 35 Quad notched band UWB antenna©[92]

FIGURE 36 Extended curved ground arm isolator©[95]

4 | UWB/MIMO ANTENNAS WITH ISOLATION TECHNIQUES

The isolation between the UWB/MIMO antennas is controlled with different isolation enhancement or mutual coupling reduction techniques. Some of them are discussed here for the research community. Two elements UWB MIMO antennas of size 41.0×30.0 mm^2 on FR-4 dielectric substrate was designed with curved ground arm to control the effect of mutual coupling between radiators. In this antenna, direction of main radiation was oriented oppositely to get >20.0 dB isolation. Peak gain in band was 6.5 dBi, and efficiency was 55% to 80%. The design is shown in Figure 36.[96]

An antenna with T-shaped slot, and extending branches in ground were etched. When antenna resonates, current concentrates in the slot so it does not couple directly to radiators. It was observed that higher mode of the resonance can be used to enhance the isolation better than 20 dB in the higher frequency band by reducing coupling by extending ground branches in the symmetric axis at an angle of $45°$.[97] A method of application of electric resonator was used to reduce mutual coupling was reported in literature. This method was applied by using unit cell for required isolation and was also used in two element array design. The size of unit cell was 10.6×5.6 mm^2 on RT/5880 substrate ($\varepsilon_r = 2.2$ and height = 1.575 mm). More than 15.0 dB of isolation was achieved at 2.45 GHz. The inclusion of metamaterial in front of antenna produced negligible effect on antenna matching. The antenna gain of 6.0 dBi was achieved by using unit cell. The design occupied 130×71.7 mm^2 area and is shown in Figure 37.[98]

A flag shaped stub was added at the middle of ground, and rectangular slit was also constructed on stub to control mutual coupling. Through design optimization of stub, strip and slots, required impedance bandwidth was achieved.[99] An antenna occupied $24.0 \times 24.0 \times 0.8$ mm^3 on FR-4 substrate to cover 3.0 to 10.9 GHz frequency band to achieve nearly 3.0 dB gain in the whole band and achieved 80% efficiency. In this antenna, stepped slots and spacing between adjacent feed were used to improve isolation, which maintained better than 20.0 dB isolation in band.[100]

Two-port antenna was designed to improve isolation between radiating elements. Orthogonal placement of radiating patches reduces the mutual coupling between elements. The antenna uses partially stepped ground to improve size and returnloss. The design achieved more than 21 dB isolation in band.[101]

The disc shaped monopole antenna of radius 8.0 mm was kept between two elements at 9.0 mm distance. The design covered 2.5 to 11.0 GHz range. For improvement in isolation, carbon black film with particle size <10.0 μm was used. Basically, carbon film was considered as a material by which electromagnetic signal could be observed. The feedline of the disc shaped MIMO was covered by this film. The average gain in band was greater than 2.11 dBi, isolation was better than 15.0 dB, and average efficiency was 69.2%. The size of the antenna was $50 \times 40 \times 1.6$ mm^3 on FR-4 dielectric substrate. The design is shown in Figure 38.[102]

To improve the isolation between two ports, a slot is etched at the center of the ground. The center slot helped to increase isolation of better than 10.0 dB at 2.4 GHz. The lower limit of the operation band shifts from 2.75 GHz to 2.4 GHz. This makes the antenna available for both UWB and WLAN MIMO applications. The radiation efficiency was 70% to 77.5% in band. The size of the antenna was $30 \times 40 \times 0.8$ mm^3 on FR-4 dielectric substrate. The design is shown in Figure 39.[103]

An antenna design consisted of square ring slot, four stepped rectangular arms, and microstrip feedline. Feeding lines were made stepped for better impedance matching and placed orthogonally as well as $45°$ slant
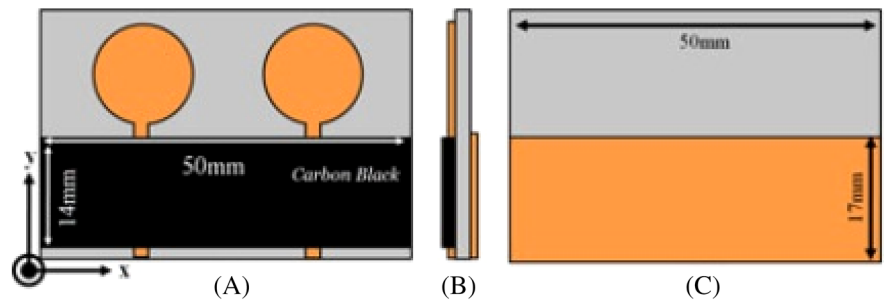
FIGURE 37 MIMO antenna: A, top view and B, bottom view©[97]

FIGURE 38 MIMO antenna with carbon film: A, top view; B, side view; and C, bottom view©[101]

FIGURE 39 MIMO antenna: A, front view; B, back view©[102]

stubs were added between ports to improve isolation. The gain in 3.0 to 12.0 GHz band was varied between 5.0 and 8.0 dBi, efficiency was >60%, and isolation was better than 20.0 dB. The size of the antenna was 66.25 × 66.25 mm^2 on FR-4 dielectric substrate. The design is shown in Figure 40.[104]

A four stubs in staircase shape were added in ground plane, these stubs suppress the surface wave to flow toward nonradiating elements thus avoided mutual coupling between radiating elements. The radiating elements were also placed in orthogonal arrangement, which also helped to improve isolation of better than 20.0 dB in 3.2 to 10.7 GHz frequency range.

A floating parasitic digitized decoupling structure was added on the backside of the substrate. This structure

was fabricated from a horizontal conducting strip with vertical stubs of unequal length. The structure results in improved isolation, as digit count affect the isolation, so large number of digits can be applied for better isolation. In this antenna ground plane is not connected to strips and gap between the strips of various length termed as digits acts as resonance element for different frequencies. The gain without decoupling structure was 4.0 dBi in design. However, when the decoupling structure was used, gain variation reduces to <2.3 dBi with a peak gain of 5.3 dBi. The decoupling structure makes the gain consistent over the radiating bandwidth of 3.1 to 10.6 GHz and also provides more than 20.0 dB isolation between antenna elements. The efficiency is maintained above 85% in design. The size of the antenna

was 33.0×45.5 mm^2 on Roger RO4003 dielectric substrate. The design is shown in Figure 41.[106]

To improve the isolation, an I-shaped slot strip was introduced between the two slot antennas. Mutual coupling between both the antenna ports is reduced by means of an isolation stub. An I-shaped stub is placed exactly between the two nearest edges of the antenna because of which an offset of Y is introduced between the isolation stub and the center of the substrate. When the rectangular slit is modified into an I-shaped structure, the isolation is brought above the 25.0 dB over several frequencies. The peak gain was 5.0 dBi, isolation was better than 15.0 dB, and efficiency was 85% in 2.8 to 12.0 GHz band. The size of the antenna was 30.0×60.0 mm^2 on FR-4 dielectric substrate.[107]

A SRR was designed in an antenna design; where L-shaped structure resonated at 6.0 GHz and another resonated at 9.5 GHz. The resonance frequency of the

decoupling SRR can be easily controlled by changing the size of the T-shaped branch. The decoupling structure improves isolation to 34.0 dB in 3.0 to 4.5 GHz band and 20.0 dB in 8.0 to 11 GHz band. The isolation in whole band is better than 19.0 dB. The peak gain in 3.0 to 12.0 GHz band was 4.0 dBi, and efficiency was 70%. The size of the antenna was 13.5×34.0 mm^2 on FR-4 dielectric substrate. The design is shown in Figure 42.[108]

MIMO antenna was designed on 23.0×29.0 mm^2 size for UWB application. This antenna was fabricated with triangular shaped element. These elements are placed in such a way that they do not face each other and this is first step of space reduction between the elements. Two inverted L-shaped stubs are used in ground plane to increase isolation, which acts as wave traps and adds resonance. The $\lambda/4$ length stubs are used for two purposes. First, as a reflector which enhances the isolation, and second, as a radiator, this adds resonances at 3.8 GHz and 6.8 GHz frequencies. CSRR is also used in design to prevent current to reach the other element in MIMO. Finally, CSRR also results in an isolation enhancement. This antenna covers frequency range 3.0 to 12.0 GHz, and has more than 15.0 dB isolation, 1.2 to 5.9 dBi gain, and 82% maximum efficiency. The design is shown in Figure 43.[109]

The correlation coefficient (ρ) and diversity gain are dependent on each other. Maximum theoretical diversity gain and correlation coefficient are related by Equation (18). The envelop correlation coefficient (ECC), which is a measurement of channel condition and diversity behavior is given by Equation (19). For the good diversity behavior by the MIMO, ECC should be <0.5.[110-112]
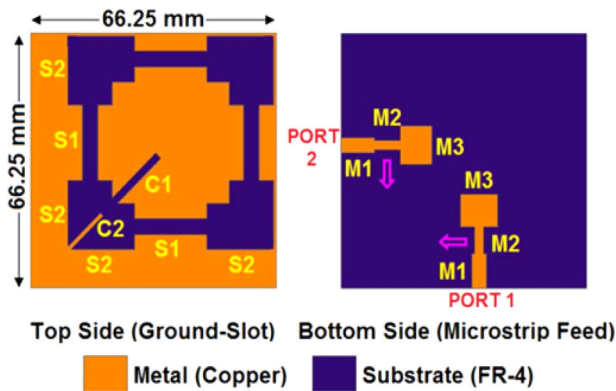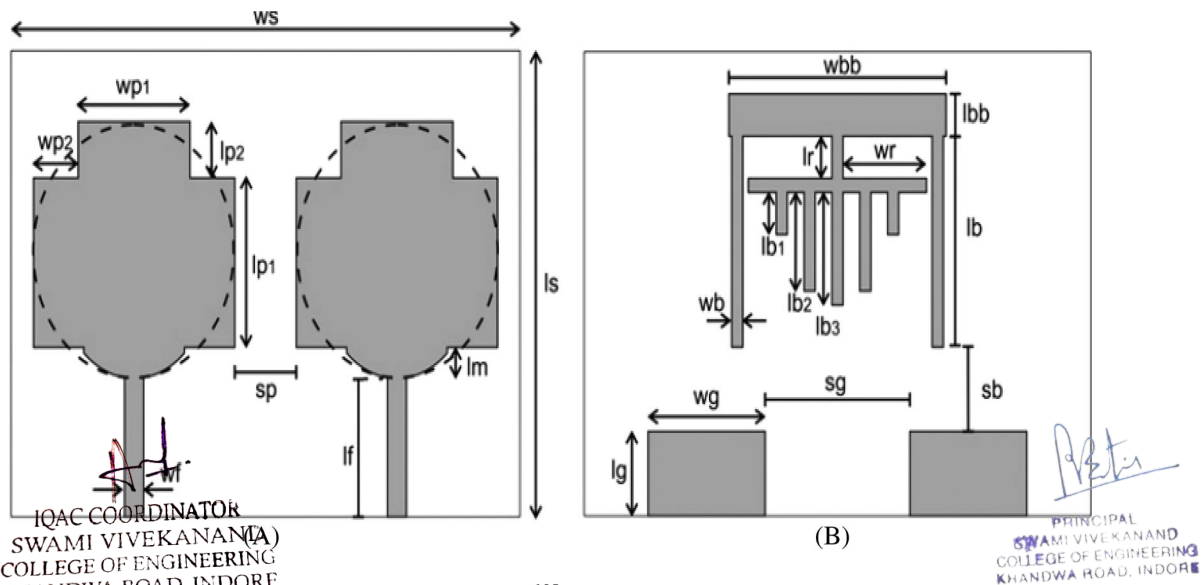

FIGURE 40 Antenna geometry©[103]

FIGURE 41 MIMO antenna: A, top view and B, bottom view©[105]

$$G_{DG} = 10*\sqrt{1 - |\rho|^2} \qquad (18)$$

$$|\rho_e(i,j,N)| = \frac{\left|\sum_{n=1}^{N} S_{i,n}^* S_{n,j}\right|}{\sqrt{\left|\prod_{k(=i,j)}\left[1 - \sum_{n=1}^{N} S_{i,n}^* S_{n.k}\right]\right|}} \qquad (19)$$

where i, j, n are the variables and N is the number of ports.

A UWB reconfigurable antenna for cognitive radio was presented for the 3.2 to 10.6 GHz frequency range. A
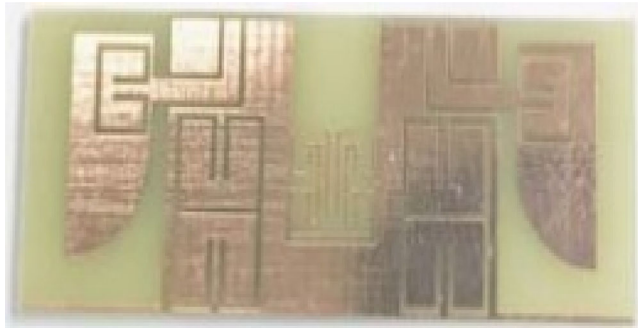

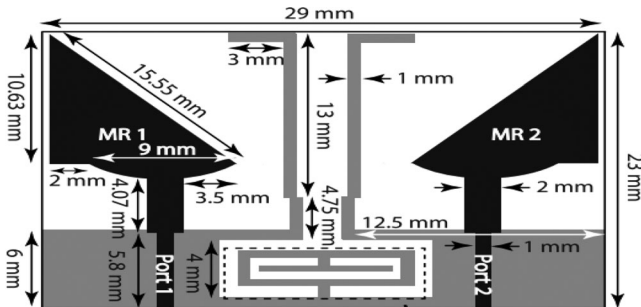**FIGURE 42**   SRR based antenna geometry[107]

FIGURE 43   UWB MIMO with CSRR©[108]

circular patch was used on 50×40 mm^2 on FR-4 dielectric substrate. For the reconfigurability, horizontal slots and PIN diodes are used. The length of slots can be adjusted by switching diodes on/off. These switches work like filters to allow desired frequency and suppress other frequencies. The antenna achieved gain of 2.48 dBi for UWB, and 2.57 to 3.95 dBi in reconfigurable mode.[113]

A printed bell-shaped monopole antenna with a short stub was designed for UWB application. The designed antenna occupied $28 \times 20 \times 1.6$ mm^3 on FR-4 dielectric substrate. The RLC parallel circuit model was used to analyze the antenna impedance in design. It is considered that short stub represents LC series circuit, and is connected in shunt with the antenna to provide broadband behavior. UWB antenna gain was 2.1 to 4.7 dBi in the UWB band.[114]

Four ports hook shaped planar MIMO with meander line radiators and partial ground structure and perfect boundary conditions was designed for wireless applications. The antenna occupied 45.9×45.9 mm^2 on FR-4 substrate and covered frequencies in 4.76 to 10.6 GHz band. Meander lines were used to show the broadband characteristics for this design. The gap between the higher arm and folded arm was responsible for wideband characteristics. The design exhibited 3.6 dBi gain and more than 66% radiation efficiency in whole band. The orthogonal placement of elements resulted in isolation improvement. The isolation in the band was 15.0 dB.[115]

A two-port antenna of size 20×34 mm^2 was designed with better than 20.0 dB isolation. The antenna uses two half hexagon radiating patches with counter facing for size reduction. Dual CSRR are used here. One is on the bottom of ground plane and other at the top of antenna. These CSRR structures act as wave trapping structure for the surface wave, and the arrangement results in better than 20.0 dB isolation.[116] Isolation can also be improved by using simple orthogonal orientation of radiating

TABLE 1   UWB antennas

Ref. no.	Frequency band (GHz)	Size (mm²)	Substrate	Gain (dBi)
34	2.78-12.9	19.0 × 21.0	FR-4	0.84-1.76
39	3.1-10.6	40.0 × 40.0	-	4.0
40	3.1-10.6	35.0 × 40.0	Taconic ORCER RF-35	<3.1
41	3.95-10.4	60.0 × 60.0	Rogers TMMI	-
42	2.9-10.6	26.0 × 40.0	RO4350B	0.9-6.5
43	3.1-10.6	36.0 × 36.0	FR-4	6.9
44	3.1-12.0	32.0 × 32.0	FR-4	1.5-4.1
45	3.1-10.6	26.0 × 31.0	RO4003	−2.0-5.8
46	3.1-10.6	32.0 × 32.0	FR-4	1.7-4.2
47	3.1-10.6	21.0 × 38.0	RO4350B	1.3-4.2

Ref. no.	Frequency band (GHz)	Size (mm²)	Substrate	Gain (dBi)
48	2.2-13.3	50.0 × 82.0	FR-4	2.44 and 4.78
49	1.8-12.0	40.0 × 68.0	FR-4	-
50	2.8-14.0	40.0 × 40.0	FR-4	4-5
51	2.49-19.41	20.0 × 20.0	Rogers 5880	5.98
52	2.85-11.9	30.0 × 30.0	FR-4	-
53	2.25-12.0	76.25 × 52.25	FR-4	3 and 5
54	2.5-12.0	23.0 × 39.8	Rogers TMM4	2.5-5.3
55	2.2-10.6	40.3 × 30.4	FR-4	3
57	2.99-10.87	30.0 × 32.0	FR-4	3.2-7.3

T A B L E 2 Lower than 3.1 GHz bands

T A B L E 3 Single and double notch band UWB antennas

Ref. no.	Frequency band (GHz)	Size (mm²)	Notch frequency/ band (GHz)	Substrate	Gain (dBi)	ECC	Rejection m agnitude (dB)
58	3.15-10.63	26.0 × 30.0	5.15-5.82, 7.25-8.39	FR-4	-	-	−1.0
67	3.1-10.6	33.0 × 26.0	5.2	FR-4	1.0-6.0	<0.03	−1.0
68	2.5-12	48.0 × 48.0	5.5	FR-4	<3.0	<0.005	−2.0
69	2.8-11.5	50.0 × 28.0	3.3-3.9	FR-4	-	<0.0003	−2.0
70	3.08-10.98	30.0 × 30.0	4.96-5.96	FR-4	5	<0.013	−2.5
71	2.95-10.8	44.0 × 44.0	5.10-5.95	FR-4	2.4-4.0	<0.04	−1.5
72	3.08-11.8	38.5 × 38.5	5.03-5.97	FR-4	1.4-3.6	<0.02	−1.5
75	3.0-12.0	47.0 × 25.7	4.59-6.0, 8.92-9.9	FR-4	2.0-5.45	<0.001	−1.0
76	3.1-10.65	0.131 λ_g × 0.131 λ_g	3.35-3.55, 5.65-5.95	-	1.7-4.2	<0.002	−1.5
77	3-13.6	20.0 × 20.0	3.0-4.2, 5.0-5.78	FR-4	0 to −6	-	−2.0
78	2.0-12.0	35.0 × 30.0	3.4-3.6, 5.725-5.825	Roger 5870	-	<0.015	−2.0

T A B L E 4 More than two notch band UWB antennas

Ref. no.	Frequency band (GHz)	Size (mm²)	Notch frequency/band (GHz)	Substrate	Gain (dBi)	ECC	Rejection magnitude (dB)
62	2.0-11.0	50.0 × 50.0	1.78-1.91, 2.28-3.120, 5.4-6.0	FR-4	−3.5 to 6.5	-	−1.0
63	3.0-15.0	31.0 × 22.0	3.3-3.7, 5.15-5.85, 7.1-7.76	FR-4	-	-	−1.0
83	2.8-12.2	18.0 × 21.0	3.3-3.7, 5.15-6.0, 7.8-8.4	FR-4	2.0-5.0	<0.013	−1.5
92	3.1-10.6	30.0 × 45.0	3.25–3.9, 5.11-5.35, 5.5-6.06, 7.18-7.88	FR-4	-	<0.02	−2.0

patch. A four-element hexagon fractal shape antenna was designed for UWB frequency band with half circular shape ground plane for individual radiating element. In this technique more space is occupies, which in turn improves isolation. The design has better than 20.0 dB isolation in band.

All the above designs are compared in Table 1, Table 2, Table 3, Table 4, and Table 5 with their frequency bands, size, substrates, gain, and rejection magnitudes in notched bands for UWB antennas, 2.0 to 11.0 GHz and higher bands, single and double notch antennas, more than two notch antennas, and isolation approaches. It has been

TABLE 5 Results based on isolation methods

Ref. no.	Frequency band (GHz)	Size (mm²)	Substrate	Gain (dBi)	Isolation (dB)	ECC
95	2.19-11.07	40.0 × 41.0	FR-4	6.5	>20.0	<0.25
96	3.0-11.0	48.0 × 48.0	FR-4	4.0	-	-
97	1.8-4.2	130 × 71.7	Rogers RT/5880	6.0	<40.0	-
98	2.0-8.0	36.0 × 22.0	FR-4	-	>18.0	0.05
99	3.0-0.9	24.0 × 24.0	FR-4	-	>20.0	<0.002
101	2.5-11.0	50.0 × 40.0	FR-4	>2.11	>15.0	<0.02
102	3.1-10.6	30.0 × 40.0	FR-4	-	>20.0	<0.15
103	3.0-12.0	66.25 × 66.25	FR-4	5.0-8.0	>20.0	<0.005
104	0.7-2.0	20.0 × 23.0	RO4003C	-	>40.0	-
105	3.1-10.6	33.0 × 45.5	-	5.3	>20.0	<0.09
106	3.0-12.0	30.0 × 60.0	FR-4	5.0	>15.0	<0.0008
108	3.0-12.0	23.0 × 29.0	Rogers TMM4	1.2-5.9	>15.0	<0.15

observed that there is a tradeoff between the gain and the bandwidth in these antennas. In some cases, size has become the function of the bandwidth. Also, the bandwidth is dependent on the type of substrate used.

5 | ANALYSIS AND DISCUSSION

The above-discussed antennas have been analyzed for different UWB antenna designs for bandwidth enhancement, notch band characteristics, and isolation improvement. Various structures were analyzed, which modified the current path to achieve lower frequency characteristics. Slot etching is interesting method because stepped slot can resonate at some frequency as well as slots can act as filters, which can reduce the gain in selective frequency band, so the antenna can perform notch characteristics. But some specialized structures like SRR and CSRR can trap the surface current, so in MIMO antenna both ports can be isolated. The slot cutting has multiple purposes. For isolation improvement, space diversity and orthogonal polarization diversity are used. The space variation increases the size of the antenna, while orthogonal polarization saves the space without making complex structures.

The shape of the radiation pattern with both the azimuthal and elevation angles is dependent on the design of the antenna element/elements, ground plane, ground arms, slots in radiating element/ground, location of the slots, placement of elements, type of feed/feed structure, parasitic elements, neutralization line, DR, and metamaterials. Due to these, the shape of the radiation pattern may be directional, bidirectional, or omnidirectional.

The UWB antennas with minimum size of 19.0 × 21.0 mm², gain of 0.84 dBi (minimum) to 6.5 dBi

(maximum), and frequency values of 2.78 GHz (minimum) to 12.9 GHz (maximum) have been observed in Table 1. These antennas cover the applications of some part of WiMAX and WLAN spectrums also. The UWB antennas with lower than 3.1 GHz band category have been observed with minimum size of 20.0 × 20.0 mm², gain of 2.44 dBi (minimum) to 5.98 dBi (maximum), and frequency values of 1.8 GHz (minimum) to 19.4 GHz (maximum) in Table 2. These antennas cover the applications of some part of WiMAX, WLAN spectrums, RFID, ITU band, and X-band also. The single and double notch UWB antennas with minimum size of 20.0 × 20.0 mm², gain of −6.0 dBi (minimum) to 6.0 dBi (maximum), and frequency values of 2.0 GHz (minimum) to 13.6 GHz (maximum) in Table 3 have been observed. More than two notches UWB antennas with minimum size of 18.0 × 21.0 mm², gain of −3.5 dBi (minimum) to 6.5 dBi (maximum), rejection band in the range of −1.0 dB to −2.0 dB, and frequency values of 2.0 GHz (minimum) to 15.0 GHz (maximum) in Table 4 have been observed. The applications of Table 3 and Table 4 have same applications as Table 2. Similarly, MIMO antennas with/without UWB antennas with minimum size of 20.0 × 23.0 mm², gain of 2.1 dBi (minimum) to 8.0 dBi (maximum), isolation 15 dB to 40 dB, and frequency values of 0.7 GHz (minimum) to 12.0 GHz (maximum) in Table 5 have been observed. These antennas cover the applications of LTE, WLAN, WiMAX, UWB, and RFID, and so forth.

6 | CONCLUSION

The fastest growth in wireless communication showed its strong candidacy for UWB antennas an exceptional technology to replace the conventional wireless technologies.

The article includes variety of UWB antennas with their basic UWB bands, bandwidth extension, and notch designs. The article includes single and multi-element structures. In case of multi-element structures, the effect of isolation between the antennas and their effects are also considered. UWB covered most of the communication applications. UWB with MIMO has a great advantage of covering high data rate applications with high capacity, reliability of signals, and high spectral efficiency. This advantage is important because of the reflection coefficient. Most of the discussed antennas in literature have 2:1 VSWR and corresponding return loss of −9.6 dB or reflection coefficient of 0.33. With respect to the reflection coefficient of 0.33, corresponding radiated/transmitted power is 89%. Some of the discussed antennas have 3:1 VSWR and corresponding return loss of −6.0 dB or reflection coefficient of 0.5. With respect to the reflection coefficient of 0.25, corresponding radiated/transmitted power is 75%.

ORCID

Leeladhar Malviya https://orcid.org/0000-0002-7342-4766

REFERENCES

1. Barrett TW. History of Ultra WideBand (UWB) Radar & Communications: Pioneers and Innovators. Progress in Electromagnetics Symposium 2000 (PIERS2000); July 2000; Cambridge, MA.
2. Schantz H. *The Art and Science of Ultra Wideband Antennas*. Boston, MA: Artech House; 2005.
3. Schantz HG. A brief history of UWB antennas. *IEEE Aerospace Electron Syst Mag*. 2004;19(4):22-26.
4. Schantz HG. Three centuries of UWB antenna development. IEEE International Conference on Ultra-Wideband; Syracuse, NY; 2012, 506-512.
5. Stutzman WL, Thiele GA. *Antenna Theory and Design*. 3rd ed. Wiley Publication; 2012.
6. Ramsay J. Highlights of antenna history. *IEEE Antennas Propag Soc Newslett*. 1981;23(6):7-20.
7. Dellinger JH. Principles of radio transmission and reception with antenna and coil aerials. *Trans Am Inst Electr Eng*. 1919; XXXVIII(2):1347-1414.
8. Yagi H, Uda S. Projector of the sharpest beam of electric waves. *Proc Imperial Acad*. 1926;2(2):49-52.
9. Chamberlain AB, Lodge WB. The broadcast antenna. *Proc Inst Radio Eng*. 1936;24(1):11-35.
10. Brown GH. Directional antennas. *Proc Inst Radio Eng*. 1937; 25(1):78-145.
11. Kraus JD. The corner-reflector antenna. *Proc IRE*. 1940;28 (11):513-519.
12. Levy GF. Loop antennas for aircraft. *Proc IRE*. 1943;31(2): 56-66.
13. Riblet HJ. Microwave omnidirectional antennas. *Proc IRE*. 1947;35(5):474-478.
14. Kolster FA. Antenna design for television and FM reception. *Proc IRE*. 1948;36(10):1242-1248.
15. Peixeiro C. Microstrip patch antennas: an historical perspective of the development SBMO/IEEE MTT-S. International Microwave and Optoelectronics Conference (IMOC) (2011); Natal; 2011, 684-688.
16. Fubini EG. Stripline radiators. *IRE Trans Microw Theory Techn*. 1955;3(2):149-156.
17. Anguera J, Andújar A, Huynh M-C, Orlenius C, Picher C, Puente C. Advances in antenna technology for wireless handheld devices. *Int J Antennas Propag*. 2013;25.
18. Carver K, Mink J. Microstrip antenna technology. *IEEE Trans Antennas Propag*. 1981;29(1):2-24.
19. Taga T, Tsunekawa K. Performance analysis of a built-in planar inverted F-antenna for 800 MHz band portable radio units. *IEEE J Sel Areas Commun*. 1987;5(5):921-929.
20. Ogawa K, Uwano T. A diversity antenna for very small 800-MHz band portable telephones. *IEEE Trans Antennas Propag*. 1994;42(9):1342-1345.
21. Hirokawa J, Ando M, Goto N, Takahashi N, Ojima T, Uematsu M. A single-layer slotted leaky waveguide array antenna for mobile reception of direct broadcast from satellite. *IEEE Trans Veh Technol*. 1995;44(4):749-755.
22. Liu ZD, Hall PS. Dual-band antenna for hand held portable telephones. *Electron Lett*. 1996;32(7):609-610.
23. Liu ZD, Hall PS, Wake D. Dual-frequency planar inverted-F antenna. *IEEE Trans Antennas Propag*. 1997;45(10):1451-1458.
24. Douglas MG, Okoniewski M, Stuchly MA. A planar diversity antenna for handheld PCS devices. *IEEE Trans Veh Technol*. 1998;47(3):747-754.
25. Lee E, Hall PS, Gardner P. Compact wideband planar monopole antenna. *Electron Lett*. 1999;35(25):2157-2158.
26. Chen ZN, Chia MYW. Broadband planar inverted-L antennas. *IEEE Proc Microw Antennas Propag*. 2001;148(5):339-342.
27. Yang M, Chen Y. A novel U-shaped planar microstrip antenna for dual-frequency mobile telephone communications. *IEEE Trans Antennas Propag*. 2001;49(6):1002-1004.
28. Venneeren G, Rogier H, Olyslager F, de Zutter D. Low-cost planar rectangular ring antenna for operation in HiperLAN band. *Electron Lett*. 2002;38(5):208-209.
29. Howell J. Microstrip antennas. *IEEE Trans Antennas Propag*. 1975;23(1):90-93.
30. Haraz OARS. In: Kishk A, ed. *Advancement in Microstrip Antennas with Recent Applications*. InTech; 2013.
31. Fei P, Jiao Y-C, Hu W. A compact CPW-fed finger-shaped antenna for UWB application. Proceedings of the 9th International Symposium on Antennas, Propagation and EM Theory; Guangzhou; 2010, 79-82.
32. Zhang S, Lau BK, Sunesson A, He S. Closely-packed UWB MIMO/diversity antenna with different patterns and polarizations for USB dongle applications. *IEEE Trans Antennas Propag*. 2012;60(9):4372-4380.
33. Iglesias ER, Teruel OQ, Pablo-Gonzalez ML, Sanchez-Fernandez M. A compact dual mode microstrip patch antenna for MIMO applications. IEEE Antennas and Propagation Society International Symposium; Albuquerque, NM; 2006, 3651-3654.
34. Tang T, Lin K. An ultra wideband MIMO antenna with dual band-notched function. *IEEE Antennas Wirel Propag Lett*. 13 (2014):1076-1079.

35. Chandel R, Gautam A, Kanaujia B. A compact rhombus-shaped slot antenna fed by microstrip-line for UWB applications. *Int J Microw Wirel Technol*. 2017;9(2):403-409.

36. Reha A, El Amri A, Benhmammouch O, Oulad Said A, El Ouadih A, Bouchouirbat M. CPW-fed H-tree fractal antenna for WLAN, WIMAX, RFID, C-band, HiperLAN, and UWB applications. *Int J Microw Wirel Technol*. 2016;8(2):327-334.

37. Mao C-X, Qing-Xin C. Miniaturization of UWB antenna by asymmetrically extending stub from ground. *J Electromagn Waves Appl*. 2014;28(5):531-541.

38. Baudha S, Yadav MV. A novel design of a planar antenna with modified patch and defective ground plane for ultra-wideband applications. *Microw Opt Technol Lett*. 2019;61:1320-1327.

39. Hota S, Baudha S, Mangaraj BB, Yadav MV. A compact, ultrawide band planar antenna with modified circular patch and a defective ground plane for multiple applications. *Microw Opt Technol Lett*. 2019;61:2088-2097.

40. Adamiuk G, Beer S, Wiesbeck W, Zwick T. Dual-orthogonal polarized antenna for UWB-IR technology. *IEEE Antennas Wirel Propag Lett*. 2009;8:981-984.

41. Zhang S, Ying Z, Xiong J, He S. Ultra wideband MIMO/diversity antennas with a tree-like structure to enhance wideband isolation. *IEEE Antennas Wirel Propag Lett*. 2009;8:1279-1282.

42. Trivedi K, Pujara D. Mutual coupling reduction in wideband tree shaped fractal dielectric resonator antenna array using defected ground structure for MIMO applications. *Microw Opt Technol Lett*. 2017;59:2735-2742.

43. Liu L, Cheung SW, Yuk TI. Compact MIMO antenna for portable devices in UWB applications. *IEEE Trans Antennas Propag*. 2013;61(8):4257-4264.

44. Zhao H, Zhang F, Wang C, Zhang X. A universal methodology for designing a UWB diversity antenna. *J Electromagn Waves Appl*. 2014;28(10):1221-1235.

45. Huang H-F, Xiao S-G. A compact polarization diversity UWB MIMO antenna with a fork-shaped decoupling structure. *Prog Electromagn Res Lett*. 2017;69:87-92.

46. Malekpour N, Honarvar MA. Design of high-isolation compact MIMO antenna for UWB application. *Prog Electromagn Res C*. 2016;62:119-129.

47. Ren J, Hu W, Yin Y, Fan R. Compact printed MIMO antenna for UWB applications. *IEEE Antennas Wirel Propag Lett*. 2014;13:1517-1520.

48. Liu L, Cheung SW, Yuk TI. Compact multiple-input–multiple-output antenna using quasi-self-complementary antenna structures for ultra wideband applications. *IET Microw Antennas Propag*. 2014;8(13):1021-1029.

49. Toktas A. G-shaped band-notched ultra-wideband MIMO antenna system for mobile terminals. *IET Microw Antennas Propag*. 2017;11(5):718-725.

50. Kumar R, Surushe G. Design of microstrip-fed printed UWB diversity antenna with tee crossed shaped structure. *Int J Eng Sci Technol*. 2016;19(2):946-955.

51. Krishna RVS, Ram Kumar R. A slotted UWB monopole antenna with single port and double ports for dual polarization. *Int J Eng Sci Technol*. 2016;19(1):470-484.

52. Sharma M, Awasthi YK, Singh H, Kumar R, Kumari S. Compact printed high rejection triple band-notch UWB antenna with multiple wireless applications. *Int J Eng Sci Technol*. 2016;19(3):1626-1634.

53. Tao J, Feng QY. Compact isolation-enhanced UWB MIMO antenna with band-notch character. *J Electromagn Waves Appl*. 2016;30(16):2206-2214.

54. Krishna RVS, Ram Kumar R. Design and investigations of a microstrip fed open V-shape slot antenna for wideband dual slant polarization. *Int J Eng Sci Technol*. 2015;18(4):513-523.

55. Khan MS, Capobianco A, Naqvi A, Ijaz B, Asif S, Braaten BD. Planar, compact ultra-wideband polarization diversity antenna array. *IET Microw Antennas Propag*. 2015;9(15):1761-1768.

56. Abdelraheem AM, Abdalla MA. Compact curved half circular disc-monopole UWB antenna. *Int J Microw Wirel Technol*. 2016;8(2):283-290.

57. Sipal D, Abegaonkar MP, Koul SK. Easily extendable compact planar UWB MIMO antenna array. *IEEE Antennas Wirel Propag Lett*. 2017;16:2328-2331.

58. Yeo J. Miniaturized UWB stepped open-slot antenna. *Prog Electromagn Res Lett*. 2018;78:119-127.

59. Yadav A, Sethi D, Khanna RK. Slot loaded UWB antenna: dual band notched characteristics. *AEU-Int J Electron C*. 2016;70(3):331-335.

60. Mohamed HAE, Elkorany AS, Saad SA, Saleeb DA. New simple flower shaped reconfigurable band-notched UWB antenna using single varactor diode. *Prog Electromagn Res C*. 2017;76:197-206.

61. Nejatijahromi M, Naghshvarianjahromi M, Rahman MU. Compact CPW fed switchable UWB antenna as an antenna filter at narrow-frequency bands. *Prog Electromagn Res C*. 2018;81:199-209.

62. Bong H-U, Jeong M, Hussain N, Rhee S-Y, Gil S-K, Kim N. Design of an UWB antenna with two slits for 5G/WLAN-notched bands. *Microw Opt Technol Lett*. 2019;61:1295-1300.

63. Zarrabi FB, Mansouri Z, Gandji NP, Kuhestani H. Triple-notch UWB monopole antenna with fractal Koch and T-shaped stub. *AEU-Int J Electron C*. 2016;70(1):64-69.

64. Bakariya PS, Dwari S, Sarkar M. Triple band notch UWB printed monopole antenna with enhanced bandwidth. *AEU-Int J Electron C*. 2015;69(1):26-30.

65. Nasrabadi E, Rezaei P. A novel design of reconfigurable monopole antenna with switchable triple band-rejection for UWB applications. *Int J Microw Wirel Technol*. 2016;8(8):1223-1229.

66. Doddipalli S, Kothari A. Compact UWB antenna with integrated triple notch bands for WBAN applications. *IEEE Access*. 2019;7:183-190.

67. Yoo M, Lim S. SRR- and CSRR-loaded ultra-wideband(UWB) antenna with tri-band notch capability. *J Electromagn Waves Appl*. 2013;27(17):2190-2197. https://doi.org/10.1080/09205071.2013.837013.

68. Liu G, Liu Y, Gong S. Compact uniplanar UWB MIMO antenna with band-notched characteristic. *Microw Opt Technol Lett*. 2017;59:2207-2212.

69. Gao P, He S, Wei X, Xu Z, Wang N, Zheng Y. Compact printed UWB diversity slot antenna with 5.5 GHz band-notched characteristics. *IEEE Antennas Wirel Propag Lett*. 2014;13:376-379.

70. Ibrahim AA, Machac J, Shubair RM. Compact UWB MIMO antenna with pattern diversity and band rejection characteristics. *Microw Opt Technol Lett*. 2017;59:1460-1464.

71. Biswal SP, Das S. A low-profile dual port UWB-MIMO/diversity antenna with band rejection ability. *Int J RF Microw Comput Aided Eng*. 2018;28(1):e21159.

72. Liu Y, Tu Z. Compact differential band-notched stepped-slot UWB-MIMO antenna with common-mode suppression. *IEEE Antennas Wirel Propag Lett*. 2017;16:593-596.

73. Kang L, Li H, Wang X, Shi X. Compact to offset microstrip-fed MIMO antenna for band-notched UWB applications. *IEEE Antennas Wirel Propag Lett*. 2015;14:1754-1757.

74. Tripathi S, Mohan A, Yadav SK. A compact MIMO/diversity antenna with WLAN band-notch characteristics for portable UWB applications. *Prog Electromagn Res C*. 2017;77:29-38.

75. Sharbati V, Rezaei P, Fakharian MM, Beiranvand E. A switchable band-notched UWB antenna for cognitive radio applications. *IETE J Res*. 2015;61(4):423-428.

76. Satam V, Nema S. Dual notched, high gain diversity antenna for wide band applications. *Microw Opt Technol Lett*. 2017;59:1222-1226.

77. Li WT, Hei YQ, Subbaraman H, Shi XW, Chen RT. Novel printed filtenna with dual notches and good out-of-band characteristics for UWB-MIMO applications. *IEEE Microw Wirel Compon Lett*. 2016;26(10):765-767.

78. Borhani Kakhki M, Rezaei P. Reconfigurable microstrip slot antenna with DGS for UWB applications. *Int J Microw Wirel Technol*. 2017;9(7):1517-1522.

79. Wani Z, Kumar D. Dual-band-notched antenna for UWB MIMO applications. *Int J Microw Wirel Technol*. 2017;9(2):381-386.

80. Li Z, Yin C, Zhu X. Compact UWB MIMO Vivaldi antenna with dual band-notched characteristics. *IEEE Access*. 2019;7:38696-38701.

81. Gautam AK, Yadav S, Rambabu K. Design of ultra-compact UWB antenna with band-notched characteristics for MIMO applications. *IET Microw Antennas Propag*. 2018;12(12):1895-1900.

82. Chandel R, Gautam AK, Rambabu K. Tapered fed compact UWB MIMO-diversity antenna with dual band-notched characteristics. *IEEE Trans Antennas Propag*. 2018;66(4):1677-1684.

83. Jetti CR, Nandanavanam VR. A very compact MIMO antenna with triple band-notch function for portable UWB systems. *Prog Electromagn Res C*. 2018;82:13-27.

84. Zhang H, Zhao J. A new compact microstrip UWB power divider with triple notched bands. *Prog Electromagn Res Lett*. 2018;78:111-117.

85. Sharma M, Awasthi YK, Singh H. Design of CPW-fed high rejection triple band-notch UWB antenna on silicon substrate with diverse wireless applications. *Prog Electromagn Res C*. 2017;74:19-30.

86. Devi M, Gautam A, Kanaujia B. A compact ultra-wideband antenna with triple band-notch characteristics. *Int J Microw Wirel Technol*. 2016;8(7):1069-1075.

87. Yang H, Xi X, Wang L, Zhao Y, Shi X, Yuan Y. Design of reconfigurable filtering ultra-wideband antenna with switchable band-notched functions. *Int J Microw Wirel Technol*. 2019;11(4):368-375.

88. Tang Z, Wu X, Zhan J, Hu S, Xi Z, Liu Y. Compact UWB-MIMO antenna with high isolation and triple band-notched characteristics. *IEEE Access*. 2019;7:19856-19865.

89. Cui L, Liu H, Hao C. Spline novel UWB antenna with triple band-notches for WiMAX and WLAN. *Prog Electromagn Res Lett*. 2019;82:101-106.

90. Liao X-J, Yang H-C, Han N, Li Y. A semi-circle-shaped aperture UWB antenna with triple band-notched character. *J Electromagn Waves Appl*. 2011;25(2-3):257-266.

91. Borhani S, Honarvar M, Virdee B. Quad notched-band UWB BPF based on quintuple-mode resonator. *Int J Microw Wirel Technol*. 2017;9(7):1433-1439.

92. Wu L, Xia Y, Cao X, Xu Z. A miniaturized UWB-MIMO antenna with quadruple band-notched characteristics. *Int J Microw Wirel Technol*. 2018;10(8):948-955.

93. Wu L, Xia Y. Compact UWB–MIMO antenna with quad-band-notched characteristic. *Int J Microw Wirel Technol*. 2017;9(5):1147-1153.

94. Zhang X-M, Ma J, Li C-X, Ma A-S, Wang Q, Shao M-X. A new planar monopole UWB antenna with quad notched bands. *Prog Electromagn Res Lett*. 2019;81:39-44.

95. Sahu B, Singh S, Meshram MK, Singh SP. A new compact ultra-wideband filtering antenna with improved performance. *J Electromagn Waves Appl*. 2019;33(1):107-124.

96. Liu X, Wang Z, Yin Y, Ren J, Wu J. A compact ultra wideband MIMO antenna using QSCA for high isolation. *IEEE Antennas Wirel Propag Lett*. 2014;13:1497-1500.

97. Mao C, Chu Q. Compact co-radiator UWB-MIMO antenna with dual polarization. *IEEE Trans Antennas Propag*. 2014;62(9):4474-4480.

98. Aghdam SA, Bagby JS, Pla RJ. Mutual coupling reduction of closely spaced MIMO antenna based on electric resonator. *Prog Electromagn Res Lett*. 2016;64:1-6.

99. Katie MO, Jamlos MF, Mohsen Alqadami AS, Jamlos MA. Isolation enhancement of compact dual-wideband MIMO antenna using flag-shaped stub. *Microw Opt Technol Lett*. 2017;59:1028-1032.

100. Srivastava G, Mohan A, Chakraborty A. A compact multidirectional UWB MIMO slot antenna with high isolation. *Microw Opt Technol Lett*. 2017;59:243-248.

101. Malviya L, Panigrahi RK, Kartikeyan MV. A 2×2 dual-band MIMO antenna with polarization diversity for wireless applications. *Prog Electromagn Res C*. 2016;61:91-103.

102. Lin G, Sung C, Chen J, Chen L, Houng M. Isolation improvement in UWB MIMO antenna system using carbon black film. *IEEE Antennas Wirel Propag Lett*. 2017;16:222-225.

103. Deng J, Guo L, Liu X. An ultra-wideband MIMO antenna with a high isolation. *IEEE Antennas Wirel Propag Lett*. 2016;15:182-185.

104. Krishna RVSR, Kumar R. A dual-polarized square-ring slot antenna for UWB, imaging, and radar applications. *IEEE Antennas Wirel Propag Lett*. 2016;15:195-198.

105. Lin M, Li Z. A compact 4 × 4 dual band-notched UWB MIMO antenna with high isolation. 2015 IEEE 6th International Symposium one Microwave, Antenna, Propagation, and EMC Technologies (MAPE); Shanghai; 2015, 126-128.

106. Khan MS, Capobianco A, Najam AI, Shoaib I, Autizi E, Shafique MF. Compact ultra-wideband diversity antenna with a floating parasitic digitated decoupling structure. *IET Microw Antennas Propag*. 2014;8(10):747-753.

107. Kumar R, Pazare N. A CPW-fed stepped slot UWB antenna for MIMO/diversity applications. *Int J Microw Wirel Technol*. 2017;9(1):151-162.

108. Wang F, Duan Z, Li S, Wang Z-L, Gong Y-B. Compact UWB MIMO antenna with metamaterial-inspired isolator. *Prog Electromagn Res C*. 2018;84:61-74.

109. Khan MS, Capobianco A, Asif SM, Anagnostou DE, Shubair RM, Braaten BD. A compact CSRR-enabled UWB diversity antenna. *IEEE Antennas Wirel Propag Lett*. 2017;16:808-812.

110. Malviya L, Panigrahi RK, Kartikeyan MV. Four element planar MIMO antenna design for long-term evolution operation. *IETE J Res*. 2018;64(3):367-373.

111. Malviya L, Kartikeyan MV, Panigrahi RK. Multi-standard, multi-band planar multiple input multiple output antenna with diversity effects for wireless applications. *Int J RF Microw Comput Aided Eng*. 2019;29:e21551.

112. Malviya L, Panigrahi RK, Kartikeyan MV. MIMO antennas with diversity and mutual coupling reduction techniques: a review. *Int J Microw Wirel Technol*. 2017;9(8):1763-1780.

113. Niture DV, Jadhav SS, Mahajan SP. Recon UWB antenna for cognitive radio. *Prog Electromagn Res C*. 2017;79:79-88.

114. Takemura N, Ichikawa S. Broad banding of printed bell-shaped monopole antenna by using short stub for UWB applications. *Prog Electromagn Res C*. 2017;78:57-67.

115. Malviya L, Gehlod K, Shakya A. Wide-band meander line MIMO antenna for wireless applications. International Conference on Advances in Computing, Communications and Informatics (ICACCI); Bangalore; 2018, 1663-1667.

116. Mathur R, Dwari S. A compact UWB-MIMO with dual grounded CRR for isolation improvement. *Int J RF Microw Comput Aided Eng*. 2019;29:e21500.

117. Rajkumar S, Anto Amala A, Selvan KT. Isolation improvement of UWB MIMO antenna utilizing molecule fractal structure. *Electron Lett*. 2019;55(10):576-579.

AUTHOR BIOGRAPHIES

Rohit Yadav received his ME (Electronics and Telecommunication) from Shri G. S. Institute of Technology and Science, Indore (MP), India, in 2010 and BE (Electronics and communication) from ShriRam College of Engineering & Management, Morena (MP), India, in 2007. Since 2011, he has been with Swami Vivekanand College of Engineering, Indore (MP), India, serving as an Assistant Professor. His current research interest includes planar antenna and multiple-input-multiple-output (MIMO) antenna designs.

Dr. Leeladhar Malviya received his PhD from IIT Roorkee, India, in 2017. He received his ME in Electronics and Telecommunication Engineering from Shri G. S. Institute of Technology and Science, Indore (MP), India, in 2008, and BE in Electronics and Communication, from the Govt. Engineering College, Ujjain (MP), India, in 1998. Since 2001, he has been with Shri G. S. Institute of Technology and Science, Indore (MP), India, and serving as an Associate Professor. His current research interests include compact multiple-input-multiple-output (MIMO) antennas for high data rate communications for 4G, 5G, and THz planar microstrip antennas, fractal antennas, and metamaterial antennas for communication. He is a Member of IEEE, Institution of Electronics and Telecommunications Engineers (IETE, India), Institution of Engineers (IE, India), and Indian Society for Technical Education (ISTE).

DESIGN AND ANALYSIS OF VALVE SPRING USED INCOMMERCIAL VEHICLE

[1]Amit Singh, [2]Dr.Pradeep patil,[3]Vishal Wankhade,[4]Rahul Joshi

[1]ME student,[2]Associate Professor and HOD,[3]Assistant professor,[4]Assistant professor,
[1]Mechanical,
[1]Swami Vivekanand College ofEngineering,Indore, India

*Abstract :*Valve helical spring is a critical part in valve train of the IC engine. It absorbs energy while opening of the valves and release energy during closing of the valves. It is basically a compression types of helical spring used in commercial vehicles. Spring stiffness plays a vital role in design of helical valve spring. The primary part of designing of valve helical spring is to define the stiffness of spring as per requirement of engine design. Then todesign for space constraints, to design for high fatigue strength, and to design for reliability.

Index Terms– **valve spring, stiffness, fatigue strength.**

I. INTRODUCTION

A reciprocating internal combustion engine uses valves to control air and fuel flow into and out of the cylinders. All cylinders have two valves, first intake valve and second exhaust valve. Intake valve opens just before the intake stroke start. In the petrol engine this allows the air-fuel mixture to enter the cylinder or in case of diesel engine it is only air is allows to enter into the cylinder. Exhaust valve open before the exhaust stroke begins start so that the burned gases can easily escape. The valves are operated by the valve train. We have two types of valve train used for a reciprocating engine depends on the engine ,first on is overhead camshaft with rocker arms, and second one is camshaft in a block with a pushrod. The valve train consists of valves, rocker arms, pushrods, and camshaft and helical springs and the combination of all. If we analysis the data we found the critical component in the valve train is helical spring. Valve springs plays an important role in the controlling of breathing of internal combustion engine, also provide a resisting force that returns displaced valves to their closed position and seal the combustion chamber during compression and combustion. Spring is used to store energy and to absorb shock, or to maintain a force between contacting surfaces. They are generally made of an elastic material formed into the shape of a helix which returns to its natural length when unloaded.

II. METHODOLOGY

Firstly we take design requirement from the engine manufacturer, then we design the component using CAD software after that we performed CAE analysis using HYPERWORKS tools. If there is mismatch between the design requirements and results then make modification as per condition, then manufacture a final product. After that we perform some physical, then again perform fatigue life cycle analysis using CAE software for its sustainability.

III. DESIGN REQUIREMENTS

The reciprocating internal combustion engine is that engine in which the combustion is take place inside the engine cylinder. They are differentiate in manly two categories, first one is as per fuel is used and second one a type of stroke is used. Our research is fully based on four stroke engines in which valve train mechanism is used to control breathing of internal combustion engine. The valve train mechanism is consisting of those parts which actuate the inlet and exhaust valve at the required time with respect to position of piston and crankshaft. In this mechanism the most cruises part is helical spring, may be it is cheapest than all other parts but if this part is disturbed in functioning all engine work and efficiency will disturbed.so the focus of our research is design of valve spring there are some basic requirements followed.

Performance			
	Length of spring	On load	
Free length	58.5 mm	0	Newton's
Installed length	45.5mm	274 ± 1.4	Newton's
required length	41.9mm	850 ± 1.4	Newton's

IV. COMPUTER AIDED DESIGN

CAD stands for Computer-Aided Design; with the help of computer aided design software we can create new design, modified it or may analysis it also. There are so many cad software are used in industries currently like pro-e, cre-o, catia, solid works etc.CAD software are used to increase the productivity, improve the quality of design, improve communication between deign and requirement virtually. That is not only for mechanical engineering but it is also useful for other engineering's also. That's

Page 169

software are very useful in automobile industries for making virtual prototype. In our case we use creo parametric 2.0 as a CAD software, and design our model as per given dimensions.

V. FINITE ELEMENT ANALYSIS

Generally we have three types of technique to solve any engineering problem, first one is Analytical method in which we reached to our solution through formulas and hand calculations, it is a classical approach , it is assumed to 100 % accurate , but this solution only applicable for simple problems . A second technique is numerical method; it is basically a mathematical presentation of a problem in which we use matrix to solve any engineering problem using CAE software, in this technique we does not need to make prototype , it is a simple technique in which we design and analysis our product using computer system. Using this technique we can easily test our product, or make changes according to requirements, but the results cannot be believed blindly, we need to verify our results by other any techniques. A third one technique is physical experiments, in this technique we need to make a real product prototype and test it, if the test will goes failed need to design and modify, and again test is so we can see it was very long term process and very costly also, along with that, we needed an experienced workers for this work. So finally we solved our problem through numerical method, the numerical method basically based on discretization to convert our model from infinite to finite one, assume we have a geometry have infinite number of points, so if we want to analysis it , we have to solve infinite number of equations means we can't achieve the exact solution of our problem. So with the help of discretization, divide our model into countable number of nodes and elements, at the end we got final and exact answer of our equation.

5.1 Meshing

Meshing is process to generate elements in our model or in other term to replace surface or volume by element generation. Basically it is a process of subdivision of geometry in to discrete geometry. There are four types of elements used in mesh generation according to cad model geometry. The followings are described bellowed.

1 D Element – 1 D element are used in one dimensional type of meshing, there are manly three type of 1D elements are used in industries and they are rod , bar and beam.
**Rod**- used where only axial load is applicable, no twisting in the elements like- civil truss members.
Bar- Used where element subjected to multiracial loading like- bolt joint, weld join etc.
Beam- It is same as bar but also support unsymmetrical cross section.

2 D Element – Two dimensional elements are used where two of the dimensions are very large as compared to third one. This type of mashing is used widely in the industries, because it is very simple to manage other than 3 D meshing. There are two types of elements are used in the industries, tria and quad elements.

3 D Element- This type of meshing is used where, there is an no possibility for 2D type of meshing, manly a geometry has variable thickness in shape and have to small curvatures, there are two types of 3D meshing is used in the industries, hex and tetra.
In our case we used tetra type of meshing because our geometry is in 3D , there is a no possibility of 2D meshing and has small curvatures , which need to be cover very carefully.
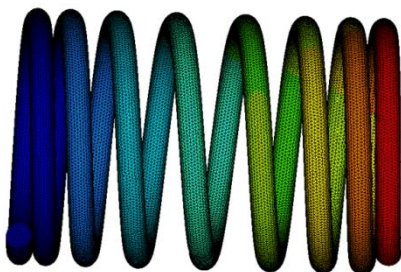

5.2 Meshing Quality

Modelling with Different types of element provides probability to introduce numerical incompatibilities in your model. Incompatibilities arise due to element degrees of freedom do not match at a common node. And mechanisms occur due to some forms of incompatibility or incomplete connectivity.

5.3 Boundary Condition
At our first condition we have to fix one end in all degree of freedom, and applied force at the other end for static structural analysis.

Page 170
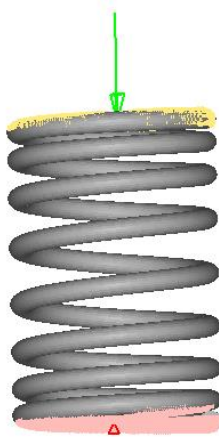
5.4 Analysis

We used optistruct as a solver for this equation, because optistruct considered as a implicit type of solver in which time steps are very large that's why it needs less time as compared to explicit type of solver. In industries mostly all type of static structural analysis solved by optistruct solver.

VI. FINITE ELEMENT ANALYSIS

As the results shows the maximum displacement is 26.06mm and the maximum stress is 694.2 mp, that displacement is not

meet the design requirement and it will failed with respect to safety of factor.
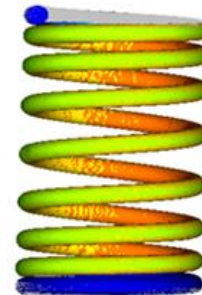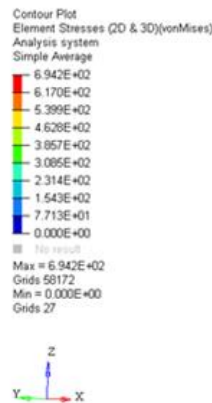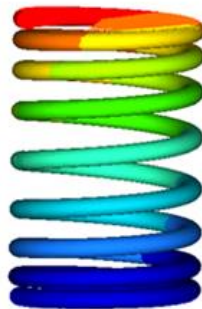
Maximum Displacement- 26.06mm
Maximum Stress   -694.2 mpa

6.1 Comparison and modification

After applying installation load of 274 N we got displacement up to 26.06 and stress 694.2 mpa, we need to achieve first displacement is 13.0 mm and a permissible stress at the same load valve to meet our design requirement.
There are two ways to meet this design requirement; first one is to make modification in basic dimensions of the helical spring and second modification we can make in material properties of heliacal spring, we changed the elasticity of modular up to 4.21E+05 after that we got desired displacement and permissible stress.

Page 171
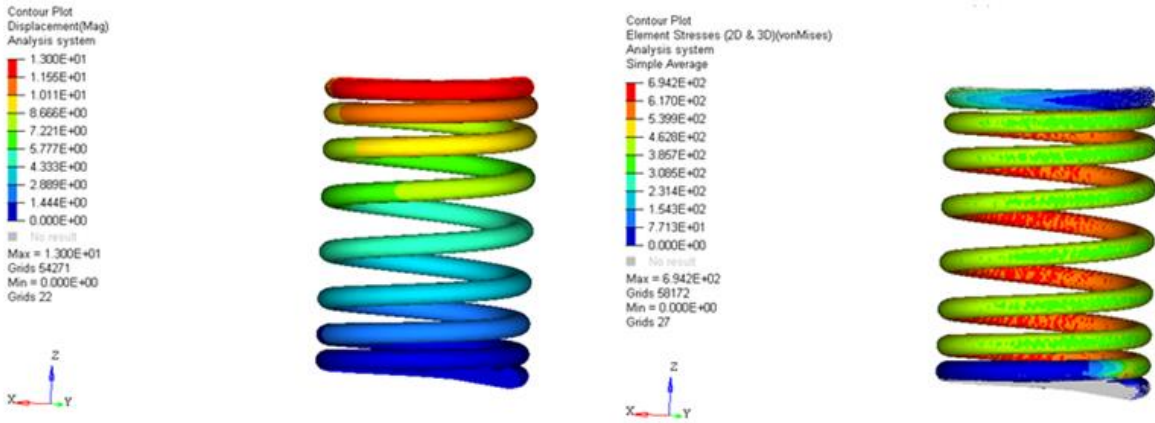
Maximum Displacement- 13.0 mm
Maximum Stress   - 694.2mpa

After applied load of 350 mpa required to operate valve opening.
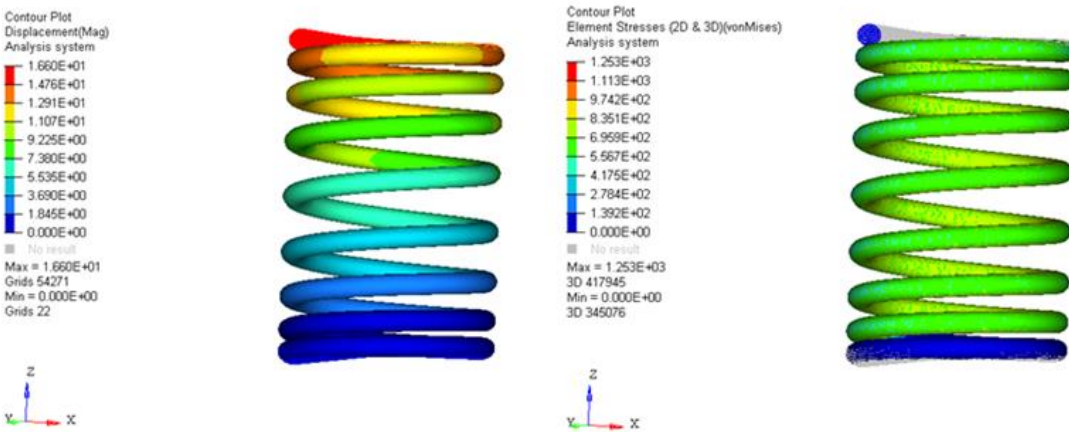
Maximum Displacement- 16.60 mm
Maximum Stress   - 1253mpa

VII. MANUFACTURING

Generally for manufacturing of valve spring we considered two methods low temperature and high temperature according to heat treatment after cooling. With the low temperature heat treatment, the spring is submitted to stress free annealing process after cooling in order to reduce internal stress; this is basically unwanted lowering component strength by this heat treatment. As the second one manly used in the industries to increase stiffness and ductility of spring material.in this process the spring is heated to a temperature above AC3 after cooling and then is quenched. Using this process we can control stiffness, ductility and internal stress of the spring.

There are some conditions are described below according to stiffness –
CONDITION C - Results from heavy cold working (generally 45-50% reduction) of solution treated material.
CONDITION CH900- Heat Condition C material to 900 F (482 C), holds for 1 hour, air cool.
CONDITION A1750- After fabrication, heat solution treated material to 1750 F (955 C), hold for 10 minutes, cool rapidly to room temperature.
CONDITION R100- Within 1 hour of treating to Condition A1750, cool to -100 F (-73 C) and hold for 8 hours.
CONDITION RH 950- From Condition R100 material, heat to 950 F (510 C), hold for 90 minutes, air cool.
CONDITION T- After fabrication, heat to 1400 F (760 C) and hold for 90 minutes. Within 60 minutes, cool to 55 F (13 C), and hold for 1/2 hour.
 CONDITION TH1050- from Condition T, heat to 1050 F (565 C) and hold for 90 minutes, air cool.

Page 172

VIII. PHYSICAL TESTING

After manufacturing of valve helical spring, we test it to calibrate CAE results and physical results and also some other test to know the physical properties of modified material.Firstly we take we take a helical spring and measure its free length by verniercaliper. The measured value is 58.5.After measuring the free length, we are going to calibrate load v/s displacement value, and this can be tested by valve spring pressure testing machine.We applied the load of valve 274N and get the displacement value is 13.0 mm , then load for valve opening is 350N and get displacement of 16.6mm which is approximate same as our CAE results.

IX. FATIGUE LIFE TESTING

In the automobile industries valve spring subjected to high repeated load and are required to reliable for long period of time. The valve helical spring are designed for higher stress so the spring needs to be designed for higher fatigue strength.
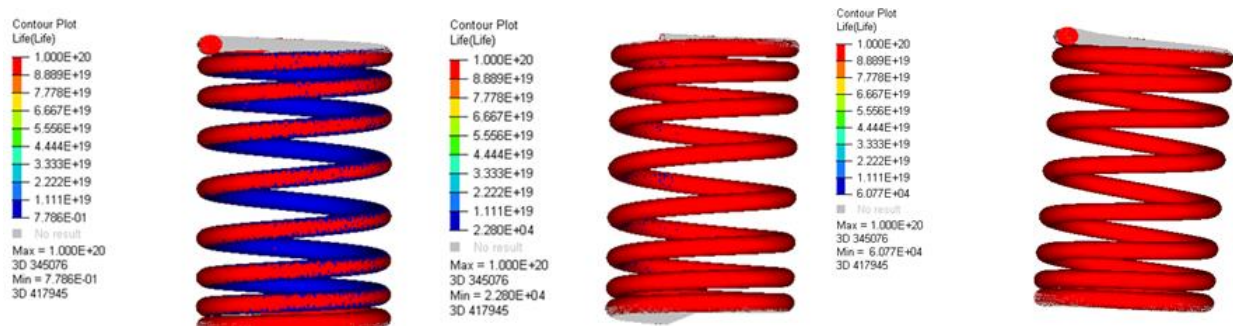
There are three cases for fatigue life test first one is normal steel material with 310 mpa yield stress, when we test it of fatigue we got minimum life of spring is 7.786E-01 that is not useable for the engine, after changing the material property we again test fatigue and we got minimum life of spring is 2.280E+04, then in the third case we changed the diameter of wire from 4.21 to 6mm, and the minimum life of spring we got 6.077E+04 showed in blue region or other than this blue region all component is in red region , the life of red region is more than E+06 which is consider as infinite life , so our helical spring is in safe in both case.

X. CONCLUSION

May be considered the cost of valve helical spring is very low as compared to whole engine sub parts, but the failure of valve helical spring can cause major damages in the engine. And also as per the literature the performance and reliability of an engine is depends on valve spring performance, so that is not a negligible thing in the internal combustion engine , although it is most crucial part of the engine and valve train mechanism. We need to design the valve helical spring by predicting all cause of failure.In our research the spring failed to meet the basic design requirement, after upgrading the modules of elasticity up to 4.21E+05, we meet the design requirement and make the spring stiffer. But in real that is not so easy to gain a desired stiffness that can be gain by heat treatment process , the specific heat treatment we used in our material is heat to 1400 F (760 C) and hold for 90 minutes. Within 60 minutes, cool to 55 F (13 C), and hold for 1/2 hour. This design is also safe in fluctuation loading, have high fatigue strength, and have a maximum permissible stress up to 1260mpa.

XI. REFERENCES

I.   YuxinPenga,b, ShilongWangb, JieZhoub, Song Leib," Structural design, numerical simulation and control system of a machine tool for stranded wire helical springs, Journal of Manufacturing Systems, 2012".

II.   Sid Ali Kaoua, KamelTaibia, NaceraBenghanem, KrimoAzouaoui, Mohammed Azzaza,"Numerical modelling of twin helical spring under tensile loading Applied Mathematical Modelling, 2011.

III.   William H. Skewis Failure Modes of Mechanical Springs Supported System Technology Corporation.

IV.   Sudhakar V "FAILURE ANALYSIS OF AUTOMOBILE VALVE SPRING" Elsevier journals pg.no 513-514.

V.   "A combined analytical, numerical, and experimental study of shape-memory-alloy helical springs" Reza Mirzaeifara, Reginald DesRochesb, ArashYavarib

VI.   GT Conference: Valve Train Validation for New Engine Program- GT Conference: Valve Train Validation for New Engine Program

VII.   H. Yamagata and O. Izumi: Nippon Kinzoku Gakkaishi, 44 (1990) 982 (in Japanese).

Page 173

VIII. The valve spring- Chuo Spring Co., Ltd., Corporate Catalogue, (2003) (in Japanese).

IX. Failure analysis of an automobile valve spring, received, college of science of technology, central Michigan University, Mount Pleasant, MI 48859, USA.

X. Helical coil buckling mechanism for a stiff nanowire on an elastomeric substrate, Center for Applied Mechanics, State Key Laboratory for Strength and Vibration of Mechanical Structure, School of Aero space, Xi'an Jiao tong University, Xi'an 710049, China b Department of Mechanic a land Aero space Engineering, North Carolina State University, NC27695,USA c Columbia, Nano mechanics Research Center, Department of Earth and Environmental Engineering, Columbia University, New York, NY 10027,USA.

XI. Multiracial fatigue and failure analysis of helical compression springs Engineering Failure Analysis 13 (2006) 1303–1313.

XII. Bhandari V B. Design of machine elements.

XIII. BharathrinathGorakhnathKadam, P. H. Jain., Swapnil S. Kulkarni."Design and Analysis of Exhaust Valve spring used in Two wheeler" International Journal of Scientific Research and Management Studies Volume 1 Issue 10, pg: 307-316 .

XIV. CingaramKushal Chary, Dr. Sridara Reddy "DESIGN AND ANALYSIS OF HELICAL COMPRESSION SPRING OF IC ENGINE" International Advanced Research Journal in Science, Engineering and Technology Vol. 3, Issue 10, pg no 153-157.

XV. Syed Mujahid Husain and Siraj Sheikh "DESIGN AND ANALYSIS OF ROCKER ARM" International journal of mechanical engineering and robotics research.

XVI. GoliUdaya Kumar FAILURE ANALYSIS OF INTERNAL COMBUSTION ENGINE VALVES BY USING ANSYS American International Journal of Research in Science, Technology, Engineering &Mathemara, Reginald DesRochesb, ArashYavarib

XVII. Youlong Chen a, Yilun Liu a,n, Yuan Yan a, Yong Zhu b, Xi Chen "Helical coil buckling mechanism for a stiff nanowire on an elastomeric substrate"

XVIII. Chang-Hsuan Chiu a,*, Chung-Li Hwan b, Han-Shuin Tsai a, Wei-Ping Lee a "An experimental investigation into the mechanical behaviors of helical composite springs"

XIX. L. Del Llano-Vizcaya a, C. Rubio-Gonza´lez a,*, G. Mesmacque b, T. Cervantes-Herna´ndez a "Multiaxial fatigue and failure analysis of helical compression springs"

Page 174